Topics in three flavor chiral dynamics

Dissertation

zur

Erlangung des Doktorgrades (Dr. rer. nat.)

der

Mathematisch-Naturwissenschaftlichen Fakultät

der

Rheinischen Friedrich-Wilhelms-Universität Bonn

vorgelegt von

Robin Nißler

aus

Ostfildern-Ruit

Bonn 2007

Angefertigt mit Genehmigung der Mathematisch-Naturwissenschaftlichen Fakultät der Rheinischen Friedrich-Wilhelms-Universität Bonn

Erscheinungsjahr: 2008

Referent:	Prof. Dr. Ulf-G. Meißner
Koreferent:	PD Dr. A. Rusetsky

Tag der Promotion: 22. Januar 2008

„Wenn die moderne Physik in zunehmendem Maße sich damit abfinden muß, daß ihr Vorstellungsbereich unanschaulich bleibt, dann ist dieser Verzicht nicht von irgendeiner Kommission von Forschern diktiert. Er ist vom Walten des Ge-stells herausgefordert, das die Bestellbarkeit der Natur als Bestand verlangt. Darum kann die Physik bei allem Rückzug aus dem bis vor kurzem allein maßgebenden, nur den Gegenständen zugewandten Vorstellen auf eines niemals verzichten: daß sich die Natur in irgendeiner rechnerisch feststellbaren Weise meldet und als ein System von Informationen bestellbar bleibt.“

Martin Heidegger, *Die Technik und die Kehre*[*]

---

[*] Verlag Günther Neske, Stuttgart, 1962.
Zur Erläuterung: Als *Ge-stell* bezeichnet Heidegger „das Wesen der Technik“, deren „Wegbereiterin“ die „neuzeitliche physikalische Theorie der Natur ist“.

Topics in three flavor chiral dynamics

In this work, we investigate several processes in low-energy hadron physics by combining chiral perturbation theory (ChPT), the effective field theory of quantum chromodynamics (QCD) at low energies, with a unitarization method based on the Bethe-Salpeter equation. Such so-called chiral unitary approaches are capable of describing processes in the three flavor sector of the strong interaction which involve substantial effects from final-state interactions and the excitation of (subthreshold) resonances, a domain where the perturbative framework of ChPT is not applicable.

In part I of this work we study η and η' decays which constitute a perfect tool to examine symmetries and symmetry breaking patterns of QCD being incorporated in a model-independent fashion in ChPT. In particular, these decays allow to investigate the breaking of isospin symmetry due to the light quark mass difference $m_d - m_u$ as well as effects of anomalies stemming from the quantum nature of QCD. For these reasons the decays of η and η' have also attracted considerable experimental interest. They are currently under investigation at several facilities including KLOE@DAΦNE, Crystal Ball at MAMI, WASA-at-COSY, VES at IHEP, and CLEO at CESR.

In part II we investigate low-energy meson-baryon scattering in the strangeness $S = -1$ sector which is dominated by the $\Lambda(1405)$ resonance immediately below the $\bar{K}N$ threshold. The $\bar{K}N$ interaction below threshold is of relevance for the quest of possible deeply bound $\bar{K}$-nuclear clusters and has recently received an additional tight constraint: the K^-p scattering length as determined from kaonic hydrogen by the KEK and the DEAR collaborations.

Apart from successfully describing a large amount of experimental data and furnishing predictions for yet unmeasured quantities, our calculations allow to interrelate different experimental observables providing important consistency tests of experiments. *E.g.* the DEAR results are shown to be inconsistent with previous K^-p scattering data and we demonstrate that the Dalitz plot parameters of the two decay modes $\eta \to 3\pi^0$, $\eta \to \pi^+\pi^-\pi^0$ as determined in the (first) analysis of the KLOE Collaboration are not compatible. In fact, they violate an important isospin rule. By performing a large number of fits to experimental data with randomized starting points we are furthermore able to give for the first time in chiral unitary approaches error estimates for our results and predictions.

Most of the contents of this thesis have been published under the following references:

- B. Borasoy and R. Nißler, *Hadronic η and η' decays*,
  Eur. Phys. J. A **26** (2005) 383 [arXiv:hep-ph/0510384].

- B. Borasoy, U.-G. Meißner and R. Nißler, *On the extraction of the quark mass ratio $(m_d - m_u)/m_s$ from $\Gamma(\eta' \to \pi^0\pi^+\pi^-)/\Gamma(\eta' \to \eta\pi^+\pi^-)$*,
  Phys. Lett. B **643** (2006) 41 [arXiv:hep-ph/0609010].

- B. Borasoy and R. Nißler, *$\eta, \eta' \to \pi^+\pi^-l^+l^-$ in a chiral unitary approach*,
  Eur. Phys. J. A **33** (2007) 95 [arXiv:0705.0954 [hep-ph]].

- B. Borasoy, R. Nißler and W. Weise, *Kaonic hydrogen and K^-p scattering*,
  Phys. Rev. Lett. **94** (2005) 213401 [arXiv:hep-ph/0410305].

- B. Borasoy, R. Nißler and W. Weise, *Chiral dynamics of kaon nucleon interactions, revisited*,
  Eur. Phys. J. A **25** (2005) 79 [arXiv:hep-ph/0505239].
- B. Borasoy, U.-G. Meißner and R. Nißler, *$K^- p$ scattering length from scattering experiments*,
  Phys. Rev. C **74** (2006) 055201 [arXiv:hep-ph/0606108].

Contents

Introduction

The interaction of hadrons at low energies is still one of the less well understood fields of physics. The reason can be traced back to the fact that the fundamental field theory of the strong interaction, quantum chromodynamics (QCD), features a running coupling "constant" which varies according to the energy scale of the process under consideration. While at high energies[†] the coupling constant is small—a phenomenon known as asymptotic freedom [1]—at low energies one enters the strongly coupled regime where perturbation theory cannot be applied. However, based on the symmetry properties of QCD it is possible to construct in a model-independent way a low-energy effective field theory of QCD whose active degrees of freedom are those observed in experiment, the (non-elementary) hadrons, instead of quarks and gluons which are the fundamental particles in QCD. This effective theory is called chiral perturbation theory (ChPT). It was initiated by Weinberg [2] and later on systematized and brought to its present-day form by Gasser and Leutwyler [3, 4].

Apart from Lorentz invariance and the discrete symmetries parity, time-reversal, and charge conjugation, ChPT is predicated on the approximate symmetry of QCD under chiral rotations of the quark fields, which is exact in the (hypothetical) limit of massless quarks, and on the spontaneous breakdown of chiral symmetry due to a non-invariant ground state. In ChPT Green functions are expanded in powers of quark masses and small momenta giving rise to a consistent power counting of the low-energy expansion. The high-energy behavior of QCD is encoded in the coupling constants occurring in the chiral effective Lagrangian; they have to be determined from experimental input or—possibly—lattice simulations of QCD. Clearly, the chiral expansion is only meaningful if the masses of the quarks are in fact small compared to the QCD scale $\Lambda_{\mathrm{QCD}} \approx 200\,\mathrm{MeV}$ which is certainly true for the up- and down-quarks, but may be questioned in case of the strange quark which happens to be considerably heavier than the up- and down-quarks. The remaining quarks charm, bottom, and top are much heavier and thus not relevant for the dynamics at low energies. While ChPT works well in the non-strange sector at very low energies, *e.g.* for $\pi\pi$ scattering, the convergence of the chiral expansion is generally worse at higher energies where the strange quark has to be taken into account. The question whether the strange quark is still in the chiral regime may be addressed by carefully investigating processes involving strange particles such as kaon-nucleon scattering.

The quantum field theory QCD exhibits characteristic anomalies which manifest themselves in hadronic reactions, *e.g.* in specific η and η' decays, and in the large mass

---

[†] To be more precise, the perturbative treatment of QCD is usually applicable for energies of at least a few GeV.

of the η' compared to the rest of the light pseudoscalar mesons. The latter is related to the axial U(1) anomaly of QCD. Apart from sharing the symmetries of QCD, ChPT also includes the anomalies of QCD in a model-independent way. For instance, the chiral anomalies are incorporated at the level of the effective theory in the Wess-Zumino-Witten Lagrangian [5, 6] whose coupling constants are fixed by the fundamental parameter N_c, the number of colors in QCD.

In this work we study several hadronic reactions in the three flavor sector of the strong interaction which reflect fundamental low-energy properties of QCD: some important decay modes of the η and the η' as well as $\bar{K}N$ scattering. It is an experimental fact that in the respective energy regime strong final-state interactions and resonances can play an essential role rendering the perturbative expansion of ChPT inapplicable. For example the $\bar{K}N$ interaction at low energies is dominated by the $\Lambda(1405)$ resonance only slightly below the $\bar{K}N$ threshold and the $\rho(770)$ yields significant contributions to final-state interactions in many η' decays. One thus has to resort to non-perturbative techniques which are able to resum the relevant contributions and generate resonances dynamically. To this end we employ the Bethe-Salpeter equation (BSE) which involves relativistic kinematics and guarantees exact two-particle unitarity of the S-matrix. The interaction kernel, that is iterated in the BSE, is derived up to a given chiral order from the chiral effective Lagrangian ensuring the perturbative matching of the unitarized and the ChPT amplitudes. Such so-called chiral unitary approaches have proven successful in describing many hadronic reactions involving resonances and substantial final-state interactions.

The possibility to study symmetries and symmetry breaking patterns of QCD by means of η and η' decays has also triggered a lot of experimental activities in this field. Various decay modes of these pseudoscalar mesons are currently under investigation, *e.g.* at KLOE@DAΦNE, Crystal Ball at MAMI, WASA-at-COSY, VES at IHEP, and CLEO at CESR. The close interplay of theoretical and experimental investigations has turned out to be particularly beneficial and leads to a better understanding of this interesting area of hadron physics. In this context we point at the formation of the network *EtaMesonNet* which has coordinated activities at different European accelerators and the exchange of information among experimental and theory groups from 2004 to 2007. It has been part of the Integrated Infrastructure Initiative *Study of strongly interacting matter* of the European Union and is likely to be continued focusing on η' physics.

Recent experimental developments in the study of hadronic atoms such as experiments with kaonic hydrogen by the KEK and the DEAR collaborations have provided new tight constraints in the area of $\bar{K}N$ interactions which will be complemented by the upcoming measurement of kaonic deuterium with SIDDHARTA at DAΦNE, a follow-up of the DEAR experiment.

In view of this variety of ongoing experimental activities it is clear that also theoretical efforts and improvements are necessary to gain deeper insights. The aim of the present work is to provide a well-grounded theoretical description of η, η' decays and $\bar{K}N$ scattering which is connected as closely as possible to the underlying theory QCD while keeping the approach efficient and technically feasible. All processes under consideration have in common that they involve interesting features of low-energy QCD while at the same time being not adequately described by pure ChPT due to the importance of non-perturbative effects.

This work is organized as follows: In Chapter 1 we present a short introduction to chiral perturbation theory with special focus on the inclusion of the η' meson which is not taken into account as a dynamical field in standard ChPT (where only the octet of pseudoscalar mesons is included). In addition, we discuss the Wess-Zumino-Witten Lagrangian which accounts for the effects of the chiral anomalies of QCD and briefly touch upon the inclusion of baryons in ChPT. In Chapter 2 we explain the unitarization of scattering amplitudes by means of the Bethe-Salpeter equation. The use of this method guarantees exact unitarity of the two-particle S-matrix while resonances are generated dynamically and can be associated with poles of the S-matrix in the complex energy plane. The section on resonance poles, where we also examine constraints imposed by causality, completes our discussion of the chiral unitary approach utilized in this work.

The applications of our framework are divided into two parts. In Part I we present the results of investigating several η and η' decays. Chapter 3 is devoted to the important hadronic decay modes $\eta, \eta' \to 3\pi$, $\eta' \to \eta\pi\pi$. We place particular emphasis on the decays into three pions which proceed mainly due to the isospin-breaking quark mass difference $m_d - m_u$. We also examine the possibility to extract the ratio $(m_d - m_u)/m_s$ from hadronic η' decays. In Chapter 4 we study the decays of η and η' into $\pi^+\pi^-$ and a lepton-antilepton pair. These processes involve vertices from the Wess-Zumino-Witten Lagrangian and are therefore called anomalous decays.

Part II deals with antikaon-nucleon scattering in the vicinity of the $\bar{K}N$ threshold. Here, we focus on the question whether the new results from kaonic hydrogen experiments are compatible with previous low-energy scattering data. Furthermore, we critically examine the pole structure of the S-matrix below the $\bar{K}N$ threshold where the $\Lambda(1405)$ resonance is situated.

We conclude the work with a short outlook. Lengthy tables and some additional material are relegated to the appendices.

Chapter 1

Chiral Perturbation Theory

1.1 QCD Lagrangian

Quantum Chromodynamics (QCD) is the quantum field theory of the strong interactions. It is a non-Abelian gauge theory, based on the gauge group $\mathrm{SU}(3)_c$ which is associated with the color degree of freedom. QCD describes the interaction of six types (flavors) of spin-1/2 particles, the quarks, mediated by massless gauge bosons, the gluons. There are eight different gluons corresponding to the $\mathrm{SU}(3)_c$ octet. Each quark flavor forms a color triplet. Apart from their color charge, quarks also carry an electric charge with up-, charm- and top-quarks having charge $+2/3$ and down-, strange- and bottom-quarks having charge $-1/3$ in units of the elementary charge e (with $e > 0$). Therefore, quarks also take part in electromagnetic interactions.

The Lagrangian of QCD (without electromagnetism) reads

$$\mathcal{L}_{\mathrm{QCD}} = \bar{\psi}_q^i \; [i\gamma^\mu (D_\mu)_{ij} - \delta_{ij}\; m_q] \; \psi_q^j - \frac{1}{4} G^a_{\mu\nu}\, G^{a\mu\nu} - \frac{g_s^2 \theta_0}{64\pi^2} G^a_{\mu\nu}\, \tilde{G}^{a\mu\nu} \,, \qquad (1.1)$$
$$(D_\mu)_{ij} = \delta_{ij}\partial_\mu + i g_s\, t^a_{ij} A^a_\mu \,,$$

where g_s is the coupling constant of QCD. Note that here and in the following we use the standard convention that repeated indices are summed over (unless otherwise indicated). Each quark field of color i, flavor q and mass m_q is represented by a four-component Dirac spinor $\psi_q^i(x)$. The gluonic gauge fields are denoted by $A^a_\mu(x)$ with associated field strength tensors $G^a_{\mu\nu} = \partial_\mu A^a_\nu - \partial_\nu A^a_\mu - g_s f^{abc} A^b_\mu A^c_\nu$, where f^{abc} are the structure constants of the symmetry group $\mathrm{SU}(3)_c$ with generators t^a. The eight SU(3) generators are related to the Gell-Mann matrices λ^a by $t^a = \lambda^a/2$. Explicit expressions for the Gell-Mann matrices and the structure constants f^{abc} can be found in Appendix A.1. The last term in the QCD Lagrangian involves the dual field strength tensor $\tilde{G}^{a\mu\nu} = \epsilon^{\mu\nu\alpha\beta} G^a_{\alpha\beta}$ and an additional parameter, the so-called vacuum angle θ_0. Since this term is odd under parity and time-reversal, it can induce measurable P and CP violation of the strong interactions. Up to now there is, however, no experimental indication of a non-zero value of θ_0 and we set $\theta_0 \equiv 0$ throughout this work.

It is yet another experimental fact that the masses of the u, d and s quarks are considerably smaller than those of c, b and t. In this work we are only interested in low-energy processes on the scale of the hadronic spectrum where the c, b and t quarks can be regarded as heavy particles. Instead of treating them as dynamical degrees of freedom they can rather be integrated out of the theory so that their effects are hidden in the coupling constants which govern the interactions of the remaining particles. If, on the other hand, the masses of the light quarks u, d, s are set to zero, one observes that the QCD Lagrangian, whose fermionic piece is then given by

$$\mathcal{L}_0 = i\bar{q}\not{D}q\,, \tag{1.2}$$

with $q = (u, d, s)^T$ and $\not{D} = \gamma^\mu D_\mu$, has an additional symmetry: It is invariant under separate U(3) transformations of the left- and right-handed quark fields

$$q_L = \frac{1}{2}(\mathbb{1} - \gamma^5)\, q, \qquad\qquad q_R = \frac{1}{2}(\mathbb{1} + \gamma^5)\, q \tag{1.3}$$

which decouple completely in the massless Lagrangian

$$\mathcal{L}_0 = i\bar{q}\not{D}q = i\bar{q}_L\not{D}q_L + i\bar{q}_R\not{D}q_R\ . \tag{1.4}$$

The full group of chiral transformations $\mathrm{U}(3)_L \times \mathrm{U}(3)_R$ can be decomposed into four irreducible subgroups $\mathrm{U}(1)_L \times \mathrm{U}(1)_R \times \mathrm{SU}(3)_L \times \mathrm{SU}(3)_R$. Left- and right-handed chiral transformations $L \in \mathrm{U}(3)_L$, $R \in \mathrm{U}(3)_R$ can also be expressed in terms of vector and axial-vector transformations defined by $L = R$ and $L = R^\dagger$, respectively, which leads to the equivalent decomposition $\mathrm{U}(1)_V \times \mathrm{U}(1)_A \times \mathrm{SU}(3)_V \times \mathrm{SU}(3)_A$. In virtue of Noether's theorem one expects conserved currents corresponding to the global symmetries of the Lagrangian. In fact $\mathrm{U}(1)_V$ symmetry, which also holds in the presence of non-vanishing quark masses, is associated with baryon number conservation in the strong interactions. The (approximate) symmetry under $\mathrm{SU}(3)_V$ transformations is realized in the flavor symmetry of the hadronic spectrum. In contrast, there are no experimentally confirmed conservation laws corresponding to the axial-vector symmetries. In case of $\mathrm{U}(1)_A$ this can be traced back to the fact that despite being a symmetry of the Lagrangian taken as a classical object, axial U(1) symmetry is anomalously broken at the quantum level of the theory. It is thus not a symmetry of QCD and we cannot expect a conserved quantum number associated with it. The axial anomaly of the strong interactions has important consequences for the nature of the η' meson and will be discussed in more detail in Sections 1.4 and 1.5.

Finally, an assumed invariance under chiral $\mathrm{SU}(3)_A$ transformations would induce parity doubling in the hadronic spectrum; *e.g.* the octet of pseudoscalar mesons should be accompanied by an octet of scalar mesons with similar masses. Since no such parity degeneracy is found in nature, one is led to the assumption that chiral $\mathrm{SU}(3)_L \times \mathrm{SU}(3)_R$ is spontaneously broken down to its subgroup $\mathrm{SU}(3)_V$. In general, spontaneous breakdown of a symmetry occurs if the Lagrangian, which describes a physical system, is symmetric under a certain transformation, but the ground state of the system is not. One example from a completely different field of physics is the spontaneous breakdown of rotational invariance of a ferromagnet which is cooled down below its Curie temperature so that the emerging magnetization singles out one particular direction in space.

According to Goldstone's theorem the spontaneous breakdown of a continuous symmetry implies the existence of a massless and spinless particle with the quantum numbers of the generator of the broken symmetry [7]. For a ferromagnet these excitations are known as magnons, quantized spin waves which change the direction of the local magnetization. In case of the broken chiral $\mathrm{SU}(3)_L \times \mathrm{SU}(3)_R$ symmetry of QCD we expect eight Goldstone bosons with spin zero and odd parity ($J^P = 0^-$).

The spectrum of the hadrons does not include any massless particles, but it does include an octet of light mesons ($\pi^+, \pi^-, \pi^0, K^+, K^-, K^0, \bar{K}^0, \eta$). These lowest-lying excitations in the hadronic spectrum are known to have $J^P = 0^-$ and are separated from the rest of the spectrum by a mass gap which is characteristic for systems with spontaneously broken symmetry. We will identify the eight pseudoscalar mesons with the Goldstone bosons of massless QCD, keeping in mind that chiral symmetry is not an exact symmetry of the strong interactions, but rather explicitly broken by the quark mass terms in the QCD Lagrangian which intertwines left- and right-handed quarks by virtue of

$$\mathcal{L}_{\mathcal{M}} = -\bar{q}\mathcal{M}q = -\bar{q}_L\mathcal{M}q_R - \bar{q}_R\mathcal{M}q_L \, , \tag{1.5}$$

where $\mathcal{M} = \mathrm{diag}(m_u, m_d, m_s)$ is the real-valued quark mass matrix.

The mechanism of chiral symmetry breaking puts stringent constraints on the interaction among the pseudoscalar mesons (*e.g.* they completely decouple in the limit of vanishing masses and momenta) and, by treating the non-vanishing masses of the three light quarks as perturbative corrections to the idealized case of massless quarks, it moreover allows to relate the masses of the pseudoscalar mesons to the quark masses in QCD (up to electromagnetic contributions which can be treated separately).

1.2 Construction of the effective Lagrangian

In order to construct an effective Lagrangian which describes the interaction of the octet of pseudoscalar mesons, *i.e.* the Goldstone bosons of QCD, we must find a suitable representation of the meson fields. Long ago such chiral Lagrangians were investigated by Weinberg [8] in the context of chiral SU(2) symmetry. Later on the general prescription of how to construct an effective field theory based on the assumption of a spontaneously broken symmetry was elaborated by Callan, Coleman, Wess and Zumino [9]. Here, we will follow the discussion given in [10]. For other introductions to chiral perturbation theory (ChPT) of varied detailedness and with different focuses see, *e.g.*, [11–15] and the textbook [16].

We consider a physical system whose Lagrangian has a symmetry G (a compact Lie group of global field transformations) which is broken down spontaneously to a subgroup $H \subset G$ by a non-invariant ground state. According to Goldstone's theorem, there exist $n = \dim G - \dim H$ Goldstone bosons which we will summarize by the n-component, real-valued field $\varphi(x)$. Given an element $g \in G$, the Goldstone bosons transform according to a representation F of the group G,

$$\varphi \to \varphi' = F(g, \varphi) \, , \tag{1.6}$$

which obeys the representation property

$$F(g, F(\tilde{g}, \varphi)) = F(g\tilde{g}, \varphi), \qquad g, \tilde{g} \in G \, . \tag{1.7}$$

Our aim is to find such a representation which—as it turns out—uniquely associates a subset of G with all field configurations φ. First, we verify that the elements $h \in H$ which leave the vacuum state (denoted by $\varphi \equiv 0$) invariant,

$$F(h,0) = 0 \quad \forall\, h \in H \ , \tag{1.8}$$

indeed form a subgroup of G. Let e be the identity in G and $h, \tilde{h} \in H$, then

$$\begin{aligned}
&F(e,0) = 0 \quad \Rightarrow e \in H\,, \\
&F(h\tilde{h},0) = F(h, F(\tilde{h},0)) = F(h,0) = 0 \quad \Rightarrow h\tilde{h} \in H\,, \\
&0 = F(e,0) = F(h^{-1}h,0) = F(h^{-1}, F(h,0)) = F(h^{-1},0) \quad \Rightarrow h^{-1} \in H\,.
\end{aligned} \tag{1.9}$$

Moreover, since for any $g \in G$ we have

$$F(gh,0) = F(g, F(h,0)) = F(g,0) \quad \forall\, h \in H \ , \tag{1.10}$$

the function $F(g,0)$ maps the elements of the left cosets* G/H onto the values of the Goldstone boson fields. This mapping is injective and thus invertible on its image, for let $g, \tilde{g} \in G$ with $F(g,0) = F(\tilde{g},0)$ then

$$\begin{aligned}
0 = F(g^{-1}g,0) = F(g^{-1}, F(g,0)) = F(g^{-1}, F(\tilde{g},0)) = F(g^{-1}\tilde{g},0) \\
\Rightarrow g^{-1}\tilde{g} \in H \ \Rightarrow \tilde{g} \in gH \ .
\end{aligned} \tag{1.11}$$

Since $\dim G/H = n$ the values of the Goldstone boson fields can in fact be identified with elements of the coset space. We now choose a representative element q for each left coset $gH \in G/H$. As G/H is a set of equivalence classes, this choice is, of course, not unique. With a suitable $h \in H$ every element $g \in G$ can then be decomposed as $g = qh$. The transformation of the Goldstone boson fields $\varphi = F(q,0)$ under $g \in G$ is therefore given by

$$\varphi \to \varphi' = F(g,\varphi) = F(g, F(q,0)) = F(gq,0) = F(q'h,0) = F(q',0)\,, \tag{1.12}$$

where q' represents the left coset associated with the transformed fields φ' and we made use of the unique decomposition $gq = q'h$ with $h \in H$ appropriately.

In the case of three flavor QCD we have $G = \mathrm{SU}(3)_L \times \mathrm{SU}(3)_R$ and $H = \mathrm{SU}(3)_V$. The coset space G/H is again isomorphic to SU(3), thus the Goldstone boson fields can be represented by matrix valued fields $\hat{U}(x) \in \mathrm{SU}(3)$. Corresponding to the decomposition $g = qh$ one may for example choose the representation

$$g = (\hat{L},\hat{R}) = (\hat{L}, \hat{R}\hat{L}^\dagger\hat{L}) = (\mathbb{1}, \hat{R}\hat{L}^\dagger)(\hat{L},\hat{L}) \quad \Rightarrow \hat{U} := \hat{R}\hat{L}^\dagger \tag{1.13}$$

or

$$g = (\hat{L},\hat{R}) = (\hat{L}\hat{R}^\dagger\hat{R}, \hat{R}) = (\hat{L}\hat{R}^\dagger, \mathbb{1})(\hat{R},\hat{R}) \quad \Rightarrow \tilde{U} := \hat{L}\hat{R}^\dagger \tag{1.14}$$

---

*A left (right) coset of a group G with respect to the subgroup $H \subset G$ is an equivalence class of elements in G which only differ by right (left) multiplication with a member $h \in H$ and is denoted by gH (Hg).

with $\hat{L}, \hat{R} \in \mathrm{SU}(3)$. Picking out the first choice, the behavior of $\hat{U}$ under a chiral transformation $\tilde{g} \in G$ is given by

$$\begin{aligned}(\mathbb{1}, \hat{U}) \to (\mathbb{1}, \hat{U}') = \tilde{g}(\mathbb{1}, \hat{U}) = (\tilde{L}, \tilde{R})(\mathbb{1}, \hat{U}) = (\tilde{L}, \tilde{R}\hat{U}) = (\mathbb{1}, \tilde{R}\hat{U}\tilde{L}^\dagger)(\tilde{L}, \tilde{L}) \\ \Rightarrow \hat{U} \to \hat{U}' = \tilde{R}\hat{U}\tilde{L}^\dagger \end{aligned} \tag{1.15}$$

Conventionally, one defines $\hat{U}(x)$ by means of the exponential representation

$$\hat{U}(x) = \exp\left(\frac{2i}{f}\, t^a \varphi^a(x)\right) , \tag{1.16}$$

where $t^a = \lambda^a/2$ are the generators of SU(3) and f is the pseudoscalar decay constant in the chiral limit. This constant measures the strength with which the pseudoscalar mesons decay via the axial-vector currents $j^a_{\mu 5} = \bar{q}\gamma_\mu\gamma_5 t^a q$, $a = 1, \ldots, 8$ into the hadronic vacuum and is defined by the matrix element

$$\langle 0|\, j^a_{\mu 5}(x) \left|\varphi^b(p)\right\rangle = i e^{-ip\cdot x} p_\mu\, f\, \delta^{ab} \tag{1.17}$$

in the chiral limit. Experimentally, the decay constant of the charged pions may be inferred from the weak decay $\pi^+ \to \mu^+\nu_\mu$ which leads to a value of $F_\pi = (92.4 \pm 0.3)\,\mathrm{MeV}$ [17]. Within the framework of chiral perturbation theory, it is possible to extrapolate the physical decay constant F_π down to its value in the chiral limit of vanishing quark masses. To one-loop order in SU(2) ChPT one obtains $f \approx 88\,\mathrm{MeV}$ [3], whereas a recent two-loop calculation yields $f = (86.2 \pm 0.5)\,\mathrm{MeV}$ [18].

Expressing the Goldstone boson fields φ^a in terms of the fields in the physical basis (but still in the chiral limit) we arrive at

$$t^a\varphi^a = \frac{1}{\sqrt{2}} \begin{pmatrix} \frac{1}{\sqrt{2}}\tilde{\pi}^0 + \frac{1}{\sqrt{6}}\eta_8 & \pi^+ & K^+ \\ \pi^- & -\frac{1}{\sqrt{2}}\tilde{\pi}^0 + \frac{1}{\sqrt{6}}\eta_8 & K^0 \\ K^- & \bar{K}^0 & -\sqrt{\frac{2}{3}}\eta_8 \end{pmatrix} =: \frac{1}{\sqrt{2}}\,\hat{\phi} \, . \tag{1.18}$$

There is yet another representation of the pseudoscalar mesons which is frequently used in the literature, in particular for the description of meson-baryon interactions, *cf.* Sect. 1.6. It is obtained by choosing the axial-vector type transformations $q = (u^\dagger, u)$, $u \in \mathrm{SU}(3)$, as the representative elements of the coset space G/H. In this case, a chiral transformation $g = (\hat{L}, \hat{R})$ acts as

$$gq = (\hat{L}, \hat{R})(u^\dagger, u) = (\hat{L}u^\dagger, \hat{R}u) = (u'^\dagger, u')(K, K) \quad \text{with } (K, K) \in \mathrm{SU}(3)_V \ , \tag{1.19}$$

from which one extracts the transformation property of u

$$u \to u' = \hat{R}uK^\dagger = Ku\hat{L}^\dagger \ . \tag{1.20}$$

The SU(3) element K is implicitly defined as a function of u, $\hat{L}$, and $\hat{R}$ by the above equation and is usually referred to as the compensator field. From the transformation of u^2,

$$u^2 \to u'^2 = \hat{R}uK^\dagger Ku\hat{L}^\dagger = \hat{R}u^2\hat{L}^\dagger \ , \tag{1.21}$$

it is obvious to identify $u^2(x) = \hat{U}(x)$, so that

$$u(x) = \exp\left(\frac{i}{f}\, t^a \varphi^a(x)\right) = \exp\left(\frac{i}{\sqrt{2}f}\, \hat{\phi}(x)\right) . \tag{1.22}$$

Due to its simple behavior under chiral transformations it is most convenient to choose the representation $\hat{U}(x)$, Eq. (1.16), for the construction of the chiral effective Lagrangian which is then given by a function of $\hat{U}$ and derivatives thereof

$$\mathcal{L}_{\hat{\phi}} = \mathcal{L}_{\hat{\phi}}(\hat{U}, \partial\hat{U}, \partial^2\hat{U}, \ldots) . \tag{1.23}$$

The final results of a calculation should of course be independent of the particular choice of the field parametrization. Following the general principles for the construction of a low-energy effective field theory, $\mathcal{L}_{\hat{\phi}}$ has to respect the same symmetries as the underlying fundamental theory, in our case QCD.[†] Hence, it has to obey Lorentz-invariance, C, P, T, and, in particular, chiral $\mathrm{SU}(3)_L \times \mathrm{SU}(3)_R$ symmetry. Constituting a low-energy theory, $\mathcal{L}_{\hat{\phi}}$ is naturally organized in powers of (small) momenta or—equivalently—in powers of derivatives on the meson fields which defines the so-called chiral counting scheme. Lorentz-invariance implies that only even powers of derivatives occur. At zeroth chiral order, *i.e.* without derivatives, the only building block for the construction of $\mathcal{L}_{\hat{\phi}}$ which respects all symmetries is $\hat{U}\hat{U}^\dagger = \mathbb{1}$. Thus, the zeroth order Lagrangian $\mathcal{L}_{\hat{\phi}}^{(0)}$ is just an irrelevant constant. At second chiral order one finds

$$\mathcal{L}_{\hat{\phi}}^{(2)} = \frac{f^2}{4}\langle \partial_\mu \hat{U} \partial^\mu \hat{U}^\dagger \rangle , \tag{1.24}$$

where $\langle \ldots \rangle$ denotes the trace in flavor space. The coefficient $f^2/4$ is fixed by the requirement that the kinetic terms of the Goldstone bosons be normalized in the standard way

$$\begin{aligned} \mathcal{L}_{\hat{\phi}}^{(2)} &= \frac{f^2}{4}\left\langle \frac{2i}{f} t^a \partial_\mu \varphi^a \frac{-2i}{f} t^b \partial^\mu \varphi^b \right\rangle + \cdots \\ &= \partial_\mu \varphi^a \partial^\mu \varphi^b \left\langle t^a t^b \right\rangle + \cdots = \frac{1}{2} \partial_\mu \varphi^a \partial^\mu \varphi^a + \cdots , \end{aligned} \tag{1.25}$$

where the ellipsis indicate terms with at least four Goldstone boson fields and we have used $\langle t^a t^b \rangle = \delta^{ab}/2$.

When going to higher chiral orders, more and more independent terms are allowed by the above-named symmetries. In general, their coefficients—which are called low-energy constants (LECs)—are not subject to any constraints and have to be fixed by experimental input or lattice QCD calculations. In some instances their size can also be estimated by phenomenological models such as resonance saturation. The explicit form of the fourth order Lagrangian will be given in the next section where we generalize the effective Lagrangian to the inclusion of external sources and symmetry-breaking terms.

[†] Moreover, the effective Lagrangian also has to reproduce the symmetry-breaking patterns of the underlying theory such as anomalies or explicit symmetry violations by non-invariant terms. These issues are discussed in Sects. 1.4 and 1.3, respectively.

1.3 External sources

A valuable tool to study matrix elements in quantum field theory is furnished by the path integral formalism [19]. In order to examine matrix elements of a given current $J(x)$ one introduces a classical source term $S(x)$ in the Lagrangian of the theory which is coupled to $J(x)$. *E.g.* for a theory with scalar fields $\varphi(x)$ and a Lagrangian $\mathcal{L} = \mathcal{L}[\varphi]$ [‡] we set $\mathcal{L}[\varphi, S] := \mathcal{L}[\varphi] + JS$. The fundamental object in the path integral formalism, the so-called generating functional $W[S]$, is then defined by

$$W[S] = \int \mathcal{D}\varphi \exp\left\{ i \int d^4x \; \mathcal{L}[\varphi, S] \right\} . \tag{1.26}$$

The vacuum expectation value of the operator J may be computed by taking the functional derivative of the generating functional, see *e.g.* [20]:

$$\langle 0|\, J(y)\, |0\rangle = \frac{1}{W[0]} \left(-i \frac{\delta}{\delta S(y)} \right) W[S] \bigg|_{S=0} . \tag{1.27}$$

We now apply the method of external sources to the case of three-flavor QCD. To this end we introduce scalar (s), pseudoscalar (p), vector(v_μ), and axial-vector (a_μ) sources which are represented by Hermitian, color neutral matrices in flavor space. The modified QCD Lagrangian then reads

$$\mathcal{L}_{\text{QCD}} = -\frac{1}{4} G^a_{\mu\nu} G^{a\mu\nu} + \bar{q} i \not{D} q + \bar{q}\gamma^\mu (v_\mu + \gamma^5 a_\mu) q - \bar{q}(s - i\gamma^5 p) q . \tag{1.28}$$

For the specific choice $v_\mu = a_\mu = p = 0$, $s = \mathcal{M}$ with $\mathcal{M} = \text{diag}(m_u, m_d, m_s)$ the original Lagrangian of QCD is recovered. Formally, the Lagrangian in Eq. (1.28) is invariant under local $\text{U}(3)_L \times \text{U}(3)_R$ transformations of the quark fields,

$$q(x) \to q'(x) = L(x)\, \frac{1}{2}(\mathbb{1} - \gamma^5) q(x) + R(x)\, \frac{1}{2}(\mathbb{1} + \gamma^5) q(x) \tag{1.29}$$

with $L(x), R(x) \in \text{U}(3)$, provided that the external fields transform according to

$$\begin{aligned} (s + ip) &\to R(s + ip) L^\dagger , \\ l_\mu &\to L\, l_\mu L^\dagger + i L \partial_\mu L^\dagger \quad \text{with} \quad l_\mu = v_\mu - a_\mu , \\ r_\mu &\to R\, r_\mu R^\dagger + i R \partial_\mu R^\dagger \quad \text{with} \quad r_\mu = v_\mu + a_\mu . \end{aligned} \tag{1.30}$$

The full generating functional

$$W_{\text{QCD}}[v, a, s, p] = \int \mathcal{D}q \mathcal{D}\bar{q} \mathcal{D}A \exp\left\{ i \int d^4x \; \mathcal{L}_{\text{QCD}}[q, \bar{q}, A, v, a, s, p] \right\} \tag{1.31}$$

is, however, not invariant under such transformations as it is affected by anomalies stemming from the non-trivial transformation properties of the fermionic measure in the

---

[‡] In this section we use square brackets for the arguments of functionals in order to distinguish them from ordinary functions for which parentheses are employed.

path integral. One such anomaly is the axial U(1) anomaly which has been mentioned earlier and will be discussed in some detail in Sect. 1.4.2, the other anomalies are the so-called chiral anomalies which involve the external vector and axial-vector fields. They have important consequences for the anomalous decays of π^0, η, η' and will be reviewed in Sect. 1.4.3.

Postponing the discussion of QCD anomalies we restrict ourselves to the subgroup of chiral $\mathrm{SU}(3)_L \times \mathrm{SU}(3)_R$ transformations and remark that the chiral anomalies appear only at next-to-leading order in the chiral counting scheme. The construction of the effective Lagrangian in the presence of external sources presented in this section will enable us to systematically treat the effects of non-vanishing quark masses and the (non-anomalous) coupling to external photons. Following the construction principles for an effective field theory, the effective Lagrangian corresponding to the modified QCD Lagrangian, Eq. (1.28), has to be invariant under chiral $\mathrm{SU}(3)_L \times \mathrm{SU}(3)_R$ gauge transformations. For this reason, we introduce a covariant derivative of the meson fields

$$\nabla_\mu \hat{U} = \partial_\mu \hat{U} - i[\hat{v}_\mu, \hat{U}] - i\{\hat{a}_\mu, \hat{U}\} = \partial_\mu \hat{U} + i\hat{U}\hat{l}_\mu - i\hat{r}_\mu \hat{U}\,, \tag{1.32}$$

where the hats over the external fields indicate that only the traceless parts are employed here, *i.e.* $\hat{v}_\mu = v_\mu - \langle v_\mu \rangle /3$ and so on. The covariant derivative transforms in the same way as $\hat{U}$ under chiral transformations $\hat{L}, \hat{R} \in \mathrm{SU}(3)$

$$\nabla_\mu \hat{U} \to \hat{R}\, \nabla_\mu \hat{U} \hat{L}^\dagger\ . \tag{1.33}$$

Furthermore, we define field strength tensors for the external left- and right-handed fields

$$\hat{L}_{\mu\nu} = \partial_\mu \hat{l}_\nu - \partial_\nu \hat{l}_\mu - i[\hat{l}_\mu, \hat{l}_\nu]\,, \qquad \hat{R}_{\mu\nu} = \partial_\mu \hat{r}_\nu - \partial_\nu \hat{r}_\mu - i[\hat{r}_\mu, \hat{r}_\nu] \tag{1.34}$$

which are needed for the construction of a gauge invariant effective Lagrangian. They transform as

$$\hat{L}_{\mu\nu} \to \hat{L}\hat{L}_{\mu\nu}\hat{L}^\dagger, \qquad \hat{R}_{\mu\nu} \to \hat{R}\hat{R}_{\mu\nu}\hat{R}^\dagger\ . \tag{1.35}$$

The scalar and pseudoscalar external fields are conventionally summarized in the quantity

$$\chi = 2B_0(s + ip)\,, \tag{1.36}$$

where B_0 is a real constant which will be determined later on.[§]

In the standard counting scheme of chiral perturbation theory, the external vector and axial-vector fields are counted as $\mathcal{O}(p)$ because they enter at the same level as the derivative operator ∂_μ in the covariant derivative Eq. (1.32). Accordingly, the field strength tensors $\hat{L}_{\mu\nu}$, $\hat{R}_{\mu\nu}$ are of order $\mathcal{O}(p^2)$. The combination χ is also booked as $\mathcal{O}(p^2)$ since it contains the quark mass matrix $\mathcal{M}$ which can be related to the squared masses of the pseudoscalar mesons as we will see later.

With these conventions one finds the chiral effective Lagrangian at order $\mathcal{O}(p^2)$ [4]

$$\mathcal{L}^{(2)}_{\hat{\phi}} = \frac{f^2}{4}\langle \nabla_\mu \hat{U} \nabla^\mu \hat{U} \rangle + \frac{f^2}{4}\langle \hat{U}^\dagger \chi + \chi^\dagger \hat{U} \rangle \tag{1.37}$$

[§] Note that B_0 is only real in the absence of CP violation, see [4].

where the first term generalizes the Lagrangian of Eq. (1.24) and the second term brings in the quark masses. Its normalization factor was chosen for later convenience. Note that at order $\mathcal{O}(p^2)$ there are no terms involving the field strength tensors $\hat{L}_{\mu\nu}$, $\hat{R}_{\mu\nu}$, *i.e.* external vector and axial-vector fields such as photons or weak currents only couple to the mesons via the covariant derivative $\nabla_\mu \hat{U}$.

Being the model-independent low-energy effective theory of QCD, ChPT reproduces QCD Green functions as a perturbative series in powers of small momenta and quark masses. Matrix elements derived from the generating functional of QCD can thus be perturbatively related to corresponding matrix elements derived from the generating functional of ChPT [2, 3]. To give one important example, we calculate the vacuum expectation value of the operator $\bar{u}u$ which is obtained by taking the functional derivative of the generating functional of QCD with respect to the auxiliary field ξ that enters the scalar source $s_\xi = \mathrm{diag}(m_u + \xi, m_d, m_s)$,

$$\langle 0|\, \bar{u}u \,|0\rangle = \frac{1}{W_{\mathrm{QCD}}[0,0,\mathcal{M},0]} \left(i\frac{\delta}{\delta\xi} \right) W_{\mathrm{QCD}}[0,0,s_\xi,0] \Big|_{\xi=0} . \tag{1.38}$$

Performing the same operations on the generating functional of the effective theory at lowest order,

$$W_{\hat{\phi}}^{(2)}[\hat{v},\hat{a},s,p] = \int \mathcal{D}\hat{U} \exp\left\{ i \int d^4x\, \mathcal{L}_{\hat{\phi}}^{(2)}[\hat{U},\hat{v},\hat{a},s,p] \right\} , \tag{1.39}$$

we compute

$$\begin{aligned}
\langle 0|\, \bar{u}u \,|0\rangle &= \frac{1}{W_{\hat{\phi}}^{(2)}[0,0,\mathcal{M},0]} \left(i\frac{\delta}{\delta\xi} \right) W_{\hat{\phi}}^{(2)}[0,0,s_\xi,0] \Big|_{\xi=0} \\
&= \frac{-f^2 B_0}{W_{\hat{\phi}}^{(2)}[0,0,\mathcal{M},0]} \int \mathcal{D}\hat{U} \frac{1}{2}(\hat{U}^\dagger + \hat{U})_{11} \exp\left\{ i \int d^4x\, \mathcal{L}_{\hat{\phi}}^{(2)}[\hat{U},0,0,\mathcal{M},0] \right\} \\
&= -f^2 B_0 + \mathcal{O}(\mathcal{M}) , \qquad (1.40)
\end{aligned}$$

where in the last step we used $\hat{U}^\dagger + \hat{U} = 2(\mathbb{1} - \hat{\phi}^2/f^2 + \hat{\phi}^4/(6f^4) + \ldots)$. The constant piece produces the result $-f^2 B_0$ whereas the remaining $\hat{\phi}$ dependent terms generate vacuum diagrams as exemplified in Fig. 1.1. Their contributions are of higher order in the chiral counting scheme, which will be explained later on, and vanish in the chiral limit. The vacuum expectation values of $\bar{d}d$ and $\bar{s}s$ are derived in complete analogy resulting in

$$\langle 0|\, \bar{u}u \,|0\rangle = \langle 0|\, \bar{d}d \,|0\rangle = \langle 0|\, \bar{s}s \,|0\rangle = -f^2 B_0 (1 + \mathcal{O}(\mathcal{M})) . \tag{1.41}$$

The constant B_0 is thus proportional to the vacuum expectation value of the scalar quark-antiquark densities in the chiral limit and can be regarded as the order parameter of chiral symmetry breakdown.

In standard ChPT B_0 is considered as a large quantity which is of zeroth chiral order. As a side note we remark that there also exists a different counting scheme which is referred to as generalized ChPT [21]. In this framework B_0 is regarded as a small scale, *i.e.* the scalar quark condensate is treated as a small quantity, and B_0 is assigned

Figure 1.1: Pseudoscalar meson loops which contribute to the vacuum expectation value $\langle 0|\,\bar{q}q\,|0\rangle$.

the chiral order $\mathcal{O}(p)$, whereas the external fields s and p are also counted as $\mathcal{O}(p)$. By utilizing B_0 and $s+ip$ as separate building blocks for the construction of the effective Lagrangian one finds six independent terms at order $\mathcal{O}(p^2)$ with additional LECs not present in $\mathcal{L}^{(2)}_{\hat{\phi}}$, Eq. (1.37). Moreover, the generalized chiral Lagrangian also contains terms of odd chiral power starting at $\mathcal{O}(p^3)$. In this work, however, we stick to the standard chiral counting scheme and do not discuss generalized ChPT any further here.

By expanding the Lagrangian $\mathcal{L}^{(2)}_{\hat{\phi}}$ up to second order in the meson fields and setting the external fields to their physical values, *i.e.* $\hat{v}=\hat{a}=p=0$, $s=\mathcal{M}$, we obtain mass terms for the pseudoscalar mesons

$$\begin{aligned}\mathcal{L}^{(2)}_{\text{mass}} &= -B_0\langle\hat{\phi}^2\mathcal{M}\rangle\\ &= -B_0\Big\{\frac{1}{2}(m_u+m_d)(\tilde{\pi}^0)^2+(m_u+m_d)\pi^+\pi^-\\ &\qquad +(m_u+m_s)K^+K^-+(m_d+m_s)K^0\bar{K}^0\\ &\qquad +\frac{1}{6}(m_u+m_d+4m_s)(\eta_8)^2+\frac{1}{\sqrt{3}}(m_u-m_d)\tilde{\pi}^0\eta_8\Big\}\,, \end{aligned}\tag{1.42}$$

where the last term entails $\tilde{\pi}^0$-η_8 mixing and is proportional to the isospin-breaking quark mass difference m_u-m_d. From Eq. (1.42) we may read off the leading order mass formulae

$$\begin{aligned} m^2_{\pi^0} &= 2B_0\hat{m}-\frac{1}{4}B_0\frac{(m_d-m_u)^2}{m_s-\hat{m}}\,, & m^2_{\pi^\pm} &= 2B_0\hat{m}\,,\\ m^2_{K^0} &= B_0(m_d+m_s)\,, & m^2_{K^\pm} &= B_0(m_u+m_s)\,,\\ m^2_{\eta} &= \frac{2}{3}B_0(\hat{m}+2m_s)+\frac{1}{4}B_0\frac{(m_d-m_u)^2}{m_s-\hat{m}}\,, \end{aligned}\tag{1.43}$$

where $\hat{m}=(m_u+m_d)/2$ is the average light quark mass. The mass relations hold up to corrections of order $\mathcal{O}(\mathcal{M}^2)$ and were first derived by Gell-Mann, Oakes, and Renner [22]. In the isospin limit of equal up- and down-quark masses they reduce to

$$m^2_\pi = 2B_0\hat{m}\,,\qquad m^2_K = B_0(\hat{m}+m_s)\,,\qquad m^2_\eta=\frac{2}{3}B_0(\hat{m}+2m_s)\,,\tag{1.44}$$

and can be readily employed to obtain the so-called Gell-Mann–Okubo formula [23, 24]

$$3m^2_\eta = 4m^2_K - m^2_\pi\tag{1.45}$$

which predicts $m_\eta = 566\,\mathrm{MeV}$, not far from the measured η mass of $547\,\mathrm{MeV}$ [17].

Higher order corrections to the above relations are obtained by taking contributions from higher order effective Lagrangians $\mathcal{L}_{\hat\phi}^{(4)}$, $\mathcal{L}_{\hat\phi}^{(6)}$, …into account, but—since we are dealing with a quantum field theory—also contributions from loop graphs have to be included. Typically, such loop integrals are divergent and in order to arrive at a meaningful result, the occurring divergences have to be absorbed by renormalizing coupling constants of the theory. If the loop integrals are regularized by means of a regularization scheme which preserves the symmetries of the Lagrangian (such as dimensional regularization), it is clear that all infinities require only counter terms that share these symmetries. Since by construction the full chiral effective Lagrangian contains all such terms, every divergence which occurs in loop calculations within ChPT can be absorbed into an appropriate counter term. Obviously, the full chiral effective Lagrangian, which consists of infinitely many terms constructed out of the building blocks $\hat U$, $\nabla_\mu \hat U$, χ, $\hat L_{\mu\nu}$, $\hat R_{\mu\nu}$ and further derivatives thereof, involves terms of mass dimension higher than four. Chiral perturbation theory is therefore a non-renormalizable theory in the usual sense. However, chiral power counting ensures that loop diagrams are indeed suppressed with respect to tree graphs so that they do not alter the coupling constants at lower chiral orders. By employing the general arguments given by Weinberg [2], this statement can be made more explicit. Consider a connected diagram with ℓ loops and N_k vertices of order $\mathcal{O}(p^k)$. The chiral order ν of the diagram is then given by

$$\nu = 2 + 2\ell + \sum_{k=2,4,6,\ldots} (k-2) N_k \ . \tag{1.46}$$

Clearly, the chiral order is increased when the number of loops grows. In other words, the chiral expansion is in accordance with the loop expansion. One-loop graphs with lowest order vertices contribute at fourth chiral order; their divergences can thus be absorbed by counter terms of order $\mathcal{O}(p^4)$. For two-loop diagrams, only counter terms from $\mathcal{L}_{\hat\phi}^{(6)}$ and higher are required, and so on.

For completeness we also display the chiral effective Lagrangian of order $\mathcal{O}(p^4)$ which was first constructed by Gasser and Leutwyler [4]. It reads

$$\begin{aligned}
\mathcal{L}_{\hat\phi}^{(4)} &= L_1 \big\langle \nabla_\mu \hat U^\dagger \nabla^\mu \hat U \big\rangle^2 + L_2 \big\langle \nabla_\mu \hat U^\dagger \nabla_\nu \hat U \big\rangle \big\langle \nabla^\mu \hat U^\dagger \nabla^\nu \hat U \big\rangle \\
&\quad + L_3 \big\langle \nabla_\mu \hat U^\dagger \nabla^\mu \hat U \nabla_\nu \hat U^\dagger \nabla^\nu \hat U \big\rangle + L_4 \big\langle \nabla_\mu \hat U^\dagger \nabla^\mu \hat U \big\rangle \big\langle \hat U^\dagger \chi + \chi^\dagger \hat U \big\rangle \\
&\quad + L_5 \big\langle \nabla_\mu \hat U^\dagger \nabla^\mu \hat U (\hat U^\dagger \chi + \chi^\dagger \hat U) \big\rangle + L_6 \big\langle \hat U^\dagger \chi + \chi^\dagger \hat U \big\rangle^2 \\
&\quad + L_7 \big\langle \hat U^\dagger \chi - \chi^\dagger \hat U \big\rangle^2 + L_8 \big\langle \hat U^\dagger \chi \hat U^\dagger \chi + \chi^\dagger \hat U \chi^\dagger \hat U \big\rangle \\
&\quad - i L_9 \big\langle \hat L_{\mu\nu} \nabla^\mu \hat U^\dagger \nabla^\nu \hat U + \hat R_{\mu\nu} \nabla^\mu \hat U \nabla^\nu \hat U^\dagger \big\rangle + L_{10} \big\langle \hat L_{\mu\nu} \hat U^\dagger \hat R^{\mu\nu} \hat U \big\rangle \\
&\quad + H_1 \big\langle \hat L_{\mu\nu} \hat L^{\mu\nu} + \hat R_{\mu\nu} \hat R^{\mu\nu} \big\rangle + H_2 \big\langle \chi^\dagger \chi \big\rangle \,,
\end{aligned} \tag{1.47}$$

where $L_1, \ldots, L_{10}$ are low-energy constants. The contact terms involving H_1 and H_2 do not contain any meson fields and are thus of no physical significance, but they are allowed by symmetry and are in fact needed as counter terms for the renormalization of one-loop graphs. The coefficients H_1, H_2 are sometimes called high-energy constants.

By expanding the Lagrangians $\mathcal{L}_{\hat\phi}^{(2)}$ and $\mathcal{L}_{\hat\phi}^{(4)}$ in powers of the meson fields one observes that they only produce contact terms with an even number of mesons. Hence, these interactions conserve the meson number modulo two which is, of course, not a symmetry of QCD—consider, *e.g.*, the QCD-allowed process $K^+K^- \to \pi^+\pi^-\pi^0$. This peculiar conservation law is due to the fact that the effective Lagrangians are invariant under the transformation

$$\hat{U} \to \hat{U}^\dagger \,, \qquad\qquad \chi \to \chi^\dagger \,, \qquad\qquad \hat{a}_\mu \to -\hat{a}_\mu \,. \tag{1.48}$$

The first operation effectively replaces $\hat{\phi}$ by $-\hat{\phi}$. This transformation is similar to the parity transformation, but without affecting the space-time coordinates. QCD, however, is only symmetric under the true parity transformation P. For instance, the simplest process which is allowed by QCD, but cannot be described by the Lagrangians discussed above is $K^+K^- \to \pi^+\pi^-\pi^0$.

Terms in the effective action which are invariant under the transformation in Eq. (1.48) are said to be of *natural parity*, whereas terms that violate this symmetry are of *unnatural parity*. The latter can only be constructed by means of the totally antisymmetric tensor $\epsilon^{\mu\nu\alpha\beta}$ which implies that a Lorentz invariant term of unnatural parity necessarily involves at least four derivatives or external (axial) vector fields. Thus, it has to be of fourth chiral order or higher. In fact one finds that the leading terms of unnatural parity which obey chiral symmetry are of order $\mathcal{O}(p^6)$. Nonetheless, there are also contributions at $\mathcal{O}(p^4)$ which are, however, related to the chiral anomalies of QCD and are summarized by the so-called Wess-Zumino-Witten action. This issue will be discussed in more detail in the following section on anomalies.

1.4 Anomalies

1.4.1 Path integral analysis

In the limit of vanishing quark masses the classical QCD Lagrangian with three flavors is invariant under chiral $\mathrm{U}(3)_L \times \mathrm{U}(3)_R$ transformations of the quark fields q. While this invariance holds at the classical level of the theory, it does not need to be guaranteed when quantum corrections are taken into account. This phenomenon was first observed by analyzing matrix elements describing the decay $\pi^0 \to \gamma\gamma$ for which the predecessor of chiral perturbation theory, the hypothesis of partial conservation of the axial current (PCAC), predicted a tiny branching ratio [25]. The much larger branching ratio observed in experiment could be explained by a loop contribution in QCD which breaks chiral symmetry [26, 27], a so-called anomaly.

In the path integral formalism the occurrence of an anomaly can be traced back to a non-trivial transformation of the fermionic measure under the field transformation in question [28]. The analysis of path integrals thus leads to a generalized definition of symmetries in quantum field theory: A continuous field transformation is a symmetry of the theory (implying the existence of a conserved current according to Noether's theorem) if and only if the Lagrangian *and* the path integral measure are invariant under this transformation.

To keep things simple, we start out with an analysis of QCD anomalies in the chiral limit and in the absence of external sources which follows the presentation given in [29].

Later on, the discussion is generalized to the inclusion of external vector and axial-vector fields.

Let $S(x)$ be a unitary local matrix transformation which acts on the column of quark fields as $q(x) \to q'(x) = S(x)\, q(x)$. It induces the following transformation of the fermionic measure in the path integral

$$\mathcal{D}q\,\mathcal{D}\bar{q} \to \mathcal{D}q'\,\mathcal{D}\bar{q}' = (\det \mathcal{J}\ \det \bar{\mathcal{J}})^{-1}\ \mathcal{D}q\,\mathcal{D}\bar{q}\ , \tag{1.49}$$

where the Jacobians of the transformation are given by

$$\mathcal{J}_{xn,ym} = S(x)_{nm}\delta^4(x-y), \qquad \bar{\mathcal{J}}_{xn,ym} = [\gamma^0 S^\dagger(x)\gamma^0]_{nm}\delta^4(x-y)\ . \tag{1.50}$$

The indices n, m comprise flavor, color and Dirac spinor indices whereas the delta functions represent the unit element in continuous space-time. In other words the Jacobian matrices are “unit matrices” in Minkowski space. The fact that the Jacobian enters as its inverse in Eq. (1.49) stems from the fermionic nature of the quarks.

First, we consider the case of a vector type chiral transformation $S \in \mathrm{U}(3)_V$ which may be written as

$$S(x) = \exp(i\alpha(x)t) \tag{1.51}$$

with t an ordinary Hermitian matrix in flavor space and $\alpha(x)$ an arbitrary real function. Since $S(x)$ commutes with γ^0, we have

$$\bar{\mathcal{J}}\,\mathcal{J} = \mathbb{1}\ . \tag{1.52}$$

Hence, the measure is invariant under this transformation.

Next, we investigate axial-vector type chiral transformations $S \in \mathrm{U}(3)_A$ which are of the form

$$S(x) = \exp(i\gamma^5\alpha(x)t) = \cos(\alpha(x)t) + i\gamma^5\sin(\alpha(x)t)\,, \tag{1.53}$$

where t is again an ordinary Hermitian 3×3 matrix and $\alpha(x)$ an arbitrary real function. In virtue of the second relation in Eq. (1.53), one finds

$$\gamma^0 S^\dagger \gamma^0 = S \quad \Rightarrow \quad \bar{\mathcal{J}} = \mathcal{J} \tag{1.54}$$

and the fermionic measure thus transforms non-trivially

$$\mathcal{D}q\,\mathcal{D}\bar{q} \to \mathcal{D}q'\,\mathcal{D}\bar{q}' = (\det \mathcal{J})^{-2}\ \mathcal{D}q\,\mathcal{D}\bar{q}\ . \tag{1.55}$$

We now restrict ourselves to the infinitesimal local chiral transformation

$$S(x) = \mathbb{1} + i\gamma^5\alpha(x)t + \mathcal{O}(\alpha^2) \tag{1.56}$$

which implies for the Jacobian matrix

$$[\mathcal{J} - \mathbb{1}]_{xn,ym} = i\alpha(x)[\gamma^5 t]_{nm}\delta^4(x-y) + \mathcal{O}(\alpha^2)\ . \tag{1.57}$$

Making use of the matrix identity $\det M = \exp(\mathrm{tr} \ln M)$ for an arbitrary ordinary matrix M and the expansion of the logarithm $\ln(1+\epsilon) = \epsilon + \mathcal{O}(\epsilon^2)$, we write

$$\begin{aligned}(\det \mathcal{J})^{-2} &= \exp\{-2\sum_{x,n} \ln \mathcal{J}_{xn,xn}\} \\ &= \exp\Big\{-2i\int d^4x\alpha(x)\,\mathrm{tr}(\gamma^5 t)\lim_{y\to x}\delta^4(x-y)\Big\} + \mathcal{O}(\alpha^2) \\ &= \exp\Big\{i\int d^4x\alpha(x)\mathcal{A}(x)\Big\} + \mathcal{O}(\alpha^2)\ , \end{aligned} \tag{1.58}$$

where we set $\mathcal{A}(x) = -2\,\mathrm{tr}(\gamma^5 t)\lim_{y\to x}\delta^4(x-y)$. As it stands, Eq. (1.58) is ill-defined. The trace $\mathrm{tr}(\gamma^5 t)$ over flavor, color and Dirac indices vanishes whereas in the limit $y \to x$ the delta function is infinite. In order to get a definite result, we need to introduce a regulator. We choose a regularization scheme which preserves Lorentz and gauge-invariance and exponentially damps out contributions with large eigenvalues of the QCD covariant derivative $\slashed{D}$, *i.e.* ultraviolet modes. We define

$$\mathcal{A}(x) = -2\lim_{M\to\infty}\lim_{y\to x}\mathrm{tr}\Big(\gamma^5 t\, e^{-\slashed{D}_x^2/M^2}\Big)\delta^4(x-y)\,, \tag{1.59}$$

where M is a large regulator mass. Employing the Fourier representation of the delta function we write

$$\begin{aligned}\mathcal{A}(x) &= -2\lim_{M\to\infty}\lim_{y\to x}\int\frac{d^4k}{(2\pi)^4}\,\mathrm{tr}\Big(\gamma^5 t\, e^{-\slashed{D}_x^2/M^2}\Big)e^{ik\cdot(x-y)} \\ &= -2\lim_{M\to\infty}\lim_{y\to x}\int\frac{d^4k}{(2\pi)^4}e^{ik\cdot(x-y)}\,\mathrm{tr}\Big(\gamma^5 t\, e^{-(i\slashed{k}+\slashed{D}_x)^2/M^2}\Big) \\ &= -2\lim_{M\to\infty}\int\frac{d^4k}{(2\pi)^4}\,\mathrm{tr}\Big(\gamma^5 t\, e^{-(i\slashed{k}+\slashed{D}_x)^2/M^2}\Big) \\ &= -2\lim_{M\to\infty}M^4\int\frac{d^4\kappa}{(2\pi)^4}\,\mathrm{tr}\Big(\gamma^5 t\, e^{-(i\slashed{\kappa}+\slashed{D}_x/M)^2}\Big)\,, \end{aligned} \tag{1.60}$$

where we used

$$\slashed{D}_x e^{ik\cdot x} = e^{ik\cdot x}(i\slashed{k} + \slashed{D}_x) \tag{1.61}$$

and introduced the dimensionless variable $\kappa = k/M$ in the last line. To analyze the limit $M \to \infty$ we expand the argument of the exponential

$$-(i\slashed{\kappa} + \slashed{D}_x/M)^2 = \kappa^2 - \frac{2i\kappa_\mu D_x^\mu}{M} - \frac{\slashed{D}_x^2}{M^2}\ . \tag{1.62}$$

Only terms which have at most four powers of M in the denominator yield non-vanishing contributions when the regulator mass is sent to infinity. On the other hand, the trace over Dirac indices vanishes unless the regulator function involves at least four gamma matrices. We are thus left with

$$\mathcal{A}(x) = -\int\frac{d^4\kappa}{(2\pi)^4}\,e^{\kappa^2}\,\mathrm{tr}\big(\gamma^5 t\,\slashed{D}_x^4\big)\,, \tag{1.63}$$

where the dependence on the regularization scale M has disappeared.

The integral can be evaluated by a Wick rotation to Euclidean space-time

$$\int \frac{d^4\kappa}{(2\pi)^4}\, e^{\kappa^2} = i \int \frac{d^4\kappa_E}{(2\pi)^4}\, e^{-\kappa_E^2} = i \int\limits_0^\infty \frac{d\zeta}{8\pi^2}\, \zeta^3\, e^{-\zeta^2} = \frac{i}{16\pi^2}\ . \tag{1.64}$$

To compute the trace over Dirac indices we write

$$\begin{aligned} \not{D}^2 &= \gamma^\mu \gamma^\nu D_\mu D_\nu \\ &= \Big(\frac{1}{2}\{\gamma^\mu, \gamma^\nu\} + \frac{1}{2}[\gamma^\mu, \gamma^\nu]\Big) D_\mu D_\nu \\ &= D^2 + \frac{1}{4}[\gamma^\mu, \gamma^\nu][D_\mu, D_\nu] \\ &= D^2 + \frac{1}{4}[\gamma^\mu, \gamma^\nu]\, i g_s\, t^a G^a_{\mu\nu} \end{aligned} \tag{1.65}$$

which leads to the Dirac trace

$$\mathrm{tr}_D\big(\gamma^5[\gamma^\mu, \gamma^\nu][\gamma^\alpha, \gamma^\beta]\big) = 4\,\mathrm{tr}_D\big(\gamma^5\gamma^\mu\gamma^\nu\gamma^\alpha\gamma^\beta\big) = 16i\,\epsilon^{\mu\nu\alpha\beta}\ . \tag{1.66}$$

Finally, we obtain the result

$$\begin{aligned} \mathcal{A}(x) &= -\frac{g_s^2}{16\pi^2}\epsilon^{\mu\nu\alpha\beta} G^a_{\mu\nu}(x) G^b_{\alpha\beta}(x)\, \mathrm{tr}_c(t^a t^b)\, \langle t\rangle \\ &= -\frac{g_s^2}{32\pi^2}\epsilon^{\mu\nu\alpha\beta} G^a_{\mu\nu}(x) G^a_{\alpha\beta}(x)\, \langle t\rangle\ , \end{aligned} \tag{1.67}$$

where we have evaluated the trace over colors, tr_c, and the trace over flavors, $\langle \ldots \rangle$, remains.

1.4.2 Axial U(1) anomaly

In the case of chiral SU(3) transformations of axial-vector type the matrix t in Eq. (1.67) is traceless, *i.e.* the anomaly function vanishes. Thus, chiral $\mathrm{SU}(3)_A$ symmetry holds at the quantum level of QCD and the associated currents $j^a_{\mu 5} = \bar{q}\gamma_\mu\gamma_5 t^a q$ are conserved, $\partial^\mu j^a_{\mu 5} = 0$.

If, however, we consider axial U(1) transformations for which t is the unit matrix in flavor space, the anomaly function is non-zero and reads

$$\mathcal{A}(x) = -\frac{g_s^2 N_f}{32\pi^2}\epsilon^{\mu\nu\alpha\beta} G^a_{\mu\nu}(x) G^a_{\alpha\beta}(x)\,, \tag{1.68}$$

where $N_f = 3$ is the number of flavors. Although the classical Lagrangian of QCD is invariant under $\mathrm{U}(1)_A$ transformations, the full quantum theory is not. As we will explain in Sect. 1.4.4 a non-zero anomaly function has the same effect as if under the transformation in question the Lagrangian would change by an additive term instead of remaining invariant. Accordingly, the divergence of the singlet axial current $j^0_{\mu 5} =$

$\bar{q}\gamma_\mu\gamma_5 t^0 q$ with $t^0 = \mathbb{1}/\sqrt{2N_f}$,[‡] which is associated with axial U(1) transformations, is related to $\mathcal{A}$ via

$$\partial^\mu j^0_{\mu 5}(x) = \frac{-1}{\sqrt{2N_f}}\,\mathcal{A}(x) = \frac{g_s^2\sqrt{2N_f}}{64\pi^2}\epsilon^{\mu\nu\alpha\beta}G^a_{\mu\nu}(x)G^a_{\alpha\beta}(x) \tag{1.69}$$

and hence $j^0_{\mu 5}$ is not conserved. This implies that we cannot expect a ninth Goldstone boson associated with the generator of axial U(1) transformations.

Strictly speaking Eq. (1.68) alone is not sufficient for QCD to be non-invariant under $\mathrm{U}(1)_A$ transformations. The problem is that by introducing the so-called Chern-Simons class

$$K^\mu = 2\epsilon^{\mu\nu\alpha\beta}\left[A^a_\nu\partial_\alpha A^a_\beta - \frac{g_s}{3}f^{abc}A^a_\nu A^b_\alpha A^c_\beta\right] \tag{1.70}$$

the anomaly function $\mathcal{A}$ can be expressed in terms of the total derivative

$$\partial_\mu K^\mu = \frac{1}{2}\epsilon^{\mu\nu\alpha\beta}G^a_{\mu\nu}G^a_{\alpha\beta}\ . \tag{1.71}$$

According to Gauß' theorem the space-time integral of the total derivative $\partial_\mu K^\mu$ may be written as a surface integral of K^μ which is zero for gauge field configurations that vanish sufficiently rapidly at infinity. However, it was shown by ‘t Hooft that QCD allows for topologically non-trivial field configurations (known as instantons) which vanish slowly enough at infinity to yield a non-zero value of the surface integral [30]. Moreover, the corresponding conserved current

$$\tilde{K}^\mu = \bar{q}\gamma^\mu\gamma^5 q - \frac{g_s^2 N_f}{16\pi^2}K^\mu \tag{1.72}$$

is not $\mathrm{SU}(3)_c$ gauge invariant and thus cannot represent an observable quantity. Far from being a proof, these arguments make it nevertheless plausible that axial U(1) is indeed not a symmetry of QCD—in accordance with the experimental observation that the lightest pseudoscalar flavor-singlet particle, the η', has a mass which is much larger than the masses of the octet of Goldstone bosons.

Three-flavor QCD possesses an interesting limit that is reached by generalizing the gauge group $\mathrm{SU}(3)_c$ to an arbitrary number of colors, $\mathrm{SU}(N_c)$, and sending N_c to infinity while keeping the product $g_s^2 N_c$ fixed [31]. Since the anomaly function, Eq. (1.68), which involves $\mathrm{tr}_c(t^a t^b) = \delta^{ab}/2$ is independent of N_c, but proportional to g_s^2 it vanishes as $1/N_c$ in the limit $N_c \to \infty$. Thus, the symmetry under axial U(1) transformations is restored rendering the existence of a ninth Goldstone boson possible. It can be shown that in the large N_c counting scheme the pseudoscalar singlet decay constant in the chiral limit, f_0, is of order $\mathcal{O}(N_c^{1/2})$. By taking the divergence of the matrix element

$$\langle 0|\, j^0_{\mu 5}(x)\,|\eta_0(p)\rangle = ie^{-ip\cdot x}p_\mu\, f_0 \tag{1.73}$$

one finds

$$\langle 0|\,\partial^\mu j^0_{\mu 5}(0)\,|\eta_0(p)\rangle = f_0 m^2_{\eta_0} = \frac{-1}{\sqrt{6}}\,\langle 0|\,\mathcal{A}(0)\,|\eta_0(p)\rangle \tag{1.74}$$

and—bearing in mind that $\mathcal{A}$ is of order $\mathcal{O}(N_c^{-1})$—one concludes that for massless quarks the squared mass of the singlet particle $m^2_{\eta_0}$ (and accordingly the squared mass of the physical state η') indeed vanishes as $1/N_c$ in the large N_c limit [32].

[‡] The matrix t^0 is normalized in such a way that $\langle t^a t^b\rangle = \delta^{ab}/2 \quad \forall\ a,b \in \{0,1,2,\ldots,8\}$.

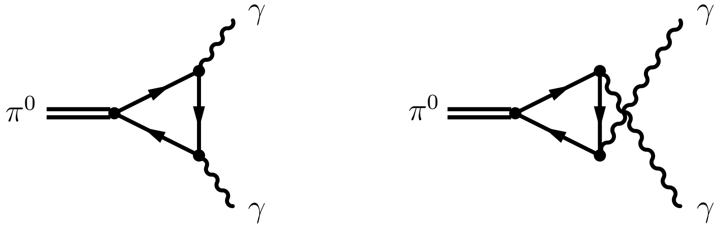

Figure 1.2: Quark loop diagrams which generate the anomalous contribution to the decay $\pi^0 \to 2\gamma$.

1.4.3 Chiral anomalies

Quarks do not only carry SU(3) color charges, they also carry electromagnetic charge and therefore couple to photons. The derivation of the anomaly function given in Eq. (1.67) is, however, not restricted to the case of gluonic gauge fields, it proceeds in an analogous manner if photonic gauge fields are considered. In this case one finds

$$\mathcal{A}(x) = -\frac{e^2 N_c}{16\pi^2}\epsilon^{\mu\nu\alpha\beta}F_{\mu\nu}(x)F_{\alpha\beta}(x)\left\langle Q^2 t\right\rangle \,, \tag{1.75}$$

where $Q = \mathrm{diag}(2/3, -1/3, -1/3)$ is the quark charge matrix and $F_{\mu\nu}$ denotes the electromagnetic field strength tensor. The trace over color indices is trivial here and yields the number of colors N_c $(= 3)$.

The anomaly function is non-zero for axial U(1) transformations ($t = \mathbb{1}$) and specific $\mathrm{SU}(3)_A$ transformations with $t = \lambda^8$ and $t = \lambda^3$ in the basis of Gell-Mann matrices. The latter is actually a pure isospin SU(2) anomaly in the presence of an electromagnetic field which was historically the first one to be discovered.[†] In 1969 Bell and Jackiw [27] and Adler [26] presented a direct calculation of the anomaly by carefully examining the triangle diagrams shown in Fig. 1.2 and could thus explain the relatively large decay rate of $\pi^0 \to 2\gamma$, for which in the absence of the anomaly chiral symmetry (or more precisely PCAC) would predict a much smaller value.

The appearance of the factor N_c in the anomaly function, Eq. (1.75), and the smallness of non-anomalous higher order corrections in ChPT has led to the conclusion that the decay width of $\pi^0 \to 2\gamma$ constitutes a direct test of the number of colors in QCD. This claim is in fact advocated in many textbooks on strong interaction physics. Recently, however, it was pointed out in a paper by Bär and Wiese [33] that in order to keep the gauge group $\mathrm{SU}(N_c)$ of QCD free of anomalies for an arbitrary number of colors, the quark charges also have to be N_c-dependent. The quark charge matrix is then given by

$$Q = \mathrm{diag}\left\{\frac{1}{2}\left(\frac{1}{N_c}+1\right), \frac{1}{2}\left(\frac{1}{N_c}-1\right), \frac{1}{2}\left(\frac{1}{N_c}-1\right)\right\}. \tag{1.76}$$

Hence, the N_c dependence in Eq. (1.75) exactly cancels for the processes $\tilde{\pi}^0 \to 2\gamma$ ($t = \lambda^3$) and $\eta_8 \to 2\gamma$ ($t = \lambda^8$) and N_c only enters in subleading corrections to the physical processes π^0, $\eta \to 2\gamma$, *e.g.* by mixing with the singlet state η_0, see also [34, 35].

[†] Note that pure two-flavor QCD is anomaly-free since the contributions of up- and down-quarks to the gluonic anomaly function Eq. (1.67) cancel, $\left\langle\lambda^3\right\rangle = 0$.

We still have not explored the full content of the chiral anomalies in QCD. For the generalized QCD Lagrangian with external sources, Eq. (1.28), they do not just involve the vector field $\hat{v}_\mu$ (through which photons are introduced), but also the axial-vector field $\hat{a}_\mu$. The full form of the anomaly function was derived by Bardeen [36] and reads

$$\mathcal{A} = -\frac{N_c}{16\pi^2}\epsilon^{\mu\nu\alpha\beta}\Big\langle\Big(\hat{v}_{\mu\nu}\hat{v}_{\alpha\beta} + \frac{4}{3}\nabla_\mu\hat{a}_\nu\nabla_\alpha\hat{a}_\beta + \frac{2i}{3}\{\hat{v}_{\mu\nu},\hat{a}_\alpha\hat{a}_\beta\} \\ + \frac{8i}{3}\hat{a}_\mu\hat{v}_{\alpha\beta}\hat{a}_\nu + \frac{4}{3}\hat{a}_\mu\hat{a}_\nu\hat{a}_\alpha\hat{a}_\beta\Big)t\Big\rangle \tag{1.77}$$

with

$$\begin{aligned}\hat{v}_{\mu\nu} &= \partial_\mu\hat{v}_\nu - \partial_\nu\hat{v}_\mu - i[\hat{v}_\mu,\hat{v}_\nu]\,,\\ \nabla_\mu\hat{a}_\nu &= \partial_\mu\hat{a}_\nu - i[\hat{v}_\mu,\hat{a}_\nu]\,.\end{aligned} \tag{1.78}$$

In the language of Feynman diagrams the third and fourth term in Eq. (1.77) are related to box type graphs (*box anomaly*) and contribute, *e.g.*, to the decay $\eta \to \pi^+\pi^-\gamma$, while the last term corresponds to a pentagon shaped loop graph which appears in the process $K^+K^- \to \pi^+\pi^-\pi^0$.

1.4.4 Wess-Zumino-Witten term

The anomalies of QCD discussed in this section arise from the fermionic part of the QCD path integral and are thus directly related to the Fermi nature of the quarks. In contrast, the effective low-energy theory which describes the interaction of Goldstone *bosons* is free of such anomalies. The construction of the unique effective field theory at low energies, however, requires that this theory does not only obey exactly the same symmetries as the underlying theory, it also has to exhibit the same symmetry breaking patterns. Hence, one must find a way to include the effect of the QCD anomalies in chiral perturbation theory.

In this respect it is crucial to observe that the anomalies, which show up in the transformation property of the fermionic measure $\mathcal{D}q\mathcal{D}\bar{q}$ of the QCD path integral, have the same effect as if the QCD Lagrangian itself were not invariant under the pertinent transformations. This becomes obvious by employing Eq. (1.58) in the transformation of the path integral

$$\begin{aligned}&\int \mathcal{D}q'\,\mathcal{D}\bar{q}'\,\mathcal{D}A\exp\left\{i\int d^4x\,\mathcal{L}_{\mathrm{QCD}}[q',\bar{q}',A]\right\}\\ &\quad= \int \mathcal{D}q\,\mathcal{D}\bar{q}\,\mathcal{D}A\,(\det\mathcal{J})^{-2}\exp\left\{i\int d^4x\,\mathcal{L}_{\mathrm{QCD}}[q,\bar{q},A]\right\}\\ &\quad= \int \mathcal{D}q\,\mathcal{D}\bar{q}\,\mathcal{D}A\exp\left\{i\int d^4x\,\mathcal{L}_{\mathrm{QCD}}[q,\bar{q},A] + \alpha(x)\mathcal{A}(x)\right\}\;.\end{aligned} \tag{1.79}$$

The effect of the anomalies can thus be mimicked by a non-invariant Lagrangian which transforms as $\mathcal{L} \to \mathcal{L} + \alpha\mathcal{A}$. This is the key point for the construction of the effective

Lagrangian: One has to include an additional, non-invariant term that transforms according to $\mathcal{L}_{\hat{\phi}} \to \mathcal{L}_{\hat{\phi}} + \alpha\mathcal{A}$, where the transformation behavior is dictated by the chiral anomalies of QCD.

In 1971 Wess and Zumino worked out consistency conditions which have to be satisfied in the presence of the anomalies by analyzing the anomalous Ward identities of QCD [5]. They showed that the effect of the chiral anomalies cannot be expressed as a single local effective Lagrangian and instead gave a Taylor expansion for it. Later Witten provided an elegant representation of the chiral anomalies as an integral over a five-dimensional space with physical four-dimensional spacetime as the boundary [6].

The Wess-Zumino-Witten (WZW) action is most compactly written in terms of differential forms of the external chiral sources $\hat{l}_\mu$ and $\hat{r}_\mu$

$$\hat{l} = dx^\mu \hat{l}_\mu \,, \quad \hat{r} = dx^\mu \hat{r}_\mu \,, \quad d = dx^\mu \partial_\mu \,. \tag{1.80}$$

The quantities dx^0, dx^1, dx^2, dx^3 are treated as Grassmann variables generating the volume element $dx^\mu dx^\nu dx^\alpha dx^\beta = d^4x\ \epsilon^{\mu\nu\alpha\beta}$. In this notation the WZW action reads [37]

$$S_{\mathrm{WZW}} = -\frac{iN_c}{240\pi^2} \int\limits_{M_5} \langle \Sigma^5 \rangle - \frac{iN_c}{48\pi^2} \int\limits_{M_4} \left\{ W(1,\hat{l},\hat{r}) - W(0,\hat{l},\hat{r}) \right\} ,$$

$$\begin{aligned} W(x^5,\hat{l},\hat{r}) = \Big\langle & \hat{U}\,\hat{l}^3\,\hat{U}^\dagger\,\hat{r} + \frac{1}{4}\,\hat{U}\,\hat{l}\,\hat{U}^\dagger\,\hat{r}\,\hat{U}\,\hat{l}\,\hat{U}^\dagger\,\hat{r} + i\,\hat{U}\,d\hat{l}\,\hat{l}\,\hat{U}^\dagger\,\hat{r} + i\,d\hat{r}\,\hat{U}\,\hat{l}\,\hat{U}^\dagger\,\hat{r} \\ & - i\,\Sigma\,\hat{l}\,\hat{U}^\dagger\,\hat{r}\,\hat{U}\,\hat{l} + \Sigma\,\hat{U}^\dagger\,d\hat{r}\,\hat{U}\,\hat{l} - \Sigma^2\,\hat{U}^\dagger\,\hat{r}\,\hat{U}\,\hat{l} + \Sigma\,\hat{l}\,d\hat{l} + \Sigma\,d\hat{l}\,\hat{l} \\ & - i\,\Sigma\,\hat{l}^3 + \frac{1}{2}\,\Sigma\,\hat{l}\,\Sigma\,\hat{l} - i\,\Sigma^3\,\hat{l} \Big\rangle - (L \leftrightarrow R) \end{aligned} \tag{1.81}$$

with $\Sigma \equiv \hat{U}^\dagger\, d\hat{U}$. The first integral is taken over the five-dimensional manifold M_5 which is the direct product of Minkowski space M_4 and the compact interval $0 \leq x^5 \leq 1$, while the Grassmann algebra is supplemented by a fifth element dx^5. The matrix-valued field $\hat{U}(x,x^5)$ is a function on this five-dimensional manifold and interpolates smoothly between the identity matrix $\hat{U}(x,0) = \mathbb{1}$ and the meson field $\hat{U}(x,1) = \hat{U}(x)$. In the second term the integration over dx^5 has already been performed and we are left with the usual integration over Minkowski space M_4 and the fields $\hat{U}(x)$. The operation $(L \leftrightarrow R)$ indicates an interchange of the 1-forms $\hat{l}$ and $\hat{r}$ as well as an interchange of $\hat{U}$ and $\hat{U}^\dagger$. As the WZW action is directly connected to the anomaly structure of QCD, unlike all other terms in ChPT it does not involve any free parameters (LECs). Applying the chiral counting rules discussed in Sect. 1.3 one verifies that the WZW contributes at chiral order $\mathcal{O}(p^4)$.

Eq. (1.81) can alternatively be written in terms of vector and axial-vector differential forms, $\hat{v}$ and $\hat{a}$, which are defined by

$$\hat{l} = \hat{v} - \hat{a}\,, \qquad \hat{r} = \hat{v} + \hat{a}\,. \tag{1.82}$$

The coupling of the mesons to an external photon field $A = dx^\mu A_\mu$ is described by $\hat{a} = 0$ and $\hat{v} = -e\,Q\,A$ with Q being the quark charge matrix.

1.5 The η'

1.5.1 Inclusion of the singlet field

The pseudoscalar mesons η and η' are known to be admixtures of the singlet and octet states η_0 and η_8, which have the same quantum numbers (I = S = 0). In order to find a uniform description of η and η' decays it is therefore mandatory to include both particles as dynamical fields in a consistent framework.

Due to the axial U(1) anomaly of QCD which destroys the symmetry of the theory under axial U(1) transformations, the singlet state η_0 is prevented from being a Goldstone boson in the chiral limit of vanishing quark masses. However, as alluded in Sect. 1.4.2 the axial anomaly vanishes for $N_c \to \infty$ and the η_0 is converted into an additional Goldstone boson in this limit. The properties of the effective theory which includes the singlet field as a ninth Goldstone boson have been studied long ago [38–40]. Note, though, that the chiral limit and the large N_c limit do not commute in general. A consistent counting scheme therefore requires a simultaneous expansion in powers of small momenta and quark masses as well as $1/N_c$ and was worked out in [4, 37, 41, 42].

While large N_c ChPT is theoretically clear-cut and appealing, it is faced with phenomenological difficulties. First, the mass of the η', $m_{\eta'} = 958$ MeV, is almost twice as large as the mass of the η meson, which makes the perturbative treatment of $m_{\eta'}$ at least doubtful. In particular loops involving the η' can be numerically substantial when standard dimensional regularization is employed. Second, $m_{\eta'}$ exceeds the masses of the lowest hadronic resonances such as the $\rho(770)$ and the $\omega(782)$. Therefore, the conventional loop-wise expansion of ChPT is usually inappropriate for a realistic description of η' decays. Resonances have to be either included explicitly in the theory or generated dynamically by means of non-perturbative methods. In addition, strong final-state interactions have to be accounted for since phase space in η' decays can be rather large.

In [43] it was demonstrated that in order to construct a generalization of standard SU(3) ChPT which includes the singlet field η_0 as a dynamical state, it is not necessary to work in the limit $N_c \to \infty$. Large N_c arguments are solely needed to establish a firm counting scheme in the presence of the η'. Here we adopt the approach of [43] for the construction of the chiral effective Lagrangian while postponing the question of power counting and renormalization to the end of this section.

As the starting point for the construction of the effective Lagrangian including the η_0 we note that the axial U(1) anomaly of QCD (*cf.* Eq. (1.67)) generates a Lagrangian term which has the same structure as the θ-term in the QCD Lagrangian, Eq. (1.1). By replacing θ_0 with a local, external source $\theta(x)$ (in addition to the scalar, pseudoscalar, vector and axial-vector sources introduced in Sect. 1.3) and by postulating the transformation property

$$\theta(x) \to \theta(x) - i \ln \det L(x) + i \ln \det R(x) \tag{1.83}$$

under local chiral transformations $L(x), R(x) \in \mathrm{U}(3)$ it is possible to transmute QCD into a theory which is invariant under axial U(1) transformations and whose change under local $\mathrm{SU}(3)_L \times \mathrm{SU}(3)_R$ transformations is exactly given by the Wess-Zumino term discussed in the previous section. One easily verifies that for the infinitesimal axial-vector type transformation in Eq. (1.56) with $t = \mathbb{1}$ and $N_f = 3$ the θ source transforms according to

$$\theta(x) \to \theta(x) - 6\,\alpha(x) \tag{1.84}$$

and thus exactly compensates the term generated by the axial U(1) anomaly. Ordinary QCD is recovered by setting $v_\mu(x) = a_\mu(x) = p(x) = 0$, $s(x) = \mathcal{M}$, $\theta(x) = \theta_0$.

These properties of generalized QCD are transferred to the level of the effective theory and constrain the construction of the effective Lagrangian. We now have nine pseudoscalar meson fields which may be summarized in the matrix $\bar{U}(x) \in \mathrm{U}(3)$ with

$$\bar{U}(x) = \exp\left\{ i\frac{\sqrt{2}}{f}\,\hat{\phi}(x) + \frac{i}{3}\,\varphi_0(x)\mathbb{1} \right\} . \tag{1.85}$$

The phase of $\bar{U}$, $\ln\det\bar{U}(x) = i\varphi_0(x)$, describes the singlet state. As in the case of SU(3) ChPT the field $\bar{U}$ again transforms linearly (see Eq. (1.2))

$$\bar{U}(x) \to R(x)\bar{U}(x)L^\dagger(x) \tag{1.86}$$

which implies for φ_0

$$\varphi_0(x) \to \varphi_0(x) + i\ln\det L(x) - i\ln\det R(x) . \tag{1.87}$$

Hence, the combination $\bar{\varphi}_0 = \varphi_0 + \theta$ is invariant under chiral transformations. The U(3) effective Lagrangian can then be constructed in terms of the meson fields $\bar{U}$, φ_0 and the external sources s, p, a_μ, v_μ, θ as well as derivatives thereof. In particular, the covariant derivatives of φ_0 and θ are given by

$$D_\mu\varphi_0 = \partial_\mu\varphi_0 - 2\,\langle a_\mu\rangle , \qquad\qquad D_\mu\theta = \partial_\mu\theta + 2\,\langle a_\mu\rangle . \tag{1.88}$$

However, there arises a complication in the construction of the effective Lagrangian that stems from the fact that the singlet axial current $j^0_{\mu5} = \bar{q}\gamma_\mu\gamma_5 q/\sqrt{6}$ carries anomalous dimension and its matrix elements, *e.g.*

$$\langle 0|\, j^0_{\mu5}\,|P(p)\rangle = ie^{-ip\cdot x}p_\mu\, F^0_P \qquad \text{with} \quad P = \pi^0, \eta, \eta' , \tag{1.89}$$

where $F^0_{\pi^0}$, F^0_η, $F^0_{\eta'}$ represent the singlet decay constants, depend on the running scale of QCD [26, 44]. When the renormalization scale is altered, the operator $j^0_{\mu5}$ receives multiplicative renormalization

$$j^0_{\mu5} \to Z j^0_{\mu5} , \tag{1.90}$$

where Z is a scale-dependent constant. In virtue of the operator relation

$$\partial^\mu j^0_{\mu5} = \sqrt{6}\,\omega \qquad \text{with} \quad \omega = \frac{g_s^2}{64\pi^2}\epsilon^{\mu\nu\alpha\beta}G^a_{\mu\nu}G^a_{\alpha\beta} , \tag{1.91}$$

which holds in the chiral limit, it is obvious that also the operator ω accompanying the external source θ in the generalized QCD Lagrangian receives renormalization which is, however, inhomogeneous if one allows for non-zero quark masses. In [37] it was shown that the renormalization of the two operators $j^0_{\mu5}$ and ω can be completely absorbed by the singlet component of the axial source a_μ provided it behaves as

$$\langle a_\mu\rangle \to Z^{-1}\langle a_\mu\rangle + \frac{1}{2}(Z^{-1} - 1)\partial_\mu\theta \tag{1.92}$$

under a change of the QCD renormalization scale while θ, which is renormalization group invariant, remains fixed. We note in passing that in analogy to Eq. (1.92) the renormalization of the operators $\bar{q}_R^i q_L^j$ can be absorbed in the external sources s and p, whereas the combination χ defined in Eq. (1.36), which involves the multiplicative, scale-dependent parameter B_0, remains invariant with respect to the QCD renormalization scale.

The scale dependence of $\langle a_\mu \rangle$ is transferred to the level of the effective theory. In order to arrive at a renormalization group invariant effective Lagrangian one finds that the singlet field φ_0 must be renormalized according to

$$\varphi_0 \to Z^{-1}\varphi + (Z^{-1} - 1)\theta \,, \tag{1.93}$$

which corresponds to

$$\bar{\varphi}_0 \to Z^{-1}\bar{\varphi}_0 \,, \qquad D_\mu\varphi_0 \to Z^{-1}D_\mu\varphi_0 \,, \qquad D_\mu\theta \to Z^{-1}D_\mu\theta \,. \tag{1.94}$$

As explained in [43] the scale dependence of $\bar{\varphi}_0$ can be absorbed by a suitable combination of low-energy constants which we denote by $\sqrt{\lambda}$. We therefore identify the singlet field with

$$\eta_0 = \sqrt{\lambda}\,\varphi_0 \,, \tag{1.95}$$

whose scale dependence vanishes for $\theta \equiv 0$. Note that within large N_c ChPT this choice of η_0 would be inconvenient since $\sqrt{\lambda}$ comprises LECs of different order in the large N_c counting scheme. The singlet and octet fields are collected in the matrix

$$U(x) = \exp\left\{ i\frac{\sqrt{2}}{f}\,\phi(x) \right\} \tag{1.96}$$

with

$$\phi = \begin{pmatrix} \frac{1}{\sqrt{2}}\tilde{\pi}^0 + \frac{1}{\sqrt{6}}\eta_8 + \frac{1}{\sqrt{3}}\eta_0 & \pi^+ & K^+ \\ \pi^- & -\frac{1}{\sqrt{2}}\tilde{\pi}^0 + \frac{1}{\sqrt{6}}\eta_8 + \frac{1}{\sqrt{3}}\eta_0 & K^0 \\ K^- & \bar{K}^0 & -\sqrt{\frac{2}{3}}\eta_8 + \frac{1}{\sqrt{3}}\eta_0 \end{pmatrix} , \tag{1.97}$$

which transforms in the same way under chiral rotations as the previous field matrix $\bar{U}$. The normalization of the singlet field η_0 has been adjusted such that it has the same kinetic term as the octet fields.

With this choice of variables the U(3) effective Lagrangian which includes terms with up to two derivatives or one insertion of χ reads [37, 42, 43]

$$\begin{aligned} \mathcal{L}_\phi^{(0,2)} &= -V_0 + V_1\langle \nabla_\mu U^\dagger \nabla^\mu U \rangle + V_2\langle U^\dagger\chi + \chi^\dagger U \rangle + iV_3\langle U^\dagger\chi - \chi^\dagger U \rangle \\ &\quad + V_4\langle U^\dagger\nabla_\mu U \rangle\langle U^\dagger\nabla^\mu U \rangle + iV_5\nabla_\mu\theta\langle U^\dagger\nabla^\mu U \rangle + V_6\nabla_\mu\theta\nabla^\mu\theta \,. \end{aligned} \tag{1.98}$$

The covariant derivatives are defined by

$$\begin{aligned} \nabla_\mu U &= \partial_\mu U - i(v_\mu + \tilde{a}_\mu)U + iU(v_\mu - \tilde{a}_\mu) \,, \\ \nabla_\mu\theta &= \frac{\sqrt{6\lambda}}{f}D_\mu\theta = \frac{\sqrt{6\lambda}}{f}\partial_\mu\theta + 2\,\langle \tilde{a}_\mu \rangle \;, \end{aligned} \tag{1.99}$$

where the axial-vector connection $\tilde{a}_\mu$ is given by

$$\tilde{a}_\mu = \hat{a}_\mu + \frac{\sqrt{6\lambda}}{3f} \langle a_\mu \rangle \ . \tag{1.100}$$

Recall that $\hat{a}_\mu$ represents the octet component of the axial-vector source. Under a change of the QCD renormalization scale the fields U and $\nabla_\mu U$ pick up the phase $\exp\{i\sqrt{6\lambda}(1-Z)\theta/(3f)\}$ whereas the covariant derivative $\nabla_\mu \theta$ remains invariant.

The coefficients V_i in $\mathcal{L}_\phi^{(0,2)}$ are analytic functions of the scale-independent chiral invariant $\sqrt{\lambda}\bar{\varphi}_0 = \eta_0 + \sqrt{\lambda}\theta$. Parity conservation implies that the V_i are all even functions of $\sqrt{\lambda}\bar{\varphi}_0$ except V_3, which is odd. For $\theta = 0$ they can be expanded in powers of the singlet field

$$\begin{aligned} V_i\left[\frac{\eta_0}{f}\right] &= v_i^{(0)} + v_i^{(2)}\frac{\eta_0^2}{f^2} + v_i^{(4)}\frac{\eta_0^4}{f^4} + \ldots \qquad \text{for} \quad i = 0,1,2,4,5,6 \\ V_3\left[\frac{\eta_0}{f}\right] &= v_3^{(1)}\frac{\eta_0}{f} + v_3^{(3)}\frac{\eta_0^3}{f^3} + \ldots \end{aligned} \tag{1.101}$$

with expansion coefficients $v_i^{(j)}$ that are not fixed by chiral symmetry. Three of them are actually dictated by the canonical normalization of the kinetic and the mass term in the Lagrangian

$$v_1^{(0)} = v_2^{(0)} = \frac{f^2}{4}\,, \qquad v_4^{(0)} = 0 \ . \tag{1.102}$$

The coefficient functions V_i with $i = 0, 1, 4, 5, 6$ do not depend on the QCD renormalization scale whereas the combinations $V_2 - iV_3$ and $V_2 + iV_3$ have to compensate for the scale dependence of U and $U^\dagger$, respectively. While the inclusion of the additional source θ is necessary for the construction of the U(3) effective Lagrangian, for actual calculations it will be kept at $\theta \equiv 0$ in this work. A nonzero value of θ would imply CP violating effects in the strong interactions which are beyond the scope of the present investigation. For $\theta \equiv 0$ all building blocks in $\mathcal{L}_\phi^{(0,2)}$ are separately independent of the QCD renormalization scale.

We now come back to the question of power counting. We do not make use of large N_c counting rules where the mass of the η' is ranked as a small quantity, but instead treat the singlet field as a massive degree of freedom with its mass being counted as of zeroth chiral order. In principle, this approach spoils the standard chiral counting scheme since loops which involve the η' are not suppressed. One way to recover power counting is the use of infrared regularization for the loop integrals which preserves Lorentz and chiral invariance [45]. Originally infrared regularization was designed to deal with the problem of power counting in relativistic baryon ChPT, but it has also been successfully applied within the framework of U(3) ChPT to calculate static properties of the pseudoscalar mesons such as masses, decay constants and mixing parameters [43, 46] and also η' decays [47].

However, as already discussed at the beginning of this section, η and in particular η' decays are usually not adequately described without taking resonances and strong final-state interactions into account. In this work this is accomplished by utilizing the Bethe-Salpeter equation (BSE) [48] which iterates two-particle rescattering to infinite order and generates resonances dynamically. The use of such a non-perturbative method, which will be explained in Sect. 2.1, necessarily breaks power counting. Instead the chiral expansion is applied to the interaction kernel which is worked out up to a given chiral order and then iterated by means of the BSE. When considering anomalous decays of η and η' such as $\eta, \eta' \to \pi^+\pi^-\gamma^*$ (see Chapter 4) the occurrence of a vertex of unnatural parity causes the iterated meson-meson rescattering, which solely involves vertices of natural parity, to start at the one-loop level. In this case we include the full one-loop calculation of the decay amplitude in ChPT which is then supplemented by the non-perturbative BSE solution. Within the one-loop calculation power-counting violating contributions due to the propagation of the heavy singlet particle η_0 in loops are absorbed manually into the pertinent U(3) coupling constants. In this context one can take advantage of the fact that in the chiral limit the octet and singlet pieces of the Lagrangian $\mathcal{L}_\phi^{(0,2)}$ decouple completely [37].

1.5.2 η-η' mixing

Since both the pseudoscalar octet field η_8 and the singlet field η_0 have quantum numbers $I = S = 0$ they may in general mix to form the corresponding mass eigenstates η and η'. Isospin symmetry is not an exact symmetry of the strong interactions since it relies on the assumption of equal up- and down-quark masses which is only approximately realized in nature. In other words, isospin is broken by the non-vanishing quark mass difference $m_u - m_d$. In addition, up- and down-quarks carry different electric charges which lead to isospin-breaking via electromagnetic effects. If isospin breaking is taken into account, one finds that all three neutral and strangeless light pseudoscalar mesons π^0, η, η' are admixtures of the flavor eigenstates $\tilde{\pi}^0$, η_8, η_0. Since we are dealing with neutral particles only, electromagnetic contributions are actually suppressed here and can be neglected.

The mixing pattern of η and η' has been worked out in the framework of U(3) ChPT up to second chiral order [46]. In this work the problem of power counting in the presence of the massive singlet field was solved by employing infrared regularization for the loop integrals [45]. In the calculation of mixing parameters, however, only tadpole integrals occur up to one-loop order. In the case of Goldstone boson tadpoles, infrared regularization yields the same result as dimensional regularization whereas η_0 tadpoles are set to zero in this framework as they do not contain any infrared physics and can thus be completely absorbed by redefining appropriate low-energy constants. Hence, the result of infrared regularization coincides with our ad hoc renormalization advocated in the previous section and we may use the result of [46] without any modification. For the inclusion of isospin-breaking see, *e.g.*, [49].

Following [46] the mixing parameters are determined by diagonalizing both the kinetic and the mass terms in the chiral effective Lagrangian. Since we count $m_{\eta'}$ as a quantity of zeroth chiral order, already at leading chiral order they also receive contributions from the $\mathcal{O}(p^4)$ Lagrangian

$$\mathcal{L}_\phi^{(4)} = \sum_{i=0}^{57} \beta_i \left[\frac{\eta_0}{f}\right] \mathcal{O}_i \ . \tag{1.103}$$

The functions β_i can be expanded in η_0/f in the same manner as the V_i in Eq. (1.98) with expansion coefficients $\beta_i^{(j)}$. The operators relevant for the evaluation of the mixing parameters read

$$\begin{aligned}
&\mathcal{O}_4 = -\left\langle C^\mu C_\mu \right\rangle \left\langle M \right\rangle \,, &&\mathcal{O}_5 = -\left\langle C^\mu C_\mu M \right\rangle \,, &&\mathcal{O}_7 = \left\langle N \right\rangle \left\langle N \right\rangle \,, \\
&\mathcal{O}_8 = \frac{1}{2} \left\langle MM + NN \right\rangle \,, &&\mathcal{O}_{17} = \left\langle C^\mu \right\rangle \left\langle C_\mu \right\rangle \left\langle M \right\rangle \,, &&\mathcal{O}_{18} = -\left\langle C^\mu \right\rangle \left\langle C_\mu M \right\rangle \,, \qquad (1.104)
\end{aligned}$$

where we made use of the abbreviations

$$C_\mu = U^\dagger \nabla_\mu U \,, \qquad M = U^\dagger \chi + \chi^\dagger U \,, \qquad N = U^\dagger \chi - \chi^\dagger U \,. \qquad (1.105)$$

At leading order in isospin-breaking and at second chiral order the mass eigenstates π^0, η, η' are related to the flavor fields $\tilde{\pi}^0$, η_8, η_0 by [46]

$$\begin{pmatrix} \tilde{\pi}^0 \\ \eta_8 \\ \eta_0 \end{pmatrix} = \begin{pmatrix} 1 + R_{\tilde{\pi}^0\pi^0} & R_{\tilde{\pi}^0\eta} & R_{\tilde{\pi}^0\eta'} \\ R_{8\pi^0} & 1 + R_{8\eta} & R_{8\eta'} \\ R_{0\pi^0} & R_{0\eta} & 1 + R_{0\eta'} \end{pmatrix} \begin{pmatrix} \pi^0 \\ \eta \\ \eta' \end{pmatrix} \,, \qquad (1.106)$$

with mixing parameters

$$\begin{aligned}
R^{(0)}_{8\pi^0} &= \frac{m_\epsilon^2}{\sqrt{3}(m_\eta^2 - m_\pi^2)} \,, & R^{(0)}_{\tilde{\pi}^0\eta} &= -R^{(0)}_{8\pi^0} \,, \\
R^{(2)}_{8\pi^0} &= R^{(0)}_{8\pi^0} \Big(R^{(2)}_{\tilde{\pi}^0\pi^0} + \frac{2}{3}\Delta_{\mathrm{GMO}} \Big) \,, & R^{(2)}_{\tilde{\pi}^0\eta} &= -R^{(0)}_{8\pi^0} \Big(R^{(2)}_{8\eta} + \frac{2}{3}\Delta_{\mathrm{GMO}} \Big) \,, \\
R^{(2)}_{0\eta} &= \frac{4\tilde{v}_2^{(1)}(m_\eta^2 - m_\pi^2)}{\sqrt{2} f^2 m_0^2} \,, & R^{(2)}_{8\eta'} &= -R^{(2)}_{0\eta} + \frac{8\beta^{(0)}_{5,18}(m_\eta^2 - m_\pi^2)}{\sqrt{2} f^2} \,, \\
R^{(2)}_{0\pi^0} &= 3 R^{(0)}_{8\pi^0} R^{(2)}_{0\eta} \,, & R^{(2)}_{\tilde{\pi}^0\eta'} &= 2 R^{(0)}_{8\pi^0} R^{(2)}_{8\eta'} \,, \qquad (1.107)
\end{aligned}$$

and terms corresponding to wave function renormalization

$$\begin{aligned}
R^{(2)}_{\tilde{\pi}^0\pi^0} &= \frac{1}{f^2} \Big(-6\beta_4^{(0)}(m_\eta^2 + m_\pi^2) - 4\beta_5^{(0)} m_\pi^2 + \frac{1}{3}\Delta_\pi + \frac{1}{6}\Delta_K \Big) \,, \\
R^{(2)}_{8\eta} &= \frac{1}{f^2} \Big(-6\beta_4^{(0)}(m_\eta^2 + m_\pi^2) - 4\beta_5^{(0)} m_\eta^2 + \frac{1}{2}\Delta_K \Big) \,, \\
R^{(2)}_{0\eta'} &= \frac{1}{f^2} \Big(-2\beta^{(0)}_{4,5,17,18}(m_\eta^2 + m_\pi^2) \Big) \,. \qquad (1.108)
\end{aligned}$$

Here the superscript on R denotes the chiral order and for the LECs we have employed the abbreviations

$$\begin{aligned}
\tilde{v}_2^{(1)} &= \frac{1}{4} f^2 - \frac{1}{2}\sqrt{6} v_3^{(1)} \,, \\
\beta^{(0)}_{5,18} &= \beta_5^{(0)} + \frac{3}{2}\beta_{18}^{(0)} \,, \\
\beta^{(0)}_{4,5,17,18} &= 3\beta_4^{(0)} + \beta_5^{(0)} - 9\beta_{17}^{(0)} + 3\beta_{18}^{(0)} \,. \qquad (1.109)
\end{aligned}$$

The masses m_π, m_K, m_η are the leading order contributions to the pseudoscalar meson masses in the isospin limit as defined in Eq. (1.44). Isospin breaking is incorporated in the scale-invariant combination $m_\epsilon^2 = B_0(m_d - m_u)$, while the next-to-leading order (NLO) correction to the Gell-Mann–Okubo formula, Eq. (1.45), is expressed in terms of the dimensionless quantity $\Delta_{\rm GMO}$

$$\left(4m_K^2 - m_\pi^2 - 3m_\eta^2\right)_{\rm phys} = (m_\eta^2 - m_\pi^2)\Delta_{\rm GMO} + \mathcal{O}(\mathcal{M}^3) \tag{1.110}$$

with

$$\begin{aligned}\Delta_{\rm GMO} = {}& \frac{6(m_\eta^2 - m_\pi^2)}{f^2}\left(\beta_5^{(0)} - 12\beta_7^{(0)} - 6\beta_8^{(0)} + \frac{4(\tilde{v}_2^{(1)})^2}{f^2 m_0^2}\right) \\ & - \frac{1}{f^2(m_\eta^2 - m_\pi^2)}\left(4m_K^2\Delta_K - m_\pi^2\Delta_\pi - 3m_\eta^2\Delta_\eta\right) .\end{aligned} \tag{1.111}$$

The symbol $m_0^2 = 2v_0^{(2)}/f^2$ stands for the mass of the η' meson in the chiral limit. Finally, there are contributions from tadpole integrals, whose finite, non-analytic pieces are denoted by

$$\Delta_P = \left(\int \frac{id^dl}{(2\pi)^d}\frac{1}{l^2 - m_P^2 + i\epsilon}\right)_{\rm finite} = \frac{m_P^2}{16\pi^2}\ln\frac{m_P^2}{\mu^2} , \tag{1.112}$$

where μ is the scale introduced in dimensional regularization.

Note that for a non-vanishing contribution from the combination $\beta_{5,18}^{(0)}$ the η-η' mixing pattern in Eq. (1.106) does not correspond to an orthogonal transformation as often assumed in the literature, see *e.g.* [50–53]. We remark that a non-orthogonal mixing scheme of η and η' was indeed also found in [54] in the framework of the Nambu–Jona-Lasinio model.

For completeness we also display the NLO results for other static quantities that are needed for one-loop calculations within U(3) ChPT, *cf.* [46]. To begin with we show the wave function renormalization for the kaon fields which supplements Eq. (1.108)

$$R_K^{(2)} = \frac{1}{f^2}\Big(-6\beta_4^{(0)}(m_\eta^2 + m_\pi^2) - 4\beta_5^{(0)}m_K^2 + \frac{1}{8}\Delta_\pi + \frac{1}{4}\Delta_K + \frac{1}{8}\Delta_\eta\Big) . \tag{1.113}$$

Next we give the NLO expressions for the pseudoscalar decay constants

$$\begin{aligned}F_\pi &= f\left[1 + \frac{1}{f^2}\left(6\beta_4^{(0)}(m_\eta^2 + m_\pi^2) + 4\beta_5^{(0)}m_\pi^2 - \Delta_\pi + \frac{1}{2}\Delta_K\right)\right] , \\ F_K &= f\left[1 + \frac{1}{f^2}\left(6\beta_4^{(0)}(m_\eta^2 + m_\pi^2) + 4\beta_5^{(0)}m_K^2 - \frac{3}{8}\Delta_\pi - \frac{3}{4}\Delta_K - \frac{3}{8}\Delta_\eta\right)\right] , \\ F_\eta &= f\left[1 + \frac{1}{f^2}\left(6\beta_4^{(0)}(m_\eta^2 + m_\pi^2) + 4\beta_5^{(0)}m_\eta^2 - \frac{3}{2}\Delta_K\right)\right] , \\ F_{\eta'} &= f\Bigg[1 + \frac{1}{f^2}\Bigg(6v_5^{(0)} + 2\left(1 - \frac{6v_5^{(0)}}{f^2}\right)\beta_{4,5,17,18}^{(0)}(m_\eta^2 + m_\pi^2) \\ &\qquad + (6\beta_{46}^{(0)} + 18\beta_{47}^{(0)} - 6\beta_{53}^{(0)} - 3\sqrt{6}\beta_{52}^{(1)})(m_\eta^2 + m_\pi^2)\Bigg)\Bigg] ,\end{aligned} \tag{1.114}$$

where $F_{\eta'}$ is the scale-invariant combination

$$F_{\eta'} = \frac{f}{\sqrt{6\lambda}} F^0_{\eta'} \,. \tag{1.115}$$

Remember that the singlet decay constant $F^0_{\eta'}$ depends on the running scale of QCD and is thus not an observable [42, 46]. The LECs in the last line of Eq. (1.114) arise from terms of the fourth order Lagrangian which we have not displayed up to now. The full list of $\mathcal{O}(p^4)$ terms can be found in Appendix A.2.

1.5.3 Unnatural parity Lagrangian

The Wess-Zumino-Witten action discussed in Sect. 1.4.4 in the context of SU(3) ChPT completely saturates the anomalous Ward identities of QCD. Since the octet field $\hat{U}$ and the U(3) field U transform in the same way under chiral rotations, a straightforward generalization of S_{WZW} (*cf.* Eq. (1.81)) to the U(3) framework is indeed possible—the chiral anomalies of QCD are still reproduced [37]. However, the singlet piece of the axial-vector source, $\langle a_\mu \rangle$, introduces a scale dependence which spoils the renormalization group invariance of S_{WZW}. This drawback can be cured by taking into account additional contact terms of unnatural parity which arise in the U(3) formalism at order $\mathcal{O}(p^4)$ and are chirally symmetric.

We prefer to work with a renormalization group invariant extension of the WZW action (for $\theta \equiv 0$) which is obtained from Eq. (1.81) by substituting $\hat{U} \to U$, $\hat{v} \to v$, $\hat{a} \to \tilde{a}$. Consequently, the left- and right-handed field strength tensors are defined according to

$$\begin{aligned} L_{\mu\nu} &= \partial_\mu(v_\nu - \tilde{a}_\nu) - \partial_\nu(v_\mu - \tilde{a}_\mu) - i[v_\mu - \tilde{a}_\mu, v_\nu - \tilde{a}_\nu] \,, \\ R_{\mu\nu} &= \partial_\mu(v_\nu + \tilde{a}_\nu) - \partial_\nu(v_\mu + \tilde{a}_\mu) - i[v_\mu + \tilde{a}_\mu, v_\nu + \tilde{a}_\nu] \,. \end{aligned} \tag{1.116}$$

The additional terms in the U(3) Lagrangian $\mathcal{L}^{(4)}_\phi$ have been constructed in [37]. With our conventions they also do not depend on the QCD renormalization scale and read

$$\begin{aligned} \mathcal{L}^{(4)}_{\text{u.p.}} = \frac{1}{2}\,\epsilon^{\mu\nu\alpha\beta}\Big\{ & 2\,W_1 \big\langle L_{\mu\nu} U^\dagger R_{\alpha\beta} U \big\rangle + W_2 \big\langle L_{\mu\nu} L_{\alpha\beta} + R_{\mu\nu} R_{\alpha\beta} \big\rangle \\ & + i\,W_3 \big\langle L_{\mu\nu} D_\alpha U^\dagger D_\beta U + R_{\mu\nu} D_\alpha U D_\beta U^\dagger \big\rangle \\ & + 2\,W_4 \big\langle L_{\mu\nu} \big\rangle \big\langle R_{\alpha\beta} \big\rangle + W_5 \big(\big\langle L_{\mu\nu} \big\rangle \big\langle L_{\alpha\beta} \big\rangle + \big\langle R_{\mu\nu} \big\rangle \big\langle R_{\alpha\beta} \big\rangle \big) \\ & - i\,W_6 \nabla_\mu\theta \big\langle L_{\nu\alpha} U^\dagger \nabla_\beta U - R_{\nu\alpha} \nabla_\beta U U^\dagger \big\rangle \Big\} \,, \end{aligned} \tag{1.117}$$

where $W_1, \ldots, W_5$ are odd functions of the chirally invariant combination $\eta_0 + \sqrt{\lambda}\theta$ and W_6 is even. As usual their expansion coefficients are denoted by $w_i^{(j)}$. At leading order the Lagrangian $\mathcal{L}^{(4)}_{\text{u.p.}}$ solely contributes to processes involving the η'. Hence, it does not renormalize the WZW action which completely determines the $\mathcal{O}(p^4)$ terms of unnatural parity in the SU(3) sector. Although it obviously contributes to η decays via η-η' mixing, these corrections do also not affect the WZW term since they are of next-to-leading order in the chiral counting scheme.

The $\mathcal{O}(p^6)$ Lagrangian of SU(3) ChPT contains 23 independent structures of unnatural parity [55]. While to our knowledge there has been no attempt to construct the most general effective Lagrangian at $\mathcal{O}(p^6)$ in the U(3) framework, it is clear that there will arise numerous more terms. In this work we restrict ourselves to the construction of those few terms which are relevant for the processes under consideration, namely $\eta, \eta' \to \pi^+\pi^-\gamma^*$, see Chapter 4.

1.6 Inclusion of baryons

In Part II of this work we study the interaction of the lightest pseudoscalar mesons and baryons. To this end we need to construct an effective Lagrangian which includes the lowest lying octet of spin-1/2 baryons (p, n, Λ, Σ^+, Σ^0, Σ^-, Ξ^0, Ξ^-), *i.e.* their kinetic and mass terms as well as their interaction with the octet of pseudoscalar Goldstone bosons, see *e.g.* the extensive reviews [15, 56]. For simplicity we do not consider the interaction of baryons with the η' here. The Dirac spinors which describe the baryon fields are summarized in the matrix

$$B = t^a\Psi^a = \begin{pmatrix} \frac{1}{\sqrt{2}}\Sigma^0 + \frac{1}{\sqrt{6}}\Lambda & \Sigma^+ & p \\ \Sigma^- & -\frac{1}{\sqrt{2}}\Sigma^0 + \frac{1}{\sqrt{6}}\Lambda & n \\ \Xi^- & \Xi^0 & -\frac{2}{\sqrt{6}}\Lambda \end{pmatrix} . \tag{1.118}$$

It is standard to choose a representation whose behavior under local chiral transformations is given by

$$B(x) \to K(x)B(x)K^\dagger(x) , \tag{1.119}$$

where K is the compensator field which is implicitly defined in terms of the chiral rotations $L(x) \in \mathrm{SU}(3)_L$, $R(x) \in \mathrm{SU}(3)_R$ and the Goldstone boson field $u(x)$, *cf.* Eq. (1.20). Therefore utilizing the representation u of the pseudoscalar mesons suggests itself and we introduce the derivative term u_μ and the connection Γ_μ,

$$\begin{aligned} u_\mu &= i\big(\partial_\mu u + iul_\mu\big)u^\dagger + iu^\dagger\big(\partial_\mu u - ir_\mu u\big) = iu^\dagger\nabla_\mu\hat{U}u^\dagger , \\ \Gamma_\mu &= \frac{1}{2}\Big(u(\partial_\mu - il_\mu)u^\dagger + u^\dagger(\partial_\mu - ir_\mu)u\Big) \end{aligned} \tag{1.120}$$

which transform according to

$$u_\mu \to Ku_\mu K^\dagger , \qquad \Gamma_\mu \to K\Gamma_\mu K^\dagger + K\partial_\mu K^\dagger . \tag{1.121}$$

The covariant derivative of the baryon fields is defined by

$$D_\mu B = \partial_\mu B + [\Gamma_\mu, B] \tag{1.122}$$

and transforms in the expected way,

$$D_\mu B \to K\, D_\mu B\, K^\dagger . \tag{1.123}$$

The occurrence of a commutator in $D_\mu B$ is sometimes emphasized by the notation $[D_\mu, B] \equiv D_\mu B$.

The leading order meson-baryon Lagrangian, which consists of terms with not more than one derivative, reads [57]

$$\mathcal{L}_{\hat{\phi}B}^{(1)} = \langle \bar{B}(i\not{D} - M_0)B) \rangle - \frac{D}{2}\langle \bar{B}\gamma^\mu\gamma_5\{u_\mu, B\}\rangle - \frac{F}{2}\langle \bar{B}\gamma^\mu\gamma_5[u_\mu, B]\rangle \,, \tag{1.124}$$

where M_0 is the common mass of the baryon octet in the chiral limit, and the constants D, F determine the axial-vector coupling of the baryons to the mesons. They are related to the axial-vector coupling constant of the nucleon, g_A, via $D{+}F = g_A$. Since M_0 is large (at the order of 1 GeV) compared to the meson masses it is clearly counted as a quantity of zeroth chiral order. When going to higher orders in the perturbative expansion, loops have to be taken into account and there arise the same problems of chiral power counting as in the case of the η'. In this work, however, we do not aim at a perturbative treatment of meson-baryon interactions, but instead employ non-perturbative methods based on the Bethe-Salpeter equation. Here chiral power counting is only invoked to specify the tree level terms which are then iterated in the Bethe-Salpeter equation to infinite order.

We also utilize the Lagrangian of second chiral order which contains 13 independent structures [57–59]. Only seven of them are needed in the present work:

$$\begin{aligned}\mathcal{L}_{\hat{\phi}B}^{(2)} &= b_D\langle \bar{B}\{\chi_+, B\}\rangle + b_F\langle \bar{B}[\chi_+, B]\rangle + b_0\langle \bar{B}B\rangle\langle \chi_+\rangle \\ &\quad + d_1\langle \bar{B}\{u_\mu, [u^\mu, B]\}\rangle + d_2\langle \bar{B}[u_\mu, [u^\mu, B]]\rangle \\ &\quad + d_3\langle \bar{B}u_\mu\rangle\langle u^\mu B\rangle + d_4\langle \bar{B}B\rangle\langle u^\mu u_\mu\rangle \,,\end{aligned} \tag{1.125}$$

where the quark masses enter in the combination

$$\chi_+ = u^\dagger \chi u^\dagger + u\chi^\dagger u \tag{1.126}$$

and the b_i, d_i are low-energy constants of dimension mass^{-1}.

Chapter 2

Unitarized two-particle scattering

2.1 Bethe-Salpeter equation

Chiral perturbation theory has proven very successful in describing static and dynamic properties of the octet of light pseudoscalar mesons, such as the masses and decay constants, $\pi\pi$ and πK scattering as well as η and kaon decays. Due to its model-independent connection to QCD it is capable of precisely determining mass ratios of the three light quarks from experimental observables. In this respect, ChPT also helps to make contact between results from lattice QCD calculations and the real world where several limits have to be taken (lattice → continuum, finite volume → infinite volume, large quark masses on the lattice → "physical" quark masses[*]). Furthermore, the inclusion of baryons in ChPT establishes the basis of a coherent description of low-energy baryon properties (*e.g.* masses and form factors), meson-baryon scattering and photon-nucleon processes.

As already hinted at in the previous chapter, the range of applicability of ChPT is, however, restricted by the onset of excited states in the hadronic spectrum which have been integrated out of the theory. In the case of meson-meson scattering this boundary is given by the mass of the lightest vector meson, the $\rho(770)$, which appears as a resonance in $\pi\pi$ scattering. When considering meson-baryon interactions one is also faced with low-lying excitations such as the $\Delta(1232)$ in πN scattering or the $\Lambda(1405)$ in the strangeness $S=-1$ channels.

There have been many attempts to construct methods which allow for a realistic description of hadronic processes in the resonance region while agreeing with ChPT in the low-energy limit. On the one hand, there are approaches based on dispersion relations which are matched to the respective ChPT amplitude in its domain of validity. While constituting an accurate, theoretically sound tool, these calculations are technically very involved and have so far only been applied to relatively simple processes, see *e.g.* [60]. Moreover, they heavily depend on precise experimental input which is only available for a rather limited number of processes. On the other hand, resummation techniques have been employed which take ChPT scattering amplitudes as their input and iterate them to infinite order. Since the guiding principle of these methods is exact unitarity of

---

[*] Quark masses depend on the running scale of QCD and are thus no physical observables in the usual sense.

the two-particle S-matrix, they are often referred to as chiral unitary approaches. They can easily be applied to comparatively complex systems with many coupled channels and have provided a successful description of many low-energy hadronic processes involving resonances which they are able to generate dynamically via infinite two-particle rescattering, see *e.g.* [61–63]. The main drawback of chiral unitary approaches is that the summation of a chain of loop diagrams generally violates crossing symmetry and does not guarantee analyticity of the scattering amplitudes. As a consequence of the missing crossing symmetry, the perturbative renormalization procedure of ChPT cannot be applied within chiral unitary approaches. However, crossing symmetry and renormalizability can in principle be restored up to any given order in the chiral expansion by adding the diagrams not included in the summed-up bubble chain. We will come back to the question of the renormalization of unitarized amplitudes further below in this section.

Apart from these two extensions of ChPT also hybrid approaches such as N/D structures have been used in the literature where the numerator N corresponds to a ChPT amplitude and the denominator D is determined by dispersive techniques. An example dealing with η decays can be found in [52].

Finally, there exist, of course, many generalizations of ChPT which explicitly include additional degrees of freedom in the effective Lagrangian, *e.g.* the nonet of light vector mesons (ρ, ω, K^*, ϕ) or the baryon decuplet with $J^P = 3/2^+$ (Δ, Σ^*, Ξ^*, Ω). Yet these supplementary terms in the Lagrangian usually bring in many new, unconstrained couplings which have to be determined from experimental input. Also establishing a power counting in the presence of these massive fields is not straightforward.

In this work we choose to work with a chiral unitary approach keeping in mind that it entails theoretical shortcomings concerning crossing symmetry, renormalizability and analyticity. The unitarization of the two-particle scattering S-matrix is accomplished by employing the Bethe-Salpeter equation (BSE), an integral equation for the T-matrix which guarantees fully relativistic kinematics and allows for a clear interpretation of the amplitudes in terms of Feynman graphs [48].

For simplicity we consider the scattering of two spinless particles with masses M, m and initial (final) four-momenta p, q (p', q') which is driven by the point-like interaction $\hat{V}(p', p, P)$ where the total four-momentum is denoted by $P = p + q = p' + q'$. The inclusion of baryons in the BSE will be discussed in Chapter 5 which deals with kaon-nucleon interactions. The BSE for the full scattering amplitude T reads

$$T(p', p, P) = \hat{V}(p', p, P) - \int \frac{d^d l}{(2\pi)^d}\, T(p', l, P)\, \tilde{G}(l, P)\, \hat{V}(l, p, P)\,, \tag{2.1}$$

where $\tilde{G}$ is the two-particle propagator. If the interaction kernel $\hat{V}$ and the propagator $\tilde{G}$ were known to arbitrary precision, the BSE would indeed generate the solution for T without any approximation (below the threshold of three-particle production). The BSE is depicted diagrammatically in Fig. 2.1. Clearly, Eq. (2.1) is an iterative equation for T and using the shorthand notation

$$T = \hat{V} - T\tilde{G}\hat{V}\,, \tag{2.2}$$

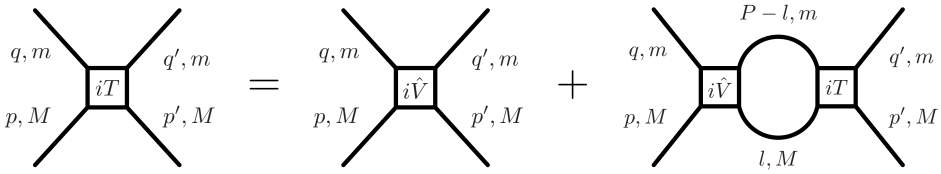

Figure 2.1: Diagrammatic illustration of the Bethe-Salpeter equation. The total four-momentum is denoted by $P = p + q = p' + q'$.

it may be expanded in powers of $\hat{V}$ according to

$$T = \hat{V} - \hat{V}\tilde{G}\hat{V} + \hat{V}\tilde{G}\hat{V}\tilde{G}\hat{V} - \ldots \ . \tag{2.3}$$

The solution T of the BSE is thus nothing else than the infinite summation of a bubble chain in the s-channel.

Since the full interaction kernel and the exact propagator are not known, we have to find reasonable approximations to them. For $\hat{V}$ it is natural to employ vertices from chiral perturbation theory at leading (and possibly next-to-leading) order as it describes the interactions of hadrons at low energies in a model-independent fashion. The two-particle propagator $\tilde{G}$ is approximated by the standard bosonic propagator

$$\tilde{G}(l, P) = \frac{i}{[l^2 - M^2 + i\epsilon][(P-l)^2 - m^2 + i\epsilon]} \ , \tag{2.4}$$

where we use the physical masses of the particles. This ensures that thresholds occur at the correct energies and is of particular importance in the case of multi-channel scattering. The signs in Eqs. (2.1), (2.4) have been chosen such that with a vertex $i\hat{V}$ (where $\hat{V}$ is real) the diagrams in Fig. 2.1 correspond to Eq. (2.1) when employing the usual Feynman rules.

We would now like to find the solution of the BSE. For simplicity let us first consider a pure s-wave interaction, *i.e.* the interaction kernel $\hat{V}(p', p, P)$ is just a function of P^2 including possible off-shell terms

$$\begin{aligned} \hat{V}(p', p, P) = \hat{V}_{\text{on}}(P^2) &+ (p^2 - M^2)\hat{V}^{(1)}_{\text{off}}(P^2) + (q^2 - m^2)\hat{V}^{(2)}_{\text{off}}(P^2) \\ &+ (p'^2 - M^2)\hat{V}^{(3)}_{\text{off}}(P^2) + (q'^2 - m^2)\hat{V}^{(4)}_{\text{off}}(P^2) \, . \end{aligned} \tag{2.5}$$

Note that here we have restricted ourselves to purely linear off-shell terms. In general $\hat{V}$ may also involve higher order and mixed off-shell contributions for which the above decomposition is not unique and hence not appropriate. Moreover, if $\hat{V}$ involves contributions to higher partial waves such as the terms $p' \cdot p$, $(p' \cdot p)^2$, …, one first has to perform a partial wave expansion of the interaction kernel which leads to a BSE in each partial wave, see the discussion in [64, 65].

Postulating the same structure for the solution T as for $\hat{V}$, *cf.* Eq. (2.5), we find that the BSE generates the following expression for the on-shell T-matrix

$$\begin{aligned} T_{\mathrm{on}} = \hat{V}_{\mathrm{on}} &- \int \frac{i d^d l}{(2\pi)^d} \frac{T_{\mathrm{on}} \hat{V}_{\mathrm{on}}}{[l^2 - M^2 + i\epsilon][(P-l)^2 - m^2 + i\epsilon]} \\ &- \int \frac{d^d l}{(2\pi)^d} \frac{T_{\mathrm{on}} \hat{V}^{(3)}_{\mathrm{off}} + T^{(1)}_{\mathrm{off}} \hat{V}_{\mathrm{on}} + (l^2 - M^2) T^{(1)}_{\mathrm{off}} \hat{V}^{(3)}_{\mathrm{off}}}{(P-l)^2 - m^2 + i\epsilon} \\ &- \int \frac{d^d l}{(2\pi)^d} \frac{T_{\mathrm{on}} \hat{V}^{(4)}_{\mathrm{off}} + T^{(2)}_{\mathrm{off}} \hat{V}_{\mathrm{on}} + ((P-l)^2 - m^2) T^{(2)}_{\mathrm{off}} \hat{V}^{(4)}_{\mathrm{off}}}{l^2 - M^2 + i\epsilon} \\ &- \int \frac{d^d l}{(2\pi)^d} \Big\{ T^{(1)}_{\mathrm{off}} \hat{V}^{(4)}_{\mathrm{off}} + T^{(2)}_{\mathrm{off}} \hat{V}^{(3)}_{\mathrm{off}} \Big\} \;, \end{aligned} \tag{2.6}$$

where we have suppressed the argument P^2 of the on- and off-shell parts of $\hat{V}$ and T for brevity. Since they do not depend on the variable of integration, they may be drawn out of the integrals over l . The off-shell pieces of $\hat{V}$ and T are thus proportional either to tadpole integrals which yield chiral logarithms (*cf.* Eq. (1.112)) or to power divergences which vanish in dimensional regularization. While, admittedly, chiral logarithms are at the heart of chiral perturbation theory reflecting the fact that the expansion in powers of small quark masses is not an ordinary Taylor series, but involves non-analytic terms, when it comes to the phenomenology of meson-meson or meson-baryon scattering in a non-perturbative region one is usually not interested in the behavior of the amplitudes when approaching the chiral limit. In this context it is reassuring that the contributions of chiral logarithms are usually numerically small. Hence one may argue that the effects of the off-shell pieces of $\hat{V}$ and T can be compensated numerically by readjusting appropriate couplings of the chiral effective Lagrangian. See also the investigation of pion form factors in [66] where the results of a two-loop calculation in ChPT are compared to a dispersive approach.

Dropping all off-shell terms in Eq. (2.6) we are left with the algebraic form of the BSE in the so-called on-shell approximation

$$T_{\mathrm{on}}(P^2) = \hat{V}_{\mathrm{on}}(P^2) - T_{\mathrm{on}}(P^2) \hat{G}(P^2) \hat{V}_{\mathrm{on}}(P^2) \;, \tag{2.7}$$

where $\hat{G}$ is the scalar loop integral

$$\hat{G}(P^2) = \int \frac{i d^d l}{(2\pi)^d} \frac{1}{[l^2 - M^2 + i\epsilon][(P-l)^2 - m^2 + i\epsilon]} \;. \tag{2.8}$$

Making use of dimensional regularization one obtains for the finite piece G of $\hat{G}$

$$\begin{aligned} G(P^2) &= \frac{1}{16\pi^2} \bigg[-1 + \ln \frac{mM}{\mu^2} + \frac{m^2 - M^2}{P^2} \ln \frac{m}{M} \\ &\qquad\qquad - \frac{2\sqrt{\lambda_{mM}(P^2)}}{P^2} \operatorname{artanh} \frac{\sqrt{\lambda_{mM}(P^2)}}{(m+M)^2 - P^2} \bigg] \;, \\ \lambda_{mM}(P^2) &= \big((m-M)^2 - P^2\big)\big((m+M)^2 - P^2\big) \;, \end{aligned} \tag{2.9}$$

where μ is the regularization scale.

So far we have not addressed the question of renormalization. The loop integral in the on-shell BSE, Eq. (2.7), and also the additional ones in the off-shell formulation, Eq. (2.6), are divergent and in order to arrive at a meaningful result these divergences have to be absorbed by suitable counter terms. Owing to the fact that the summation of a bubble sum in the s-channel violates crossing symmetry it is clear that the renormalization of the BSE cannot be accomplished by a local effective Lagrangian which produces counter terms that are crossing symmetric by construction [67]. However, it is at least possible to show that the infinities of the loop integrals may be absorbed by redefining the interaction kernel $\hat{V}$ appropriately. Let δG denote the infinite piece of $\hat{G}$ for $d \to 4$, so that $\hat{G} = G + \delta G$. In this work we employ the so-called $\overline{\mathrm{MS}}$ scheme where δG reads

$$\delta G = \frac{\mu^{d-4}}{16\pi^2}\left(\frac{1}{d-4} - \frac{1}{2}\big[\ln(4\pi) - \gamma_E + 1\big]\right) \equiv \bar{\lambda} \ . \tag{2.10}$$

Here $\gamma_E \approx 0.5772$ is the Euler-Mascheroni constant. After decomposing

$$\hat{V}_{\rm on} = V_{\rm on} + \delta V_{\rm on} \qquad \text{with} \quad \delta V_{\rm on} = \hat{V}_{\rm on}\delta G\, \hat{V}_{\rm on}(1 + \delta G\, \hat{V}_{\rm on})^{-1} \tag{2.11}$$

one easily verifies that the on-shell BSE, Eq. (2.7), is transferred into an equation which solely involves finite quantities

$$T_{\rm on}(P^2) = V_{\rm on}(P^2) - T_{\rm on}(P^2)G(P^2)V_{\rm on}(P^2) \ . \tag{2.12}$$

While the renormalization procedure outlined here differs from renormalization in the usual sense where the divergences are absorbed by local counter terms, it nevertheless makes the use of finite quantities in the BSE plausible: The infinite piece of $\hat{G}$ is canceled by an appropriate term in the kernel $\hat{V}$.

As illustrated in [64] for a polynomial interaction kernel $\hat{V}$ it is in fact not necessary to employ the on-shell approximation in order to transform the Bethe-Salpeter integral equation (2.1) into an algebraic relation, see also [68]. The key point is to rewrite the interaction kernel as a matrix in “off-shell space” and make an analogous ansatz for T. *E.g.* for our simple s-wave kernel defined in Eq. (2.5) we would write

$$\hat{V} = \Big(1,\ \ p'^2 - M^2,\ \ q'^2 - m^2\Big) \underbrace{\begin{pmatrix} \hat{V}_{\rm on} & \hat{V}_{\rm off}^{(1)} & \hat{V}_{\rm off}^{(2)} \\ \hat{V}_{\rm off}^{(3)} & 0 & 0 \\ \hat{V}_{\rm off}^{(4)} & 0 & 0 \end{pmatrix}}_{\breve{V}} \begin{pmatrix} 1 \\ p^2 - M^2 \\ q^2 - m^2 \end{pmatrix} \tag{2.13}$$

and would eventually find an algebraic equation for the pertinent matrix $\breve{T}$ which can be solved by matrix inversion. For details the reader is referred to [64].

Although it is hence possible to find the exact solution of the BSE including the full off-shell dependence of the interaction kernel, in this work we will utilize the simpler on-shell version of the BSE for two reasons. First, as far as meson-meson or meson-baryon scattering is concerned, the off-shell contributions are generally small and can be compensated by re-adjusting free coupling constants in the kernel. Note, however, that when the coupling of photons to the bubble chain is taken into account, which is, *e.g.*, of relevance for the description of meson photoproduction, off-shell effects can be sizable and should not be neglected [65]. Second, the off-shell pieces of $\hat{V}$ are not unique—they depend on the choice of the field parametrization in the Lagrangian [67]. While this unphysical representation dependence drops out at each loop order in ChPT, it does not cancel in the bubble sum generated by the BSE.

In order to solve the BSE for more complicated interaction kernels it is convenient to first perform a partial wave decomposition of $V_{\text{on}}(p', p, P)$ (from now on we drop the subscript "on")

$$V(p', p, P) = \sum_{\ell=0}^{\infty} (2\ell + 1)\tilde{V}_\ell(P^2)\, P_\ell(\cos\theta) \ , \tag{2.14}$$

where θ is the center-of-mass (c.m.) scattering angle and P_ℓ denotes the ℓ^{th} Legendre polynomial. Since the BSE is a relativistic equation we prefer to work with a manifestly covariant form of the partial wave decomposition which is based on the relation

$$4|\mathbf{p}_{\text{cm}}||\mathbf{p}'_{\text{cm}}| \cos\theta = t - u - \frac{1}{s}(p^2 - q^2)(p'^2 - q'^2) \ . \tag{2.15}$$

The Mandelstam variables are defined by

$$\begin{aligned} s &= (p + q)^2 = (p' + q')^2 = P^2 \,, \\ t &= (p - p')^2 = (q - q')^2 \,, \\ u &= (p - q')^2 = (q - p')^2 \,, \end{aligned} \tag{2.16}$$

and the moduli of the c.m. momenta can also be expressed in terms of Lorentz scalars

$$\begin{aligned} |\mathbf{p}_{\text{cm}}|^2 &= \frac{1}{4s}\big(s - p^2 + q^2\big)^2 - q^2 \ , \\ |\mathbf{p}'_{\text{cm}}|^2 &= \frac{1}{4s}\big(s - p'^2 + q'^2\big)^2 - q'^2 \ . \end{aligned} \tag{2.17}$$

We define a set of orthogonal functions J_ℓ which are proportional to the Legendre polynomials. They are polynomials of order ℓ in $t - u$ and the first three of them read

$$\begin{aligned} J_0 &= P_0(\cos\theta) = 1 \,, \\ J_1 &= |\mathbf{p}_{\text{cm}}||\mathbf{p}'_{\text{cm}}|\, P_1(\cos\theta) = \frac{1}{4}(t - u) - \frac{1}{4s}(p^2 - q^2)(p'^2 - q'^2) \,, \\ J_2 &= \frac{2}{3}|\mathbf{p}_{\text{cm}}|^2|\mathbf{p}'_{\text{cm}}|^2\, P_2(\cos\theta) = J_1^2 - \frac{1}{3}|\mathbf{p}_{\text{cm}}|^2|\mathbf{p}'_{\text{cm}}|^2 \ . \end{aligned} \tag{2.18}$$

In this work we only consider s- and p-waves, *i.e.* only J_0 and J_1 are needed. Assuming that the momenta of the particles are put on their respective mass shells, the partial wave decomposition of V in terms of the J_ℓ is given by

$$V(p', p, P) = \sum_{\ell=0}^{\infty} V_\ell(s)\, J_\ell(s, t - u) \,. \tag{2.19}$$

Due to the orthogonality of the J_ℓ (or of the Legendre polynomials) the partial wave amplitudes V_ℓ decouple in the BSE, so that we get a BSE for each partial wave

$$T_\ell(s) = V_\ell(s) - T_\ell(s) G_\ell(s) V_\ell(s) \,, \tag{2.20}$$

where T is decomposed in the same manner as V and G_ℓ differs from G in Eq. (2.12) by kinematical factors which depend on ℓ. For example we have

$$G_0(s) = G(s) \,, \qquad G_1(s) = \left[\frac{1}{12s}\big(s - m^2 + M^2\big)^2 - \frac{1}{3} M^2 \right] G(s) \,. \tag{2.21}$$

Now we would like to briefly discuss the generalization of the BSE to multi-channel scattering. All quantities in Eq. (2.1) are then replaced by matrices in channel space, in particular $\tilde{G}$ turns into a diagonal matrix. Time-reversal invariance implies that $\tilde{V}$ is a symmetric matrix and therefore also T. The renormalized on-shell form of the partial wave BSE, Eq. (2.20), is now a matrix equation and can directly be solved via matrix inversion which yields

$$T_\ell = V_\ell (\mathbb{1} + G_\ell V_\ell)^{-1} \ . \tag{2.22}$$

By virtue of

$$\begin{aligned} 0 &= T_\ell(\mathbb{1} + G_\ell V_\ell) - V_\ell = (T_\ell - V_\ell)(\mathbb{1} + G_\ell V_\ell) + V_\ell G_\ell V_\ell \\ &= (T_\ell - V_\ell + V_\ell G_\ell T_\ell)(\mathbb{1} + G_\ell V_\ell) \end{aligned} \tag{2.23}$$

it follows that T_ℓ also solves the alternative BSE

$$T_\ell = V_\ell - V_\ell G_\ell T_\ell \ , \tag{2.24}$$

so that we may as well write

$$T_\ell = (\mathbb{1} + V_\ell G_\ell)^{-1} \, V_\ell \ . \tag{2.25}$$

Finally, in the spirit of dispersion theory we introduce a subtraction constant $a(\mu)$ which cancels the scale dependence of the finite piece G of the scalar loop integral in dimensional regularization and corresponds to a specific choice of higher order counter terms [69, 70]. Without changing the notation we thus replace G from Eq. (2.9) according to

$$G(s) \to G(s) + a(\mu) \tag{2.26}$$

so that $G_\ell(s)$ turns into a scale-independent quantity and we allow for different numerical values of the subtraction constant in each partial wave ℓ and each two-particle channel.

In the simplest case the interaction kernel of the BSE, V_ℓ, is derived from the tree level terms of the leading order chiral Lagrangian. It is clear that the solution T_ℓ then reproduces the leading order ChPT result by virtue of the expansion

$$T_\ell = V_\ell - V_\ell G_\ell V_\ell + \dots \tag{2.27}$$

owing to the fact that the loop expansion complies with the chiral counting scheme (assuming that possible power-counting violating terms from loops with heavy particles such as the η' have been treated appropriately, see the discussion in Sect. 1.5.1).

This matching procedure between the unitarized and the perturbative amplitude can be generalized to higher chiral orders [69, 70]. If, for instance, one has the full one-loop scattering amplitude of ChPT at one's disposal, one may ensure that T_ℓ reproduces this result by defining

$$V_\ell = A_\ell^{(\text{1-loop})} + A_\ell^{(\text{LO})} G_\ell \, A_\ell^{(\text{LO})} \,, \tag{2.28}$$

where $A_\ell^{(\text{LO})}$ is the partial wave projected leading order amplitude from ChPT and $A_\ell^{(\text{1-loop})} = A_\ell^{(\text{LO})} + A_\ell^{(\text{NLO})}$ denotes the ℓ^{th} partial wave of the full one-loop result. The second term on the r.h.s. of Eq. (2.28) compensates exactly that piece of the one-loop amplitude which is generated by the BSE. By construction T_ℓ thus matches to the one-loop result of ChPT and the amplitudes in the chiral unitary approach and in ChPT start to deviate only at the two-loop level. While in principle the matching procedure can be accomplished at any given loop order, one should keep in mind that in combination with the on-shell approximation the partial wave projection of graphs more complicated than contact interactions (*e.g.* Born diagrams in meson-baryon scattering or t-channel loops) may entail additional singularities in unphysical regions of the respective processes. In coupled channels calculations with significantly different masses of the particles the unphysical regions of one particular channel may overlap with the physical region of another channel transferring the artificial singularities of the partial wave projection to physical observables where they should not appear. Hence one has to be very careful when including complicated diagrams with a non-trivial analytic structure in the interaction kernel of the BSE. We will come back to this point in Chapter 5. Moreover, one has to make sure that the interaction kernel remains real-valued when it involves contributions from loop diagrams because otherwise exact unitarity of the S-matrix would be spoilt.

2.2 Unitarity

In this section we explain that the solution of the BSE indeed yields a unitary S-matrix and to stay general we work in the multi-channel formulation. The partial wave S-matrix of two-particle scattering is defined by

$$S_\ell(s) = \mathbb{1} + iC_\ell(s)\, T_\ell(s)\, C_\ell(s) \,, \tag{2.29}$$

where the C_ℓ are real diagonal matrices and the first two have entries

$$C_0^{ii} = \theta\big(\sqrt{s} - (m_i + M_i)\big)\sqrt{\frac{|\mathbf{p}_{\text{cm}}^i|}{4\pi\sqrt{s}}} \,, \qquad C_1^{ii} = \theta\big(\sqrt{s} - (m_i + M_i)\big)\sqrt{\frac{|\mathbf{p}_{\text{cm}}^i|^3}{12\pi\sqrt{s}}} \tag{2.30}$$

for each channel i. The step functions ensure that only channels which are open, *i.e.* above their respective thresholds, appear in the S-matrix which is a measurable quantity after all. Unitarity of the S-matrix imposes a constraint on the T-matrix which is derived via

$$\begin{aligned} S_\ell^\dagger S_\ell &= \mathbb{1} + iC_\ell(T_\ell - T_\ell^\dagger)C_\ell + C_\ell T_\ell^\dagger C_\ell^2\, T_\ell\, C_\ell \overset{!}{=} \mathbb{1} \\ \Rightarrow \quad -i(T_\ell - T_\ell^\dagger) &= 2\,\text{Im}\, T_\ell = T_\ell^\dagger C_\ell^2\, T_\ell \,, \end{aligned} \tag{2.31}$$

where in the second line we have used the symmetry of T_ℓ. After multiplying by $(T_\ell^\dagger)^{-1}$ from the left and by T_ℓ^{-1} from the right, the unitarity constraint on T_ℓ can be reformulated as a simple relation for T_ℓ^{-1}

$$\begin{aligned} C_\ell^2 = -i\big((T_\ell^\dagger)^{-1} - T_\ell^{-1}\big) &= -2\,\mathrm{Im}\,T_\ell^{-1} \\ \Rightarrow \quad \mathrm{Im}\,T_\ell^{-1} &= -\frac{1}{2}\,C_\ell^2\ . \end{aligned} \tag{2.32}$$

One the other hand, we know that the solution of the BSE satisfies (*cf.* Eq. (2.22))

$$T_\ell^{-1} = V_\ell^{-1} + G_\ell\ , \tag{2.33}$$

i.e. for a real interaction kernel V_ℓ we have

$$\mathrm{Im}\,T_\ell^{-1} = \mathrm{Im}\,G_\ell\ , \tag{2.34}$$

but since $\mathrm{Im}\,G_\ell = -C_\ell^2/2$, we conclude that the solution of the BSE corresponds to an S-matrix which is exactly unitary.

At the threshold of channel i the imaginary part of G_ℓ^{ii} vanishes as a square root function and is thus not differentiable, *cf.* Eq. (2.30). This threshold singularity of channel i shows up in all other (open) channels of the T-matrix. In particular it leads to characteristic sudden changes of the slope of cross sections which can be (and have been) observed in experiment. They are known as *cusps.*

The diagonal elements of S_ℓ are conventionally parametrized as

$$S_\ell^{ii}(s) = \eta_\ell^i(s)\exp\big[2i\,\delta_\ell^i(s)\big] \qquad \text{with} \quad 0 \le \eta_\ell^i \le 1\ , \tag{2.35}$$

where δ_ℓ^i is the (real) phase shift and η_ℓ^i the inelasticity. For elastic scattering, *i.e.* if only channel i is open, one has $\eta_\ell^i = 1$ and unitarity of the S-matrix is evident.

2.3 Resonance poles

The BSE is able to generate resonances dynamically. By this we mean that the infinite sum of rescattering graphs may produce a pole of $T_\ell(s)$ at some value s_0 which is generally a complex number. For convenience we will regard T_ℓ as a function of the invariant energy $W = \sqrt{s}$ in this section without changing the notation, *i.e.* $T_\ell = T_\ell(W)$ (and analogously for the other functions). If $W_0 = \sqrt{s_0}$ is real, such a pole corresponds to a bound state solution, if W_0 is complex, one speaks of a resonance.

The analytic continuation of $T_\ell(W)$ from the real axis, where it describes physical observables, to the complex W plane is not completely straightforward. While the interaction kernel $V_\ell(W)$ is assumed to be an analytic function of W, the loop functions collected in $G_\ell(W)$ contain non-analytic pieces. Apart from a possible singularity at $W = 0$ which is connected to the partial wave decomposition for $\ell \ge 1$ and has no relevance for physical observables, $G_\ell(W)$ exhibits a branch point at the threshold $W_i = m_i + M_i$ of each channel i. That is when winding once around W_i in the complex plane one ends up at a value of G_ℓ which differs from the initial value. These branch points reflect the fact that the loop integral G in Eq. (2.9) is actually a double-valued

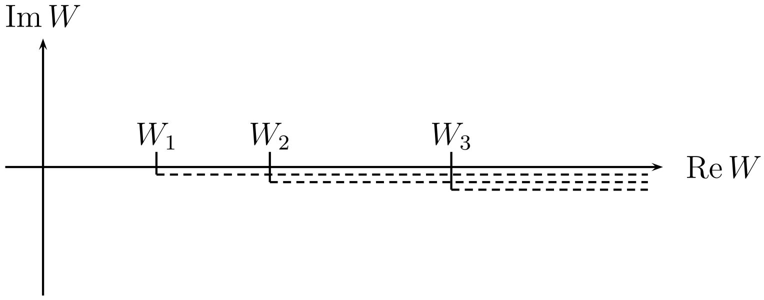

Figure 2.2: Cut structure of the physical Riemann sheet with three branch points that are located at the thresholds W_1, W_2, W_3. The unphysical Riemann sheets which are directly connected to the physical real axis are reached by passing through all the cuts below the real axis.

function in the complex W plane. In order to work with a well-defined loop function one introduces two so-called Riemann sheets (duplicates of the complex W plane) which have a cut just below the real axis ranging from threshold to $+\infty$ and are glued together along the two cuts so that they form a two-dimensional manifold. For each channel two Riemann sheets have to be introduced so that for N channels one arrives at a relatively complicated structure of $2N$ Riemann sheets, see Fig 2.2 for an illustration.

From all $2N$ real axes the *physical* real axis is singled out by the unitarity condition

$$\operatorname{Im} G(W) = -\frac{|\mathbf{p}_{\mathrm{cm}}|}{8\pi W} \qquad \text{for} \quad W > m + M \tag{2.36}$$

which is required for each channel. Accordingly, the *physical* Riemann sheet is the one that contains the physical real axis and the cuts below this axis are often referred to as the unitarity cuts. Note that our definition of the branch cut of $G(W)$ is in accordance with the convention that the square root function has a branch cut just below the negative real axis and that $\operatorname{artanh}(x)$ has two cuts from -1 to $-\infty$ below the real axis and from $+1$ to $+\infty$ above the real axis, respectively, *cf.* Eq. (2.9).

The postulate of maximal analyticity, which is one of the foundations of S-matrix theory, states that on the physical Riemann sheet the scattering amplitude has only those singularities which are direct consequences of general physical principles such as unitarity and crossing symmetry. We will see to what extent this assumption holds within chiral unitary approaches. On the other hand, maximal analyticity allows for poles on unphysical Riemann sheets. In this context poles of $T_\ell(W)$ on Riemann sheets which are directly connected to the physical real axis are of particular interest since they are related to resonance structures in physical observables. We will explain the argument for the simplified case of one-channel s-wave scattering. Assume that $T_0(W)$ has a simple pole at W_0 on its unphysical Riemann sheet below the unitarity cut, *i.e.* $\operatorname{Re} W_0 \equiv E_0 > m + M$, $\operatorname{Im} W_0 \equiv -\Gamma_0/2 < 0$. Since the scattering amplitude $T_0(W)$ is a meromorphic function in a neighborhood of W_0, it may be expanded as a Laurent series

$$T_0(W) = \frac{c_{-1}}{W - W_0} + c_0 + c_1(W - W_0) + c_2(W - W_0)^2 + \dots \tag{2.37}$$

with complex coefficients c_i. If W_0 is close to the real axis, the values of $T_0(W)$ for real W in the vicinity of E_0 will be dominated by the pole term and we find that in this region the cross section $\sigma(W) = |T_0(W)|^2/(16\pi W^2)$ shows the typical Breit-Wigner form of a resonance

$$\sigma(W) \approx \frac{1}{16\pi W^2} \frac{|c_{-1}|^2}{(W-E_0)^2 + \Gamma_0^2/4} , \tag{2.38}$$

which is peaked roughly at $W \approx E_0$. Accordingly, E_0 and Γ_0 are associated with the mass and the width of the resonance, respectively. Unitarity at $W = E_0$ imposes the constraint $|c_{-1}|^2 = -4\pi W\,\Gamma_0\,\mathrm{Re}(c_{-1})/|\mathbf{p}_{\mathrm{cm}}|$ which implies the standard form of a Breit-Wigner resonance with $c_{-1} = -4\pi W\,\Gamma_0/|\mathbf{p}_{\mathrm{cm}}|$ if c_{-1} is real. Note that in the presence of several poles on unphysical Riemann sheets or close to threshold singularities in multi-channel calculations, cross section observables may deviate substantially from the Breit-Wigner shape. In fact, employing the pole which is closest to the physical real axis, the relation

$$W_0 = E_0 - \frac{i}{2}\Gamma_0 \tag{2.39}$$

is then taken as the definition of the mass and the width of the resonance [17].

There is a second, slightly more general indication of a resonance pole close to the real axis. Assume that the partial wave S-matrix has a pole on the unphysical sheet at $W_0 = E_0 - i\Gamma_0/2$ (with $\Gamma_0 > 0$). Unitarity then dictates the form

$$S_\ell = e^{2i\delta_\ell} = S_\ell^{\mathrm{res}} \exp\big[2i\delta_\ell^{\mathrm{bg}}\big] \qquad \text{with} \quad S_\ell^{\mathrm{res}} = \frac{W - E_0 - i\Gamma_0/2}{W - E_0 + i\Gamma_0/2} , \tag{2.40}$$

where the background phase shift $\delta_\ell^{\mathrm{bg}}$ describes the deviation from the pure pole term. The resonant piece of the S-matrix changes quickly from $S_\ell^{\mathrm{res}} = i$ at $W = E_0 - \Gamma_0/2$ via $S_\ell^{\mathrm{res}} = -1$ at $W = E_0$ to $S_\ell^{\mathrm{res}} = -i$ at $W = E_0 + \Gamma_0/2$, *i.e.* the corresponding phase shift $\delta_\ell^{\mathrm{res}}$ increases by $\pi/2$ in this interval which is small when the pole is close to the real axis. Since the background phase shift usually varies comparatively slowly, a rapid increase of δ_ℓ by (at least) $\pi/2$ is a clear signature of a resonance independent of a possible peak of the cross section. The steep rise of the partial wave phase shift can, *e.g.*, be seen in speed plots. The "speed" SP of the amplitude is defined by [71]

$$\mathrm{SP}[T_\ell(W)] = \left|\frac{dT_\ell(W)}{dW}\right| \tag{2.41}$$

and exhibits a pronounced peak at the energy of the resonance.

The observation that complex poles of the S- or T-matrix are related to resonance structures on the physical real axis can be generalized in a straightforward way to scattering processes which involve several coupled channels, see *e.g.* [72]. We point out once more that for multi-channel problems with their complicated structure of many Riemann sheets only those poles are relevant which are located on a Riemann sheet that is directly connected to the physical real axis between two thresholds and whose distance from this interval on the real axis is "not too large". The precise meaning of the last statement heavily depends on the given kinematical constraints, but certainly the imaginary part of the pole position has to be considerably smaller in magnitude than the relevant energy scale of the system.

Within the framework of non-relativistic potential scattering it can be proven that for a finite-range potential the S-matrix is an analytic function of the (non-relativistic) energy W on the physical Riemann sheet except for possible simple poles which are located on the negative real axis and correspond to bound states. On the unphysical Riemann sheets $S_\ell(W)$ is a meromorphic function, for a proof see *e.g.* [73]. These observations have formed the basis of relativistic S-matrix theory which takes analyticity of the S-matrix as one of its postulates. (Note, however, that in the relativistic formulation bound state poles are situated on the *positive* real axis below the lowest threshold.)

While in chiral unitary approaches the use of the BSE guarantees that the S-matrix is exactly unitary this does not say much about its analytic properties. In fact, as we will illustrate by making use of a simple toy model, poles of S_ℓ (or T_ℓ) on the physical Riemann sheet are not excluded within chiral unitary approaches. However, due to an argument by Wigner such poles may induce violations of causality if they are close to the real axis. We will come back to this point at the end of this section. Let us first set up the toy model for one-channel s-wave scattering which incorporates the main analytic properties of a chiral unitary framework. Consider an interaction kernel

$$V(W) = a + b\,W \tag{2.42}$$

with real constants a, b. Poles of $T = V/(1+VG)$ obviously correspond to zeros of $1 + VG$. We are thus lead to the equations

$$\begin{aligned} 1 + \big(a + b\,\mathrm{Re}(W_0)\big)\,\mathrm{Re}(G) - b\,\mathrm{Im}(W_0)\,\mathrm{Im}(G) &= 0\,, \\ \big(a + b\,\mathrm{Re}(W_0)\big)\,\mathrm{Im}(G) + b\,\mathrm{Im}(W_0)\,\mathrm{Re}(G) &= 0\,, \end{aligned} \tag{2.43}$$

which imply the following conditions for the parameters a and b

$$\begin{aligned} a &= \frac{1}{|G(W_0)|^2}\left[\mathrm{Re}(G(W_0)) - \frac{\mathrm{Im}(G(W_0))}{\mathrm{Im}(W_0)}\,\mathrm{Re}(W_0)\right]\,, \\ b &= \frac{1}{|G(W_0)|^2}\,\frac{\mathrm{Im}(G(W_0))}{\mathrm{Im}(W_0)}\;. \end{aligned} \tag{2.44}$$

From the second equation we can read off that a pole of T above the physical real axis where $\mathrm{Im}(G) < 0$ is indeed possible if b is negative. The larger $|b|$ gets the more does the pole position W_0 approach the real axis. The value of a, on the other hand, may be adjusted in such a way that the real part of W_0 is above threshold and therefore in the physically relevant region.

The interaction kernels derived from ChPT are certainly much more complicated than the toy model interaction considered here. In addition the interplay of many coupled channels generally induces involved expressions for the T- or S-matrix elements. Nevertheless, the conclusion remains the same: Depending on the values of the free parameters in the interaction kernel (the LECs) one cannot exclude that the BSE generates solutions for T_ℓ which have poles above the real axis on the physical Riemann sheet. In principle this observation could be utilized to constrain the values of the LECs to certain regions where none of these unphysical poles occur. However, given the intricate, highly non-linear expressions for the amplitudes T_ℓ this procedure is usually not feasible. Instead we choose to follow a different, more pragmatic path and first fit the undetermined parameters freely to achieve good agreement with experimental data, *i.e.* T_ℓ is only evaluated on the real axis. Afterwards we check whether the fits exhibit near-by poles on the physical Riemann sheet and use this as an exclusion criterion.

One might argue that the postulate of maximal analyticity of the S-matrix which is based on the examination of potential scattering in non-relativistic quantum mechanics does not apply to chiral unitary approaches and that there is thus no problem with poles on the physical Riemann sheet. Yet there is a more fundamental argument why there must not be any near-by poles above the physical real axis. It is based on the fact that the derivative of the phase shift with respect to energy measures the time delay τ of a scattered particle (or rather its wave packet) compared to the unscattered case [74]

$$\frac{d\delta_\ell(W)}{dW} = \tau \ . \tag{2.45}$$

In particular if the particle is temporarily captured in the interaction region to form a resonant state, the time delay will be large and the phase shift rapidly increases. This is the common indication of a resonance. On the other hand if the interaction has a finite range R, causality requires that the scattered particle cannot leave the interaction region before the incident particle has reached it. Therefore the time advance of the scattered particle has an upper limit, or formulated in terms of the time delay τ we have

$$\tau \gtrsim -\frac{R}{c} \ , \tag{2.46}$$

where c is the speed of light. This immediately yields a lower limit for the slope of the phase shift which was derived by Wigner [74]

$$\frac{d\delta_\ell(W)}{dW} \gtrsim -R \tag{2.47}$$

and we have set $c = 1$ as usual. This remarkably simple result is based on causality in the classical sense, whereas Wigner also calculated quantum corrections to Eq. (2.47) which account for the wave nature of the particles. Here we are only interested in an estimate of the order of magnitude and stick to the simple form.

The causality condition Eq. (2.47) can be utilized to derive an estimate of how far poles on the physical Riemann sheet have to stay away from the real axis. Suppose that the S-matrix has a pole on the upper have plane of the physical sheet at $W_0 = E_0 + i\Upsilon_0/2$ (with $\Upsilon_0 > 0$). Just as in Eq. (2.40) it takes the form

$$S_\ell(W) = \exp\big[2i\,\delta_\ell(W)\big] = \underbrace{\frac{W - E_0 + i\Upsilon_0/2}{W - E_0 - i\Upsilon_0/2}}_{S_\ell^{\text{pole}}} \exp\big[2i\,\delta_\ell^{\text{bg}}(W)\big] \ . \tag{2.48}$$

The derivative of the phase shift can then be expressed as

$$\frac{d}{dW}\delta_\ell = -\frac{i}{2}\frac{d}{dW}\ln S_\ell = -\frac{i}{2}\frac{d}{dW}\ln S_\ell^{\text{pole}} + \frac{d}{dW}\delta_\ell^{\text{bg}} \ . \tag{2.49}$$

Assuming that the background phase shift varies only slowly with energy we may neglect the last term and arrive at

$$\left.\frac{d\delta_\ell}{dW}\right|_{W=E_0} \approx -\frac{2}{\Upsilon_0} \ , \tag{2.50}$$

which in conjuction with Eq. (2.47) leads to the inequality

$$\Upsilon_0 \gtrsim \frac{2}{R} \, . \tag{2.51}$$

The range of the strong interactions is of the order of 1 fm. Consequently, we find that causality requires the S-matrix not to have poles above the real axis with $\Upsilon_0 \lesssim 400\,\mathrm{MeV}$. We will use this criterion to discard possible solutions of the BSE as unphysical.

Eq. (2.51) is meant as a rule of thumb. Certainly there are corrections to it due to quantum effects or in case the variation of the background phase is not negligible. Nevertheless it should give the right order of magnitude. We point out that this condition is already a weak assumption in view of the fact that one usually requires the S-matrix to be free of poles in the whole physical sheet, *e.g.* when employing dispersion relations.

Part I

η and η' decays

Chapter 3

Hadronic decays of η and η' [§]

3.1 Introduction

The hadronic decays of η and η' offer a possibility to study symmetries and symmetry breaking patterns in strong interactions. The η-η' system offers a testing ground for chiral SU(3) symmetry in QCD and the role of both spontaneous and explicit chiral symmetry breaking, the latter one induced by the light quark masses. In the absence of η-η' mixing, η would be the pure member η_8 of the octet of Goldstone bosons which arise due to spontaneous breakdown of chiral symmetry.

The isospin-violating decays $\eta, \eta' \to 3\pi$ can only occur due to an isospin-breaking quark mass difference $m_u - m_d$ or electromagnetic effects. While for most processes isospin-violation of the strong interactions is masked by electromagnetic effects, these corrections are expected to be small for the three pion decays of η and η' (Sutherland's theorem) [77] which has been confirmed in an effective Lagrangian framework [78, 79]. Neglecting electromagnetic corrections the decay amplitude is directly proportional to $m_u - m_d$. In principle it is therefore possible to determine the quark mass difference $m_u - m_d$ (or rather the ratio $(m_d - m_u)/(m_s - \hat{m})$ with $\hat{m} = (m_u + m_d)/2$) from the three pion decays of η and η'. Combining the one-loop results of ChPT [80] and dispersion relations this has been accomplished for the decay $\eta \to 3\pi$ [81, 82]. Very recently the result of a two-loop calculation in ChPT became available [83]. Long ago it was claimed in the literature that the quark mass ratio $(m_d - m_u)/(m_s - \hat{m})$ may also be extracted in a very simple manner from the branching ratio $\Gamma(\eta' \to \pi^+\pi^-\pi^0)/\Gamma(\eta' \to \eta\pi^+\pi^-)$ involving an isospin-breaking and an isospin-conserving hadronic decay mode of the η' [84]. We have critically examined the assumptions made in [84] within our chiral unitary framework.

Moreover, reactions involving the η' might provide insight into gluonic effects through the axial U(1) anomaly of QCD. The divergence of the singlet axial-vector current acquires an additional term involving the gluonic field strength tensor that remains in the chiral limit of vanishing light quark masses. This term prevents the pseudoscalar singlet η_0 from being a Goldstone boson which is phenomenologically manifested in its relatively large mass, $m_{\eta'} = 958\,\mathrm{MeV}$, *cf.* Sect. 1.5 for details.

[§] The contents of this chapter have been published in [75, 76].

An appropriate theoretical framework to investigate low-energy hadronic physics is provided by chiral perturbation theory, the effective field theory of QCD. In ChPT Green functions are expanded perturbatively in powers of Goldstone boson masses and small three-momenta. However, final-state interactions in $\eta \rightarrow 3\pi$ have been shown to be substantial both in a complete one-loop calculation in SU(3) ChPT [80] and using dispersion relations [81, 82, 85].

In η' decays final-state interactions are expected to be even more important due to larger phase space and the presence of nearby resonances. It is claimed, *e.g.*, that the exchange of the scalar resonance $a_0(980)$ dominates the decays $\eta' \rightarrow \eta\pi\pi$ [86] which has been confirmed both in a full one-loop calculation utilizing infrared regularization [47] and in a chiral unitary approach [49]. In the latter work, resonances are generated dynamically by iterating the chiral effective potentials to infinite order in a BSE, whereas in [47] the effects of the $a_0(980)$ are hidden in a combination of coupling constants of the effective Lagrangian.

In the present investigation we extend the approach of [49] by including p-wave interactions. This also allows us to obtain more realistic predictions for the decay $\eta' \rightarrow \pi^+\pi^-\pi^0$, where p-waves can—in principle—yield sizable contributions to the decay width and Dalitz slope parameters. We will illustrate that meson-meson scattering phase shifts along with available data on η, η' hadronic decays provide a set of tight constraints which must be met by theoretical approaches.

The physics of η and η' decays is a very lively field and investigations at many experimental facilities such as KLOE@DAΦNE, WASA-at-COSY, Crystal Ball at MAMI, VES at IHEP, CLEO at CESR, WASA@CELSIUS are currently being performed or have been finished lately. In this chapter we study the implications of two recent experiments by the KLOE [87] and the VES [88] Collaborations which have determined the Dalitz plot distributions of $\eta \rightarrow 3\pi$ and $\eta' \rightarrow \eta\pi^+\pi^-$, respectively, with high statistics. One should note that the preliminary result for the slope parameter of the $\eta \rightarrow 3\pi^0$ decay specified by the KLOE Collaboration in [87] is considerably smaller in magnitude than the one determined by another high precision experiment performed by the Crystal Ball (CB) Collaboration [89]. Very recently and after the publication of our results [75] where we pointed at questions of consistency between the KLOE numbers for the charged and the neutral three pion decay, the KLOE Collaboration has come forward with a reanalysis of their data [90] which resolves the discrepancy between the first analysis and the CB result. Nevertheless we will repeat here the critical discussion of the first KLOE results [87] as published in [75]. The new VES data are taken into account separately. It turns out that they furnish additional tight constraints on the chiral unitary framework that we utilize.

This chapter is organized as follows. In the next section we explain how the chiral unitary approach is applied to the hadronic decays of η and η'. It also includes a discussion of constraints imposed by unitarity. In Sect. 3.3 we present our results based on available data of the hadronic decay modes excluding the results of the KLOE and the VES Collaborations and we discuss the changes which arise if the new results by KLOE [87] (first analysis) and VES [88] are included. A critical examination of the $\eta \rightarrow 3\pi$ data of KLOE based on purely phenomenological arguments is presented in Sect. 3.4. In Sect. 3.5 we analyze the assumptions made in [84] and comment on the possibility to

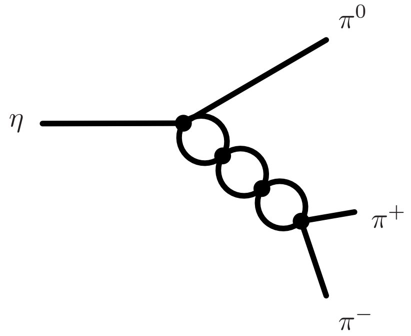

Figure 3.1: Shown is a possible contribution to final-state interactions in the decay $\eta \to \pi^+\pi^-\pi^0$.

extract $m_u - m_d$ from hadronic η' decays. We summarize our findings in Sect. 3.6.

3.2 Chiral unitary approach

3.2.1 Final state interactions

It was noted long ago that the tree level result of ChPT for the decay width of $\eta \to \pi^+\pi^-\pi^0$ (which coincides with the PCAC prediction) [91] underestimates the experimental value by roughly a factor of four. One-loop corrections have been shown to be important [80], but even when they are taken into account the resulting decay width remains considerably below the measured value [17]. In $\eta' \to 3\pi$ one expects even larger contributions from final-state interactions [49], whereas for $\eta' \to \eta\pi\pi$ reasonable agreement with experiment can also be achieved in a perturbative approach employing infrared regularization [47] which for this process provides a consistent counting scheme. In the present combined analysis of these three dominant hadronic decay modes of η and η' we include final-state interactions in a non-perturbative fashion as introduced in [49], but extending the work of [49] by taking p-waves into account and by improving the fit procedure for the unknown couplings in the chiral Lagrangian via Monte Carlo techniques.

The underlying idea of our approach is that the initial particle, *i.e.* the η or η', decays into three mesons and that two out of these rescatter (elastically or inelastically) an arbitrary number of times, see Fig. 3.1 for illustration. All occurring vertices are derived from the effective Lagrangian and are thus constrained by chiral symmetry. Interactions of the third meson with the pair of rescattering mesons are neglected which turns out to be a good approximation, particularly for the decays $\eta \to 3\pi$ and $\eta' \to \eta\pi\pi$. In the decays under consideration the two-particle states either carry one elementary charge or no net charge. Charge conservation prevents transitions between these two sets, while the different channels of one set are generally coupled. There are nine uncharged combinations of mesons

$$\pi^0\pi^0,\ \pi^+\pi^-,\ \eta\pi^0,\ K^+K^-,\ K^0\bar{K}^0,\ \eta\eta,\ \eta'\pi^0,\ \eta'\eta,\ \eta'\eta', \tag{3.1}$$

and a set of four positively charged channels

$$\pi^0\pi^+,\ \eta\pi^+,\ K^+\bar{K}^0,\ \eta'\pi^+ \,. \tag{3.2}$$

The negatively charged channels are related to the former via charge conjugation. For the p-waves there arise some simplifications in the uncharged channels. Due to Bose symmetry contributions from identical particles vanish and the remaining two-particle states can be classified according to their behavior under charge conjugation. While for $J = 1$ $\pi^+\pi^-$ and $K\bar{K}$ must be C-odd combinations, the other pairs are C-even, so that transitions between the two classes of states are forbidden.

The infinite rescattering of meson pairs is accomplished by utilizing the Bethe-Salpeter equation, see Chapter 2. From the U(3) effective Lagrangian up to fourth chiral order we derive tree level scattering amplitudes which are comprised in the interaction kernel of the BSE with coupled channels. The full list of $\mathcal{O}(p^4)$ terms in the Lagrangian is compiled in App. A.2 where we also specify the terms relevant for the present investigation. Since the vertices derived from $\mathcal{L}_\phi^{(4)}$ involve no more than four momenta, the partial wave decomposition of the interaction kernel V is limited to s-, p-, and d-waves

$$V = \sum_{\ell=0}^{2} V_\ell J_\ell \,. \tag{3.3}$$

For each partial wave we have the BSE, Eq. (2.20),

$$T_\ell = V_\ell - T_\ell G_\ell V_\ell$$

in the on-shell approximation. The loop integrals in G_ℓ are equipped with subtraction constants as explained at the end of Sect. 2.1. The symmetry factor for two identical particles in a loop is absorbed into the V_ℓ by multiplying the scattering amplitudes by a factor of $1/\sqrt{2}$ for each pair of identical particles. In the present work we restrict ourselves to s- and p-waves and drop the d-wave part T_2. As we will see in the following, this is a justified approximation since very good agreement with available data is achieved.

We now explain how the infinite chain of rescattering processes is included in the decay amplitudes to describe final-state interactions in a non-perturbative manner. We introduce a common notation for the decay modes investigated in this chapter and define Mandelstam variables

$$s = (p_h - p_i)^2, \quad t = (p_h - p_j)^2, \quad u = (p_h - p_k)^2 \tag{3.4}$$

for the generic process $h \to i\,j\,k$ and the $p_{h,i,j,k}$ represent the four-momenta of the particles. Since all decays under consideration happen to have a particle-antiparticle pair in the final state, *i.e.* either $\pi^+\pi^-$ or $\pi^0\pi^0$, which we denote by j and k with $j = \bar{k}$, C-invariance dictates that the decay amplitude $\mathcal{A}_{hijk}(s,t,u)$ is symmetric under $t \leftrightarrow u$. The full amplitude $\mathcal{A}_{hijk}$, which includes s- and p-wave final-state interactions, is constructed in such a way that it reproduces the tree level result and the unitarity corrections from one-loop ChPT. It reads

$$\begin{aligned}\mathcal{A}_{hijk}(s,t,u) = A_{hijk}(s,t,u) &+ \left(\sum_{\ell=0}^{1} J_\ell(s,t-u)\big[T_\ell(s) - V_\ell(s)\big]\right)_{hi,jk} \\ &+ \left(\sum_{\ell=0}^{1} J_\ell(t,u-s)\big[T_\ell(t) - V_\ell(t)\big]\right)_{hj,ik} \\ &+ \left(\sum_{\ell=0}^{1} J_\ell(u,s-t)\big[T_\ell(u) - V_\ell(u)\big]\right)_{hk,ij} \quad , \end{aligned} \tag{3.5}$$

where A_{hijk} is the complete tree level amplitude from ChPT up to fourth chiral order. The differences $T_\ell - V_\ell$ are introduced to avoid double-counting of tree graphs—the terms in parentheses start to contribute at the one-loop level. Depending on the subscripts of the parentheses which denote the pertinent meson pairs, T_ℓ and V_ℓ represent either the matrices of charged or uncharged channels. For identical particles in the final state ($\pi^0\pi^0$) they must be multiplied by a combinatorial factor of $\sqrt{2}$, in order to cancel the symmetry factor which was absorbed into the interaction kernel. We note that $\mathcal{A}_{hijk}$ does not involve the full one-loop result from ChPT since due to the on-shell approximation tadpole terms have been neglected. However, these contributions can be compensated numerically by redefining the couplings of the effective Lagrangian [63]. For consistency we also drop the tadpole contributions included in the corrections to the pseudoscalar decay constants, wave function renormalization and in π^0-η-η' mixing, see Sect. 1.5.2.

When neglecting isospin breaking via electromagnetic effects which is justified by Sutherland's theorem [77], the decay amplitudes of $\eta, \eta' \to 3\pi$ are directly proportional to the light quark mass difference $m_u - m_d$. Within ChPT this quantity is encoded in the combination

$$m_\epsilon^2 = B_0(m_d - m_u) \tag{3.6}$$

which is independent of the QCD renormalization scale. According to a theorem by Dashen [92] the electromagnetic contributions to the self-energies of m_{π^+} and m_{K^+} are equal in the chiral limit while those of the neutral mesons vanish (up to corrections of order e^4). In conjuction with the Gell-Mann–Oakes–Renner relations (1.43) this result can be utilized to express m_ϵ^2 in terms of physical masses

$$\begin{aligned} m_\epsilon^2 &= \big(m_{K^0}^2 - m_{K^+}^2\big)_{\text{QCD}} \\ &= \big(m_{K^0}^2 - m_{K^+}^2\big)_{\text{phys}} - \big(m_{K^0}^2 - m_{K^+}^2\big)_{\text{em}} \\ &= \big(m_{K^0}^2 - m_{K^+}^2 - m_{\pi^0}^2 + m_{\pi^+}^2\big)_{\text{phys}} \end{aligned} \tag{3.7}$$

up to corrections of $\mathcal{O}(e^2p^2, (m_d - m_u)p^2)$. Hence by making use of Dashen's theorem one is able to predict the decay width of $\eta \to 3\pi$ from a ChPT calculation, or one may turn the argument around and take possible deviations between theoretical and experimental results for $\Gamma(\eta \to 3\pi)$ as an indication for a violation of Dashen's theorem. We will come back to this issue in Sect. 3.3, where we discuss the numerical results of our calculation.

3.2.2 Unitarity

The approach described above incorporates the relevant pieces of the ChPT one-loop amplitude, fulfills unitarity constraints from two-particle scattering and has a clear diagrammatic representation of the final-state interactions: the summation of a bubble sum in each of the three two-particle channels. However, it does not account for three-body interactions in the final state, either mediated by the interaction of one of the two rescattering particles with the third, spectating particle or by a genuine three-body force. Therefore, the approach does not guarantee exact unitarity of the resulting S-matrix which implies a relation for the imaginary part of the decay amplitude $\mathcal{A}_{hijk}$, see *e.g.* [93],

$$\operatorname{Im}\mathcal{A}_{hijk} = \frac{1}{2}\sum_{a,b,c}(2\pi)^4\delta^{(4)}(p_i+p_j+p_k-p_a-p_b-p_c)\;\mathcal{T}^*_{abc,ijk}\;\mathcal{A}_{habc}\;, \tag{3.8}$$

where $\mathcal{T}^*_{abc,ijk}$ represents the complex conjugate of the scattering amplitude for $ijk \to abc$ and the sum, which includes the integration over phase space, runs over all possible three-particle states which h can decay into. A diagrammatic representation of the unitarity condition is shown in Fig. 3.2. For $\mathcal{T}_{abc,ijk}$ we make an approximation similar to the one already applied to $\mathcal{A}_{hijk}$, *i.e.* we drop the last diagram on the r.h.s. of Fig. 3.2 and keep only the graphs involving exclusively two-particle rescattering. The first term on the r.h.s. of Fig. 3.2 can be expressed in terms of the unitarized two-body scattering amplitude T, and Eq. (3.8) reduces to

$$\begin{aligned}
\operatorname{Im}\mathcal{A}_{hijk}(s,t,u) &= \sum_{\ell=0}^{1}\frac{1}{16\pi^2}\\
\times\Bigg[&\sum_{b,c}\int\frac{d^3p_b}{2p_b^0}\frac{d^3p_c}{2p_c^0}\Big\{J_\ell(s,t'-u')\,[T_\ell^{bc,jk}(s)]^*\mathcal{A}_{hibc}(s,t',u')\,\delta^{(4)}(p_b+p_c-p_j-p_k)\Big\}\\
&\sum_{a,c}\int\frac{d^3p_a}{2p_a^0}\frac{d^3p_c}{2p_c^0}\Big\{J_\ell(t,u'-s')\,[T_\ell^{ac,ik}(t)]^*\mathcal{A}_{hajc}(s',t,u')\,\delta^{(4)}(p_a+p_c-p_i-p_k)\Big\}\\
&\sum_{a,b}\int\frac{d^3p_a}{2p_a^0}\frac{d^3p_b}{2p_b^0}\Big\{J_\ell(u,s'-t')\,[T_\ell^{ab,ij}(u)]^*\mathcal{A}_{habk}(s',t',u)\,\delta^{(4)}(p_a+p_b-p_i-p_j)\Big\}\Bigg],
\end{aligned} \tag{3.9}$$

where, in analogy to the definition of $\mathcal{A}$, we only include two-particle rescattering in the s and p partial waves. The Mandelstam variables s', t', u' are defined by

$$s' = (p_h - p_a)^2\,,\qquad t' = (p_h - p_b)^2\,,\qquad u' = (p_h - p_c)^2\,. \tag{3.10}$$

However, the two spectator approximations utilized for the decay amplitude $\mathcal{A}$ within our approach, which determines the l.h.s. of Eq. (3.9), and on the r.h.s. of Eq. (3.9) do not coincide. Contributions like the one shown in Fig. 3.3 appear on the r.h.s. of Eq. (3.9), whereas such graphs are not included in our approach and are thus missing in $\operatorname{Im}\mathcal{A}$ on the l.h.s. Notice that Fig. 3.3 does not represent the full graph, but only a contribution to its imaginary part according to Cutkosky's cutting rules [94]. The violation of Eq. (3.9) gives

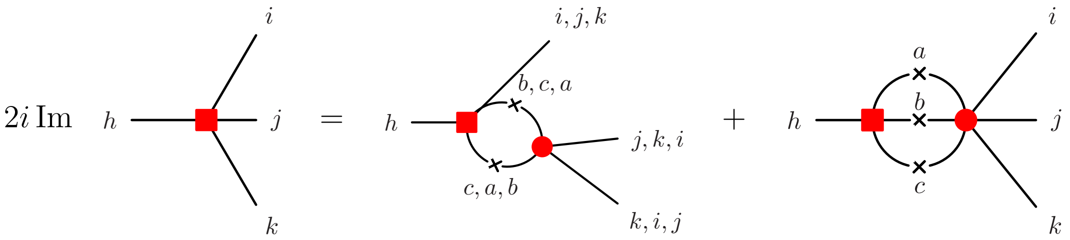

Figure 3.2: Diagrammatic representation of the unitarity relation in Eq. (3.8). The crosses indicate on-shell particles and phase space integration according to Cutkosky's cutting rules [94].

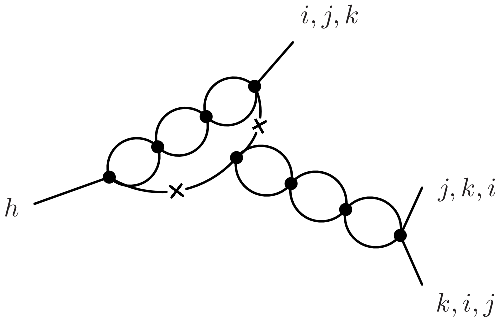

Figure 3.3: Contribution which is included on the r.h.s. of Eq. (3.8), but not in the decay amplitude $\mathcal{A}$ on the l.h.s. The crosses indicate on-shell particles and phase space integration according to the Cutkosky cutting rules [94].

us the possibility to estimate the importance of this class of three-body contributions which go beyond pure two-particle rescattering as embodied in $\mathcal{A}$. As we will discuss below, it turns out that these deviations are rather small for $\eta \to 3\pi$ and $\eta' \to \eta\pi\pi$ where phase space is narrow and dropping the last term in Fig. 3.2 appears to be a good approximation. This observation is confirmed by a new two-loop calculation of $\eta \to 3\pi$ where the contribution of the three particle cut is found to be small [83]. Assuming that structures involving more complicated iterated two-body interactions or three-body contact terms yield contributions comparable in size to the violation of Eq. (3.9) we conclude that our approach approximates the physical amplitude reasonably well.

For $\eta' \to 3\pi$, where phase space is about seven times larger than for $\eta \to 3\pi$, the violation of Eq. (3.9) comes out considerably more severe. However, this does not imply that our approach, which involves only two-particle rescattering, is not suited to describe $\eta' \to 3\pi$ since for the large phase space of this decay mode neglecting the last term in Fig. 3.2 is indeed not justified and hence Eq. (3.9) is not an appropriate estimate of unitarity corrections not included in the approach. Certainly the consistent inclusion of three-body interactions in our chiral unitary framework—possibly following the steps outlined by Mandelstam [95]—would constitute a major improvement of the approach, but is beyond the scope of the present work.

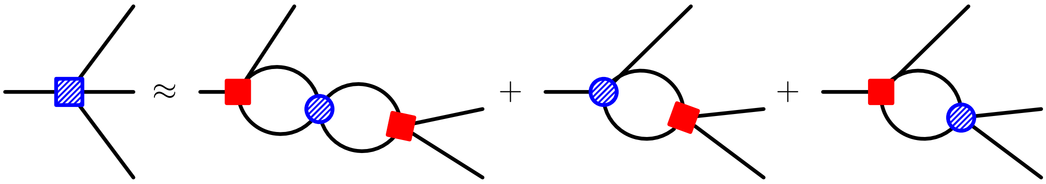

Figure 3.4: Isospin decomposition of the full amplitude for $\eta^{(\prime)} \to 3\pi$ (left-hand side) according to Eq. (3.12). The isospin-breaking vertices $V_\ell^{(\mathrm{ib})}$ are represented by shaded circles whereas the isospin-conserving $T_\ell^{(\mathrm{ic})}$ are symbolized by filled boxes.

3.2.3 Isospin decomposition

In order to study the importance of the various two-particle channels in the final-state interactions and corresponding contributions from well-known resonances such as $\rho(770)$, $f_0(980)$, $a_0(980)$ and the correlated $\pi\pi$ interaction known as the $\sigma(600)$, we perform a decomposition into isospin channels. Assigning one common mass for all particles of an isospin multiplet this can straightforwardly be done for the isospin-conserving decay modes $\eta' \to \eta\pi\pi$. To this aim, we decompose the interaction kernel of the Bethe-Salpeter equation, Eq. (2.20), into an isospin-conserving and an isospin-breaking part, $V_\ell^{(\mathrm{ic})}$ and $V_\ell^{(\mathrm{ib})}$, respectively, so that

$$V_\ell = O\, V_\ell^{(\mathrm{ic})}\, O^T + O\, V_\ell^{(\mathrm{ib})}\, O^T \ , \tag{3.11}$$

where O represents the orthogonal matrix which transforms from the isospin to the physical basis. Analogous to the definition of T_ℓ we can construct the unitarized amplitude $T_\ell^{(\mathrm{ic})}$ in the isospin limit by replacing V_ℓ by $V_\ell^{(\mathrm{ic})}$ in Eq. (2.20). After substituting in Eq. (3.5) the pieces of the form $[T_\ell - V_\ell]$ by $O[T_\ell^{(\mathrm{ic})} - V_\ell^{(\mathrm{ic})}]O^T$, the influence of the different isospin channels may be examined by omitting one specific combination of isospin and angular momentum quantum numbers.

The situation is slightly more complicated for the isospin-breaking decays of η and η' into three pions. Retaining only one isospin-breaking vertex and inserting it at all possible places in the bubble chain, the decay amplitude in terms of isospin channels is found by replacing in Eq. (3.5) the pieces of the form $[T_\ell - V_\ell]$ by

$$O[T_\ell^{(\mathrm{ic})}\, G_\ell\, V_\ell^{(\mathrm{ib})}\, G_\ell\, T_\ell^{(\mathrm{ic})} - T_\ell^{(\mathrm{ic})}\, G_\ell\, V_\ell^{(\mathrm{ib})} - V_\ell^{(\mathrm{ib})}\, G_\ell\, T_\ell^{(\mathrm{ic})}]O^T \ . \tag{3.12}$$

While the second and third term in the bracket describe the insertion of the isospin-breaking vertex at both ends of the bubble chain, the first one includes insertions at all intermediate points, see Fig. 3.4. Note that Eq. (3.12) indeed corresponds to a sum of graphs—the minus signs are due to our definition of the BSE in Eq. (2.20).

3.3 Results

3.3.1 Preface

We now turn to the discussion of the numerical results of the calculation which are obtained from a combined analysis of the decay widths, branching ratios, and slope parameters of the considered decays as well as phase shifts in meson-meson scattering. Our results, which are published in [75, 76], are based on the 2004 edition of *"The Review of Particle Physics"* [96]. Apart from the recent experimental results of the KLOE and the VES Collaborations which we discuss explicitly, the 2006 edition [17] has entailed slight changes in the partial decay widths of η and η' due to new experiments. However, the smallness of the changes makes us confident that none of our conclusions has to be altered. We will indicate the revised numbers from [17] at the pertinent places for comparison.

The widths of $\eta \to 3\pi$ and $\eta' \to \eta\pi\pi$ have been measured roughly at the 5–10 % precision level, while for $\eta' \to 3\pi^0$ the experimental uncertainty is considerably larger and only an upper limit exists for $\Gamma(\eta' \to \pi^+\pi^-\pi^0)$ [96]. Moreover, some of these decay widths are constrained by the well-measured branching ratios

$$r_1 = \frac{\Gamma(\eta \to 3\pi^0)}{\Gamma(\eta \to \pi^+\pi^-\pi^0)} , \qquad r_2 = \frac{\Gamma(\eta' \to 3\pi^0)}{\Gamma(\eta' \to \eta\pi^0\pi^0)} . \tag{3.13}$$

The Dalitz plot distribution of the decay $h \to i\,j\,k$ (with $j = \bar{k}$) is conventionally described in terms of the two variables

$$\begin{aligned} x &= \frac{\sqrt{3}(u-t)}{2m_h(m_h - m_i - 2m_{jk})} , \\ y &= \frac{(m_i + 2m_{jk})\big[(m_h - m_i)^2 - s\big]}{2m_h m_{jk}(m_h - m_i - 2m_{jk})} - 1 , \end{aligned} \tag{3.14}$$

where the $m_{h,i,j,k}$ denote the masses of the respective particles ($m_j = m_k = m_{jk}$) and the Mandelstam variables have been defined in Eq. (3.4). In $\eta \to 3\pi$ measurements, *e.g.* [97], a slightly simpler definition of y, where $(m_{\pi^0} + 2m_{\pi^+})/m_{\pi^+}$ is replaced by 3, is usually employed,

$$y = \frac{3\big[(m_h - m_i)^2 - s\big]}{2m_h(m_h - m_i - 2m_{jk})} - 1 , \tag{3.15}$$

but the difference is at the level of 1 % and can be safely neglected. The squared absolute value of the amplitude, $|\mathcal{A}_{hijk}(x,y)|^2$, is then expanded for $\eta' \to \eta\pi\pi$ and the charged decay modes of $\eta, \eta' \to 3\pi$ as

$$|\mathcal{A}(x,y)|^2 = |N|^2\big[1 + ay + by^2 + cx^2 + dy^3 + \cdots\big] , \tag{3.16}$$

while for the decays into three identical particles Bose symmetry dictates the form

$$|\mathcal{A}(x,y)|^2 = |N'|^2\big[1 + g(y^2 + x^2) + \cdots\big] . \tag{3.17}$$

The value of the single Dalitz plot parameter g which describes the decay $\eta \to 3\pi^0$ was debated controversially over the last few years after the first analysis of the KLOE Collaboration [87] became available. There a value of $g_{\text{KLOE}} = -0.026 \pm 0.010 \pm 0.008$ was found—in conflict with the number given by the Particle Data Group [96], which is identical with the result of a high-statistics measurement by the Crystal Ball (CB) Collaboration [89], $g_{\text{CB}} = -0.062 \pm 0.008$. Very recently and after our critical examination of the KLOE results in [75], the members of the KLOE Collaboration have reanalyzed their data and found inconsistencies in the treatment of the η mass in their first analysis. Having corrected this issue, they now arrive at $g_{\mathrm{KLOE}} = -0.054 \pm 0.008^{+0.008}_{-0.012}$ [90] resolving the discrepancy between the different experiments. In this context it is interesting to note that this value is also confirmed by a recent result of the WASA@CELSIUS experiment which yields $g_{\mathrm{WASA}} = -0.052 \pm 0.020 \pm 0.020$ [98], admittedly with large error bars. Moreover, the slope parameter g is currently being analyzed using the data sample collected with the Crystal Ball detector at MAMI-B which is roughly three times larger than the previous one taken with CB at the Brookhaven National Laboratory [89]. Apparently, preliminary results confirm the old CB value [99]. Final certainty about the value of g might be provided by the third high precision experiment aiming at a determination of g, the WASA-at-COSY experiment in Jülich [100].

For the Dalitz plot parameters a, b, c of $\eta \to \pi^+\pi^-\pi^0$ the experimental situation is also not without controversy. We employ the numbers of [97] since it is the most recent published measurement before the KLOE experiment and the results appear to be consistent with the bulk of the other experiments listed by the Particle Data Group [96]. They differ somewhat from the results of the KLOE Collaboration [87, 101], in particular for the Dalitz parameter b. Note that for $\eta \to \pi^+\pi^-\pi^0$ the two analyses of the KLOE Collaboration agree within error bars. For the first time they have extended the Dalitz plot parametrization to third order in x, y and find a non-zero value for d.

Recently the Dalitz plot parameters of $\eta' \to \eta\pi^+\pi^-$ have been determined with high statistics by the VES experiment [88]. While as a first step we will employ in our fits the experimental Dalitz parameters provided by the Particle Data Group [96], we will discuss in Sects. 3.3.7 and 3.3.8 the modifications of our results when the numbers of the first KLOE analysis [87] and the new data set of the VES Collaboration [88] are taken into account, respectively. Note that the slope parameters of $\eta' \to 3\pi$ have not yet been determined experimentally with significant statistics, but such a measurement is intended at WASA-at-COSY [100], at MAMI-C [102] and with KLOE-2 at DAΦNE [103].

From the unitarized partial-wave T-matrix in Eq. (2.20) one may also derive the phase shifts in meson-meson scattering. Hence, our approach is further constrained by the experimental phase shifts for $\pi\pi \to \pi\pi, K\bar{K}$ scattering. The results of the fit are presented in the next subsection.

The coupled-channels framework involves several parameters, *i.e.* the low-energy constants (LECs) of the chiral effective Lagrangian up to fourth order and the subtraction constants a in the loop integrals G which are embodied in the coupled-channels T-matrix. It turns out that only the fit to the $\pi\pi$ phase shifts in the $I = J = 1$ channel (which includes the ρ resonance) requires a non-zero value of the corresponding subtraction constant $a_{\pi\pi}^{(I=J=1)}(\mu)$. The regularization scale of G is set to $\mu = 1\,\mathrm{GeV}$ for all channels. As a guiding principle for the importance of the LECs and in order to reduce their number, we make use of large N_c arguments in the effective Lagrangian, *cf.* [37], and set all LECs to zero which are of order $\mathcal{O}(1/N_c^2)$ and thus suppressed by at least three powers of $1/N_c$ with respect to the leading coefficients. Their effects are expected to be small and can be partially compensated by readjusting the leading and subleading coefficients in our fits. Furthermore, we set those parameters to zero by hand to which the processes under consideration turn out to be less sensitive. We find that with the exception of $v_1^{(2)}$ and

$\beta_{14}^{(0)}$ all parameters of order $\mathcal{O}(1/N_c)$ have a negligible effect when varying them within small ranges around zero and can be safely neglected. To summarize, we only keep the LECs

$$\begin{gathered}\beta_0^{(0)},\,\beta_3^{(0)},\,\beta_5^{(0)},\,\beta_8^{(0)} = \mathcal{O}(N_c)\,,\\ v_0^{(2)},\,v_3^{(1)},\,\beta_1^{(0)},\,\beta_2^{(0)},\,\beta_4^{(0)},\,\beta_6^{(0)},\,\beta_7^{(0)},\,\beta_{13}^{(0)},\,\beta_{18}^{(0)},\, = \mathcal{O}(1)\,,\\ v_1^{(2)},\,\beta_{14}^{(0)} = \mathcal{O}(1/N_c)\,.\end{gathered} \tag{3.18}$$

The coefficient $v_0^{(2)}$ is related to the mass of the η' in the chiral limit, m_0, and has been constrained to the range $0.00183\,\mathrm{GeV}^4 \ldots 0.00523\,\mathrm{GeV}^4$ in [46]. The rest of the parameters may be varied within small ranges around zero for which we employ large N_c arguments. The coefficient of the kinetic term in the Lagrangian of second chiral order, which is counted as $\mathcal{O}(N_c)$, is $f^2/4$, *cf.* Eq. (1.102). Consequently, the boundaries for LECs of order $\mathcal{O}(N_c^k)$ are naturally given by $\pm N_c^{k-1} f^2/(4\Lambda_\chi^n)$, where n depends on the dimension of the constant under consideration and $\Lambda_\chi \approx 4\pi f \approx 1\,\mathrm{GeV}$ is the scale of spontaneous chiral symmetry breaking. In conventional ChPT the β_0 term is usually not listed, since it can be absorbed into other contact terms by virtue of a Cayley-Hamilton matrix identity. However, this transformation mixes different orders in $1/N_c$, hence we prefer to keep this term explicitly, in order to retain the clean large N_c behavior of the β_i's.

By fitting to all available data sets of the investigated hadronic η, η' decays which are collected in [96] and to the phase shifts an overall χ^2 function is calculated. To this end, we compute χ^2 values for all observables, *i.e.* phase shifts, decay widths, branching ratios and Dalitz plot parametrizations, divide them by the number of experimental data points and take the sum afterwards, *cf.* the treatment in [104]. In contrast to the conventional definition of the χ^2 function where each *data point* is weighted equally, this method ensures that the contribution from each *observable* is weighted in the same way in the total χ^2. Thereby one-point observables (such as decay widths) will not be subdued by observables with many data points (such as the phase shifts) as it may happen using the standard definition.

In order to find the minima of the overall χ^2 function, we perform a random walk in parameter space, where only steps which lead to a smaller χ^2 value are allowed, and a very large number of random walks with randomized starting points is carried out. We observe four different classes of fits which are all in very good agreement with the currently available data on hadronic decays from [96], but differ in the description of the decays $\eta' \to 3\pi$ where experimental constraints are scarce.

As a matter of fact the constraints set by the experimental data from [96] turn out to be rather mild in view of the number of parameters included in our approach. We therefore do not attempt to give 1σ errors of our results in the usual way by taking into account all fits with an overall χ^2/d.o.f. less than

$$\frac{\chi^2_{\mathrm{min}}}{\mathrm{d.o.f.}} + \frac{\Delta\chi^2}{\mathrm{d.o.f.}} \tag{3.19}$$

with $\Delta\chi^2/\mathrm{d.o.f.} \approx 1$ [17], see also the discussion in Sect. 4.5. Instead the errors which we specify in the following for all parameters and observables are rather intended to

I	J	Riemann sheet	$\mathrm{Re}\sqrt{s_0}$ [MeV]	$\mathrm{Im}\sqrt{s_0}$ [MeV]	$\sqrt{s_0}$ [109] [MeV]	associated resonance
0	0	III	464 ± 6	-211 ± 17	$442 - 227i$	σ
1	1	IV	749 ± 3	-69.5 ± 1.2	$759 - 70.5i$	$\rho(770)$
0	0	IV	988 ± 11	-17 ± 10	$994 - 14i$	$f_0(980)$
0	0	V	998 ± 10	-29 ± 11	—	$f_0(980)$
0	0	VI	916 ± 52	-88 ± 37	—	$f_0(980)$
1	0	IV	1023 ± 24	-69 ± 6	$1055 - 21i$	$a_0(980)$
1	0	V	876 ± 43	-105 ± 17	—	$a_0(980)$
1	0	VI	848 ± 47	-95 ± 17	—	$a_0(980)$

Table 3.1: Positions $\sqrt{s_0}$ of resonance poles in the complex $\sqrt{s}$ plane associated with isospin I and angular momentum J. Our results are compared to the pole positions found in a similar chiral unitary framework [109]. See text for details.

illustrate how small variations of the total χ^2 affect the results. To this end we take into account fits with χ^2 values which are at most 15 % larger than the minimum value. Surely this choice is somewhat arbitrary, but it enables us to separate the observed four different classes of fits with their different features.

3.3.2 Phase shifts and resonance poles

In Fig. 3.5 we show the results for the phase shifts of four meson-meson channels: the $I = 0, 2$ s-wave and $I = 1$ p-wave $\pi\pi \to \pi\pi$ scattering as well as $\pi\pi \to K\bar{K}$ with $I = J = 0$. The agreement with the experimental data points is remarkably good. The shaded areas indicate the variation of the results when the overall χ^2 value of the fits is allowed to exceed the minimum by at most 15 %, see the discussion in the previous subsection. The variation is particularly small for $I = J = 1$ $\pi\pi$ scattering which involves the $\rho(770)$ resonance. This fact is, however, not surprising since this channel is controlled by an additional fit parameter, the subtraction constant $a_{\pi\pi}^{(I=J=1)}$, and is only weakly constrained by the Dalitz plots of $\eta \to 3\pi$ and $\eta' \to \eta\pi\pi$ (for which precise experimental data exist) as they are dominated by s-waves.

We have furthermore extracted the resonance poles of T_ℓ in the complex $\sqrt{s}$ plane which are generated dynamically within the chiral unitary approach. The results are compiled in Table 3.1. Due to the multi-sheeted structure of the scattering amplitude it is necessary to specify on which of the unphysical Riemann sheets the poles are located. We use Roman numerals to denote the various Riemann sheets where "I" corresponds to the physical sheet, "II" to the unphysical sheet which is connected to the physical real axis between the two lowest thresholds at $\sqrt{s} = 2m_{\pi^0}$ and $\sqrt{s} = 2m_{\pi^+}$ and so on for the remaining thresholds in ascending order ($\pi^0\pi^0$, $\pi^+\pi^-$, $\eta\pi^0$, K^+K^-, $K^0\bar{K}^0$, $\eta\eta$, $\eta'\pi^0$, $\eta'\eta$, $\eta'\eta'$ for the neutral channels). Riemann sheets which are not directly connected to the physical real axis are not considered here since poles on these sheets do not have much influence on physical observables. The pole corresponding to the ρ resonance is found on

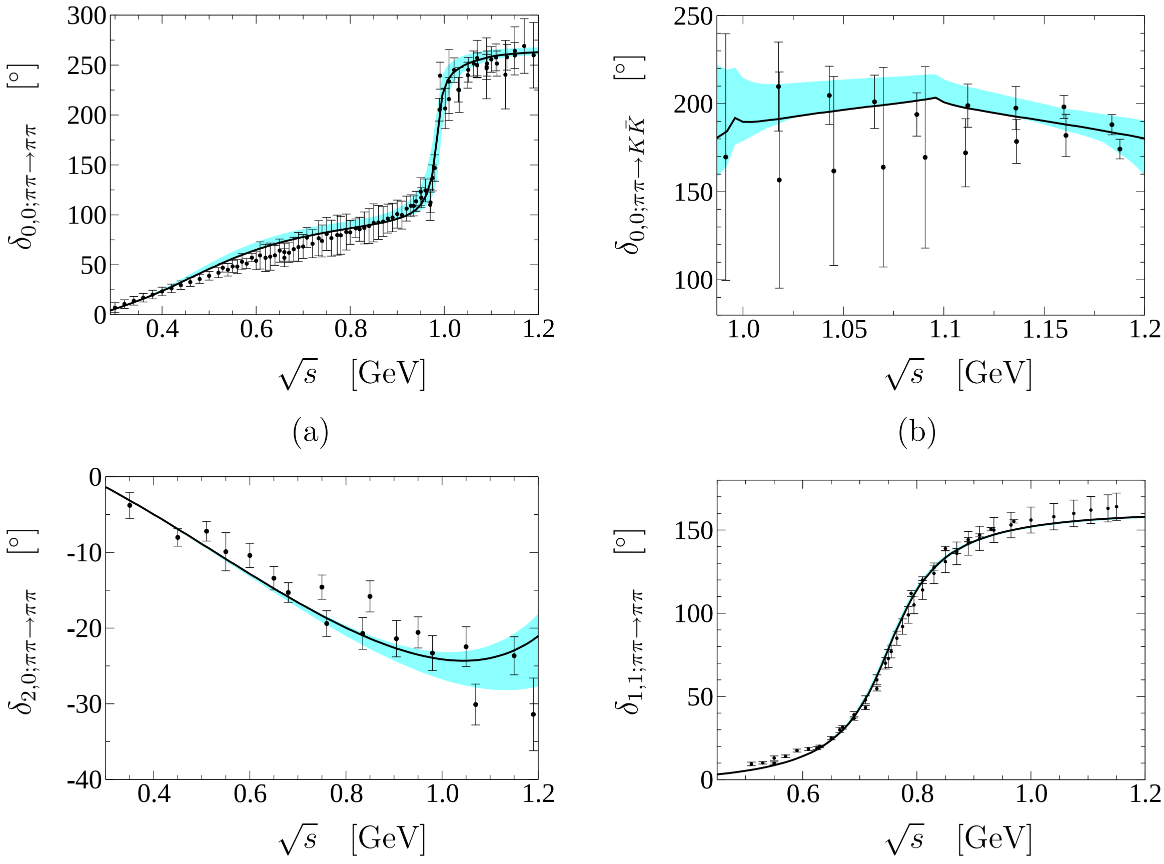

(a) (b)

(c) (d)

Figure 3.5: Results for the phase shifts $\delta_{I,J}$ of meson-meson scattering for isospin I and partial wave J. The shaded area indicates the range of fits taken into account within our approach, while the solid line represents the best fit in each particular channel. The data are taken from (a) [105], (b) [106], (c) [107], (d) [108].

Riemann sheet "IV" which is connected to the real axis between the $\eta\pi^0$ and the K^+K^- threshold. The tiny error band of the $I = J = 1$ phase shift in Fig. 3.5 is reflected by small errors of the position of the ρ pole. Using the relation (*cf.* Eq. (2.39))

$$\sqrt{s_0} = M - \frac{i}{2}\Gamma \tag{3.20}$$

we may translate the pole position $\sqrt{s_0}$ into the mass M and the width Γ of the corresponding resonance. We obtain $M_\rho = (749 \pm 3)\,\text{MeV}$, $\Gamma_\rho = (139 \pm 3)\,\text{MeV}$ which is to be compared to the measured values $M_\rho = (775.5 \pm 0.4)\,\text{MeV}$, $\Gamma_\rho = (149.4 \pm 1.0)\,\text{MeV}$ quoted in [17], *i.e.* even though we did not impose explicit constraints on the position of the pole the numbers turn out to be in the right ballpark. The pole associated with the σ is not as tightly fixed as the ρ pole. We find $M_\sigma = (464 \pm 6)\,\text{MeV}$, $\Gamma_\sigma = (422 \pm 33)\,\text{MeV}$, in reasonable agreement with a recent, precise extraction of these parameters using Roy equations, $M_\sigma = 441^{+16}_{-8}\,\text{MeV}$, $\Gamma_\sigma = 544^{+18}_{-25}\,\text{MeV}$ [110].

The $f_0(980)$ resonance in the $I = J = 0$ channels is located right at the K^+K^- and $K^0\bar{K}^0$ thresholds and may therefore be identified with poles on the three nearby Riemann sheets "IV", "V", "VI". We indeed find poles close to the real axis on all these sheets, yet at different values of $\sqrt{s}$, see Table 3.1. The pole on Riemann sheet "VI" is relatively far away from the real axis whereas the one on sheet "V" only influences the small interval between the two $K\bar{K}$ thresholds. Hence the pole on sheet "IV" is certainly the most relevant one for the $f_0(980)$ resonance and yields $M_{f_0} = (988 \pm 11)\,\text{MeV}$, $\Gamma_{f_0} = (33 \pm 20)\,\text{MeV}$.

For lack of experimental data the phase shifts of $I = 1$ s-wave meson-meson scattering are not constrained by the fit. Nevertheless the chiral unitary approach generates poles in the isospin one amplitude at the energy of the $a_0(980)$. As in the case of the $f_0(980)$ we find poles on all close-by Riemann sheets out of which the one on sheet "IV" is again closest to the real axis. Its distance from the real axis is significantly larger than that of the corresponding $f_0(980)$ pole on sheet "IV" leading to $M_{a_0} = (1023 \pm 24)\,\text{MeV}$, $\Gamma_{a_0} = (139 \pm 11)\,\text{MeV}$.

Due to the presence of the $K\bar{K}$ thresholds roughly at 990 MeV the scalar mesons $a_0(980)$, $f_0(980)$ do not appear as simple Breit-Wigner resonances in physical observables such as cross sections. It is therefore hard to determine their masses and, in particular, their widths directly from experiment without making use of model-dependent assumptions. While for the masses the PDG quotes comparatively small errors, $M_{f_0} = (980 \pm 10)\,\text{MeV}$, $M_{a_0} = (984.7 \pm 1.2)\,\text{MeV}$, the widths are much less precisely known $\Gamma_{f_0} = (40 \ldots 100)\,\text{MeV}$, $\Gamma_{a_0} = (50 \ldots 100)\,\text{MeV}$ [17].

In Table 3.1 we also compare our results to the pole positions obtained in a similar chiral unitary approach [109]. The agreement is good with exception of the width of the $a_0(980)$ which comes out considerably smaller in [109]. Notice that in [109] the calculation is performed in the isospin limit where the two $K\bar{K}$ thresholds coincide and sheet "V" is not present. The Riemann sheet "VI" has not been examined in that work and no error estimates for the pole positions are given.

3.3.3 $\eta \to 3\pi$

The results for the decays $\eta \to 3\pi$, which agree very well with the experimental values, are shown in Table 3.2. We also compare our results to the very recent two-loop calculation in ChPT [83]. Most remarkably our approach is able to reproduce the precise value of the $\eta \to 3\pi^0$ Dalitz parameter g measured by the Crystal Ball Collaboration [89] (and prevailing the PDG average value [96]) which could neither be met in previous investigations [49, 81] nor in the new two-loop calculation [83], where even a positive central value is found for g. The different result compared to [49] is mainly due to the larger number of chiral parameters taken into account in the present work and the improved fitting routine utilized. With regard to [83] one should mention that while the LECs are treated as fit parameters in our approach, in the perturbative framework of [83] they are taken as fixed input parameters. At $\mathcal{O}(p^2)$ and $\mathcal{O}(p^4)$ in ChPT the LECs have been determined from phenomenological input within certain errors, see [4]. Up to now experimental data and information from lattice QCD is, however, not sufficient to constrain the numerous LECs at $\mathcal{O}(p^6)$. In [83] the relevant LECs at sixth chiral order have therefore been estimated using the method of resonance saturation, which introduces some model-dependence, and no error ranges are given for the values of these LECs. The errors of the Dalitz plot parameters quoted in [83] do thus not reflect the uncertainty in the determination of the LECs, but merely represent the fitting errors resulting from the extraction of the Dalitz coefficients by fitting the polynomials in Eqs. (3.16), (3.17) to the full amplitudes squared.

In Table 3.2 we also display the updated PDG numbers for the branching ratios and decay widths [17] as well as the new results of the CLEO experiment [111] (using an η width of $(1.30 \pm 0.07)\,\mathrm{keV}$ [17]). In a conservative manner we have added the statistical and systematic uncertainties from [111] linearly. Since these new experimental results appeared after the publication of our investigation [75] they are not included in the fit, but they are sufficiently close to the old numbers so that none of our conclusions has to be altered.

When electromagnetic effects are neglected (which is justified according to Sutherland's theorem [77]), the isospin-violating decay of η into three pions can only take place via a finite quark mass difference $m_u - m_d$. The decay amplitude is therefore proportional to m_ϵ^2 defined in Eq. (3.6) and we have employed the value which follows from Dashen's theorem, Eq. (3.7). Deviations of the calculated decay widths from the measured numbers could thus be interpreted as a hint to non-negligible subleading corrections to the leading order result by Dashen. In order to quantify these deviations, one commonly defines the double quark mass ratio

$$Q^2 = \frac{m_s - \hat{m}}{m_d - m_u} \frac{m_s + \hat{m}}{m_d + m_u} \,, \tag{3.21}$$

for which Dashen's theorem yields $Q_{\text{Dashen}} = 24.1$. Differing Q-values lead to decay widths which are related to the original one, Γ_{Dashen}, by

$$\Gamma = \left(\frac{Q_{\text{Dashen}}}{Q} \right)^4 \Gamma_{\text{Dashen}} \,. \tag{3.22}$$

Taking into account theoretical as well as experimental uncertainties we find from a comparison of our results with data $Q = 24.0 \pm 0.6$ which is consistent with the result of

	$\Gamma_{\eta\to 3\pi^0}$ [eV]	$\Gamma_{\eta\to\pi^+\pi^-\pi^0}$ [eV]	r_1
this work	422 ± 13	290 ± 8	1.46 ± 0.02
ChPT 2-loop [83]	—	—	1.47
exp. (PDG '04) [96]	419 ± 27	292 ± 21	1.44 ± 0.04
exp. (PDG '06) [17]	421 ± 22	294 ± 16	1.43 ± 0.04
exp. (CLEO) [111]	442 ± 34	294 ± 25	1.496 ± 0.078

	a	b	c
this work	-1.20 ± 0.07	0.28 ± 0.05	0.05 ± 0.02
ChPT 2-loop [83]	-1.27 ± 0.08	0.39 ± 0.10	0.06 ± 0.06
exp. [97]	-1.22 ± 0.07	0.22 ± 0.11	0.06 ± 0.02

	g
this work	-0.062 ± 0.006
ChPT 2-loop [83]	0.026 ± 0.064
exp. (PDG) [17, 96]	-0.062 ± 0.008

Table 3.2: Results for the partial decay widths of $\eta \to 3\pi$, the branching ratio r_1, and the Dalitz plot parameters compared to the new two-loop calculation in ChPT [83] and experimental data. See text for further details.

[49]. Note, however, that this obvious agreement with Dashen's theorem merely reflects the fact that our approach is capable of reproducing the experimental decay widths of $\eta \to 3\pi$. Due to the larger number of chiral parameters with increased ranges compared to [49] and the improved fitting procedure we can easily compensate the effects from variations in Q by readjusting the chiral parameters of our approach. We have checked that variations of Q in the range of $20 \ldots 24$ which covers the various (and partially contradictory) results in the literature [112] can be accommodated within this approach. Therefore, our analysis does not allow for conclusions on the size of the violation of Dashen's theorem. We remark that the new two-loop calculation [83] yields $Q = 23.2$ compatible with our result and indicating only small corrections to Dashen's theorem.

Extending the work of [49] we have also taken p-wave final-state interactions into account. By setting these contributions to zero, we find that the decay width of $\eta \to \pi^+\pi^-\pi^0$ is reduced by a tiny fraction of $0.7\,\%$ implying rapid convergence of the partial wave expansion. The Dalitz plot parameters, which are more sensitive to the precise form of the amplitude than the width, are also only moderately altered. Without p-waves we obtain $a = -1.15 \pm 0.07$, $b = 0.29 \pm 0.05$, $c = 0.01 \pm 0.02$. (Relative to its small central value the change of the coefficient c may appear large, but on the absolute scale set by the Dalitz distribution, which is normalized to one at $x = y = 0$, it is small.) Note that due to Bose symmetry there is no p-wave contribution to the decay into three neutral pions.

Certainly, the most important isospin channel of final-state interactions in $\eta \to 3\pi$ is the $I = 0$ s-wave rescattering which is dominated by $\pi\pi$ interactions. Omitting this channel reduces the decay width by $73\,\%$ on average. The other two s-wave channels with isospin one and two, respectively, interfere destructively with the former. To be more precise, taking out the $I = 1$ part, which mainly reflects $\pi\eta$ interactions, enlarges the decay width of $\eta \to \pi^+\pi^-\pi^0$ ($\eta \to 3\pi^0$) by 9 % (10 %), while setting the $I = 2$ channel, which is purely $\pi\pi$ rescattering, to zero results in an enhancement of the decay widths by 16 % (20 %). The only relevant p-wave contributions arise from the $I = 1$ channels. Neglecting these channels reduces the $\eta \to \pi^+\pi^-\pi^0$ decay width by roughly 1 %. The numerical difference to the 0.7 % stated above is due to the fact that for the decomposition into isospin channels we use isospin-symmetrized masses, while otherwise we employ the physical values of the masses.

Finally, we have also examined to which extent the amplitude violates three-particle unitarity in the spectator approximation as described in Sect. 3.2.2. In order to quantify the violation of Eq. (3.9), we compute the absolute value of the difference between l.h.s. and r.h.s. divided by the modulus of the amplitude $\mathcal{A}_{hijk}$. Averaged over the whole Dalitz plot we find this violation to be $(2.5 \pm 0.3)\,\%$ for the process $\eta \to \pi^+\pi^-\pi^0$ and—even smaller—$(1.3 \pm 0.3)\,\%$ for the decay into three neutral pions. The fact that the violation of Eq. (3.9) is so small is non-trivial since only two-body unitarity, but not three-body unitarity is implemented in our approach. This may suggest that three-body effects (such as multiple scattering of one particle in the final state with the other two or a genuine three-body interaction) are of the same order of magnitude.

3.3.4 $\eta' \to 3\pi$

Only sparse experimental information exists on the decays of the η' into three pions. The experimental decay width of $\eta' \to 3\pi^0$ is [96]*

$$\Gamma^{(\mathrm{exp})}(\eta' \to 3\pi^0) = (315 \pm 78)\,\mathrm{eV} \tag{3.23}$$

which is nicely met within our approach:

$$\Gamma^{(\mathrm{theo})}(\eta' \to 3\pi^0) = (330 \pm 33)\,\mathrm{eV}\,. \tag{3.24}$$

For the decay into $\pi^+\pi^-\pi^0$ only a weak experimental upper limit exists [17, 96]

$$\Gamma^{(\mathrm{exp})}(\eta' \to \pi^+\pi^-\pi^0) < 10\,\mathrm{keV}\,. \tag{3.25}$$

Due to the large phase space available in these two decay modes of the η', final-state interactions are expected to be of greater importance. Indeed we find that in contrast to the processes $\eta \to 3\pi$ and $\eta' \to \eta\pi\pi$ the Dalitz plot distribution of $\eta' \to 3\pi$ can—depending on the values of the chiral parameters—mostly not be well parametrized by a simple second or third order polynomial in x and y. Nevertheless, it happens that all our fits may be classified into four groups mainly due to the different values of the lower order coefficients in x and y. The numerical results for these most relevant coefficients are compiled in Tables 3.3 and 3.4 along with the predicted width of $\eta' \to \pi^+\pi^-\pi^0$ and the order of the polynomial in x and y which is needed to obtain a reasonable approximation to the Dalitz plot distribution resulting from our approach. Note that

---

*The updated value in [17] is $\Gamma(\eta' \to 3\pi^0) = (320 \pm 60)\,\mathrm{eV}$.

	cluster 1	cluster 2	cluster 3	cluster 4
$\Gamma_{\eta'\to\pi^+\pi^-\pi^0}$ [eV]	470 ± 200	520 ± 200	740 ± 420	620 ± 180
coeff. y (“a”)	0.6 ± 5.2	2.4 ± 1.7	0.3 ± 1.1	4.4 ± 1.2
coeff. y^2 (“b”)	10.0 ± 11.0	2.1 ± 7.5	-5.2 ± 1.5	14.9 ± 6.7
coeff. x^2 (“c”)	0.1 ± 3.6	-0.7 ± 1.4	0.1 ± 1.6	-3.7 ± 1.5
coeff. y^3 (“d”)	-6.1 ± 11.5	-0.6 ± 14.0	-8.8 ± 7.8	27.5 ± 18.1
coeff. x^2y	-10.8 ± 11.2	2.0 ± 3.0	-7.4 ± 5.6	-1.5 ± 2.8
coeff. y^4	0.6 ± 12.2	-3.2 ± 7.3	23.3 ± 20.7	24.5 ± 11.6
coeff. x^2y^2	13.9 ± 23.6	11.8 ± 22.4	-17.7 ± 9.4	39.0 ± 12.7
coeff. x^4	-0.5 ± 11.5	-1.2 ± 16.1	15.4 ± 9.8	-20.5 ± 9.4
poly. order	$6-8$	$4-8$	≥ 8	≥ 8

Table 3.3: Results for the decay width of $\eta' \to \pi^+\pi^-\pi^0$ and the leading Dalitz plot parameters. The last line denotes the order of the polynomial which is needed to describe the Dalitz plot distribution.

due to charge conjugation invariance, only even powers of x appear. Examples of two very different Dalitz plots are shown in Fig. 3.6. Despite these differing predictions one should keep in mind that all fits describe all available experimental data in [96] at the same level of accuracy. The Dalitz plot distributions of these decays pose therefore tight constraints for our approach and must be compared with ongoing experiments at the WASA-at-COSY facility [100] and at MAMI-C [102] as well as with upcoming measurements at KLOE-2 [103].

While in $\eta' \to 3\pi^0$ p-wave contributions in two-body rescattering are forbidden by Bose symmetry, they can be large in $\eta' \to \pi^+\pi^-\pi^0$ due to large phase space. Interestingly, their size varies significantly depending on the cluster of fit parameters. They are largest for the fits of cluster 4 where setting them to zero diminishes the decay width by 50 % on average. The partial width is reduced by 44 % (28 %) for cluster 3 (cluster 1), while

	cluster 1	cluster 2	cluster 3	cluster 4
coeff. x^2, y^2 (“g”)	0.1 ± 1.7	-2.7 ± 1.0	-2.1 ± 0.7	-0.2 ± 0.6
coeff. y^3	-0.5 ± 1.4	-1.7 ± 0.7	-0.2 ± 0.6	-0.8 ± 0.6
coeff. x^2y	1.6 ± 4.1	5.0 ± 1.9	0.6 ± 1.8	2.3 ± 1.7
coeff. y^4	0.2 ± 1.4	2.6 ± 1.5	1.6 ± 0.8	-0.1 ± 1.1
coeff. x^2y^2	0.4 ± 2.9	5.3 ± 2.8	3.5 ± 1.7	0.2 ± 2.5
coeff. x^4	0.1 ± 1.5	2.7 ± 1.5	1.7 ± 0.9	0.1 ± 1.2
poly. order	$3-6$	$5-6$	$4-6$	$3-5$

Table 3.4: Results for the leading Dalitz plot parameters of $\eta' \to 3\pi^0$. The last line denotes the order of the polynomial which is needed to describe the Dalitz plot distribution.

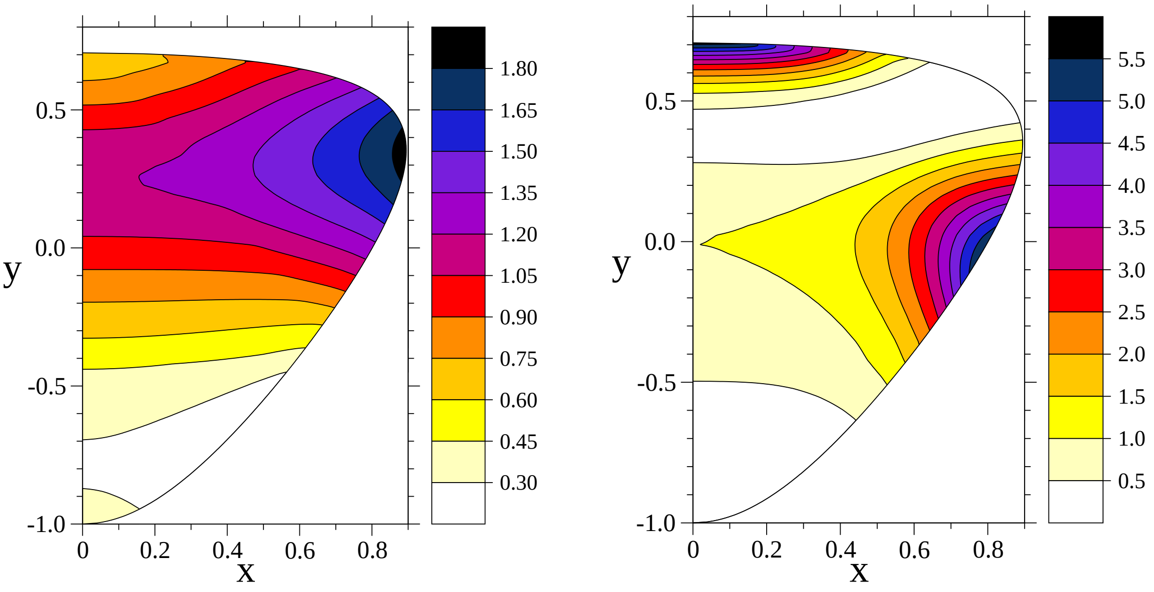

(a) (b)

Figure 3.6: Sample $\eta' \to \pi^+\pi^-\pi^0$ Dalitz plot distribution $|\mathcal{A}(x,y)/\mathcal{A}(0,0)|^2$ of cluster 2 which can be described by a fourth order polynomial in x and y (a) and of cluster 3 which must be parametrized by a polynomial of eighth order (b). Due to their symmetry under $x \to -x$ only the right halves of the Dalitz plots are shown.

for the parameter sets of cluster 2 suppressing the p-wave contributions alters the width by less than 10 %. The large higher order coefficients of the $\eta' \to \pi^+\pi^-\pi^0$ Dalitz plot distribution are mainly due to p-wave contributions. If p-waves are omitted, the fits of clusters 3 and 4 can be well parametrized by polynomials of fifth order in x and y, while for most fits in clusters 1 and 2 a sixth order polynomial would be sufficient, *cf.* Table 3.3. Note that due to C-invariance p-wave final-state interactions with the quantum numbers of the $\rho^0(770)$ meson do not occur.

In $\eta' \to 3\pi$ the contributions from the various isospin channels depend sensitively on the cluster, *e.g.*, omitting the $I = J = 0$ channel in $\eta' \to 3\pi^0$ reduces the decay width by 84 % for cluster 1, while it is enhanced by 132 % on average for the fits of cluster 3. For brevity we refrain from giving the full list of isospin contributions.

3.3.5 $\eta' \to \eta\pi\pi$

In Tables 3.5 and 3.6 we show the results for the dominant hadronic decay modes of the η', namely the decays into $\eta\pi^+\pi^-$ and $\eta\pi^0\pi^0$. They are all in very good agreement with the experimental data from [96]. Furthermore, we have calculated the branching ratio r_2, Eq. (3.13), which links the two neutral decay modes $\eta' \to 3\pi^0$ and $\eta' \to \eta\pi^0\pi^0$. We find

$$r_2^{(\text{theo})} = (71 \pm 7) \times 10^{-4}, \qquad r_2^{(\text{exp})} = (74 \pm 12) \times 10^{-4} \quad [17,\, 96], \tag{3.26}$$

and the accordance with experiment is again persuasive.

In the isospin limit, $m_u = m_d$, the decay width $\Gamma(\eta' \to \eta\pi^+\pi^-)$ would be exactly

	$\Gamma_{\eta'\to\eta\pi^+\pi^-}$ [96]†	a [113]	b	c
this work	81 ± 4 keV	-0.116 ± 0.024	0.000 ± 0.019	0.016 ± 0.035
exp.	89 ± 11 keV	-0.16 ± 0.06		

Table 3.5: Results for the partial decay width of $\eta'\to\eta\pi^+\pi^-$ and the Dalitz plot parameters compared to experimental data as indicated in the first line.

	$\Gamma_{\eta'\to\eta\pi^0\pi^0}$ [96]†	a [114]	b [114]	c [114]
this work	46 ± 3 keV	-0.122 ± 0.025	0.003 ± 0.018	0.019 ± 0.039
exp.	42 ± 6 keV	-0.116 ± 0.026	0.003 ± 0.017	0.00 ± 0.03

Table 3.6: Results for the partial decay width of $\eta'\to\eta\pi^0\pi^0$ and the Dalitz plot parameters compared to experimental data as indicated in the first line.

given by 2 $\Gamma(\eta'\to\eta\pi^0\pi^0)$, due to the symmetry factor for identical particles in the latter process. If, however, one is interested in the isospin-breaking contributions in the amplitude of $\eta'\to\eta\pi\pi$, one ought to disentangle it from phase space effects which are caused by the different masses of charged and neutral pions. With an isospin-symmetric decay amplitude, but physical masses in the phase space factors, we find a ratio

$$r_3=\frac{\Gamma(\eta'\to\eta\pi^+\pi^-)}{\Gamma(\eta'\to\eta\pi^0\pi^0)}=1.78\pm0.02\,, \tag{3.27}$$

which is smaller than 2 and compares to $r_3=1.77\pm0.02$ when isospin-breaking is taken into account in the amplitude. (For comparison, if the amplitude is set constant and the physical pion masses are employed in the phase space integrals, the ratio is given by $r_3=1.77$.) We may thus conclude that within our approach isospin-breaking corrections in the $\eta'\to\eta\pi\pi$ decay amplitude are tiny. The branching ratio r_3 has not been measured directly. If, however, we calculate the ratio of fractions $\Gamma_i/\Gamma_{\text{total}}$ for these two decay modes using the numbers and correlation coefficients published by the Particle Data Group [96], we arrive at†

$$r_3^{(\text{exp})}=2.12\pm0.19 \tag{3.28}$$

by means of standard error propagation. Such a large branching ratio would indicate significant isospin-violating contributions in the amplitude. But the experimental uncertainties are sizable and should be reduced by the experiments with WASA-at-COSY [100], at MAMI-C [102] or with KLOE-2 at DAΦNE [103].

It turns out that p-wave final-state interactions are tiny in the processes $\eta'\to\eta\pi\pi$. The corrections to the decay widths which they generate are smaller than 0.02 % and can thus be safely neglected. Consequently, in the isospin basis the relevant two-body channels are given by s-wave interactions of isospin 0 or 1 states. When examining the influence of these two channels on the $\eta'\to\eta\pi\pi$ partial widths we observe an interesting

---

[†] The updated values in [17] are $\Gamma(\eta'\to\eta\pi^+\pi^-)=(90\pm8)\,\text{keV}$, $\Gamma(\eta'\to\eta\pi^0\pi^0)=(42\pm4)\,\text{keV}$, and $r_3=2.14\pm0.18$.

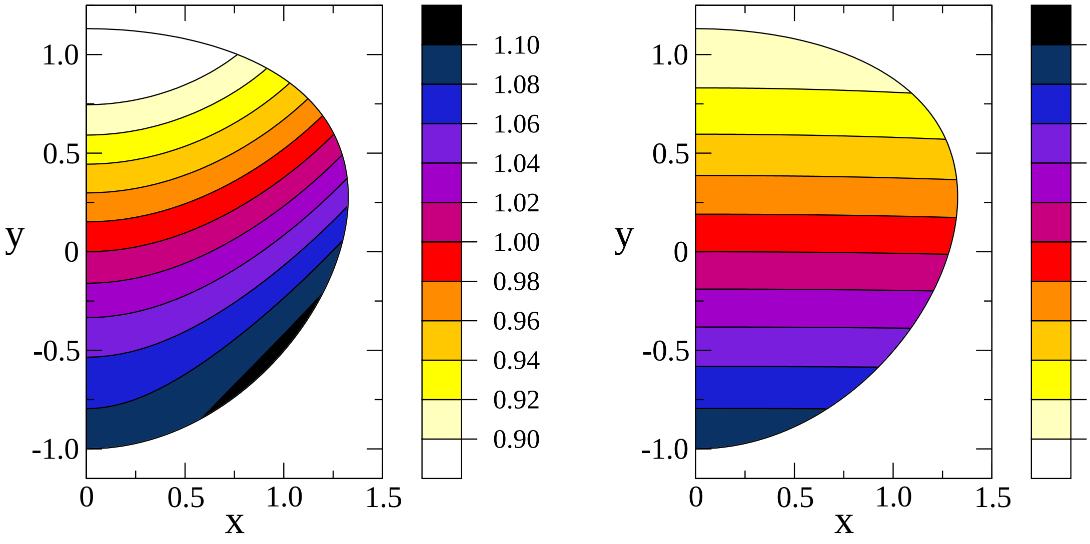

(a) (b)

Figure 3.7: Typical Dalitz plot distribution of $\eta' \to \eta\pi^+\pi^-$ for a fit in cluster 1 which is dominated by $I = 1$ final-state interactions (a) and a fit in cluster 3 which is dominated by $I = 0$ final-state interactions (b). See text for further details. Due to their symmetry under $x \to -x$ only the right halves of the Dalitz plots are shown.

pattern. By setting the $I = 0$ channel to zero for the fits of cluster 1 (cluster 2) the widths are lowered by 22 % (22 %), while suppressing the $I = 1$ part reduces them by 81 % (72 %). When the fit parameters of clusters 1 and 2 are employed, the isospin one channel which includes the tail of the $a_0(980)$ resonance thus appears to be of great importance for the decay mode $\eta' \to \eta\pi\pi$ confirming the findings of [49] and [86]. The situation is, however, reversed if one considers the fits of the remaining two clusters. Taking out the $I = 0$ channel in the final-state interactions of the fits of cluster 3 (cluster 4) diminishes the decay widths by 79 % (81 %), whereas erasing the channel with $I = 1$ reduces it by only 33 % (28 %). Accordingly, for these sets of parameters the $I = 0$ channel, which incorporates the effects of the $f_0(980)$ resonance and the $\pi\pi$ correlation at lower energies, has higher impact on the decay widths than the $a_0(980)$ channel. A precise determination of the Dalitz plot of $\eta' \to \eta\pi\pi$ could in principle resolve this difference as exemplified in Fig. 3.7 for two typical fits. Such a measurement is planned at WASA-at-COSY [115]. In addition, the two scenarios can be distinguished by their correlation with the processes $\eta' \to 3\pi$ provided within our approach. Thus, a precise measurement of $\eta' \to 3\pi$ decay parameters can also help to clarify the importance of $a_0(980)$ or $f_0(980)$ resonance contributions to the dominant decay mode of the η' into $\eta\pi\pi$.

The violation of three-particle unitarity as described in Sect. 3.2.2 is not as tiny as in the case of $\eta \to 3\pi$, but still remarkably small. Using the definition of Sect. 3.3.3 we find averaged deviations of $(11 \pm 7)\,\%$ for $\eta' \to \eta\pi^+\pi^-$ and $(10 \pm 6)\,\%$ for $\eta' \to \eta\pi^0\pi^0$.

3.3.6 Numerical values of the parameters and η-η' mixing

Before presenting numerical results for the chiral parameters we would like to stress that the values of the couplings of the effective Lagrangian employed in the coupled-channels approach are in general not identical to those in the perturbative framework. First, contributions from tadpoles (which include also effects from the so-called on-shell approximation), and t-/u-channel diagrams in the interaction kernel have been absorbed into the coupling constants. Second, the BSE sums up meson-meson scattering in the s-channel to infinite order. The contributions beyond a given chiral order are missing in the perturbative approach and lead to changes in the values of the couplings when fitting the results to data. Finally, the subtraction point in the renormalization procedure can be different in both schemes. Hence, one must expect differences in the values of the coupling constants utilized in both frameworks.

In Table 3.7 we show the numerical values of the low-energy constants as well as the non-zero subtraction constant $a_{\pi\pi}^{(I=J=1)}$ as they come out for the fits of the four different clusters. In addition we display the parameters of η-η' mixing $R_{0\eta}$, $R_{8\eta'}$ which are determined by the values of the LECs $v_3^{(1)}$, $\beta_5^{(0)}$, and $\beta_{18}^{(0)}$ in virtue of Eq. (1.107). Note that compared to the analysis in [49] we have increased the number of chiral parameters which—in conjunction with an improved fitting procedure—helped to considerably improve the agreement with experimental data on hadronic η, η' decays.

According to the mixing parameters the four clusters of fits may be divided into two groups. For clusters 1 and 2 $R_{0\eta}$ and $R_{8\eta'}$ are both of similar small size and (mainly) positive, while clusters 3 and 4 feature a large, positive $R_{0\eta}$ and an $R_{8\eta'}$ which is close to zero. Within the present analysis the second mixing parameter $R_{8\eta'}$, which characterizes the fraction of the pure octet field η_8 in the physical η', turns out to be more tightly constrained by the fit than $R_{0\eta}$ which describes the singlet content of the η. In all cases the numerical results for $R_{0\eta}$ and $R_{8\eta'}$ deviate sizably from an orthogonal mixing scheme, where $R_{0\eta} = -R_{8\eta'}$. For comparison, a mixing angle of $-20°$ in the one-mixing angle scheme as found in the literature [4] would correspond to $R_{0\eta} = -R_{8\eta'} = 0.34$.

The fitting procedure does not constrain all parameters at the same level of accuracy. While some (*e.g.* $v_3^{(1)}$, $\beta_3^{(0)}$, $\beta_5^{(0)}$, $\beta_8^{(0)}$, $\beta_{18}^{(0)}$) may vary within large ranges (partly compensating each other), others like $v_0^{(2)}$, $\beta_0^{(0)}$, $\beta_1^{(0)}$, $\beta_2^{(0)}$, and $\beta_4^{(0)}$ are relatively tightly fixed. These boundaries constitute important constraints which must be met in future coupled-channels analyses of mesonic processes within the approach described here. Apart from entering the π^0-η-η' mixing parameters, *cf.* Eq. (1.107), the coefficient $v_0^{(2)}$ also encodes the mass of the η' in the chiral limit, m_0, by virtue of

$$m_0^2 = \frac{2v_0^{(2)}}{f^2}\,. \tag{3.29}$$

The fact that the η' does not become massless in the chiral limit is a consequence of the axial U(1) anomaly of QCD which generates in the divergence of the singlet axial-vector current an additional, non-vanishing term involving the gluonic field strength tensor. In the effective theory this term is represented by $v_0^{(2)}$. Employing $f = 88\,\mathrm{MeV}$, the value of the pseudoscalar decay constant in the chiral limit [3], we find from the fits of all clusters $m_0 = (900 \pm 80)\,\mathrm{MeV}$ which is close to the physical mass of the η'.

	cluster 1	cluster 2	cluster 3	cluster 4
$v_3^{(1)}$	0.82 ± 1.65	0.23 ± 1.46	-1.92 ± 0.62	-1.47 ± 0.83
$v_0^{(2)}$	3.15 ± 0.39	3.21 ± 0.49	3.07 ± 0.42	2.89 ± 0.30
$v_1^{(2)}$	-0.16 ± 0.34	-0.12 ± 0.32	-0.07 ± 0.17	-0.13 ± 0.13
$\beta_0^{(0)} \times 10^3$	-0.12 ± 0.18	-0.07 ± 0.22	-0.06 ± 0.19	-0.02 ± 0.32
$\beta_1^{(0)} \times 10^3$	-0.47 ± 0.25	-0.57 ± 0.22	-0.49 ± 0.14	-0.49 ± 0.18
$\beta_2^{(0)} \times 10^3$	0.77 ± 0.18	0.72 ± 0.23	0.69 ± 0.19	0.64 ± 0.34
$\beta_3^{(0)} \times 10^3$	0.05 ± 0.55	0.19 ± 0.51	0.06 ± 0.26	0.11 ± 0.15
$\beta_4^{(0)} \times 10^3$	0.33 ± 0.18	0.34 ± 0.15	0.39 ± 0.12	0.42 ± 0.14
$\beta_5^{(0)} \times 10^3$	0.73 ± 0.62	0.86 ± 0.66	0.77 ± 0.83	0.48 ± 0.22
$\beta_6^{(0)} \times 10^3$	0.00 ± 0.30	0.06 ± 0.28	-0.25 ± 0.13	-0.34 ± 0.15
$\beta_7^{(0)} \times 10^3$	0.13 ± 0.25	0.42 ± 0.33	1.01 ± 0.49	0.76 ± 0.48
$\beta_8^{(0)} \times 10^3$	-0.06 ± 0.41	-0.38 ± 0.46	0.02 ± 0.51	0.15 ± 0.14
$\beta_{13}^{(0)} \times 10^3$	-0.08 ± 0.65	-0.02 ± 0.60	0.16 ± 0.42	0.23 ± 0.17
$\beta_{14}^{(0)} \times 10^3$	0.08 ± 0.35	-0.03 ± 0.31	-0.21 ± 0.22	-0.25 ± 0.14
$\beta_{18}^{(0)} \times 10^3$	0.80 ± 0.80	0.99 ± 0.82	1.51 ± 0.47	1.49 ± 0.30
$a_{\pi\pi}^{I=J=1} \times 10^2$	-6.1 ± 0.3	-6.1 ± 0.2	-6.1 ± 0.3	-6.0 ± 0.2
$R_{0\eta}$	0.13 ± 0.26	0.24 ± 0.23	0.61 ± 0.13	0.55 ± 0.17
$R_{8\eta'}$	0.22 ± 0.11	0.20 ± 0.08	-0.01 ± 0.11	-0.04 ± 0.08

Table 3.7: Numerical values of the fit parameters itemized according to the four different clusters of fits. The LECs $v_3^{(1)}$, $v_1^{(2)}$ are given in units of $10^{-3}\,\mathrm{GeV}^2$, $v_0^{(2)}$ in units of $10^{-3}\,\mathrm{GeV}^4$. The remaining parameters are dimensionless. The two η-η' mixing parameters $R_{0\eta}$ and $R_{8\eta'}$ are specific linear combinations of some of the LECs, see Eq. (1.107). The regularization scale in the loop integrals is set to $\mu = 1\,\mathrm{GeV}$.

$\eta \to \pi^+\pi^-\pi^0$				
	a	b	c	d
this work	-1.054 ± 0.025	0.185 ± 0.015	0.079 ± 0.026	0.064 ± 0.012
ChPT [83]	-1.271 ± 0.075	0.394 ± 0.102	0.055 ± 0.057	0.025 ± 0.160
KLOE [87]	-1.072 ± 0.013	0.117 ± 0.012	0.047 ± 0.011	0.13 ± 0.03
KLOE [101]	-1.090 ± 0.024	0.124 ± 0.016	0.057 ± 0.022	0.14 ± 0.03

$\eta \to 3\pi^0$	
	g
this work	-0.058 ± 0.011
ChPT [83]	0.026 ± 0.064
KLOE [87]	-0.026 ± 0.018
KLOE [90]	-0.054 ± 0.020

$\eta \to 3\pi$	
	r_1
this work	1.50 ± 0.01
ChPT [83]	1.47
PDG '04 [96]	1.44 ± 0.04
PDG '06 [17]	1.43 ± 0.04

Table 3.8: Results for the Dalitz plot parameters of $\eta \to 3\pi$ and the branching ratio r_1, Eq. (3.13), when the KLOE data [87] are included in the fit. For simplicity we have added the statistical and systematic errors specified in [87, 90, 101] linearly and display symmetrized error bars according to the larger value. Note that our coefficients c, d, and g correspond to d, f, and 2α in [83, 87, 90, 101], respectively.

3.3.7 Inclusion of the KLOE data

Recently the Dalitz plot distributions of the decays $\eta \to \pi^+\pi^-\pi^0$ and $\eta \to 3\pi^0$ have been investigated experimentally with high statistics by the KLOE Collaboration [87, 90, 101]. Employing the numbers resulting from the first analysis by the KLOE Collaboration [87] instead of the previous values from [96, 97] we obtain the results compiled in Table 3.8 where for comparison we also display the outcome of the new two-loop calculation in ChPT [83]. While within our approach it is possible to accommodate the KLOE numbers for the a and c coefficients of the $\eta \to \pi^+\pi^-\pi^0$ Dalitz plot distribution, our results do not agree with b and d. In particular, the value of the y^2-coefficient b differs from the KLOE number, which has been determined very precisely, by more than five standard deviations. Within the given boundaries for the low-energy coefficients of the chiral effective Lagrangian our approach is unable to produce a b value as small as the number advocated by the KLOE Collaboration [87]. Note that such a small value also implies unexpectedly large corrections to the well-known current algebra result $b = a^2/4$ [80, 91]. This might indicate that contributions from higher chiral orders of the effective Lagrangian could play a role for this quantity, but the two-loop calculation [83], which involves numerous LECs of sixth chiral order, results in an even larger value of b. Of course one should keep in mind that in [83] the LECs are not fitted to the experimental numbers but instead fixed via resonance saturation.

On the other hand, the result of the first KLOE analysis for the leading order coefficient of the $\eta \to 3\pi^0$ Dalitz plot, g, cannot be met within our approach—the number still remains compatible with the PDG value, -0.062 ± 0.008 [96]. Generally, we observe the pattern, that reducing the b value correlates with an enhancement of the modulus of g. Finally, fitting to the new KLOE numbers destroys the agreement of the measured branching ratio r_1, Eq. (3.13), and our result, which is significantly increased. The accordance of the rest of the calculated observables with experimental data is only marginally affected by including the KLOE results, also the partial decay widths of the two $\eta \to 3\pi$ decay modes which enter r_1 remain consistent with the—admittedly large—experimental error bars in [96].

So far we have employed the r_1 value which is determined by the Particle Data Group by performing a χ^2-fit using one decay rate and 18 branching ratios (quoted as "our fit" in [96]). The result of the recent direct measurement of r_1 [116], however, is a bit larger and has also larger error bars: $r_1 = 1.52 \pm 0.12$, where we have added statistical and systematic errors linearly.[‡] Employing this number instead of the PDG value slightly improves the fit to the KLOE data, but does not resolve the disagreement with the Dalitz parameters b and g. Taking this value for r_1 we find $a = -1.049 \pm 0.025$, $b = 0.178 \pm 0.019$, $c = 0.079 \pm 0.028$, $d = 0.064 \pm 0.012$, $g = -0.056 \pm 0.012$, $r_1 = 1.51 \pm 0.01$.

We mention in passing that after relaxing the naturalness assumption on the size of the chiral parameters described at the beginning of this section, we have found a second class of fits, which are slightly closer to the results [87] of the KLOE Collaboration for the Dalitz plot of $\eta \to \pi^+\pi^-\pi^0$. Apart from involving unnaturally large values of some of the LECs they entail a g value which is even larger in magnitude than the one of the previous fits, Table 3.8. Moreover, the agreement with the experimental phase shifts of $\pi\pi$ scattering in the $I = J = 0$ channel shown in Fig. 3.5 is considerably worsened. The branching ratio r_1, on the other hand, is not altered.

Very recently a reanalysis by the KLOE Collaboration has become available [90, 101] whose results are also shown in Table 3.8. While there are only small changes in the results of the Dalitz parameters of the $\eta \to \pi^+\pi^-\pi^0$ decay, the g coefficient in $\eta \to 3\pi^0$ has drastically increased in magnitude reconciling it with the value determined by the Crystal Ball Collaboration [89]. All in all, after the reanalysis the agreement between the KLOE numbers and our results has considerably improved the only remaining inconsistency being the smallness of the experimental b parameter in $\eta \to \pi^+\pi^-\pi^0$ which cannot be reached within our approach.

3.3.8 Inclusion of the VES data

In this section we study the changes of our results that occur if the recent VES data on the spectral shape of $\eta' \to \eta\pi^+\pi^-$ are taken into account [88]. Note that the most recent analysis of the VES Collaboration [88] has not yet been included in Ref. [17]. The VES data have much higher statistics on the Dalitz slope parameters than previous experiments and by including them in the fit we obtain the results shown in Tab. 3.9. Since the amplitudes for $\eta' \to \eta\pi^+\pi^-$ and $\eta' \to \eta\pi^0\pi^0$ are equal in the isospin limit and deviations are thus isospin-breaking and small in our approach, we only include the leading Dalitz parameter a of $\eta' \to \eta\pi^0\pi^0$ [114] and omit the higher ones which are—assuming only small isospin-violating contributions—not quite compatible with the new

---

[‡] The result of the even more recent CLEO experiment [111] is $r_1 = 1.496 \pm 0.043 \pm 0.035$, consistent with [116].

$\eta' \to \eta\pi^+\pi^-$			
	a	b	c
this work	-0.109	-0.087	-0.036
VES exp. [88]	-0.127 ± 0.024	-0.106 ± 0.042	-0.082 ± 0.025

$\eta' \to \eta\pi^0\pi^0$			
	a	b	c
this work	-0.123	-0.104	-0.041
exp. [114]	-0.116 ± 0.026		

Table 3.9: Results for the Dalitz plot parameters of $\eta' \to \eta\pi\pi$ if the VES data are included in the fit.

results of the VES experiment for $\eta' \to \eta\pi^+\pi^-$. Our results are in good agreement with the Dalitz plot parameters extracted from the VES experiment the main difference to the previous results being the larger negative values for b and c, *cf.* Table 3.5. In Tab. 3.9 only the best least-squares fit is shown which is sufficient to discuss the qualitative changes of the results compared to those presented in the previous subsections. It is important to emphasize that the inclusion of the VES data reduces the number of fit clusters to one and we observe indeed one global minimum.

The values of the low-energy constants read

$$\begin{aligned}
v_3^{(1)} &= -1.37 \cdot 10^{-3}\,\text{GeV}^2\,, & v_0^{(2)} &= 2.35 \cdot 10^{-3}\,\text{GeV}^2\,, & v_1^{(2)} &= -0.37 \cdot 10^{-3}\,\text{GeV}^4\,, \\
\beta_0^{(0)} &= -0.31 \cdot 10^{-3}\,, & \beta_1^{(0)} &= 1.00 \cdot 10^{-3}\,, & \beta_2^{(0)} &= -0.65 \cdot 10^{-3}\,, \\
\beta_3^{(0)} &= 0.41 \cdot 10^{-3}\,, & \beta_4^{(0)} &= 0.16 \cdot 10^{-3}\,, & \beta_5^{(0)} &= -0.42 \cdot 10^{-3}\,, \\
\beta_6^{(0)} &= 0.85 \cdot 10^{-3}\,, & \beta_7^{(0)} &= 4.81 \cdot 10^{-6}\,, & \beta_8^{(0)} &= -0.89 \cdot 10^{-3}\,, \\
\beta_{13}^{(0)} &= 0.18 \cdot 10^{-3}\,, & \beta_{14}^{(0)} &= 1.77 \cdot 10^{-3}\,, & \beta_{18}^{(0)} &= 0.23 \cdot 10^{-3}\,,
\end{aligned} \tag{3.30}$$

and the subtraction constant is given by $a_{\pi\pi}^{I=J=1} = -6.0 \cdot 10^{-2}$. The fit accommodating the new VES data is thus more similar to the fits of clusters 3 and 4 than to those of clusters 1 and 2 which is supported by the observation that the decay widths of $\eta' \to \eta\pi\pi$ are also dominated by isospin zero contributions. Eliminating the $I = 0$ final-state interactions reduces the widths by 65 % while taking out the $I = 1$ channels lowers them by only 35 %.

In addition the VES Collaboration has also provided a new upper limit of 1.75 % for the branching fraction of $\eta' \to \pi^0\pi^+\pi^-$ which is significantly lower than the previous upper limit of 5 % [17, 96]. This tighter bound translates to an upper limit of 3.8 keV for the partial decay width and reduces the upper limit for the branching ratio

$$r_3 = \frac{\Gamma(\eta' \to \pi^0\pi^+\pi^-)}{\Gamma(\eta' \to \eta\pi^+\pi^-)} \tag{3.31}$$

from 10 % (as quoted by the PDG) to 4.1 %. Note that our previous results without involvement of the VES data are in agreement also with these reduced upper limits.

	this work	exp.
$\Gamma(\eta' \to \pi^0\pi^+\pi^-)$ [eV]	3120	< 3800 [88]
r_3 [%]	3.9	< 4.1 [88]
$\Gamma(\eta' \to 3\pi^0)$ [eV]	330	315 ± 78 [96]
r_2 [%]	0.73	0.74 ± 0.12 [96]

Table 3.10: Decay widths and branching ratios if the VES data are taken into account.

The new results for the $\eta' \to 3\pi$ decay widths and width ratios are displayed in Tab. 3.10. We observe a strong tendency of the fits towards the upper limit $\Gamma(\eta' \to \pi^0\pi^+\pi^-) < 3.8\,\mathrm{keV}$ and, in fact, slightly improved fits with a smaller χ^2 value can be obtained if this upper limit is omitted. (In this case, the best overall fit leads to the width $\Gamma(\eta' \to \pi^0\pi^+\pi^-) = 5.73\,\mathrm{keV}$.) The result for the width ratio, $r_3 = 3.9\,\%$, has thus considerably increased if the VES data are taken into account. Furthermore, the amplitude $A(\eta' \to \pi^0\pi^+\pi^-)$ fluctuates strongly over phase space with slope parameters which can be more than one order of magnitude larger in size than those obtained without inclusion of the VES data. The Dalitz plot distribution $|A(\eta' \to \pi^0\pi^+\pi^-)|^2$ can therefore not be properly described by a low-order polynomial in the usual expansion variables x and y.

The reason for both the large decay width $\Gamma(\eta' \to \pi^0\pi^+\pi^-)$ and the strong fluctuations over phase space are mainly due to a large contribution from isospin $I = 1$ p-waves in the final-state interactions of the decay. Setting them to zero reduces the decay width of $\eta' \to \pi^0\pi^+\pi^-$ by 83 %. While for $I = 1$ p-waves the uncharged two-particle channels are C-even and, due to C-invariance, do not couple to C-odd channels related to the $\rho^0(770)$ the coupling of charged channels to the $\rho^\pm(770)$ is not forbidden. In fact, an important feature of the fits including the VES data compared to those without these is the large enhancement of the $\eta'\pi^\pm \to \pi^0\pi^\pm$ coupling which also determines the importance of the $\rho^\pm(770)$ in this decay. The pertinent Dalitz plot is shown in Fig. 3.8 and exhibits signatures of the $\rho^\pm(770)$. Note, however, that these resonances do not appear as bands of increased amplitude at fixed two-particle energies (dotted lines in Fig. 3.8), since the p-wave contributions have a kinematical zero in the middle of these bands as indicated in Fig. 3.8 (dashed lines). Thus the amplitude only peaks at the edge of the Dalitz plot. Moreover, due to the symmetry of the amplitude under $\pi^+ \leftrightarrow \pi^-$ exchange (C-invariance) the ρ^+, ρ^- peaks interfere constructively on the symmetry axis producing a pronounced peak structure at the top of the Dalitz plot, where the invariant mass of the $\pi^+\pi^-$ system is minimal. These features of the Dalitz plot of a pseudoscalar meson decaying into three pions have been pointed out long ago in [117]. For comparison we also show the Dalitz plot of the decay mode $\eta' \to 3\pi^0$ where p-wave contributions are forbidden by Bose symmetry, see Fig 3.9.

3.3.9 Cusp phenomena

Recently a method for the extraction of $\pi\pi$ scattering lengths from $K \to 3\pi$ decays was proposed by Cabibbo [118]. It is based on the observation that the cusp in the $\pi^0\pi^0$

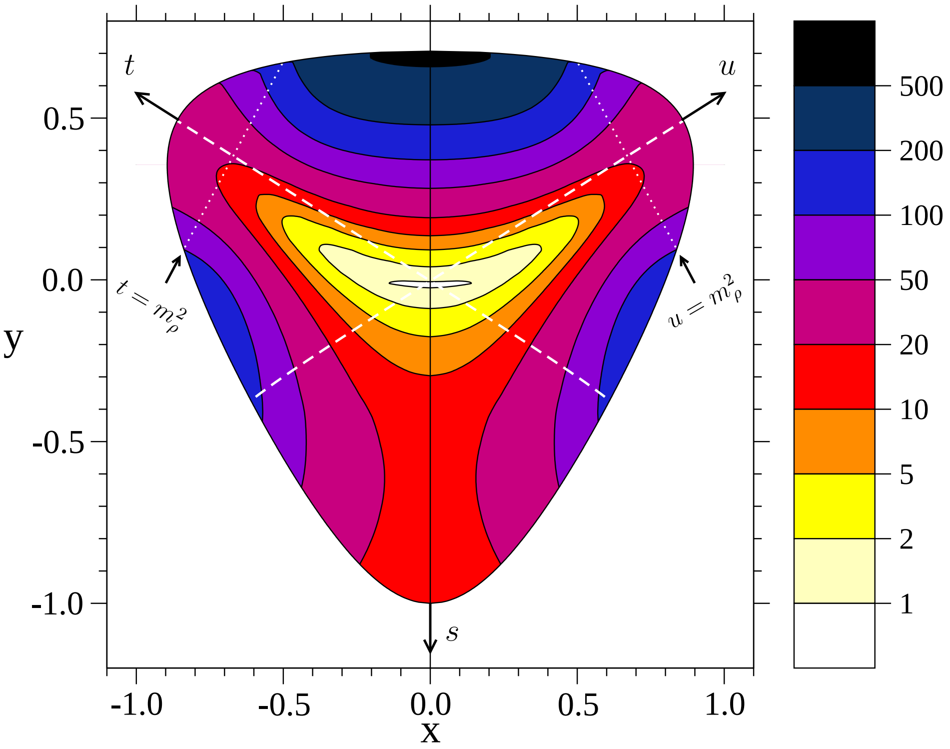

Figure 3.8: Dalitz plot distribution of $\eta' \to \pi^0\pi^+\pi^-$ for the best overall fit including the VES data for $\eta' \to \eta\pi^+\pi^-$ [88]. The p-wave contributions to $\pi^0\pi^+$ ($\pi^0\pi^-$) rescattering vanish on the rising (falling) dashed line and the invariant energies associated with the $\rho^\pm(770)$ are indicated by the dotted lines.

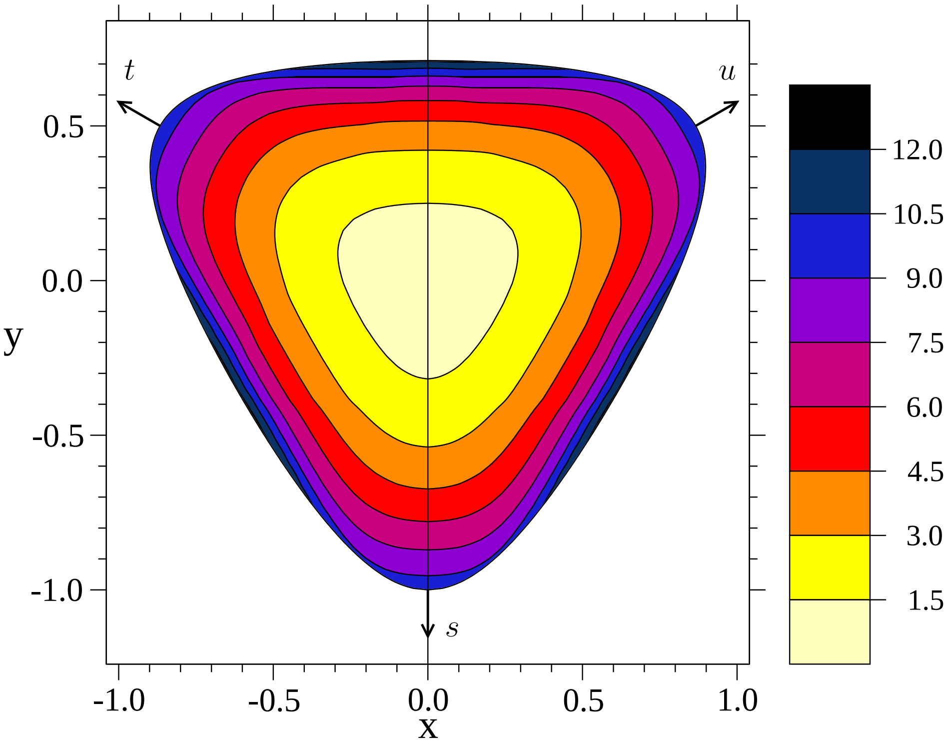

Figure 3.9: Dalitz plot distribution of $\eta' \to 3\pi^0$ for the best overall fit including the VES data for $\eta' \to \eta\pi^+\pi^-$ [88]. Due to Bose symmetry there are no p-wave contributions to this decay mode.

invariant mass distribution of $K^+ \to \pi^+\pi^0\pi^0$ which appears at the $\pi^+\pi^-$ threshold is related to the difference $a_0 - a_2$ of the $I = 0$ and $I = 2$ s-wave $\pi\pi$ scattering lengths. An accurate experimental determination of the cusp region in $K^+ \to \pi^+\pi^0\pi^0$ can therefore be used to pin down these important parameters of low-energy $\pi\pi$ scattering which is a crucial test of chiral perturbation theory, see also [119–121]. Note that the cusp effect and its implications for $\pi^0\pi^0 \to \pi^0\pi^0$ scattering were already discussed in [122].

Clearly, the same reasoning also holds for the decays of η and η' into $3\pi^0$ and for $\eta' \to \eta\pi^0\pi^0$ where, however, experimental precision is not (yet) competitive to $K \to 3\pi$ experiments such as the NA48/2 [123]. The cusp phenomenon in $\eta \to 3\pi^0$ has recently been studied theoretically in the framework of a relativistic field theory [124]. In this subsection we present the cusp structures in $\eta, \eta' \to 3\pi^0$ and $\eta' \to \eta\pi^0\pi^0$ as they arise within the chiral unitary approach to give an estimate of the size of such effects. The $\pi^0\pi^0$ spectra $f_{\pi^0\pi^0}$ are obtained from the full Dalitz plot by integrating over the x variable,

$$f_{\pi^0\pi^0}(y) = \frac{1}{|N|^2} \int\limits_{x_{\min(y)}}^{x_{\max}(y)} dx \, |\mathcal{A}(x,y)|^2 \, . \tag{3.32}$$

In Fig. 3.10 they are plotted as functions of the invariant $\pi^0\pi^0$ mass $\sqrt{s}$ for one sample fit from cluster 2. Obviously the cusp effect is tiny and might only be resolved in very high precision experiments. At the moment it seems that the necessary accuracy can exclusively be reached in $\eta \to 3\pi^0$ measurements, *e.g.* with Crystal Ball at MAMI [99].

Due to the symmetry of the Dalitz plot of $\eta \to 3\pi^0$ experimentalists usually employ an azimuthal averaging of the two-dimensional Dalitz distribution whose result is expressed in terms of the variable $z = x^2 + y^2$ so that (*cf.* Eq. (3.17))

$$|\mathcal{A}(\eta \to 3\pi^0)|^2 \approx |N'|^2[1 + g(y^2 + x^2)] = |N'|^2[1 + gz] \, . \tag{3.33}$$

Note, however, that the azimuthal symmetry of the Dalitz plot holds only at quadratic order in x and y. In Fig. 3.11 we present the z-distribution $R(z)$ calculated for our sample fit according to

$$R(z) = \frac{\int_I d\varphi \, |\mathcal{A}(x,y)|^2}{|N'|^2 \int_I d\varphi} \qquad \text{with} \quad x = \sqrt{z}\sin\varphi \, , \quad y = \sqrt{z}\cos\varphi \, , \tag{3.34}$$

where the domain of integration I extends over all values of the azimuthal angle φ allowed by phase space. For clarity we also show in Fig. 3.11 the boundaries of the Dalitz plot in the x-y plane. The z-distribution exhibits two cusps, one at $z = 0.597$, the minimal value to reach the $\pi^+\pi^-$ threshold, and one at $z = 0.882$ which corresponds to the maximal value to touch the line of $\pi^+\pi^-$ threshold, see the dashed lines in the z-distribution and the arrows in the Dalitz plot. We remark that z is defined in such a way that it gives equal weight to all points of the Dalitz plot inscribed by the dotted circle in Fig. 3.11 (corresponding to $z \leq 0.756$ indicated by the dotted line in the z-distribution) since the infinitesimal quantity dz is proportional to the area of the infinitesimal annulus of radius $r = \sqrt{z}$, $2\pi r dr = \pi dz$. For $z > 0.756$, however, the length dz corresponds to a smaller area of the Dalitz plot which deviates from a circular shape due to relativistic kinematics. Therefore the points outside the dotted circle are given more weight in $R(z)$.

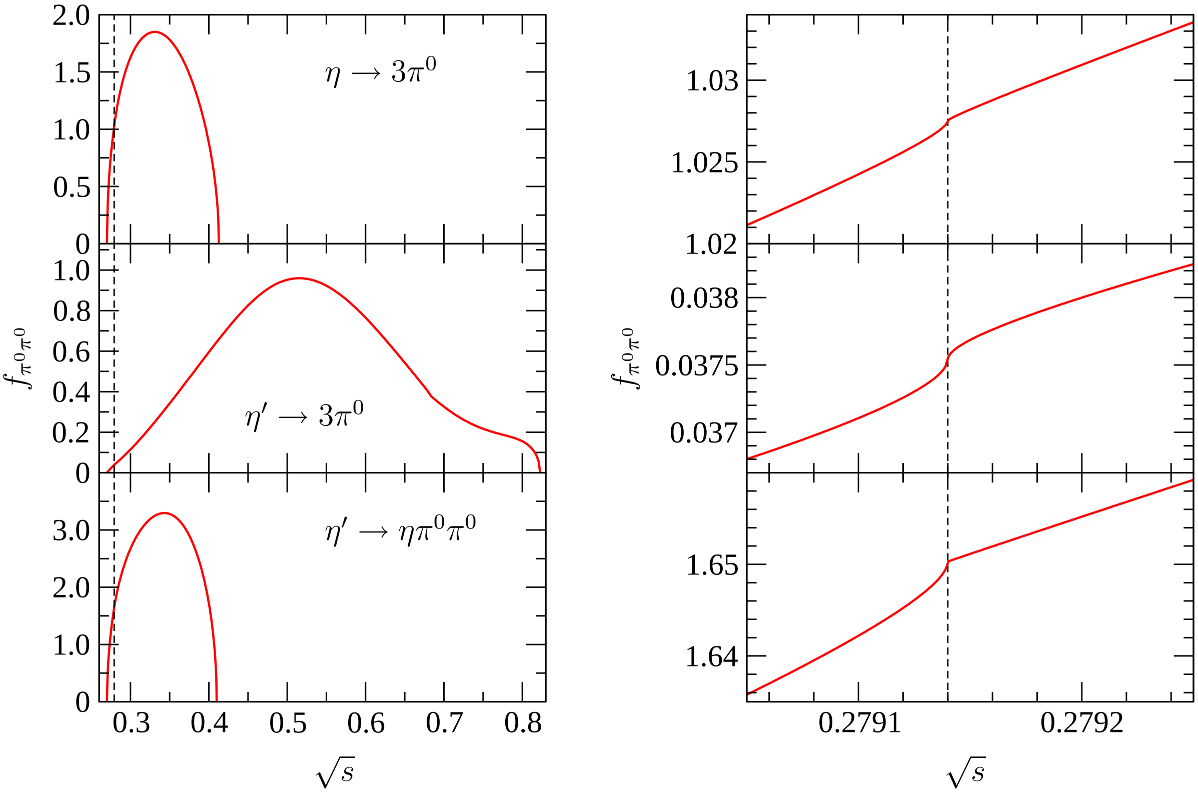

Figure 3.10: $\pi^0\pi^0$ invariant mass distributions in $\eta \to 3\pi^0$ (top), $\eta' \to 3\pi^0$ (middle) and $\eta' \to \eta\pi^0\pi^0$ (bottom) for a sample fit from cluster 2. The full available phase space is shown in the left column whereas the right column displays a zoomed view of the cusp region. The dashed line indicates the position of the $\pi^+\pi^-$ threshold.

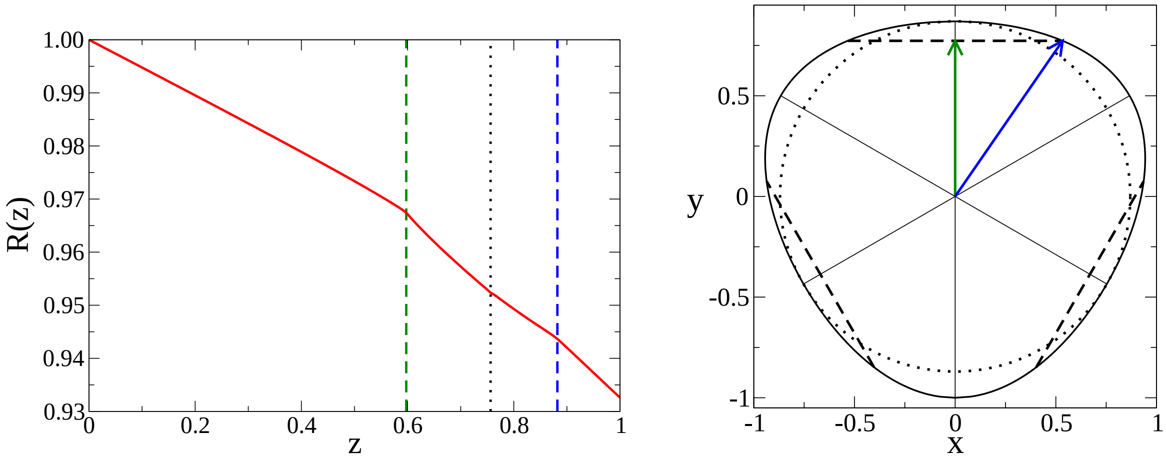

Figure 3.11: Left panel: radial distribution of the $\eta \to 3\pi^0$ Dalitz plot for the sample fit from cluster 2. The dashed lines mark the cusp positions, the dotted line corresponds to the z value of the widest circle enclosed in the Dalitz plot. Right panel: kinematic boundaries of the Dalitz plot. The dashed lines indicate the $\pi^+\pi^-$ thresholds. See text for further details.

One should keep this in mind when extracting the Dalitz slope parameter g from the z-distribution. It remains to be seen whether the interesting cusp structure of $R(z)$ may be verified in future experiments.

3.4 Dalitz plot parameters of $\eta \to 3\pi$

As pointed out in Sect. 3.3.7, within the chiral unitary approach it is not possible to accommodate the results of the first KLOE analysis [87] of the $\eta \to 3\pi$ Dalitz parameters together with the measured branching ratio of the two decay modes, r_1. In this section we will present an explanation how all these experimental quantities can be related in a phenomenological way without making use of model-dependent assumptions on the construction of the decay amplitudes.

The main ingredient is the $\Delta I = 1$ selection rule which relates the $\eta \to \pi^+\pi^-\pi^0$ decay amplitude $\mathcal{A}$ to the amplitude $\bar{\mathcal{A}}$ for $\eta \to 3\pi^0$ [80]

$$\bar{\mathcal{A}}(s,t,u) = \mathcal{A}(s,t,u) + \mathcal{A}(t,u,s) + \mathcal{A}(u,s,t)\,. \tag{3.35}$$

This rule is valid up to tiny corrections from QCD (suppressed by $\mathcal{O}(m_\epsilon^2)$) and of electromagnetic origin (suppressed by $\mathcal{O}(\alpha^2)$).[§] In analogy to the experimental parametrization of the Dalitz plot distribution, Eq. (3.16), we assume that the amplitude $\mathcal{A}$ can be well approximated by a polynomial

$$\mathcal{A}(x,y) = N\big[1 + \alpha y + \beta y^2 + \gamma x^2 + \cdots\big] \tag{3.36}$$

[§] Our chiral unitary approach iterates isospin-breaking terms and thus includes corrections to the $\Delta I = 1$ selection rule. We have checked that these are indeed numerically tiny.

with complex coefficients α, β, γ. We will drop all terms of third order and beyond and work with this minimal parametrization of $\mathcal{A}$ which is able to describe the experimental Dalitz plot distribution as measured by the KLOE Collaboration[¶] [87]

$$|\mathcal{A}(x,y)|^2 = |N|^2\big[1 + ay + by^2 + cx^2 + dy^3\big] \tag{3.37}$$

with[*]

$$a = -1.072 \pm 0.013\,, \quad b = 0.117 \pm 0.012\,, \quad c = 0.047 \pm 0.011\,, \quad d = 0.13 \pm 0.03\,. \tag{3.38}$$

Employing the $\Delta I = 1$ selection rule, Eq. (3.35), we are able to derive expressions for the leading Dalitz plot parameter of $\eta \to 3\pi^0$, g, and for the branching ratio r_1. Note that we do not include possible cusp effects in the $\eta \to 3\pi^0$ amplitude as discussed in Sect. 3.3.9 because they are expected to be small and up to now have not been verified experimentally. Since the complex normalization factor N is irrelevant for the determination of the g parameter and drops out in the branching ratio r_1, we are left with six free constants which parametrize the amplitude $\mathcal{A}$, the real and imaginary parts of α, β, and γ. Four of these can be fixed by matching $|\mathcal{A}|^2$ to the central experimental values of a, b, c, d. However, also the remaining two are constrained by the fact that the higher order terms x^2y, x^2y^2, x^4, and y^4, which automatically emerge when squaring $\mathcal{A}$, are expected to have small coefficients, since Eq. (3.37) appears to be a good parametrization of the experimental distribution. As an upper limit for the moduli of these higher coefficients not observed in experiment we choose the value of the highest order experimental coefficient in Eq. (3.38), $d = 0.13$.

Fitting the remaining two parameters in $\mathcal{A}$ within the boundaries dictated by the smallness of the higher order terms in $|\mathcal{A}|^2$ to the experimental numbers for r_1 and KLOE g we find

$$\begin{aligned} g^{(\text{theo})} &= -0.074 \pm 0.012\,, & g^{(\text{exp})} &= -0.026 \pm 0.018\ [87]\,, \\ r_1^{(\text{theo})} &= 1.47 \pm 0.03\,, & r_1^{(\text{exp})} &= 1.44 \pm 0.04\ \ \ [96]\,, \end{aligned} \tag{3.39}$$

where the theoretical uncertainties represent the propagation of the errors of the input parameters in Eq. (3.38). While the two numbers for the branching ratio r_1 are very well compatible, the calculated value of g differs by about two standard deviations from the number extracted by the KLOE Collaboration. It is, however, consistent with the value published by the Crystal Ball Collaboration [89].

We would like to point out that raising the order of the polynomial parametrization of the amplitude in Eq. (3.36) does not alter these conclusions. Although it would increase the number of adjustable parameters, at the same time more and more constraints would be generated by the fact that the numerous higher order coefficients of $|\mathcal{A}|^2$ all have to be close to zero for Eq. (3.37) to be a good parametrization of the experimental distribution. As a matter of fact, we have explicitly checked that the inclusion of, *e.g.*, a y^3 term in the

---

[¶] Note that in contrast to [87] we do not include C-violating terms proportional to x. Our coefficients c and d correspond to d and f in [87], respectively.

[*] For simplicity we have added the statistical and systematic errors specified in [87] linearly and display symmetrized error bars according to the larger value.

parametrization of the amplitude, Eq. (3.36), yields only tiny numerical improvements for the fit to g and r_1. As in Sect. 3.3.7 we have verified that our results do not change significantly, when the PDG value for r_1 is replaced by the recent direct experimental determination of this branching ratio which yields $r_1 = 1.52 \pm 0.12$ [116].† Instead of the numbers given in Eq. (3.39) we then obtain $g = -0.071 \pm 0.012$ which is only slightly closer to the KLOE number and $r_1 = 1.50 \pm 0.03$. The main restriction for the parameters is thus given by the size of the higher order coefficients of $|\mathcal{A}|^2$ and not by the value of r_1.

We have also checked to what extent the phenomenological amplitude described here fulfills the unitarity condition discussed in Sect. 3.2.2. This can be done utilizing purely experimental input and thus without making use of unitarized ChPT, since the scattering amplitude T_ℓ which enters Eq. (3.9) may be expressed by the experimentally determined phase shifts of $\pi\pi$ scattering, see [93] for the explicit expressions. The violation of three-particle unitarity turns out to be 10 % (5 %) for $\eta \to \pi^+\pi^-\pi^0$ ($\eta \to 3\pi^0$) on average over the full Dalitz plot when the parameters are fixed to physical observables as above, see Eqs. (3.38, 3.39). The phase of free normalization constant N is chosen in such a way that the unitarity violation is minimized at the center of the $\eta \to \pi^+\pi^-\pi^0$ Dalitz plot. Although the polynomial amplitude does not incorporate any constraints from unitarity the violations turn out to be rather modest. If, on the other hand, the restrictions on the size of higher order coefficients of $|\mathcal{A}|^2$ are released and the fit is forced to reproduce the central values of the branching ratio r_1 and the KLOE g value, we observe unitarity violations as large as 43 % for $\eta \to \pi^+\pi^-\pi^0$ and 45 % for $\eta \to 3\pi^0$.

After the appearance of the revised numbers due to the new KLOE analysis [90, 101] we have performed the same phenomenological study as for the previous values. Moreover, we have employed the latest PDG result for the branching ratio r_1. We now find

$$\begin{aligned} g^{(\text{theo})} &= -0.070 \pm 0.019\,, & g^{(\text{exp})} &= -0.054 \pm 0.020\ [90]\,, \\ r_1^{(\text{theo})} &= \quad 1.47 \pm 0.03\,, & r_1^{(\text{exp})} &= \quad 1.43 \pm 0.04\ \ [17]\,, \end{aligned} \tag{3.40}$$

i.e. within error bars the new numbers are consistent with the $\Delta I = 1$ rule.

3.5 Extraction of $(m_u - m_d)/m_s$ from hadronic η' decays

3.5.1 Conjecture

The light quark masses m_u, m_d, m_s are fundamental parameters of QCD and ought to be constrained as accurately as possible. The determination of the light quark mass ratios has been the goal of a variety of investigations in low-energy hadron physics, see *e.g.* [125–129]. Of particular interest is the quark mass difference $m_d - m_u$ which induces isospin breaking in QCD.

---

†The result of the even more recent CLEO experiment [111] is $r_1 = 1.496 \pm 0.043 \pm 0.035$ consistent with [116].

In principle, an accurate way of extracting $m_d - m_u$ is given by the isospin-violating decays $\eta, \eta' \to \pi^0\pi^+\pi^-$ and $\eta, \eta' \to 3\pi^0$. While for most processes isospin-violation of the strong interactions is masked by electromagnetic effects, these corrections are expected to be small for the three pion decays of the η and η' (Sutherland's theorem) [77] which has been confirmed in an effective Lagrangian framework [78]. Neglecting electromagnetic corrections the decay amplitudes are directly proportional to $m_d - m_u$. For this reason, it has been claimed in [84] that the branching ratio

$$r_3 = \frac{\Gamma(\eta' \to \pi^0\pi^+\pi^-)}{\Gamma(\eta' \to \eta\pi^+\pi^-)} \tag{3.41}$$

can be utilized in a very simple manner to extract the light quark mass difference $m_d - m_u$. To this aim, it is assumed that

a) the amplitude $A(\eta' \to \pi^0\pi^+\pi^-)$ is determined by the corresponding amplitude $A(\eta' \to \eta\pi^+\pi^-)$ according to

$$A(\eta' \to \pi^0\pi^+\pi^-) = R^{(0)}_{8\pi^0}\, A(\eta' \to \eta\pi^+\pi^-)\,, \tag{3.42}$$

where $R^{(0)}_{8\pi^0} = (\sqrt{3}/4)\,(m_d - m_u)/(m_s - \hat{m})$ is the π^0-η mixing angle at leading order, see Eq. (1.107).[‡] Eq. (3.42) implies that the decay $\eta' \to \pi^0\pi^+\pi^-$ proceeds entirely via $\eta' \to \eta\pi^+\pi^-$ followed by π^0-η mixing.

b) both amplitudes are *"essentially constant"* over phase space (see the remark in front of Eq. (19) of Ref. [84]).

Based on these two assumptions one arrives at the relation [84]

$$r_3 \approx (16.8)\,\frac{3}{16}\left(\frac{m_d - m_u}{m_s}\right)^2, \tag{3.43}$$

where the factor 16.8 represents the phase space ratio. Comparison with experimental data—for which, so far, only an upper limit exists—would then lead to a prediction for the quark mass ratio $(m_d - m_u)/(m_s - \hat{m}) \approx (m_d - m_u)/m_s$. In this section we critically examine the two assumptions which lead to the simple relation (3.43). Such an investigation is very timely in view of the recent and ongoing experimental activities on η' decays at the WASA facility at COSY [100], at MAMI-C [102] and by the VES Collaboration [88].

3.5.2 Validity of the assumptions

In the following, we will work with the double quark mass ratio

$$Q^2 = \frac{m_s - \hat{m}}{m_d - m_u}\frac{m_s + \hat{m}}{m_d + m_u} \tag{3.44}$$

instead of the mixing angle $R^{(0)}_{8\pi^0}$, since the Kaplan-Manohar reparametrization invariance [130] of the chiral effective Lagrangian is respected by Q^2 up to chiral order $\mathcal{O}(p^4)$,

---

[‡] Note that in [84] the difference $m_s - \hat{m}$ has been approximated by m_s in the denominator of $R^{(0)}_{8\pi^0}$.

	Cluster 1	Cluster 2	Cluster 3	Cluster 4
$\Gamma_{\eta'\to\pi^0\pi^+\pi^-}$ [eV]	69 ± 12	73 ± 9	141 ± 44	141 ± 26
r_3 [%]	0.09 ± 0.02	0.09 ± 0.02	0.17 ± 0.06	0.17 ± 0.03
$\Gamma_{\eta'\to3\pi^0}$ [eV]	116 ± 22	120 ± 16	217 ± 67	217 ± 40
r_2 [%]	0.26 ± 0.05	0.26 ± 0.04	0.47 ± 0.15	0.47 ± 0.08

Table 3.11: Decay widths and branching ratios in the chiral unitary approach [132] employing assumption "*a*".

whereas $R^{(0)}_{8\pi^0}$ receives corrections already at $\mathcal{O}(p^2)$. Hence, it is preferable to employ Q in phenomenological analyses in order to suppress the ambiguity stemming from this reparametrization invariance.

Following Dashen's theorem which asserts equal electromagnetic corrections for pion and kaon masses at leading chiral order [92], Q^2 can be expressed in terms of physical meson masses (*cf.* Eq. (3.7))

$$Q^2_{\text{Dashen}} = \frac{m_K^2}{m_\pi^2}\,\frac{m_K^2 - m_\pi^2}{m_{K^0}^2 - m_{K^\pm}^2 + m_{\pi^\pm}^2 - m_{\pi^0}^2} = (24.1)^2\ . \tag{3.45}$$

However, there are various investigations on the size of violations to Dashen's theorem with (partially contradictory) results for Q in the range of about $20\ldots24$ [112]. The 3π decays of η and η' provide thus a good opportunity to pin down the value of the double quark mass ratio Q^2 [81, 83, 131].

We will first investigate the validity of assumption "*a*", *i.e.* we assume that the decay $\eta' \to \pi^0\pi^+\pi^-$ proceeds entirely via $\eta' \to \eta\pi^+\pi^-$ followed by π^0-η mixing. This implies for the neutral decay

$$A(\eta' \to 3\pi^0) = 3\,R^{(0)}_{8\pi^0}\,A(\eta' \to \eta\pi^0\pi^0)\ . \tag{3.46}$$

Employing the amplitudes $A(\eta' \to \eta\,2\pi)$ from our chiral unitary approach one can thus predict the decay amplitudes for $A(\eta' \to 3\pi)$ and calculate both the decay widths $\Gamma(\eta' \to \pi^0\pi^+\pi^-)$, $\Gamma(\eta' \to 3\pi^0)$ and the branching ratios r_3 and $r_2 = \Gamma(\eta' \to 3\pi^0)/\Gamma(\eta' \to \eta\pi^0\pi^0)$. The results are shown in Table 3.11 where we have used the Q value predicted by Dashen's theorem, $Q_{\text{Dashen}} = 24.1$. The ratios are obtained by explicitly performing the integration of the amplitudes over phase space. We infer that assumption "*a*" is not justified—at least for the neutral decay where, in particular, clusters 1 and 2 are in clear disagreement with experiment. Remember that the latest PDG values are $\Gamma(\eta' \to 3\pi^0) = (320\pm60)\,\text{eV}$ and $r_3 = (0.74\pm0.12)\,\%$ [17].

Next, we employ in addition assumption "*b*". This is achieved by averaging the $\eta' \to \eta\,2\pi$ amplitudes over phase space which are then employed for $\eta' \to 3\pi$ by means of assumption "*a*". The results are displayed in Table 3.12. One observes that for clusters 1 and 2 the decay widths into 3π and hence the ratios r_2, r_3 increase, while the changes for clusters 3 and 4 are rather moderate. However, recall that the Dalitz plot parameters found in Sect. 3.3.4 clearly indicate that the assumption of a constant amplitude is not justified for $\eta' \to \pi^0\pi^+\pi^-$, particularly for clusters 3 and 4, see Table 3.3, and even more so if the new VES data are taken into account, *cf.* Sect. 3.3.8. The partial compensation

	Cluster 1	Cluster 2	Cluster 3	Cluster 4
$\Gamma_{\eta'\to\pi^0\pi^+\pi^-}$ [eV]	155 ± 7	155 ± 7	153 ± 7	154 ± 5
r_3 [%]	0.19	0.19	0.19	0.19
$\Gamma_{\eta'\to 3\pi^0}$ [eV]	238 ± 11	239 ± 10	237 ± 11	239 ± 6
r_2 [%]	0.52	0.52	0.52	0.52

Table 3.12: Decay widths and branching ratios in the chiral unitary approach employing assumptions "*a*" and "*b*". Since in this case the branching ratios only depend on phase space and Q, they do not have an error bar here.

	Cluster 1	Cluster 2	Cluster 3	Cluster 4
$\Gamma_{\eta'\to\pi^0\pi^+\pi^-}$ [eV]	470 ± 200	520 ± 200	740 ± 420	620 ± 180
r_3 [%]	0.58 ± 0.24	0.66 ± 0.27	0.92 ± 0.52	0.77 ± 0.21
$\Gamma_{\eta'\to 3\pi^0}$ [eV]	331 ± 24	326 ± 28	330 ± 33	336 ± 21
r_2 [%]	0.73 ± 0.06	0.72 ± 0.06	0.71 ± 0.07	0.73 ± 0.05

Table 3.13: Decay widths and branching ratios in the chiral unitary approach tabulated according to the four different clusters of fits.

of the effects of assumptions "*a*" and "*b*" in clusters 1, 2 and the moderate changes in clusters 3, 4 are therefore purely accidental.

We conclude that both assumptions "*a*" and "*b*" are not justified. This is further substantiated by comparison of r_2 and r_3 in Tab. 3.12 with the respective values from the full chiral unitary approach shown in Tab. 3.13. The values are in clear disagreement and, hence, both assumptions are not appropriate—at least within the chiral unitary approach.

We have also investigated the differences which result if assumption "*a*" is replaced by the decay mechanism where $\eta' \to 3\pi$ occurs due to π^0-η' mixing followed by a (virtual) transition $\pi^0 \to 3\pi$. Employing the relation $A(\eta' \to 3\pi) = R^{(2)}_{\tilde{\pi}^0\eta'}\, A(\pi^0 \to 3\pi)$ with $R^{(2)}_{\tilde{\pi}^0\eta'}$ being the π^0-η' mixing angle, see Eq. (1.107), we find the values shown in Table 3.14. Assuming the $\eta' \to 3\pi$ decays to proceed via this mechanism introduces a huge uncertainty and leads to different ratios r_2 and r_3. This underlines the observation that the decays $\eta' \to 3\pi$ cannot be expected to simply proceed either via π^0-η or π^0-η' mixing. In particular, the isospin-breaking transition due to the quark mass difference $m_d - m_u$ cannot be completely assigned to π^0-η mixing as done in assumption "*a*". Despite its appealing simplicity, the crude estimate given in Eq. (3.43) is certainly not suited to precisely determine the double quark mass ratio Q^2.

In fact, even at leading chiral order the $\eta' \to 3\pi$ decay amplitude is not entirely due to π^0-η mixing. While assumption "*a*" would yield

$$\mathcal{A}(\eta' \to \pi^0\pi^+\pi^-) = R^{(0)}_{8\pi^0}\, \mathcal{A}(\eta' \to \eta\pi^+\pi^-) = \frac{m_\epsilon^2}{9f^4}\frac{m_\pi^2}{m_\eta^2 - m_\pi^2}\big(\sqrt{6}f^2 - 12v_3^{(1)}\big)\,, \qquad (3.47)$$

the leading order tree level result in ChPT, which also involves an isospin-violating $\eta'3\pi$-

	Cluster 1	Cluster 2	Cluster 3	Cluster 4
$\Gamma_{\eta'\to\pi^0\pi^+\pi^-}$ [eV]	2450 ± 1930	1720 ± 1160	260 ± 260	290 ± 290
r_3 [%]	2.96 ± 2.30	2.10 ± 1.40	0.34 ± 0.34	0.37 ± 0.37
$\Gamma_{\eta'\to 3\pi^0}$ [eV]	1080 ± 840	800 ± 550	120 ± 120	120 ± 120
r_2 [%]	2.34 ± 1.79	1.73 ± 1.19	0.28 ± 0.28	0.28 ± 0.28

Table 3.14: Decay widths and branching ratios in the chiral unitary approach if isospin-breaking takes place solely via π^0-η' mixing. For the fits of Clusters 3 and 4 this mixing angle can actually become zero leading to vanishing decay widths $\Gamma(\eta' \to 3\pi)$ and branching ratios r_2, r_3.

vertex, reads

$$\mathcal{A}(\eta' \to \pi^0\pi^+\pi^-) = -\frac{m_\epsilon^2}{9f^4}\frac{m_\eta^2 - 2m_\pi^2}{m_\eta^2 - m_\pi^2}\left(\sqrt{6}f^2 - 12v_3^{(1)}\right). \tag{3.48}$$

On the other hand, as explained in Sect. 3.3.3 employing the chiral unitary approach does not lead to a conclusive extraction of Q due to the present experimental situation. Using the Q value predicted by Dashen's theorem we obtain the decay width ratio $r_3 = (0.35\ldots1.5)\,\%$ which is appreciably larger than the value of $0.18\,\%$ quoted in [84]. Note also that there is a tendency to even larger values of r_3 if Q is lowered, *e.g.*, for $Q = 22$ we obtain the range $r_3 = (0.4\ldots2.8)\,\%$.

3.6 Conclusions

We have investigated the hadronic decays $\eta, \eta' \to 3\pi$ and $\eta' \to \eta\pi\pi$ within a chiral unitary approach based on the Bethe-Salpeter equation. The s- and p-wave interaction kernels of the BSE are derived from the U(3) chiral effective Lagrangian up to fourth chiral order with the η' as an explicit degree of freedom. Within this approach the incoming η or η' decays into three pseudoscalar mesons and then two of these mesons rescatter—elastically or inelastically—an arbitrary number of times, while the third particle remains a spectator. The final-state interaction of the two mesons is described by the solution of the BSE and satisfies two-particle unitarity. For the decays $\eta \to 3\pi$ and $\eta' \to \eta\pi\pi$ we have also estimated to what extent constraints from three-body unitarity, which is not incorporated in the approach, are fulfilled and find that the deviations are rather modest. Although the numerical results of our approach are in very good agreement with most experimental data of hadronic η and η' decays, the consistent inclusion of three-body interactions (see *e.g.* the work of Mandelstam [95]) in the chiral unitary framework would be an important step of improvement, in particular for an accurate description of the three pion decays of the η' whose phase space is large.

The chiral parameters of the approach are fitted by means of an overall χ^2 fit to experimental data of the hadronic decay modes of η and η' and meson-meson scattering phase shifts. We obtain very good agreement with the experimental phase shifts and the data of decay widths and spectral shapes provided by the Particle Data Group [96]. In fact, we observe four different classes of fits which describe these data equally well, but differ in their predictions for yet unmeasured quantities such as the $\eta' \to \pi^+\pi^-\pi^0$ decay width (for which there exists only a weak upper limit) and the Dalitz slope parameters of $\eta' \to 3\pi$. The results obtained may be tested in future experiments foreseen at WASA-at-COSY [100], MAMI-C [102] and with KLOE-2 at DAΦNE [103]. The hadronic decays considered here along with phase shifts in meson-meson scattering pose therefore tight constraints on the approach and will allow to determine the couplings of the effective Lagrangian up to fourth chiral order within this chiral unitary approach. It is important to stress that the values of the parameters obtained from the fit are in general not the same as in the framework of ChPT which can be traced back to the absorption of loops into the coefficients and higher order effects not included in the perturbative framework.

An intriguing feature of the fits is that they accommodate the large negative slope parameter g of the decay $\eta \to 3\pi^0$ measured by the Crystal Ball Collaboration [89] which could not be met by other theoretical investigations [81, 83]. This value has very recently been confirmed both by the WASA@CELSIUS [98] and the KLOE Collaboration [90].

The importance of the various two-particle channels with different isospin and angular momentum has been examined as well. For the $\eta \to 3\pi$ decays we find that the major contribution is given by $\pi\pi$ rescattering in the s-wave $I = 0$ channel, while the $I = 1, 2$ channels interfere destructively with the former. The p-wave contribution in the charged decay is tiny, since available phase space is small. For $\eta' \to \pi^+\pi^-\pi^0$, on the other hand, phase space is considerably larger, and the size of the p-wave contributions ranges from 10 % to 50 % depending on the cluster of fits.

For the decays $\eta' \to \eta\pi\pi$ we find that the s-wave $I = 1$ channels dominate for two classes of fits which would confirm the importance of the nearby $a_0(980)$ resonance as claimed in previous investigations [49, 86]. But the other two clusters are dominated by the $I = 0$ channels. These two scenarios can be distinguished both by slightly different Dalitz plot distributions, *cf.* Fig. 3.7, and by different predictions for the $\eta' \to 3\pi$ decays. Thus, a precise measurement of $\eta' \to 3\pi$ decay parameters can also help to clarify the importance of $a_0(980)$ or $f_0(980)$ resonance contributions to the dominant decay mode of the η' into $\eta\pi\pi$.

In Sects. 3.3.7 and 3.4 we have critically examined the Dalitz plot parameters of $\eta \to \pi^0\pi^+\pi^-$ and $\eta \to 3\pi^0$ resulting from the first analysis by the KLOE Collaboration [87] which are partially in conflict with previous experiments. In particular, the first KLOE value of the Dalitz slope parameter g in $\eta \to 3\pi^0$ is considerably smaller in magnitude than determined by the Crystal Ball Collaboration. If we replace the PDG data by the KLOE Dalitz parameters from [87], we do not achieve a good overall fit anymore. It appears that the slope parameters of both $\eta \to 3\pi$ decays cannot be fitted simultaneously. In addition, fitting to the KLOE data destroys the agreement with the experimental branching ratio of both decay modes which is known to high precision. We have furthermore illustrated that utilizing the $\Delta I = 1$ selection rule which relates both decays and taking the KLOE parametrization of the charged decay as input leads in a model-independent way to a g value not consistent with the result of the first KLOE analysis [87]. The revised numbers of the new analysis [90, 101] by the KLOE Collaboration are, however, in accordance with the $\Delta I = 1$ rule.

Inclusion of the recent VES data on the $\eta' \to \eta\pi^+\pi^-$ spectral shape reduces the uncertainty of the fit results and we are left with one single minimum of the χ^2 function. In this case, the overall fit to η, η' data yields for $\eta' \to \pi^0\pi^+\pi^-$ a large contribution from the isospin $I = 1$ p-wave in the final-state interactions which can be attributed to a large coupling to the $\rho^\pm(770)$ resonances while contributions related to the $\rho^0(770)$ are forbidden by C-invariance. Consequently we observe a large decay width of roughly 3 keV for $\eta' \to \pi^0\pi^+\pi^-$ whereas the decay width of the related neutral decay mode $\eta' \to 3\pi^0$, to which p-waves do not contribute, remains fixed at the experimental value of approximately 300 eV. More precise data on η' decays are needed in order to eventually clarify this issue. An improvement of the experimental situation is foreseen in the near future due to the upcoming data from WASA-at-COSY [100], MAMI-C [102] and KLOE-2 at DAΦNE [103].

Finally, we have critically investigated the claim of Ref. [84] that the light quark mass ratio $(m_d - m_u)/(m_s - \hat{m})$ can be extracted from the decay width ratio $r_3 = \Gamma(\eta' \to \pi^0\pi^+\pi^-)/\Gamma(\eta' \to \eta\pi^+\pi^-)$. In order to study this issue we have employed our U(3) chiral unitary framework which is in very good agreement with the η, η' data on widths and spectral shapes. Our results clearly indicate that the two underlying assumptions of [84] in order to arrive at a relation between r_3 and $(m_d - m_u)/(m_s - \hat{m})$, *i.e.*, that a) the decay $\eta' \to \pi^0\pi^+\pi^-$ proceeds entirely via the decay $\eta' \to \eta\pi^+\pi^-$ followed by π^0-η mixing and that b) the decay amplitudes are constant over phase space, are not justified at all. The results from the full chiral unitary approach are in plain disagreement with these two assumptions, in particular if the new VES data are taken into account. Unfortunately, the present experimental situation which is used as input to fit the parameters of the chiral unitary approach does not allow for a precise determination of the double quark mass ratio Q^2 from hadronic η' decays.

Chapter 4

The anomalous decays $\eta, \eta' \to \pi^+\pi^- l^+ l^-$ [§]

4.1 Introduction

The decays $\eta^{(\prime)} \to \pi^+\pi^- l^+ l^-$ are interesting in several respects. First, they involve contributions from the box-anomaly of Quantum Chromodynamics, see Sect. 1.4. Second, they probe the transition form factors of the η and η'. In principle, the decays are suited to test whether double vector meson dominance is indeed realized in nature, which is also an important issue for the anomalous magnetic moment of the muon and kaon decays [134]. Moreover, since the η' is closely related to the axial U(1) anomaly of the strong interactions, one can study the phenomenological implications of the anomaly at low energies. On the experimental side, there is renewed interest in η, η' decays which are investigated at WASA-at-COSY [100], MAMI [102, 135], KLOE [87, 90, 101] and by the VES collaboration [88].

In this chapter we extend previous work [136], where the anomalous decays $\eta^{(\prime)} \to \pi^+\pi^-\gamma$ were investigated in a chiral unitary approach, to include off-shell photons since the process $\eta^{(\prime)} \to \pi^+\pi^- l^+ l^-$ can be regarded as the two-step process $\eta^{(\prime)} \to \pi^+\pi^-\gamma^* \to \pi^+\pi^- l^+ l^-$. It is worthwhile mentioning that the conventional vector dominance picture with energy-dependent widths in the vector meson propagators can be shown to be in contradiction to the one-loop result of chiral perturbation theory [52]. The present approach, on the other hand, satisfies theoretical constraints such as anomalous Ward identities, electromagnetic gauge invariance, exact two-body unitarity and matches in the low-energy limit to one-loop ChPT. Resonances are not taken into account explicitly, but are rather generated dynamically through the iteration of meson-meson interactions.

This chapter is organized as follows. In the next section we present the general structure of the amplitude, while in Sect. 4.3 the one-loop result of these decays within ChPT is derived. Some details of the chiral unitary approach are presented in Sect. 4.4 and the results are discussed in Sect. 4.5. We summarize our findings in Sect. 4.6. The full list of relevant $\mathcal{O}(p^6)$ counter terms is given in App. A.3.

[§] The contents of this chapter have been published in [133].

4.2 General structure of the amplitude

The decays $\eta^{(\prime)} \to \pi^+\pi^- l^+ l^-$ ($l^\pm$ represents either $e^\pm$ or $\mu^\pm$) are depicted in Fig. 4.1, where we also introduce the four-momenta of the particles. The invariant matrix element of the decay has the generic form

$$i\mathcal{M} = -ie\,\epsilon^{\mu\nu\alpha\beta} k_\mu p_\alpha^+ p_\beta^- A(s_{+-}, s_{+\gamma}, s_{-\gamma})\,\frac{-ig_{\nu\rho}}{k^2}\,\bar{u}(q^-, \sigma)(-ie\gamma^\rho)v(q^+, \sigma')\ , \tag{4.1}$$

with spin indices σ, σ' and $A(s_{+-}, s_{+\gamma}, s_{-\gamma})$ summarizing all contributions to $\eta^{(\prime)} \to \pi^+\pi^-\gamma^*$ (represented by the blob in Fig. 4.1). The Mandelstam variables s_{+-}, $s_{+\gamma}$, $s_{-\gamma}$ are defined as follows:

$$s_{+-} = (p^+ + p^-)^2\ , \quad s_{+\gamma} = (p^+ + k)^2\ , \quad s_{-\gamma} = (p^- + k)^2\ . \tag{4.2}$$

As a consequence of C invariance $A(s_{+-}, s_{+\gamma}, s_{-\gamma})$ is symmetric under the exchange $s_{+\gamma} \leftrightarrow s_{-\gamma}$. Clearly, the decay $\eta^{(\prime)} \to \pi^+\pi^- l^+ l^-$ proceeds via the two-step mechanism $\eta^{(\prime)} \to \pi^+\pi^-\gamma^*$ followed by $\gamma^* \to l^+ l^-$. Defining (in accordance with [17]) the n-body phase space element

$$d\Phi_n(P; p_1, \ldots, p_n) = \delta^{(4)}\Big(P - \sum_{i=1}^n p_i\Big) \prod_{i=1}^n \frac{d^3 p_i}{(2\pi)^3 2E_i} \tag{4.3}$$

and making use of the factorization

$$d\Phi_4(P; q^+, q^-, p^+, p^-) = d\Phi_3(P; k, p^+, p^-)\, d\Phi_2(k; q^+, q^-)\, (2\pi)^3 dk^2 \tag{4.4}$$

one finds the following relation between the differential decay width of $\eta^{(\prime)} \to \pi^+\pi^- l^+ l^-$ and the differential widths of the two sub-processes $\eta^{(\prime)} \to \pi^+\pi^-\gamma^*$ and $\gamma^* \to l^+ l^-$, see *e.g.* [137]:

$$d\Gamma(\eta^{(\prime)} \to \pi^+\pi^- l^+ l^-) = d\Gamma(\eta^{(\prime)} \to \pi^+\pi^-\gamma^*)\, d\Gamma(\gamma^* \to l^+ l^-)\, \frac{1}{\pi}\, \frac{1}{k^2\sqrt{k^2}}\, dk^2\ . \tag{4.5}$$

After integration over the dilepton phase space (PSll) one arrives at

$$\int\limits_{\mathrm{PS}ll} d\Gamma(\eta^{(\prime)} \to \pi^+\pi^- l^+ l^-) = d\Gamma(\eta^{(\prime)} \to \pi^+\pi^-\gamma^*)\, \Gamma(\gamma^* \to l^+ l^-)\, \frac{1}{\pi}\, \frac{1}{k^2\sqrt{k^2}}\, dk^2 \tag{4.6}$$

with

$$\Gamma(\gamma^* \to l^+ l^-) = \frac{\alpha}{3}\sqrt{k^2}\left(1 + \frac{2m_l^2}{k^2}\right)\sqrt{1 - \frac{4m_l^2}{k^2}}\ , \qquad \alpha = \frac{e^2}{4\pi}\ . \tag{4.7}$$

The task of the current work is to calculate $A(s_{+-}, s_{+\gamma}, s_{-\gamma})$ (or, equivalently, the amplitude $\mathcal{A}(\eta^{(\prime)} \to \pi^+\pi^-\gamma^*)$) within a chiral unitary approach.

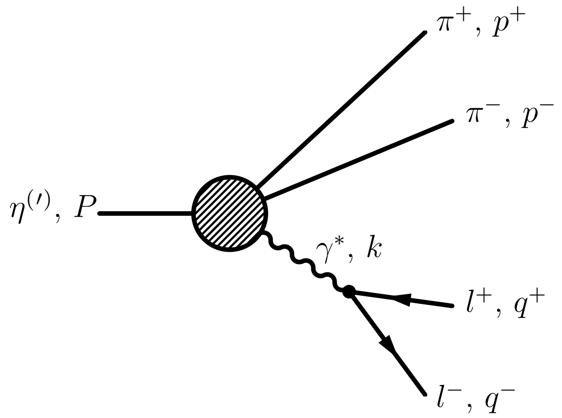

Figure 4.1: General structure of the process $\eta^{(\prime)}(P) \to \pi^+(p^+)\pi^-(p^-)l^+(q^+)l^-(q^-)$. The blob symbolizes the amplitude $\mathcal{A}(\eta^{(\prime)} \to \pi^+\pi^-\gamma^*)$. The four-momentum of the intermediate photon is denoted by $k = P - p^+ - p^- = q^+ + q^-$ with $k^2 > 0$.

4.3 One-loop calculation

In this section we present the result of the full one-loop calculation of the amplitude for $\eta^{(\prime)} \to \pi^+\pi^-\gamma^*$ in U(3) ChPT generalizing the one-loop result of [136] for the decay amplitude $\eta^{(\prime)} \to \pi^+\pi^-\gamma$. Here we will restrict ourselves to compiling the necessary formulae and outlining the basic steps of the calculation. For details we refer the reader to [136].

The amplitude $\mathcal{A}(\eta^{(\prime)} \to \pi^+\pi^-\gamma^*)$ involves the totally antisymmetric tensor $\epsilon^{\mu\nu\alpha\beta}$ and is thus of unnatural parity. At leading chiral order, the pure SU(3) process $\eta_8 \to \pi^+\pi^-\gamma^*$ is determined by the chiral anomaly of the underlying QCD Lagrangian. As discussed in Sect. 1.4.4, within ChPT the chiral QCD anomalies are accounted for by the Wess-Zumino-Witten (WZW) action [5, 6, 37, 138, 139], *cf.* Eq. (1.81),

$$\begin{aligned} S_{\text{WZW}} = &-\frac{i}{80\pi^2}\int\limits_{M_5} d^5x\,\epsilon^{ijklm}\left\langle U^\dagger\partial_i U\,U^\dagger\partial_j U\,U^\dagger\partial_k U\,U^\dagger\partial_l U\,U^\dagger\partial_m U\right\rangle \\ &+\frac{e}{16\pi^2}\int d^4x\,\epsilon^{\mu\nu\alpha\beta}A_\mu\left\langle U\partial_\nu U^\dagger U\partial_\alpha U^\dagger U\partial_\beta U^\dagger Q - U^\dagger\partial_\nu U\,U^\dagger\partial_\alpha U\,U^\dagger\partial_\beta U Q\right\rangle , \end{aligned} \tag{4.8}$$

where we have displayed only the pieces of the action relevant for the present calculation. In particular we have replaced the field strength tensors $L_{\mu\nu}$, $R_{\mu\nu}$ of the external sources by the expression corresponding to an external photon,

$$L_{\mu\nu} = R_{\mu\nu} = -eQF_{\mu\nu}\,, \tag{4.9}$$

where Q is the quark charge matrix and $F_{\mu\nu} = \partial_\mu A_\nu - \partial_\nu A_\mu$ the electromagnetic field strength tensor. The integration in the first line of Eq. (4.8) spans over a five-dimensional manifold M_5, whose boundary is Minkowskian space, and the U fields in this integral are functions on M_5. The additional fifth coordinate is defined to be timelike and the convention for the totally antisymmetric tensor is $\epsilon^{01234} = +1$, see Sect. 1.4.4 and [6, 37, 139] for further details.

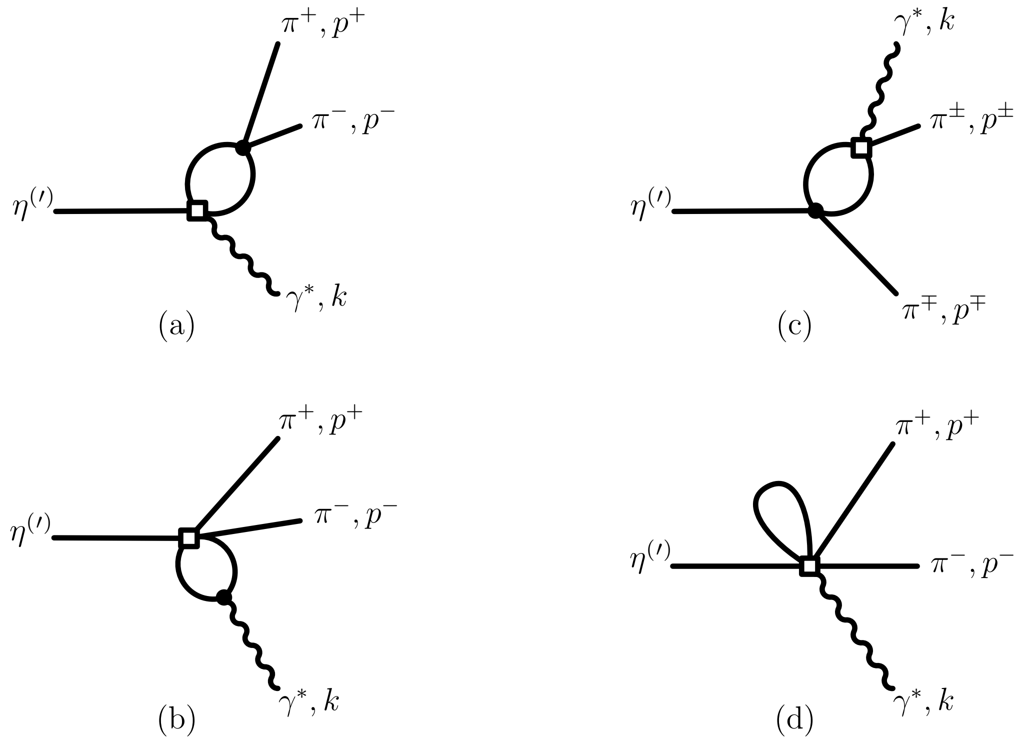

Figure 4.2: One-loop diagrams contributing to the process $\eta^{(\prime)} \to \pi^+\pi^-\gamma^*$. The empty squares denote vertices from the $\mathcal{O}(p^4)$ Lagrangian of unnatural parity, whereas vertices from the leading order Lagrangian of natural parity are indicated by a filled circle.

As explained in Sect. 1.5.3 the inclusion of the singlet field η_0 and, consequently, the extension of SU(3) ChPT to the U(3) framework introduces additional, non-anomalous terms of unnatural parity at chiral order $\mathcal{O}(p^4)$, see Eq. (1.117). The only term relevant for this calculation reads

$$\begin{aligned}\mathcal{L}_{ct}^{(4)} &= \frac{i}{2}\,\epsilon^{\mu\nu\alpha\beta}\big\langle L_{\mu\nu}D_\alpha U^\dagger D_\beta U + R_{\mu\nu}D_\alpha U D_\beta U^\dagger\big\rangle \\ &= -ie\,\epsilon^{\mu\nu\alpha\beta}\partial_\mu A_\nu\, W_3\left\langle\partial_\alpha U^\dagger\partial_\beta U Q + \partial_\alpha U\partial_\beta U^\dagger Q\right\rangle, \end{aligned} \tag{4.10}$$

where in the second line we specialized to the case of an external photon by means of Eq. (4.9). Recall that due to parity conservation W_3 is an odd function of η_0 which can be expanded in powers of the singlet field with coefficients $w_3^{(j)}$ that are not fixed by chiral symmetry.

In addition to the leading-order tree level contributions derived from Eqs. (4.8) and (4.10) there are next-to-leading order chiral corrections from one-loop graphs, decay constants, η-η' mixing, and wave function renormalization which involve terms both from the $\mathcal{O}(p^0) + \mathcal{O}(p^2)$ Lagrangian and the $\mathcal{O}(p^4)$ Lagrangian of natural parity with couplings $v_i^{(j)}$ and $\beta_i^{(j)}$, respectively. The full list of terms at $\mathcal{O}(p^4)$ can be found in App. A.2. Finally, the process $\eta^{(\prime)} \to \pi^+\pi^-\gamma^*$ receives contributions from counter terms of the unnatural parity $\mathcal{O}(p^6)$ Lagrangian, which also absorb the divergences of the one-loop integrals.

Fig. 4.2 shows the pertinent one-loop diagrams contributing to $\eta^{(\prime)} \to \pi^+\pi^-\gamma^*$ (except for contributions from wave function renormalization). The full one-loop result reads

$$\mathcal{A}^{(\text{1-loop})}(\eta^{(\prime)} \to \pi^+\pi^-\gamma^*) = -e k_\mu \epsilon_\nu p_\alpha^+ p_\beta^- \epsilon^{\mu\nu\alpha\beta} \frac{1}{4\pi^2 F_{\eta^{(\prime)}} F_\pi^2}\, \beta_{\eta^{(\prime)}}^{(\text{1-loop})} , \tag{4.11}$$

where ϵ_ν is the polarization vector of the virtual photon. For details of the calculation see [136]. The coefficients $\beta_{\eta^{(\prime)}}^{(\text{1-loop})}$ are given by

$$\begin{align} \beta_\eta^{(\text{1-loop})} = \frac{1}{\sqrt{3}} \Bigg\{ & 1 + \frac{1}{F_\eta^2} \Bigg[4\sqrt{\frac{2}{3}} \left(\sqrt{\frac{2}{3}} - 16\pi^2 w_3^{(1)r} \right) (m_K^2 - m_\pi^2) \frac{\tilde{v}_2^{(1)}}{v_0^{(2)}} - 3\Delta_\pi - 3\Delta_K \nonumber \\ & + 3I(m_K^2, m_K^2, k^2) + I(m_\pi^2, m_\pi^2, s_{+-}) + 2I(m_K^2, m_K^2, s_{+-}) \Bigg] \nonumber \\ & + 64\pi^2 \Big(\bar{w}_\eta^{(m)} + \bar{w}_\eta^{(s)} s_{+-} + \bar{w}_\eta^{(k)} k^2 \Big) \Bigg\} , \nonumber \\ \beta_{\eta'}^{(\text{1-loop})} = & \left(\sqrt{\frac{2}{3}} - 16\pi^2 w_3^{(1)r} \right) \nonumber \\ & \times \Bigg\{ 1 + \frac{1}{F_{\eta'}^2} \Bigg[4(2m_K^2 + m_\pi^2) \Big(\beta_{46}^{(0)} + 3\beta_{47}^{(0)} - \beta_{53}^{(0)} - \sqrt{\frac{3}{2}} \beta_{52}^{(1)} \Big) \nonumber \\ & \quad - 3\Delta_\pi - \frac{3}{2}\Delta_K + I(m_\pi^2, m_\pi^2, s_{+-}) + \frac{1}{2} I(m_K^2, m_K^2, s_{+-}) \nonumber \\ & \quad - 4v_1^{(2)} \Big(I'(m_\pi^2, m_{\eta'}^2, s_{+\gamma}) + I'(m_\pi^2, m_{\eta'}^2, s_{-\gamma}) \Big) \Bigg] \Bigg\} \nonumber \\ & + \frac{4}{3}\sqrt{\frac{2}{3}} (m_K^2 - m_\pi^2) \left(4\frac{\beta_{5,18}}{F_{\eta'}^2} - \frac{\tilde{v}_2^{(1)}}{v_0^{(2)}} \right) \nonumber \\ & + 32\pi^2 \sqrt{\frac{2}{3}} \Big(\bar{w}_{\eta'}^{(m)} + \bar{w}_{\eta'}^{(s)} s_{+-} + \bar{w}_{\eta'}^{(k)} k^2 \Big) . \tag{4.12} \end{align}$$

In this expression we have perturbatively substituted the pseudoscalar decay constant in the chiral limit, f, by the physical decay constants F_π, F_η, $F_{\eta'}$ of π, η, η', respectively, making of Eqs. (1.114). As in Sect. 1.5.2 we have employed the abbreviations

$$\tilde{v}_2^{(1)} = \tfrac{1}{4} f^2 - \tfrac{1}{2}\sqrt{6} v_3^{(1)} , \qquad \beta_{5,18} = \beta_5^{(0)} + \tfrac{3}{2}\beta_{18}^{(0)} . \tag{4.13}$$

The loop integrals are calculated using dimensional regularization and the pertinent regularization scale is denoted by μ. The tadpole integrals Δ_P, where P denotes a pseudoscalar meson, are defined in Eq. (1.112). The finite part of the loop integral I reads

$$\begin{align} I(m^2, M^2, p^2) = & \frac{1}{6p^2} \Big\{ - (p^2 - (m-M)^2)(p^2 - (m+M)^2) G(p^2) \tag{4.14} \\ & \qquad + (p^2 + m^2 - M^2)\Delta_m + (p^2 - m^2 + M^2)\Delta_M \Big\} \nonumber \\ & + \frac{1}{144\pi^2} (p^2 - 3m^2 - 3M^2) , \tag{4.15} \end{align}$$

where G is the finite part of the scalar one-loop integral, see Eq. (2.9). The integral I' is defined via the subtraction

$$I'(m^2, M^2, p^2) = I(m^2, M^2, p^2) - I(0, M^2, 0) \tag{4.16}$$

which guarantees chiral power counting for loops involving the η'. Since the mass of this heavy degree of freedom does not vanish in the chiral limit, its presence can in principle spoil the chiral counting scheme. However, it has been shown in [136] that all power-counting violating contributions to the process $\eta^{(\prime)} \to \pi^+\pi^-\gamma^*$ can be absorbed into a redefinition of the low-energy constant $w_3^{(1)}$; the renormalized value is denoted by $w_3^{(1)r}$.

The last terms in the expressions for $\beta_{\eta^{(\prime)}}^{(\text{1-loop})}$ in Eq. (4.12) summarize the contributions of counter terms from the $\mathcal{O}(p^6)$ Lagrangian of unnatural parity. The relations between the constants $\bar{w}_{\eta^{(\prime)}}^{(m)}$, $\bar{w}_{\eta^{(\prime)}}^{(s)}$, $\bar{w}_{\eta^{(\prime)}}^{(k)}$ and the numerous couplings of the Lagrangian of sixth chiral order are given in App. A.3.

4.4 Chiral unitary approach

From the analysis of various η and η' decays, see Chapter 3 and [132, 136], it has become clear that resonances and unitarity corrections due to final-state interactions are a necessary ingredient for the realistic description of these processes. One example is the pronounced peak structure caused by the $\rho(770)$ resonance in the $\pi^+\pi^-$ spectrum of $\eta' \to \pi^+\pi^-\gamma$ [140, 141] (see also Fig. 4.5). Hence, a conventional loop-wise expansion within ChPT is usually not sufficient to successfully describe η and—in particular—η' decays.

Instead of taking resonances into account explicitly, as *e.g.* in [137, 142, 143], we prefer to work within a chiral unitary approach which combines ChPT and a non-perturbative resummation based on the Bethe-Salpeter equation. In this framework the resulting multi-channel T-matrix of meson-meson scattering satisfies exact two-body unitarity. Our approach has the further advantages that electromagnetic gauge invariance is automatically maintained, anomalous chiral Ward identities are satisfied, and the result matches to one-loop ChPT in the low-energy limit. Resonances are generated dynamically and are identified with poles of the T-matrix in the complex energy plane.

Since this approach has already been discussed in detail in Chapters 2 and 3 we will only recapitulate the basic formulae here. From the effective Lagrangian up to fourth chiral order one extracts the partial wave interaction kernel V_ℓ for meson-meson scattering which is then iterated in the BSE

$$T_\ell = V_\ell - T_\ell \, G_\ell \, V_\ell \ . \tag{4.17}$$

The diagonal matrix G_ℓ involves the scalar loop integrals which are equipped with subtraction constants as explained at the end of Sect. 2.1. After adjusting the occurring parameters the partial-wave T-matrix resulting from the BSE accurately describes the experimental phase shifts in both the s- and p-wave channels, see Sect. 3.3.2, and we use the values of the LECs of natural parity obtained from the analysis of hadronic decay modes of η and η' in the previous chapter. The numerical values are compiled in Table 3.7.

The implementation of non-perturbative meson-meson rescattering generated by the BSE in the amplitude $\mathcal{A}(\eta^{(\prime)} \to \pi^+\pi^-\gamma^*)$ is accomplished in the same way as in [136]. The pertinent graphs are shown in Fig. 4.3 and the corresponding amplitude is added to the one-loop result presented in in the previous section. We point out that a possible double counting of one-loop contributions, which in principle could arise since the diagrams (a) and (c) in Fig. 4.3 incorporate also one-loop terms, has been properly taken care of. The amplitude corresponding to the diagram in Fig. 4.3 a is given by

$$\begin{aligned}\mathcal{A}^{(\mathrm{CCa})}(\eta^{(\prime)} \to \pi^+\pi^-\gamma^*) &= -ek_\mu \epsilon_\nu p^+_\alpha p^-_\beta \epsilon^{\mu\nu\alpha\beta} \frac{1}{4\pi^2 F_\pi^3} \\ &\qquad \times \sum_a{}' \gamma^{(\mathrm{CCa}),a}_{\eta^{(\prime)}} \, \tilde{I}(m_a^2, m_a^2, s_{+-}, C_a) \, T_1^{(a\to\pi^\pm)}(s_{+-}) \qquad (4.18)\end{aligned}$$

with coefficients

$$\begin{aligned}\gamma_\eta^{(\mathrm{CCa}),\pi^\pm} &= \gamma_\eta^{(\mathrm{CCa}),K^\pm} = \frac{1}{6}\left[\sqrt{3} + \frac{4\sqrt{2}}{3}(m_K^2 - m_\pi^2)\frac{\tilde{v}_2^{(1)}}{v_0^{(2)}}\big(\sqrt{6} - 48\pi^2 w_3^{(1)r}\big)\right], \\ \gamma_\eta^{(\mathrm{CCa}),K^0\bar{K}^0} &= -\frac{\sqrt{3}}{2}, \\ \gamma_{\eta'}^{(\mathrm{CCa}),\pi^\pm} &= \gamma_{\eta'}^{(\mathrm{CCa}),K^\pm} \\ &= \frac{1}{6}\left[\sqrt{6} - 48\pi^2 w_3^{(1)r} + \frac{4\sqrt{6}}{3}(m_K^2 - m_\pi^2)\left(4\frac{\beta_{5,18}}{F_{\eta'}^2} - \frac{\tilde{v}_2^{(1)}}{v_0^{(2)}}\right)\right], \\ \gamma_{\eta'}^{(\mathrm{CCa}),K^0\bar{K}^0} &= -2\sqrt{\frac{2}{3}}(m_K^2 - m_\pi^2)\left(4\frac{\beta_{5,18}}{F_{\eta'}^2} - \frac{\tilde{v}_2^{(1)}}{v_0^{(2)}}\right). \qquad (4.19)\end{aligned}$$

The symbol $\sum'$ in Eq. (4.18) denotes summation over the meson pairs $\pi^+\pi^-$, K^+K^- and $K^0\bar{K}^0$ and $T_1^{(a\to b)}$ represents the p-wave part of the T-matrix element for scattering of a meson pair a into a meson pair b as described by the BSE. The modified loop integral $\tilde{I}$ is given by

$$\tilde{I}(m^2, M^2, p^2, C_{mM}) = I(m^2, M^2, p^2) + (p^2 - 3m^2 - 3M^2)C_{mM} \qquad (4.20)$$

with I defined in Eq. (4.14). In order to keep the notation compact we set

$$C_\pi \equiv C_{m_\pi m_\pi}, \qquad C_K \equiv C_{m_K m_K}, \qquad C_{\pi\eta} \equiv C_{m_\pi m_\eta}, \qquad C_{\pi\eta'} \equiv C_{m_\pi m_{\eta'}}. \qquad (4.21)$$

Note that the definition of $\tilde{I}$ slightly differs from that of $\tilde{I}_1$ in [136], where the constant C was chosen to be the coefficient of p^2 instead of $(p^2 - 3m^2 - 3M^2)$. Here, we prefer to work with the decomposition in Eq. (4.20) since then the regularization scale dependence of I can be completely absorbed into the constant C. We point out that in an effective field theory framework one is free to arbitrarily modify the analytic piece of an amplitude by adjusting unconstrained counter terms.

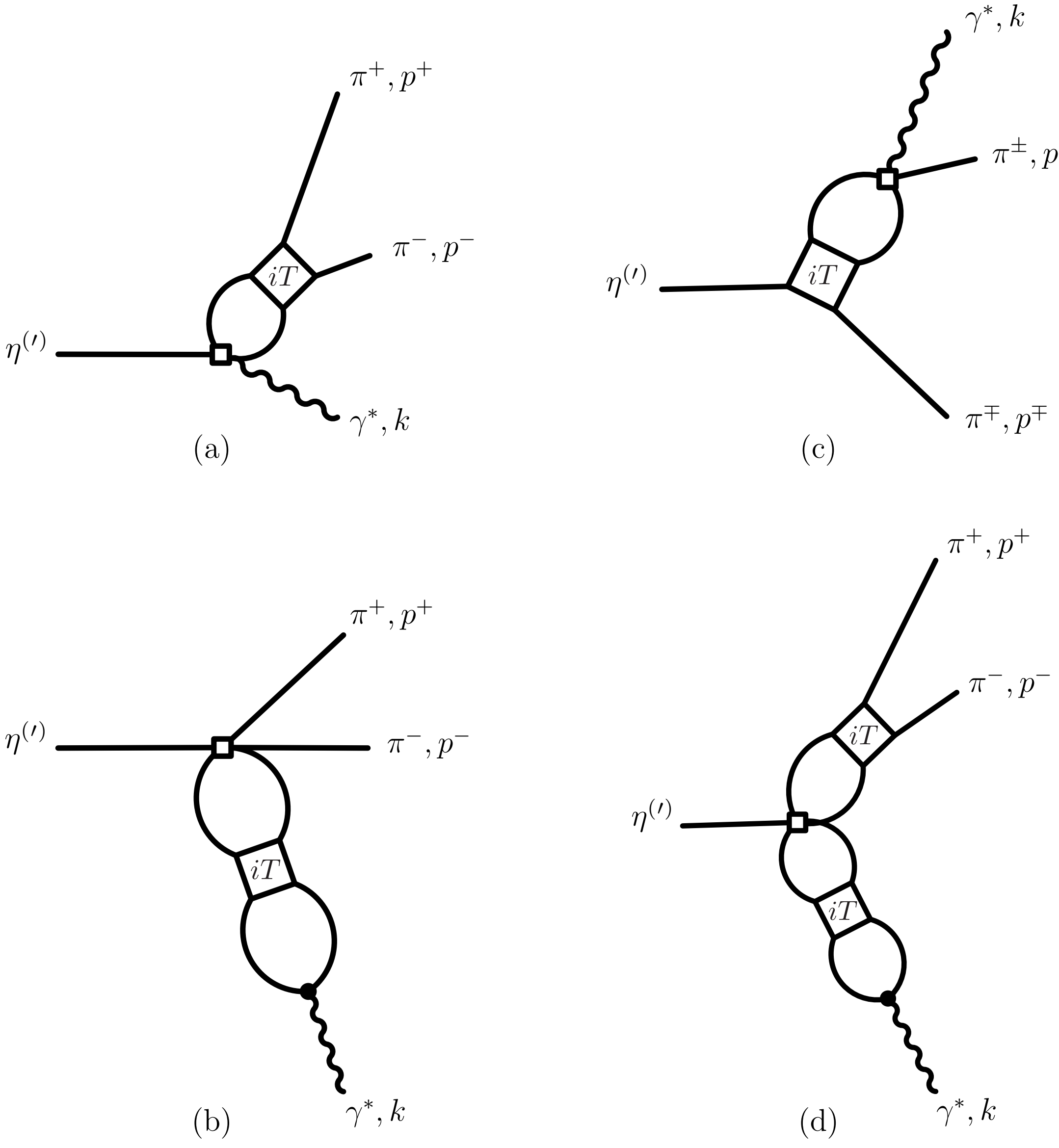

(a) (c)

(b) (d)

Figure 4.3: Set of meson-meson rescattering diagrams which contribute to the process $\eta^{(\prime)} \to \pi^+\pi^-\gamma^*$ and are taken into account in this approach. The empty squares denote vertices from the $\mathcal{O}(p^4)$ Lagrangian of unnatural parity whereas vertices from the leading order Lagrangian of natural parity are indicated by a filled circle.

The diagram in Fig. 4.3 b produces the amplitude

$$\mathcal{A}^{(\mathrm{CCb})}(\eta^{(\prime)} \to \pi^+\pi^-\gamma^*) = -e k_\mu \epsilon_\nu p_\alpha^+ p_\beta^- \epsilon^{\mu\nu\alpha\beta} \frac{1}{4\pi^2 F_\pi^5} {\sum_a}' \gamma_{\eta^{(\prime)}}^{(\mathrm{CCb}),a}\ \tilde{I}(m_K^2, m_K^2, k^2, C_K) \\ \times \Big[T_1^{(a\to\pi^\pm)}(k^2)\ \tilde{I}(m_\pi^2, m_\pi^2, k^2, C_\pi) + T_1^{(a\to K^\pm)}(k^2)\ \tilde{I}(m_K^2, m_K^2, k^2, C_K)\Big]\ , \quad (4.22)$$

where the coefficients $\gamma_{\eta^{(\prime)}}^{(\mathrm{CCb}),a}$ are given by

$$\gamma_\eta^{(\mathrm{CCb}),\pi^\pm} = \gamma_{\eta'}^{(\mathrm{CCb}),\pi^\pm} = 0\,, \qquad \gamma_\eta^{(\mathrm{CCb}),K^\pm} = -\gamma_\eta^{(\mathrm{CCb}),K^0\bar{K}^0} = \frac{\sqrt{3}}{2}\,, \\ \gamma_{\eta'}^{(\mathrm{CCb}),K^\pm} = -\gamma_{\eta'}^{(\mathrm{CCb}),K^0\bar{K}^0} = 2\sqrt{\frac{2}{3}}(m_K^2 - m_\pi^2)\left(4\frac{\beta_{5,18}}{F_{\eta'}^2} - \frac{\tilde{v}_2^{(1)}}{v_0^{(2)}}\right)\ . \quad (4.23)$$

The amplitude corresponding to graph (c) in Fig. 4.3 is given by

$$\mathcal{A}^{(\mathrm{CCc})}(\eta^{(\prime)} \to \pi^+\pi^-\gamma^*) = -e k_\mu \epsilon_\nu p_\alpha^+ p_\beta^- \epsilon^{\mu\nu\alpha\beta} \frac{1}{4\pi^2 F_\pi^3} \\ \times \frac{1}{2}\Bigg\{\frac{1}{\sqrt{3}}\big[\tilde{I}(m_\pi^2, m_\eta^2, s_{+\gamma}, C_{\pi\eta})\ T_1^{(\eta^{(\prime)}\pi^+\to\eta\pi^+)}(s_{+\gamma}) \\ + \tilde{I}(m_\pi^2, m_\eta^2, s_{-\gamma}, C_{\pi\eta})\ T_1^{(\eta^{(\prime)}\pi^-\to\eta\pi^-)}(s_{-\gamma})\big] \\ + \left(\sqrt{\frac{2}{3}} - 16\pi^2 w_3^{(1)r}\right)\big[\tilde{I}'(m_\pi^2, m_{\eta'}^2, s_{+\gamma}, C_{\pi\eta'})\ T_1^{(\eta^{(\prime)}\pi^+\to\eta'\pi^+)}(s_{+\gamma}) \\ + \tilde{I}'(m_\pi^2, m_{\eta'}^2, s_{-\gamma}, C_{\pi\eta'})\ T_1^{(\eta^{(\prime)}\pi^-\to\eta'\pi^-)}(s_{-\gamma})\big]\Bigg\}, \quad (4.24)$$

where the integral $\tilde{I}'$ is defined analogously to I', Eq. (4.16), by

$$\tilde{I}'(m^2, M^2, p^2, C_{mM}) = \tilde{I}(m^2, M^2, p^2, C_{mM}) - \tilde{I}(0, M^2, 0, C_{mM})\ . \quad (4.25)$$

Finally, we include the diagram with two insertions of iterated meson-meson rescattering, Fig. 4.3 d. The corresponding amplitude reads

$$\mathcal{A}^{(2\,\mathrm{CC})}(\eta^{(\prime)} \to \pi^+\pi^-\gamma^*) = -e k_\mu \epsilon_\nu p_\alpha^+ p_\beta^- \epsilon^{\mu\nu\alpha\beta} \frac{1}{4\pi^2 F_\pi^5} {\sum_{a,b}}' \gamma_{\eta^{(\prime)}}^{(2\,\mathrm{CC}),a,b} \\ \times \tilde{I}(m_a^2, m_a^2, s_{+-}, C_a)\ T_1^{(a\to\pi^\pm)}(s_{+-})\ \tilde{I}(m_b^2, m_b^2, k^2, C_b) \\ \times \big[T_1^{(b\to\pi^\pm)}(k^2)\, \tilde{I}(m_\pi^2, m_\pi^2, k^2, C_\pi) + T_1^{(b\to K^\pm)}(k^2)\, \tilde{I}(m_K^2, m_K^2, k^2, C_K)\big] \quad (4.26)$$

with coefficients $\gamma_{\eta^{(\prime)}}^{(2\,\mathrm{CC}),a,b}$ symmetric under the interchange $a \leftrightarrow b$

$$\begin{aligned}
\gamma_{\eta}^{(2\,\mathrm{CC}),\pi^\pm,K^\pm} &= -\gamma_{\eta}^{(2\,\mathrm{CC}),\pi^\pm,K^0\bar{K}^0} = -\frac{1}{2}\gamma_{\eta}^{(2\,\mathrm{CC}),K^\pm,K^0\bar{K}^0} = \frac{\sqrt{3}}{4}\,, \\
\gamma_{\eta'}^{(2\,\mathrm{CC}),\pi^\pm,K^\pm} &= -\gamma_{\eta'}^{(2\,\mathrm{CC}),\pi^\pm,K^0\bar{K}^0} = -\frac{1}{2}\gamma_{\eta'}^{(2\,\mathrm{CC}),K^\pm,K^0\bar{K}^0} \\
&= \sqrt{\frac{2}{3}}(m_K^2 - m_\pi^2)\left(4\frac{\beta_{5,18}}{F_{\eta'}^2} - \frac{\tilde{v}_2^{(1)}}{v_0^{(2)}}\right)
\end{aligned} \tag{4.27}$$

and zero otherwise.

4.5 Results

The chiral unitary approach utilized in this investigation involves several free parameters which must be fixed from experiment. On the one hand, there are the coupling constants of the chiral Lagrangian which can be grouped into coefficients of the natural parity part of $\mathcal{O}(p^0) + \mathcal{O}(p^2)$ and $\mathcal{O}(p^4)$, $v_i^{(j)}$ and $\beta_i^{(j)}$, respectively, and coefficients of the unnatural parity part of $\mathcal{O}(p^4)$ and $\mathcal{O}(p^6)$, $w_i^{(j)}$ and $\bar{w}_i^{(j)}$, respectively. On the other hand, there are the subtraction constants a and C in the loop integrals whose values correspond to a specific choice of the infinitely many higher order counter terms neglected in this non-perturbative approach. As mentioned earlier the coupling constants of the Lagrangian of natural parity and the subtraction constant $a_{\pi\pi}^{(I=J=1)}$ in the isospin one p-wave $\pi\pi$ channel are fixed by the previous fit to the hadronic decay modes of η and η', $\eta^{(\prime)} \to 3\pi$ and $\eta' \to \eta\pi\pi$, and the phase shifts of meson-meson scattering, *cf.* Chapter 3. This fit is in very good agreement with the bulk of the available experimental data. The subtraction constants in the other meson-meson channels do not have any relevant impact on the discussed data and can be set to zero for our purposes. The pseudoscalar decay constants are set to $F_\pi = 92.4\,\mathrm{MeV}$, $F_\eta = 1.3F_\pi$, and $F_{\eta'} = 1.1F_\pi$ [132, 136].

The couplings of the unnatural parity part of the Lagrangian and the subtraction constants C are taken as free parameters, which are constrained by fitting to the available spectra and widths of the decays $\eta^{(\prime)} \to \pi^+\pi^-\gamma$. It turns out, however, that in order to achieve agreement with the experimental data, only the subtraction constant in the pion loops, C_π, is required to have a non-vanishing value, and we set all other subtraction constants to zero for simplicity. To further reduce the number of parameters and for consistency with previous investigations [132, 136], we also set the renormalized coupling constant $w_3^{(1)r}$ of the unnatural parity Lagrangian at $\mathcal{O}(p^4)$ to zero. We have confirmed that small variations in $w_3^{(1)r}$ do not alter our conclusions. Finally, the combinations of $\mathcal{O}(p^6)$ unnatural parity couplings denoted by $\bar{w}_{\eta^{(\prime)}}^{(k)}$, which do not contribute to processes with on-shell photons and thus cannot be constrained by $\eta^{(\prime)} \to \pi^+\pi^-\gamma$, will be neglected for the time being. Changes of the results due to non-zero values of these coefficients will be discussed at the end of this section. To summarize, there are five parameters, C_π, $\bar{w}_\eta^{(m)}$, $\bar{w}_\eta^{(s)}$, $\bar{w}_{\eta'}^{(m)}$, and $\bar{w}_{\eta'}^{(s)}$ which are constrained by fitting the decays $\eta^{(\prime)} \to \pi^+\pi^-\gamma$.

Afterwards, we can predict the spectra and widths of $\eta^{(\prime)} \to \pi^+\pi^- l^+ l^-$ within this approach.

The data of $\eta^{(\prime)} \to \pi^+\pi^-\gamma$ involve the partial decay widths [17] and the di-pion spectra from [140, 141, 144, 145]. In order to perform a global least-squares fit to these different data sets we employ the following definition for the χ^2-function:

$$\frac{\chi^2}{\text{d.o.f.}} = \frac{\sum_i n_i}{N(\sum_i n_i - p)} \sum_i \frac{\chi_i^2}{n_i} \ , \tag{4.28}$$

where N is the number of observables and p the number of free parameters in the approach. The quantity χ_i^2 is the standard χ^2-value computed for the i-th data set with n_i data points. The above definition was introduced in [104] to equally weight each data set and to prevent, *e.g.*, sets with only one data point (such as decay widths) from being dominated by sets with many data points (such as spectra).

In order to quantify an error for our analysis we employ the condition [17]

$$\frac{\chi^2}{\text{d.o.f.}} \leq \frac{\chi^2_{\text{min}}}{\text{d.o.f.}} + \frac{\Delta\chi^2}{\text{d.o.f.}} \tag{4.29}$$

where $\Delta\chi^2$ is derived from the p-value of the χ^2 probability distribution function. One finds that in the present investigation employing $\Delta\chi^2/\text{d.o.f.} = 1.08$ corresponds to the 1σ confidence region. Strictly speaking, this standard definition of a confidence region, Eq. (4.29), holds only if the fit is performed to just one observable and the fit function is linear in the fit parameters. Although both constraints are not fulfilled here, one can expect Eq. (4.29) to be a reasonable approximation in the vicinity of the minimum of the χ^2-function, see also the discussion in Sect. 5.3.1. We have significantly improved our fitting routine compared to the previous investigation [136] and performed a large number of fits so that the 1σ confidence region is populated by about 1000 qualitatively different fits providing a realistic estimate of the theoretical uncertainty within this approach.

In Figs. 4.4 and 4.5 the result of the calculation is compared to the available experimental spectra which are given in terms of the photon energy for $\eta \to \pi^+\pi^-\gamma$ and in terms of the invariant mass of the $\pi^+\pi^-$ system for $\eta' \to \pi^+\pi^-\gamma$. The solid line corresponds to the best fit with an overall $\chi^2/\text{d.o.f.} = 2.23$, the error bands indicate the 1σ confidence level. For the η' decay the agreement with the two experimental spectra from [140, 141] is very good as already observed in [136]. The experimental situation for the η decay is not as consistent as for $\eta' \to \pi^+\pi^-\gamma$. First, the two spectra published in [144, 145] have not been corrected for the detection efficiency which is given separately in [144], but must be deduced in [145]. Also, in both experiments it is impossible to quantify the systematic error resulting from the correction of the detection efficiency which introduces an uncontrolled uncertainty in the data. Second, when taking into account the two data sets from [144] and [145] simultaneously in the fit, it turns out that they are not fully consistent, at least without knowledge of the complete systematic errors. As a consequence, the major part of the total $\chi^2/\text{d.o.f.}$ value is due to the disagreement between the two data sets. In fact, the best fit (solid line in Fig. 4.4) must be considered as a compromise of [144] and [145], so that under these circumstances a total $\chi^2/\text{d.o.f.}$ close to 1 cannot be achieved. If, however, only one of the two spectra is included in the fit, a total $\chi^2/\text{d.o.f.} \simeq 1$ can be obtained. In this context, further experimental

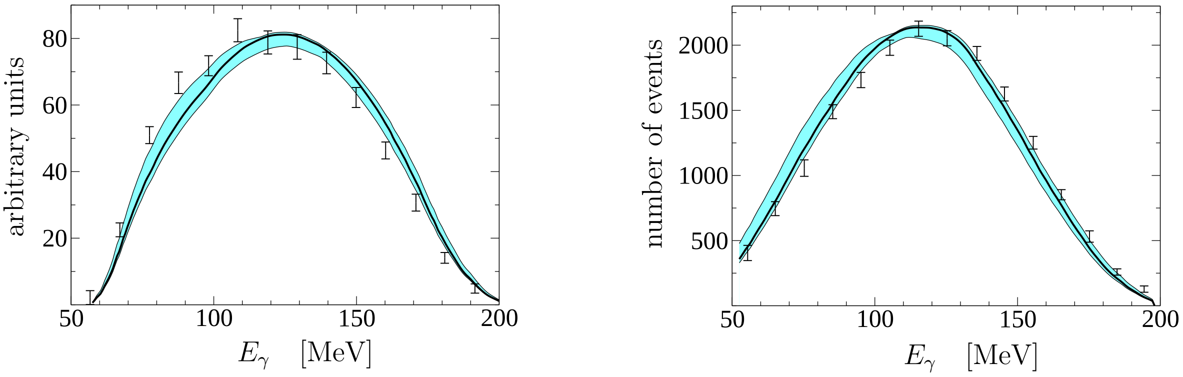

Figure 4.4: Photon spectrum of $\eta \to \pi^+\pi^-\gamma$ compared to experimental data from [144] (left) and [145] (right). The solid line corresponds to the fit with minimal χ^2, the error band indicates the 1σ confidence region. For comparison with the experimental data points, the curves have been multiplied by the experimental detection efficiencies, hence the different shapes in the two plots.

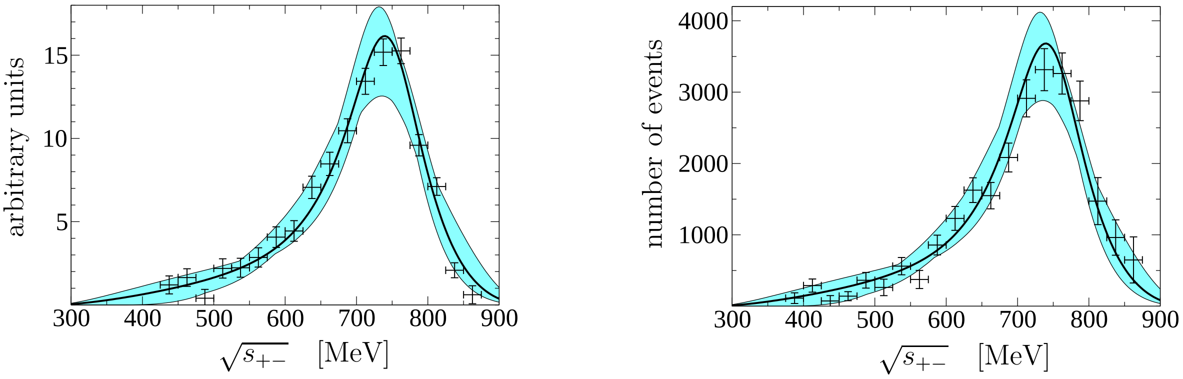

Figure 4.5: Invariant mass spectrum of the $\pi^+\pi^-$ system in $\eta' \to \pi^+\pi^-\gamma$ compared to experimental data from [140] (left) and [141] (right). The solid line corresponds to the fit with minimal χ^2, the error band indicates the 1σ confidence region. All curves are normalized to the integral of the experimental histogram.

investigations—such as [100, 146]—with substantially improved accuracy should lead to a more consistent picture of the $\eta \to \pi^+\pi^-\gamma$ spectrum.

The numerical results for the branching ratios and decay widths of $\eta^{(\prime)} \to \pi^+\pi^-\gamma$, $\eta^{(\prime)} \to \pi^+\pi^-l^+l^-$ are shown in Table 4.1. The central values of our results correspond to the fit with minimal χ^2, the error bars reflect the 1σ confidence region given within our approach. The agreement with the decay modes involving on-shell photons, which have been taken as input to the fit, is very good. The numerical values of the fit parameters, *i.e.* the counter terms $\bar{w}^{(m)}_{\eta^{(\prime)}}$, $\bar{w}^{(s)}_{\eta^{(\prime)}}$ and the subtraction constant C_π, are compiled in Table 4.2. Having fixed all parameters from data, we can make predictions for the decays into $\pi^+\pi^-$ and a lepton-antilepton pair. Up to now, the only branching ratio of this type which has been determined experimentally is $\eta \to \pi^+\pi^-e^+e^-$. We compare our result with the very recent experiment at WASA@CELSIUS [147] which has improved precision compared to the PDG number [17] and we observe nice agreement. Being somewhat on the low side, our result is also compatible with the preliminary number of

	this work	[142, 143]	[137]	experiment
BR($\eta \to \pi^+\pi^-\gamma$) [%]	$4.68^{+0.09}_{-0.09}$		6.9	4.69 ± 0.5 [17]
BR($\eta' \to \pi^+\pi^-\gamma$) [%]	$29.4^{+2.7}_{-4.3}$		25	29.4 ± 0.9 [17]
BR($\eta \to \pi^+\pi^-e^+e^-$) [$10^{-4}$]	$2.99^{+0.06}_{-0.09}$		3.6	4.3 ± 1.7 [147]
BR($\eta' \to \pi^+\pi^-e^+e^-$) [$10^{-3}$]	$2.13^{+0.17}_{-0.31}$		1.8	—
BR($\eta \to \pi^+\pi^-\mu^+\mu^-$) [$10^{-9}$]	$7.5^{+1.8}_{-0.7}$		12	—
BR($\eta' \to \pi^+\pi^-\mu^+\mu^-$) [$10^{-5}$]	$1.57^{+0.40}_{-0.47}$		2.0	—
$\Gamma(\eta \to \pi^+\pi^-\gamma)$ [eV]	$60.9^{+1.1}_{-1.2}$	62		60.8 ± 3.5 [17]
$\Gamma(\eta' \to \pi^+\pi^-\gamma)$ [keV]	60^{+6}_{-9}			60 ± 5 [17]
$\Gamma(\eta \to \pi^+\pi^-e^+e^-)$ [meV]	389^{+8}_{-11}	380		560 ± 260 [147]
$\Gamma(\eta' \to \pi^+\pi^-e^+e^-)$ [eV]	431^{+35}_{-62}			—
$\Gamma(\eta \to \pi^+\pi^-\mu^+\mu^-)$ [μeV]	$9.8^{+2.3}_{-0.9}$			—
$\Gamma(\eta' \to \pi^+\pi^-\mu^+\mu^-)$ [eV]	$3.2^{+0.9}_{-1.0}$			—

Table 4.1: Results for the branching ratios (BR) and widths (Γ) of the decay modes under consideration compared to experimental values and the theoretical analyses [142, 143] and [137]. See text for further details.

$\bar{w}_\eta^{(m)} \times 10^3$	$\bar{w}_{\eta'}^{(m)} \times 10^3$	$\bar{w}_\eta^{(s)} \times 10^3\,\mathrm{GeV}^2$	$\bar{w}_{\eta'}^{(s)} \times 10^3\,\mathrm{GeV}^2$	$C_\pi \times 10^2$
$-3.4^{+6.6}_{-2.0}$	$-20.1^{+35.1}_{-7.5}$	$1.2^{+2.6}_{-11.8}$	$-8.8^{+18.5}_{-23.8}$	$1.9^{+0.7}_{-3.6}$

Table 4.2: Numerical values of the fitted parameters at the regularization scale $\mu = 1\,\mathrm{GeV}$. The central values correspond to the fit with minimal χ^2, the error ranges are given by the 1σ confidence region.

the KLOE Collaboration [146]

$$\mathrm{BR}(\eta \to \pi^+\pi^-e^+e^-)_{\mathrm{KLOE}} = (4.6 \pm 1.4 \pm 0.5) \times 10^{-4} \tag{4.30}$$

whose error bars will be drastically reduced once the analysis of the full data sample is completed.

Moreover, we can compare our results with those of [142, 143] and [137]. In [142, 143] a chiral Lagrangian with explicit vector mesons is used to calculate both the decay widths and spectra of $\eta \to \pi^+\pi^-\gamma$ and $\eta \to \pi^+\pi^-e^+e^-$. As shown in Table 4.1 and Figs. 4.6, 4.7 the agreement with our results is very good. However, it should be remarked that the results presented in [143] depend sensitively on the numerical values employed for the meson masses. Using the final expression Eq. (4) in [143] and inserting up-to-date meson mass values from [17], one computes $\Gamma(\eta \to \pi^+\pi^-e^+e^-) = 403\,\mathrm{meV}$ instead of $380\,\mathrm{meV}$ as given in [143]. Also, the invariant mass spectra shown in Figs. 4.6, 4.7 are rescaled accordingly. In [137], on the other hand, a meson exchange model has been employed

		this work	[17]	rel. acc.
$\frac{\Gamma(\eta \to \pi^+\pi^-e^+e^-)}{\Gamma(\eta \to \pi^+\pi^-\gamma)}$	$[10^{-3}]$	$6.39\,^{+0.04}_{-0.06}$	$9\,^{+11}_{-5}$	0.9 %
$\frac{\Gamma(\eta' \to \pi^+\pi^-e^+e^-)}{\Gamma(\eta' \to \pi^+\pi^-\gamma)}$	$[10^{-3}]$	$7.24\,^{+0.04}_{-0.10}$	—	1.2 %
$\frac{\Gamma(\eta \to \pi^+\pi^-\mu^+\mu^-)}{\Gamma(\eta \to \pi^+\pi^-\gamma)}$	$[10^{-7}]$	$1.61\,^{+0.38}_{-0.12}$	—	23.1 %
$\frac{\Gamma(\eta' \to \pi^+\pi^-\mu^+\mu^-)}{\Gamma(\eta' \to \pi^+\pi^-\gamma)}$	$[10^{-5}]$	$5.4\,^{+1.6}_{-1.7}$	—	30.9 %

Table 4.3: Branching ratios of the decay modes into $\pi^+\pi^-l^+l^-$ with respect to the $\pi^+\pi^-\gamma$ decays. The experimental value quoted in the third column is taken from [17]. The relative accuracies of the theoretical results are given in the last column. For simplicity they are derived from the larger of the two error bars.

to calculate numerous decay modes of light unflavored mesons. Despite dissimilarities between [137] and our approach the numerical results are in reasonable agreement. We point out that—in contrast to our work—no theoretical error estimates are given in [137, 142, 143].

The ratios between the $\pi^+\pi^-l^+l^-$ and the $\pi^+\pi^-\gamma$ decay channels are given in Tab. 4.3. The small theoretical uncertainties for the decays into an e^+e^- pair are further reduced down to about 1% in these ratios, while the theoretical accuracies for the $\mu^+\mu^-$ decay ratios remain roughly unaffected. This indicates that the $\pi^+\pi^-e^+e^-$ and $\pi^+\pi^-\gamma$ decays are correlated which can be traced back to the shape of the QED part $\Gamma(\gamma^* \to e^+e^-)/(k^2\sqrt{k^2})$ in Eq. (4.6) describing the transition $\gamma^* \to e^+e^-$. This function possesses a pronounced peak at the virtual photon mass $k_e^2 = (1+\sqrt{21})m_e^2 \approx 5.6\,m_e^2$ and projects out the values of the subprocesses $\eta^{(\prime)} \to \pi^+\pi^-\gamma^*$ at k_e^2—close to the photon on-shell point $k^2 = 0$. For the $\mu^+\mu^-$ decays, on the other hand, the respective value $k_\mu^2 = (1+\sqrt{21})m_\mu^2 \approx 5.6\,m_\mu^2$ is relatively far apart from $k^2 = 0$ so that these decays are not immediately correlated to the $\pi^+\pi^-\gamma$ decays. We observe that for photon virtualities which are not too close to the upper boundary of phase space the rate $\Gamma(\eta^{(\prime)} \to \pi^+\pi^-\gamma^*)$ in our approach can be very well approximated by a Gaussian,

$$\Gamma(\eta^{(\prime)} \to \pi^+\pi^-\gamma^*)(k^2) \simeq \Gamma(\eta^{(\prime)} \to \pi^+\pi^-\gamma)\exp(-k^2/\Lambda^2)\,, \tag{4.31}$$

with $\Lambda = \big(97.8^{+1.8}_{-2.8}\big)$ MeV and $\Lambda = \big(167.3^{+4.5}_{-5.2}\big)$ MeV for the η and η' decay, respectively. In combination with the sharply peaked QED part the dependence on the small variations in Λ is further reduced in the branching ratios $\Gamma(\eta^{(\prime)} \to \pi^+\pi^-e^+e^-)/\Gamma(\eta^{(\prime)} \to \pi^+\pi^-\gamma)$ resulting in the small relative uncertainties of about 1% mentioned above.

In Figs. 4.6 and 4.7 we present our predictions for the $\pi^+\pi^-$ and l^+l^- invariant mass spectra, respectively. The lepton-antilepton spectra are strongly peaked right above threshold, so for illustrational purposes we have multiplied these spectra by a factor k^2 which reduces the otherwise extremely pronounced peak. Due to the tiny branching fractions of the decays into $\pi^+\pi^-\mu^+\mu^-$ it will be experimentally very challenging to

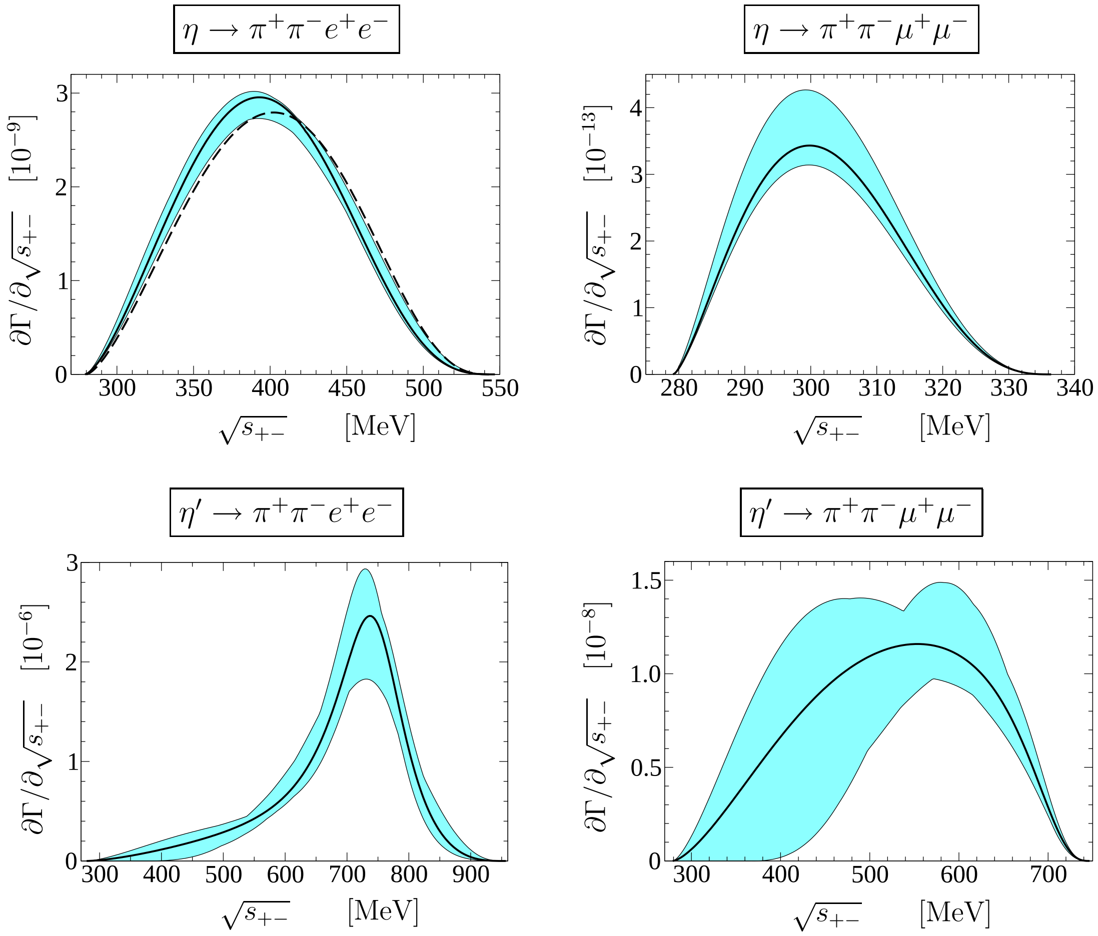

Figure 4.6: Predicted invariant mass spectra of the $\pi^+\pi^-$ system in the different decay modes. The solid lines represent the fit with minimal χ^2, the error bands indicate the 1σ confidence region. The result of [143] is represented by the dashed line in the upper left plot.

measure these kinds of spectra. The spectra of the decays involving an electron-positron pair, however, are likely to be probed at the ongoing experiments at KLOE [146] and at COSY-Jülich [100].

We reconfirm the findings of [136] regarding the importance of the different coupled channels diagrams in Fig. 4.3. The by far largest contribution to the decay amplitude stems from $\pi^+\pi^-$ final-state interactions, *cf.* Fig. 4.3a, whereas the diagram in Fig. 4.3d, which mimics the simultaneous exchange of two vector mesons within our approach, yields only small corrections. This is in contrast to the assumption of complete vector meson dominance.

The decay modes $\eta^{(\prime)} \to \pi^+\pi^- l^+ l^-$ involve $\mathcal{O}(p^6)$ counter terms which generate contributions proportional to k^2 and do not contribute to the decays with on-shell photons. Consequently, they cannot be fixed by fitting to $\eta^{(\prime)} \to \pi^+\pi^-\gamma$ data. In order to examine their impact on the results for $\eta^{(\prime)} \to \pi^+\pi^- l^+ l^-$ we have varied their values in the range $(-10 \ldots + 10) \times 10^3\,\mathrm{GeV}^{-2}$ which is motivated by the size of the other $\mathcal{O}(p^6)$ couplings, *cf.* Table 4.2. The enlargement of the error ranges for the branching ratios and widths

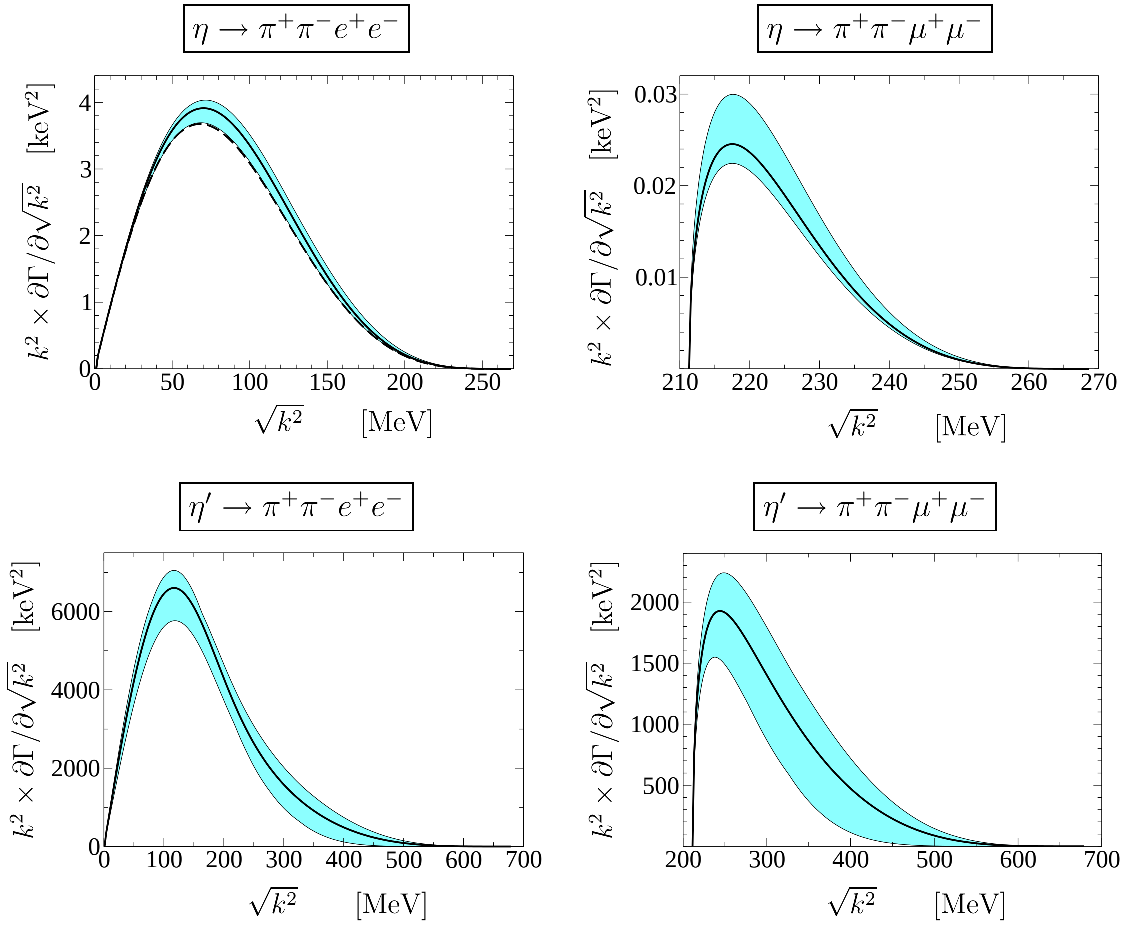

Figure 4.7: Predicted invariant mass spectra of the lepton-antilepton pair in the different decay modes. The solid lines represent the fit with minimal χ^2, the error bands indicate the 1σ confidence region. For illustrational reasons the spectra are multiplied by a factor k^2. The result of [143] is represented by the dashed line in the upper left plot.

		this work	experiment
$\mathrm{BR}(\eta \to \pi^+\pi^- e^+ e^-)$	$[10^{-4}]$	$2.99\,^{+0.08}_{-0.11}$	4.3 ± 1.7 [147]
$\mathrm{BR}(\eta' \to \pi^+\pi^- e^+ e^-)$	$[10^{-3}]$	$2.13\,^{+0.19}_{-0.32}$	—
$\mathrm{BR}(\eta \to \pi^+\pi^- \mu^+ \mu^-)$	$[10^{-9}]$	$7.5\,^{+4.5}_{-2.7}$	—
$\mathrm{BR}(\eta' \to \pi^+\pi^- \mu^+ \mu^-)$	$[10^{-5}]$	$1.57\,^{+0.96}_{-0.75}$	—
$\Gamma(\eta \to \pi^+\pi^- e^+ e^-)$	[meV]	$389\,^{+10}_{-13}$	560 ± 260 [147]
$\Gamma(\eta' \to \pi^+\pi^- e^+ e^-)$	[eV]	$431\,^{+38}_{-64}$	—
$\Gamma(\eta \to \pi^+\pi^- \mu^+ \mu^-)$	[μeV]	$9.8\,^{+5.8}_{-3.5}$	—
$\Gamma(\eta' \to \pi^+\pi^- \mu^+ \mu^-)$	[eV]	$3.2\,^{+2.0}_{-1.6}$	—

Table 4.4: This table illustrates how the uncertainties of the results grow if variations of k^2-dependent counter terms are taken into account.

		this work	[17]	rel. acc.
$\dfrac{\Gamma(\eta \to \pi^+\pi^- e^+e^-)}{\Gamma(\eta \to \pi^+\pi^-\gamma)}$	$[10^{-3}]$	$6.39\,^{+0.08}_{-0.11}$	$9\,^{+11}_{-5}$	$1.6\,\%$
$\dfrac{\Gamma(\eta' \to \pi^+\pi^- e^+e^-)}{\Gamma(\eta' \to \pi^+\pi^-\gamma)}$	$[10^{-3}]$	$7.24\,^{+0.09}_{-0.15}$	—	$1.9\,\%$
$\dfrac{\Gamma(\eta \to \pi^+\pi^- \mu^+\mu^-)}{\Gamma(\eta \to \pi^+\pi^-\gamma)}$	$[10^{-7}]$	$1.61\,^{+0.95}_{-0.55}$	—	$58.8\,\%$
$\dfrac{\Gamma(\eta' \to \pi^+\pi^- \mu^+\mu^-)}{\Gamma(\eta' \to \pi^+\pi^-\gamma)}$	$[10^{-5}]$	$5.4\,^{+3.6}_{-2.6}$	—	$66.2\,\%$

Table 4.5: Branching ratios of decay modes into $\pi^+\pi^-l^+l^-$ with respect to $\pi^+\pi^-\gamma$ decays when k^2-dependent counter terms are taken into account. The experimental value quoted in the third column is taken from [17]. The relative accuracies of the theoretical results are given in the last column. For simplicity they are derived from the larger of the two error bars.

following from this variation is tabulated in Table 4.4. It turns out that the influence of the k^2 terms is rather mild for the decays involving an electron-positron pair owing to the fact that the spectra of such decay modes are strongly enhanced at small k^2, *cf.* Fig. 4.7. For the decays into $\pi^+\pi^-\mu^+\mu^-$, on the other hand, where k^2 is bounded below by $4m_\mu^2$, the uncertainties from the 1σ confidence regions are roughly doubled by taking into account the counter terms $\bar{w}^{(k)}_{\eta^{(\prime)}}$.

Finally, in Tab. 4.5 we display the ratios $\Gamma(\eta^{(\prime)} \to \pi^+\pi^-l^+l^-)/\Gamma(\eta^{(\prime)} \to \pi^+\pi^-\gamma)$ in the presence of the k^2 terms. The relative uncertainties for the $\mu^+\mu^-$ decays are again approximately doubled with respect to Tab. 4.3 if these counter terms are taken into account.

4.6 Conclusions

In this chapter we have investigated the decays $\eta, \eta' \to \pi^+\pi^-l^+l^-$ within a chiral unitary approach based on the chiral effective Lagrangian and a coupled-channels Bethe-Salpeter equation. Utilization of the chiral effective Lagrangian guarantees that symmetries and symmetry-breaking patterns of the underlying theory QCD are incorporated in a model-independent fashion. In particular, contributions due to chiral anomalies enter through the Wess-Zumino-Witten Lagrangian which does not involve any low-energy constants. Besides, counter terms of unnatural parity at leading and next-to-leading order are also taken into account.

We have first performed a full one-loop calculation in ChPT. However, unitarity effects due to final-state interactions are important in η and, in particular, in η' decays and must be treated non-perturbatively. To this aim, meson-meson rescattering is accounted for in a Bethe-Salpeter equation which satisfies exact two-body unitarity.

This method has already been applied successfully to the anomalous decays $\eta^{(\prime)} \to$

$\gamma^{(*)}\gamma^{(*)}$ [132] and $\eta^{(\prime)} \to \pi^+\pi^-\gamma$ [136], and to the hadronic decay modes of η and η'. The parameters in our approach are fixed by the latter two processes and meson-meson scattering phase shifts, so that we obtain predictions for the decay widths and spectra of $\eta, \eta' \to \pi^+\pi^- l^+ l^-$. The decay of η into $\pi^+\pi^- e^+ e^-$ is currently under investigation at KLOE@DAΦNE and a precise check of our prediction for the branching ratio $\Gamma(\eta \to \pi^+\pi^- e^+ e^-)/\Gamma(\eta \to \pi^+\pi^-\gamma)$ will soon be available [146]. Similar investigations are being carried out with WASA in Jülich [100] where also η' decays are studied. Moreover, anomalous decay modes of the η' will be investigated at the upgraded KLOE2 facility [103].

Part II

Kaon-nucleon interactions

Chapter 5

$\bar{K}N$ scattering [§]

5.1 Introduction

The $\bar{K}N$ system provides a good testing ground for chiral SU(3) dynamics and the role of explicit chiral symmetry-breaking due to the strange quark mass. While for the very light quarks u, d the symmetry-breaking corrections are in general small, it remains unclear whether the strange quark is still light enough to be in the chiral regime. Low-energy K^-p data, such as K^-p scattering, the $\pi\Sigma$ mass spectrum and the precisely measured K^-p threshold decay ratios set important constraints for theoretical approaches. Recently they have been supplemented by the new accurate results for the strong interaction shift and width of kaonic hydrogen from the DEAR experiment [150] which reduced both the mean values and error ranges of the previous KEK experiment [151].

The existence of the $\Lambda(1405)$ resonance in the K^-p channel just below its threshold makes the loop expansion of chiral perturbation theory inapplicable. In this regard, the combination of ChPT with non-perturbative coupled-channel techniques based on driving terms of the chiral SU(3) effective Lagrangian has proven useful by generating the $\Lambda(1405)$ dynamically as an $I = 0$ $\bar{K}N$ quasibound state and a resonance in the $\pi\Sigma$ channel.

However, the recent and precise DEAR measurement appears to be in disagreement with the K^-p scattering length derived from scattering data as pointed out in [152]. In contrast, it was claimed very recently in [153, 154] (after the appearance of [148] where the question of consistency of the DEAR experiment with K^-p scattering data is reinforced) that using a chiral unitary framework both the scattering and the DEAR data can be accommodated. It is evident from these recent investigations that the K^-p system remains a topic of great interest and is under lively discussion, see also [155, 156]. The aim of this chapter is to shed some more light on this issue by providing a conservative range for the K^-p scattering length constrained solely from K^-p scattering data. This is accomplished within different variants of chiral unitary approaches and by performing a very large number of fits to experiment in order to reduce the inherent model-dependence of these frameworks. The obtained realistic range for the K^-p scattering length is then compared with the results of the DEAR and KEK experiments.

[§] The contents of this chapter have been published in [148, 149].

Moreover, the interaction of kaons and nucleons is of interest for the possible formation of deeply bound kaon nuclear states. While the strongly attractive $\bar{K}N$ interaction below threshold is responsible for generating the $\Lambda(1405)$ resonance, it does not produce a $\bar{K}N$ bound state due to the open decay channels into $\pi\Sigma$. If, however, the attractive $\bar{K}N$ coupling is still strong enough below the $\pi\Sigma$ threshold, the formation of $\bar{K}$-nuclear bound state involving light nuclei is rendered possible [157, 158]. In fact, it was claimed recently by the FINUDA Collaboration that deeply bound K^-pp states have been observed in the absorption of stopped K^- in light nuclei [159], note, however, the critical analyses of Refs. [160, 161]. In addition, no evidence for a K^-pp bound state could be found in the process $pp \rightarrow ppK^+K^-$ which was investigated very recently with COSY-ANKE [162]. On the theoretical side, an accurate description of the K^-pp three-body system relies upon realistic $\bar{K}N$ amplitudes below threshold. In this respect, chiral unitary approaches can provide important contributions to the ongoing discussion. For recent theoretical works on the K^-pp system see *e.g.* [163–165].

This chapter is organized as follows. In the next section we explain how the chiral unitary approach described in Chapter 2 can be applied to meson-baryon scattering. We also discuss some shortcomings of the framework concerning the analytic properties of the obtained solutions and touch on the inclusion of the Coulomb interaction in elastic K^-p scattering. Our results for scattering observables and the comparison with kaonic hydrogen data are presented in Sect. 5.3. Furthermore, we show the relevant $\bar{K}N$ amplitudes below threshold and study the importance of the Coulomb interaction in the process $K^-p \rightarrow K^-p$. Section 5.4 deals with the pole structures of the amplitudes in the $\Lambda(1405)$ region. We summarize our findings in Sect. 5.5.

5.2 Formalism

5.2.1 Chiral unitary approach

In this section we explain how the chiral unitary approach, which is based on the Bethe-Salpeter equation as discussed in Chapter 2, can be applied to meson-baryon scattering processes. The starting point of the calculation is the chiral effective Lagrangian $\mathcal{L}_{\hat{\phi}B}$ which describes the coupling of the pseudoscalar meson octet (π, K, η) to the ground state baryon octet $(N, \Lambda, \Sigma, \Xi)$. In this investigation the meson-baryon Lagrangian is employed up to second chiral order. The pertinent expressions for $\mathcal{L}^{(1)}_{\hat{\phi}B}$, $\mathcal{L}^{(2)}_{\hat{\phi}B}$ can be found in Chapter 1, Eqs. (1.124), (1.125), respectively.

The BSE for the meson-baryon scattering process $\phi_i(q_i)B_a(p_a) \rightarrow \phi_j(q_j)B_b(p_b)$ with total momentum $P = p_a + q_i = p_b + q_j$ reads (*cf.* Eq. (2.1))

$$\begin{aligned}\check{T}_{jb,ia}(p_b, p_a, P) &= \check{V}_{jb,ia}(p_b, p_a, P)\\ &- \sum_{c,k} \int \frac{d^dl}{(2\pi)^d}\, \check{T}_{jb,kc}(p_b, l, P)\, \frac{i}{[\not{l} - M_c + i\epsilon][(P-l)^2 - m_k^2 + i\epsilon]}\, \check{V}_{kc,ia}(l, p_a, P)\,, \quad (5.1)\end{aligned}$$

where we have employed the standard propagators of the mesons and baryons using their physical masses which ensures the correct positions of the thresholds and the sum runs over all possible meson-baryon intermediate states denoted by the flavor indices k, c. In the $S=-1$ sector we have to consider ten meson-baryon channels with total charge zero, $\pi^0\Lambda$, $\pi^0\Sigma^0$, $\pi^-\Sigma^+$, $\pi^+\Sigma^-$, K^-p, $\bar{K}^0n$, $\eta\Lambda$, $\eta\Sigma^0$, $K^0\Xi^0$, $K^+\Xi^-$. In the simplest case the interaction kernel $\check{V}$ of the BSE is given by the leading order contact term (known as the Weinberg-Tomozawa term) derived from $\mathcal{L}^{(1)}_{\hat{\phi}B}$ which has the form

$$\check{V}_{jb,ia}(p_b,p_a,P)=\frac{1}{8f^2}\,C^{(\mathrm{a})}_{jb,ia}\,(\not{q}_i+\not{q}_j)\;. \tag{5.2}$$

The coefficients $C^{(\mathrm{a})}$ are dimensionless constants and for the channels under consideration they are tabulated in App. B.1.

As shown in [65, 68] the BSE, Eq. (5.1), can be solved exactly for the Weinberg-Tomozawa interaction and in principle it should be possible to generalize the proof to arbitrary contact terms, see also [64]. In this work, however, we follow the treatment of the BSE for meson-meson scattering as advocated in Chapter 2 and make use of the on-shell approximation which simplifies Eq. (5.1) a lot. To this end we utilize the spin sum

$$\sum_{\sigma}u(p,M,\sigma)\bar{u}(p,M,\sigma)=\not{p}+M \tag{5.3}$$

and rewrite Eq. (5.1) as (dropping the $i\epsilon$ terms and the spin indices for brevity)

$$\begin{aligned}\check{T}_{jb,ia}(p_b,p_a,P)&=\check{V}_{jb,ia}(p_b,p_a,P)\\&-\sum_{k,c}\int\frac{id^dl}{(2\pi)^d}\,\check{T}_{jb,kc}(p_b,l,P)\,\frac{u(l,M_c)\bar{u}(l,M_c)}{[l^2-M_c^2][(P-l)^2-m_k^2]}\,\check{V}_{kc,ia}(l,p_a,P)\,.\end{aligned} \tag{5.4}$$

In the center-of-mass (c.m.) frame the on-shell approximation amounts to sandwiching Eq. (5.4) between spinors and putting the momenta in the combinations

$$V\equiv\bar{u}\,\check{V}\,u\,,\qquad\qquad T\equiv\bar{u}\,\check{T}\,u \tag{5.5}$$

on their respective mass shells. In addition, we perform a partial wave decomposition of the amplitudes V, T as explained in Sect. 2.1. In this way the BSE is transformed into an algebraic equation for each partial wave ℓ,

$$T^{jb,ia}_{\ell}(s)=V^{jb,ia}_{\ell}(s)-\sum_{k,c}T^{jb,kc}_{\ell}(s)\,G^{kc}_{\ell}(s)\,V^{kc,ia}_{\ell}(s)\;, \tag{5.6}$$

which is identical to Eq. (2.20). The first two of the loop functions $G^{kc}_{\ell}(s)$ are given in Eq. (2.21). Since we are primarily concerned with a narrow c.m. energy region around the $\bar{K}N$ threshold where the amplitudes are dominated by the $J=0$ resonance $\Lambda(1405)$, it is sufficient to restrict ourselves to the s-wave components. It was demonstrated in [65] that when only the Weinberg-Tomozawa term is taken into account, the difference between the s-wave part of the exact solution of Eq. (5.1) and the on-shell approximated $T_0(s)$ amounts to terms involving tadpole integrals, *cf.* Eq. (1.112), whose effects may be largely compensated by readjusting the couplings of the effective Lagrangian and/or the subtraction constants included in $G^{kc}_{\ell}(s)$, see Eq. (2.26).

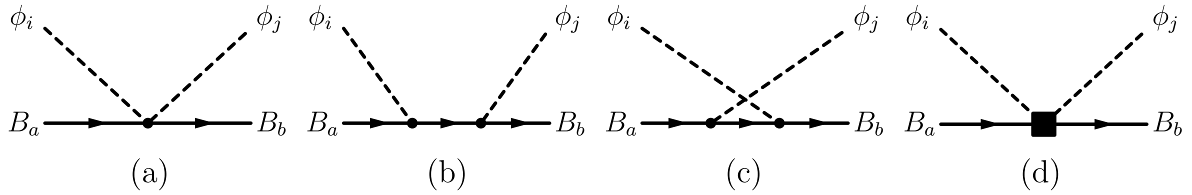

Figure 5.1: Shown are the leading order contact interaction (a), the direct (b) and crossed (c) Born term as well as the next-to-leading order contact interaction (d). Solid and dashed lines represent baryons and pseudoscalar mesons, respectively.

The algebraic BSE in Eq. (5.6) has been frequently and successfully used in the literature to describe meson-baryon interactions in the regime of low-lying resonances such as the $S_{11}(1535)$ and the $\Lambda(1405)$. Thereby, the effective meson-baryon Lagrangian from which one derives the interaction kernel V has been employed at different levels of sophistication. While only the Weinberg-Tomozawa term is taken, *e.g.*, in [166, 167], the Born terms are included in [70]. In [168], on the other hand, the Lagrangian of second chiral order is added which yields additional contact interactions.

In order to provide an estimate of the model-dependence of such approaches, we will discuss the following three different choices for the amplitude $V_{jb,ia}(\mathbf{p}', \mathbf{p}; \sigma', \sigma)$ where $\mathbf{p}$ ($\mathbf{p}'$) and σ (σ') are the c.m. three-momentum and the spin index of the incoming (outgoing) baryon. First, only the Weinberg-Tomozawa term is taken into account, see Figure 5.1 a. Subsequently, the Born diagrams are included, see Figs. 5.1 b and c. In the third approach we add the contact interactions from the Lagrangian of second chiral order, $\mathcal{L}^{(2)}_{\hat{\phi}B}$ (Fig. 5.1 d). For brevity, we will refer to these variants as "WT" (Weinberg-Tomozawa), "WTB" (Weinberg-Tomozawa + Born diagrams) and "full" (including also the higher order contact terms), respectively.

In the c.m. frame of the particles the amplitudes corresponding to the diagrams a, b, c, d in Fig. 5.1 read

$$
\begin{aligned}
V^{(\mathrm{a})}_{jb,ia} &= \frac{1}{8f^2}\, C^{(\mathrm{a})}_{jb,ia}\, N_a N_b\, (\chi^{\sigma'}_b)^T \\
&\quad \times \left[2\sqrt{s} - M_a - M_b + (2\sqrt{s} + M_a + M_b)\, \frac{\mathbf{p}' \cdot \mathbf{p} + i(\mathbf{p}' \times \mathbf{p}) \cdot \boldsymbol{\sigma}}{N_a^2 N_b^2} \right] \chi^{\sigma}_a\,, \qquad (5.7)\\
V^{(\mathrm{b})}_{jb,ia} &= -\frac{1}{12f^2} \sum_{c=1}^{8} C^{(\mathrm{b})}_{jb,c}\, C^{(\mathrm{b})}_{ia,c}\, N_a N_b\, \frac{1}{s - M_c^2}\, (\chi^{\sigma'}_b)^T \\
&\quad \times \Big[(\sqrt{s} - M_c)\big(s - \sqrt{s}\,(M_a + M_b) + M_a M_b\big) \\
&\qquad + (\sqrt{s} + M_c)\big(s + \sqrt{s}\,(M_a + M_b) + M_a M_b\big)\, \frac{\mathbf{p}' \cdot \mathbf{p} + i(\mathbf{p}' \times \mathbf{p}) \cdot \boldsymbol{\sigma}}{N_a^2 N_b^2} \Big] \chi^{\sigma}_a\,, \qquad (5.8)
\end{aligned}
$$

$$
\begin{aligned}
V^{(\mathrm{c})}_{jb,ia} &= \frac{1}{12f^2}\sum_{c=1}^{8} C^{(\mathrm{b})}_{ic,b}\, C^{(\mathrm{b})}_{jc,a}\, N_a N_b\, \frac{1}{u-M_c^2}\, (\chi^{\sigma'}_b)^T \\
&\times \Bigg[u(\sqrt{s}+M_c) + \sqrt{s}\,\big(M_a M_b + M_c(M_a+M_b)\big) - M_a M_b M_c \\
&\quad - M_a^2(M_b+M_c) - M_b^2(M_a+M_c) + \big\{u(\sqrt{s}-M_c) \\
&\quad + \sqrt{s}\,\big(M_a M_b + M_c(M_a+M_b)\big) + M_a M_b M_c \\
&\quad + M_a^2(M_b+M_c) + M_b^2(M_a+M_c)\big\}\, \frac{\mathbf{p}'\cdot\mathbf{p} + i(\mathbf{p}'\times\mathbf{p})\cdot\boldsymbol{\sigma}}{N_a^2 N_b^2} \Bigg] \chi^{\sigma}_a\,, \qquad (5.9)\\
V^{(\mathrm{d})}_{jb,ia} &= -\frac{1}{f^2}\big(C^{(\mathrm{d}_1)}_{jb,ia} - 2(E_i E_j - \mathbf{p}'\cdot\mathbf{p})\, C^{(\mathrm{d}_2)}_{jb,ia}\big)\, N_a N_b\, (\chi^{\sigma'}_b)^T \\
&\times \left[1 - \frac{\mathbf{p}'\cdot\mathbf{p} + i(\mathbf{p}'\times\mathbf{p})\cdot\boldsymbol{\sigma}}{N_a^2 N_b^2}\right] \chi^{\sigma}_a\,, \qquad (5.10)
\end{aligned}
$$

respectively. The two-component Pauli-spinor of a baryon a with spin σ is symbolized by χ^{σ}_a while the pertinent normalization factor is given by $N_a = \sqrt{E_a + M_a}$ and E_x is the c.m. energy of particle x. The Mandelstam variable u is defined by $u = (p_a - q_j)^2 = (p_b - q_i)^2$. The coefficients $C^{(\mathrm{a})}_{jb,ia}$ are fixed numbers whereas the $C^{(\mathrm{b})}_{jb,ia}$ ($C^{(\mathrm{d}_1)}_{jb,ia}$, $C^{(\mathrm{d}_2)}_{jb,ia}$) summarize LECs of the meson-baryon Lagrangian $\mathcal{L}^{(1)}_{\hat{\phi}B}$ ($\mathcal{L}^{(2)}_{\hat{\phi}B}$). They can be found in App. B.1. The s-wave part of the amplitude $V_{jb,ia}(\mathbf{p}',\mathbf{p};\sigma',\sigma)$ is projected out according to

$$
\begin{aligned}
V_0^{jb,ia}(s) &= \frac{1}{8\pi}\sum_{\sigma}\int d\Omega\; V_{jb,ia}(\mathbf{p}',\mathbf{p};\sigma,\sigma) \\
&= \frac{1}{4}\sum_{\sigma}\int_{-1}^{+1} dz\; V_{jb,ia}(\mathbf{p}',\mathbf{p};\sigma,\sigma)\,, \qquad (5.11)
\end{aligned}
$$

where in the second line we made use of the azimuthal symmetry of $V_{jb,ia}$. The remaining integration runs over the cosine of the c.m. scattering angle,

$$
z = \cos\theta_{\mathrm{cm}} = \frac{\mathbf{p}'\cdot\mathbf{p}}{|\mathbf{p}'||\mathbf{p}|}\,, \qquad (5.12)
$$

and we average over the spins σ of the baryons. Note that spin-flip terms in $V_{jb,ia}$ do not contribute to the s-wave component $V_0^{jb,ia}$. We arrive at the following s-wave amplitudes

$$
V^{(\mathrm{a})}_{jb,ia;0} = \frac{N_a N_b}{8f^2}\, C^{(\mathrm{a})}_{jb,ia}\,\big(2\sqrt{s} - M_a - M_b\big)\,, \qquad (5.13)
$$

$$
V^{(\mathrm{b})}_{jb,ia;0} = -\frac{N_a N_b}{12f^2}\sum_{c=1}^{8} C^{(\mathrm{b})}_{jb,c}\, C^{(\mathrm{b})}_{ia,c}\, \frac{1}{\sqrt{s}+M_c}\,\big(s - \sqrt{s}\,(M_a+M_b) + M_a M_b\big)\,, \qquad (5.14)
$$

$$\begin{aligned}
V^{(\mathrm{c})}_{jb,ia;0} = {} & \frac{N_a N_b}{12 f^2} \sum_{c=1}^{8} C^{(\mathrm{b})}_{ic,b} C^{(\mathrm{b})}_{jc,a} \\
& \times \Bigg[\sqrt{s} + M_c - \frac{(M_a + M_c)(M_b + M_c)}{2 N_a^2 N_b^2} \left(\sqrt{s} - M_c + M_a + M_b \right) \\
& + \frac{(M_a + M_c)(M_b + M_c)}{4 |\mathbf{p}'||\mathbf{p}|} \Bigg\{ \sqrt{s} + M_c - M_a - M_b \\
& - \frac{s + M_c^2 - m_i^2 - m_j^2 - 2 E_a E_b}{2 N_a^2 N_b^2} \left(\sqrt{s} - M_c + M_a + M_b \right) \Bigg\} \\
& \times \ln \frac{s + M_c^2 - m_i^2 - m_j^2 - 2 E_a E_b - 2 |\mathbf{p}'||\mathbf{p}|}{s + M_c^2 - m_i^2 - m_j^2 - 2 E_a E_b + 2 |\mathbf{p}'||\mathbf{p}|} \Bigg] \,, \qquad (5.15)
\end{aligned}$$

$$V^{(\mathrm{d})}_{jb,ia;0} = -\frac{N_a N_b}{f^2} \left[C^{(\mathrm{d}_1)}_{jb,ia} - 2 \left(E_i E_j + \frac{|\mathbf{p}'|^2 |\mathbf{p}|^2}{3 N_a^2 N_b^2} \right) C^{(\mathrm{d}_2)}_{jb,ia} \right] \,, \qquad (5.16)$$

which enter the different interaction kernels according to

$$V_{\mathrm{WT}} = V_0^{(\mathrm{a})} \,, \quad V_{\mathrm{WTB}} = V_0^{(\mathrm{a})} + V_0^{(\mathrm{b})} + V_0^{(\mathrm{c})} \,, \quad V_{\mathrm{full}} = V_0^{(\mathrm{a})} + V_0^{(\mathrm{b})} + V_0^{(\mathrm{c})} + V_0^{(\mathrm{d})} \,. \qquad (5.17)$$

We point out once more that the strict correspondence between the bubble chain calculated in field theory and the solution of the BSE is lost, once the on-shell approximation is carried out. As long as the interaction kernel solely involves contact terms or the s-channel Born diagram, Fig. 5.1 b, the difference amounts to tadpole terms which are usually numerically small and whose effects may be largely compensated by adjusting the free parameters of the approach, *i.e.* the subtraction constants in the loop integrals and the couplings in the effective Lagrangian. If, however, the interaction kernel includes non-local t- or u-dependent terms such as the Born diagram in Fig. 5.1 c whose partial wave expansion does not terminate, one should keep in mind that the analytic structure of the BSE amplitude will not in general be the same as that of the full amplitude calculated in field theory.

We exemplify this statement by comparing the one-loop contribution to T_0

$$T_0^{(\mathrm{c}),\text{1-loop}} = -V_0^{(\mathrm{c})} G_0 V_0^{(\mathrm{c})} \,, \qquad (5.18)$$

where the u-channel Born diagrams are treated as contact terms, see Fig. 5.2 a, with the result of the full loop calculation which involves the box graph in Fig. 5.2 b. The analytic expression of the latter diagram was given in [169] in the context of πN scattering. Here we specialize to the case of elastic $\eta\Lambda$ scattering which has a contribution where the same particles, η and Λ, are also running in the loop. For convenience we consider this contribution as it does not involve the additional complication of possible mass differences of internal and external particles, but nevertheless exhibits the features which are crucial for this discussion. The s-wave scattering amplitudes $f_0^{\eta\Lambda,\eta\Lambda}$ corresponding to the diagrams in Fig. 5.2 are plotted in Fig. 5.3. The scattering amplitude in the on-shell approximation is related to $T_0^{(\mathrm{c}),\text{1-loop}}$ via

$$f_0^{\mathrm{on}}(s) = \frac{1}{8\pi\sqrt{s}} \, T_0^{(\mathrm{c}),\text{1-loop}}(s) \,. \qquad (5.19)$$

(a) (b)

Figure 5.2: Shown are the one-loop contribution to T_0 using the interaction kernel $V^{(c)}$ in the on-shell approximation (a) and the corresponding full one-loop graph (b).

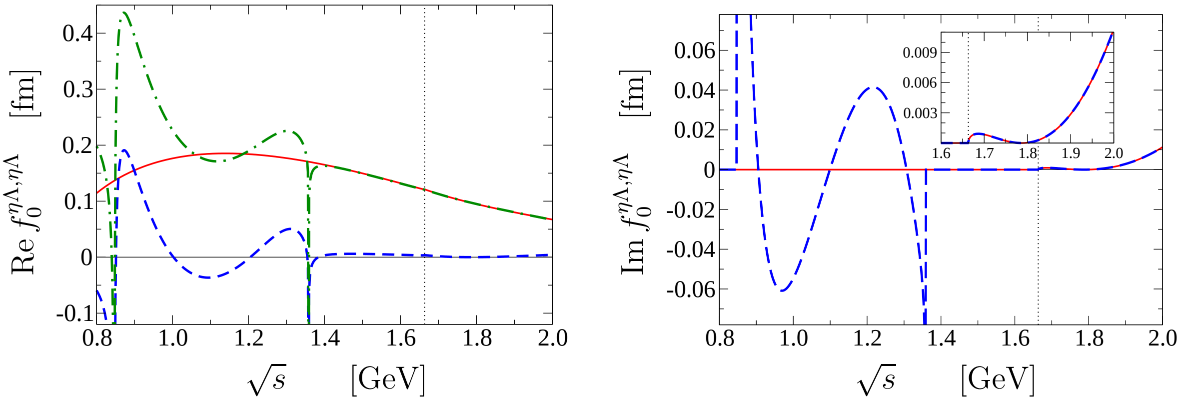

Figure 5.3: Real (left panel) and imaginary part (right panel) of the contributions to the invariant amplitude of $\eta\Lambda \to \eta\Lambda$. The solid line corresponds to the result of the full loop calculation, *cf.* Fig. 5.2 b, whereas the dashed line represents the amplitude in the on-shell approximation as defined in Eq. (5.19). The dot-dashed line is obtained by adding appropriate counter term contributions to the on-shell approximated result, see Eq. (5.22). The $\eta\Lambda$ threshold is indicated by the dotted vertical line. For better visualization, the above-threshold region of the imaginary part is shown at a larger scale in the inset.

As expected from Cutkosky's cutting rules [94] the imaginary parts resulting from the full loop calculation and from the on-shell approximation agree in the physical region, *i.e.* above threshold, see the inset in the right panel of Fig. 5.3. However, below threshold the amplitude $f_0^{\rm on}$ has an additional cut between the points

$$s_1 = \left(M_\Lambda - \frac{m_\eta^2}{M_\Lambda}\right)^2 , \qquad\qquad s_2 = M_\Lambda^2 + 2m_\eta^2 , \tag{5.20}$$

which arises from the pole of $V^{\rm (c)}_{\eta\Lambda,\eta\Lambda}$ at $u = M_\Lambda^2$, *cf.* Eqs. (5.9), (5.15). In the case of πN scattering this cut is known as the short nucleon cut [170]. Clearly, the subthreshold cut is a property of the partial wave amplitude generated by the diagrams involving the u-channel pole term, *e.g.* the one in Fig. 5.1 c. When included in loops, on the other hand, the poles of the propagators are smoothed out by the loop integration. Consequently, the one-loop diagram in Fig. 5.2 b (solid lines in Fig. 5.3) does not exhibit the singularity of the u-channel Born term and results in a smooth scattering amplitude below threshold, whereas the amplitude in the on-shell approximation, $f_0^{\rm on}$, has a non-vanishing imaginary part along the cut and develops logarithmic singularities at the end points $s_{1,2}$. The fact that these singularities appear at the loop level is an artifact of the on-shell approximation.

The problem with these deficiencies of the on-shell approximation is that in a coupled channels calculation the subthreshold amplitudes of channels with heavy particles influence the physical region of channels with lighter particles via loop effects. For instance the logarithmic singularity of $f_0^{\rm on}$ at $s_2 = M_\Lambda^2 + 2m_\eta^2 \approx 1.36\,{\rm GeV}$ lies above the $\pi\Sigma$ thresholds and may thus contribute to physical observables such as cross sections where it must not appear. Moreover, the non-vanishing imaginary part of $V_0^{\rm (c)}(s)$ for $s_1 < s < s_2$ destroys unitarity of the S-matrix when it is included in the interaction kernel of the BSE since exact unitarity is only fulfilled for real interaction kernels. In order to eliminate the unphysical subthreshold cuts and preserve unitarity we choose to set $V_0^{\rm (c)}$ to a constant real value below a certain invariant energy squared s_0 which is located between s_2 and the pertinent threshold. The constant is matched to the amplitude at $s = s_0$. We use $s_0 - s_2 = 50\,{\rm MeV}$ in all channels which appears to be a reasonable distance from the singularity and we have convinced ourselves that our conclusions do not depend on the specific choice of s_0 as long as it does not come too close to s_2. In the general case of inelastic meson-baryon scattering $\phi_i B_a \to \phi_j B_b$ with an intermediate baryon B_c in the u-channel Born diagram the end points of the subthreshold cut are given by

$$\begin{aligned} s_{1,2} = \frac{1}{2M_c^2} \Big\{ &(M_a^2 - m_j^2)(M_b^2 - m_i^2) + M_c^2\big(M_a^2 + M_b^2 - M_c^2 + m_i^2 + m_j^2\big) \\ &\mp \sqrt{\big((M_a + M_c)^2 - m_j^2\big)\big((M_a - M_c)^2 - m_j^2\big)} \\ &\times \sqrt{\big((M_b + M_c)^2 - m_i^2\big)\big((M_b - M_c)^2 - m_i^2\big)} \Big\} \end{aligned} \tag{5.21}$$

instead of Eq. (5.20).

When looking at Fig. 5.3 one might be surprised that in contrast to the imaginary parts of the amplitudes, the real parts corresponding to the full loop calculation and the on-shell approximation differ significantly. However, the real part of the amplitude is not uniquely defined—it may be partially absorbed by polynomial counter terms of subleading chiral orders. After adding a simple linear counter term amplitude

$$f_0^{(\mathrm{ct})}(s) = c_1 + c_2\, s \tag{5.22}$$

to $f_0^{\mathrm{on}}(s)$ and fitting the free constants $c_{1,2}$ to the full loop result above threshold, we observe that also the real part in the on-shell approximation agrees nicely with that of the full loop calculation for $s > s_2$. Yet in the region of the subthreshold cut both amplitudes still deviate considerably due to the unphysical singularities arising in the on-shell approximation.

To summarize, we employ the Bethe-Salpeter equation in the on-shell approximation to compute unitarized amplitudes for meson-baryon scattering. We use three different interaction kernels for the BSE which are derived from the chiral effective meson-baryon Lagrangian of first and second order. The approximations due to the on-shell formalism are uncritical for the contact terms and the s-channel Born diagram, see Figs. 5.1 a, b, d. For the u-channel Born graph, however, the on-shell approximation involves unphysical singularities which we eliminate in a pragmatic way by setting the respective contributions to a constant in the relevant energy range. In particular, these modifications guarantee exact unitarity of the S-matrix which would be lost otherwise.

5.2.2 Coulomb interaction

The Coulomb interaction has been shown to yield significant contributions to the elastic K^-p scattering amplitude up to kaon laboratory momenta of 100–150 MeV/c [171, 172]. In non-relativistic quantum mechanics the Coulomb scattering amplitude for point charges can be calculated exactly and reads [173]

$$f^{\mathrm{coul}}_{K^-p,K^-p} = \frac{1}{2|\mathbf{p}|^2 a_B \sin^2(\theta_{\mathrm{cm}}/2)}\, \frac{\Gamma(1 - i/(|\mathbf{p}|a_B))}{\Gamma(1 + i/(|\mathbf{p}|a_B))}\, \exp\left\{ \frac{2i}{|\mathbf{p}|a_B} \ln \sin \frac{\theta_{\mathrm{cm}}}{2} \right\} , \tag{5.23}$$

where $a_B = 84\,\mathrm{fm}$ is the Bohr radius of the K^-p system, while $\mathbf{p}$ and θ_{cm} denote the center-of-mass three-momentum and scattering angle, respectively. We account for the electromagnetic interaction by adding $f^{\mathrm{coul}}_{K^-p,K^-p}$ to the s-wave part of the unitarized strong elastic K^-p amplitude

$$f^{\mathrm{str}}_{K^-p,K^-p} = \frac{1}{8\pi\sqrt{s}}\, T_0^{K^-p,K^-p}(s) \ . \tag{5.24}$$

Note that there can also be important contributions from the interference of the strong and the electromagnetic interactions, *e.g.* via vertex corrections. However, in this investigation we are satisfied with a rough estimate of the size of Coulomb corrections and do not aim at a complete treatment of electromagnetic effects. Since these modifications of the strong interaction also occur in inelastic processes such as $K^-p \to \pi^\pm\Sigma^\mp$, they should—in principle—also be taken into account there.

The total elastic cross section is obtained by performing the integration of $d\sigma/d\Omega = |f^{\mathrm{coul}} + f^{\mathrm{str}}|^2$ over the c.m. scattering angle. Since this expression is divergent for forward scattering, a cutoff for the scattering angle must be introduced. In the analysis of the scattering data [174, 175], forward angles were suppressed by accepting only events with $\theta_{\rm cm}$ larger than a minimum angle $\theta_{\rm min}$. In practice the value employed in [174, 175] was $\cos\theta_{\rm min} = 0.966$. We choose the same $\theta_{\rm min}$ for a meaningful comparison with data. Some K^-p angular distributions (though of very limited quality) were reported in Ref. [174]. We have checked that our treatment of Coulomb effects reproduces the measured small-angle differential cross sections in the relevant momentum range. The dependence of our results on the infrared cutoff provided by $\theta_{\rm min}$ will be discussed in Sect. 5.3.6.

The Coulomb potential vanishes at infinity as $1/r$ and leads to an infrared divergent scattering amplitude for $|\mathbf{p}| \to 0$. In physical reality, however, the kaons are scattered off neutral hydrogen atoms rather than off protons and the range of the Coulomb interaction—given by the Bohr radius of the hydrogen atom—is therefore finite. Deviations from the pure Coulomb potential will be important, if the de Broglie wavelength of the kaons is of the order of the atomic radius, corresponding to kaon laboratory momenta of a few keV/c. The lowest experimentally accessible kaon momenta are around 100 MeV/c, four orders of magnitude higher, so the electronic shielding of the Coulomb potential can be safely neglected.

Deviations from the Coulomb scattering amplitude of point charges are expected when the wavelength of the incident kaon is comparable to the size of the proton. This translates into kaon momenta larger than 200 MeV/c. For such momenta K^-p scattering is completely dominated by the strong interaction since the Coulomb amplitude decreases as $1/|\mathbf{p}|^2$. The corrections induced by finite size effects in the Coulomb amplitude are negligible in the relevant range of kaon energies. We will therefore work with the formula given in Eq. (5.23) combined with the small-angle cutoff as mentioned before.

5.3 Results

5.3.1 Preface

In this section, we present our results for K^-p scattering and the resulting predictions for $\bar{K}N$ scattering lengths which can be related to observables in kaonic hydrogen. Additional subsections are devoted to our results for $\bar{K}N$ scattering amplitudes below threshold which are of interest for the quest of possible kaonic bound states in light nuclei, see *e.g.* [157, 158, 160, 161, 163, 164], and to the estimation of Coulomb effects in elastic K^-p scattering.

Low-energy antikaon-nucleon scattering and reactions have been studied experimentally decades ago [174–179]. The available data (admittedly with large errors) are mostly restricted to K^- momenta above 100 MeV/c. Further tight constraints are imposed by the accurately determined threshold branching ratios into the inelastic channels $\pi\Sigma$ and

$\pi^0\Lambda$ [180, 181]

$$\begin{aligned}\gamma &= \frac{\Gamma(K^-p\to\pi^+\Sigma^-)}{\Gamma(K^-p\to\pi^-\Sigma^+)} = 2.36\pm0.04\,,\\ R_c &= \frac{\Gamma(K^-p\to\pi^+\Sigma^-,\ \pi^-\Sigma^+)}{\Gamma(K^-p\to\text{all inelastic channels})} = 0.664\pm0.011\,,\\ R_n &= \frac{\Gamma(K^-p\to\pi^0\Lambda)}{\Gamma(K^-p\to\text{neutral states})} = 0.189\pm0.015\,, \qquad (5.25)\end{aligned}$$

and by the $\pi\Sigma$ invariant mass spectrum in the isospin $I=0$ channel [182]. We note that very recently (and after the publication of [148, 149]) the results of Ref. [182] have been confirmed by an experiment using the ANKE spectrometer at COSY-Jülich where the decay of the $\Lambda(1405)$ into $\pi^0\Sigma^0$ was measured [183]. We compare our results to the new data at the end of Sect. 5.3.2.

In our analysis we have restricted ourselves to pure meson-baryon scattering and have not included the processes $K^-p\to\gamma\Lambda(1405)$ [184], $\gamma p\to K^*\Lambda(1405)$ [185] which is now experimentally under investigation at SPring-8/Osaka [186] and, in the near future, also at ELSA (Bonn), and $K^-p\to\pi^0\pi^0\Sigma^0$ [187] which is already measured [188]. Reactions including the coupling to an external photon such as $K^-p\to\gamma\Lambda(1405)$ and $\gamma p\to K^*\Lambda(1405)$ require a substantial extension of the chiral unitary approach applied here as illustrated, *e.g.*, in [65, 189], whereas the three-body final state in $K^-p\to\pi^0\pi^0\Sigma^0$ introduces additional model-dependence. Hence, these processes are beyond the scope of the present investigation.

The primary goal of this study is to provide a realistic error range for the K^-p scattering length derived *exclusively* from K^-p scattering data and to compare the outcome with the recent kaonic hydrogen measurement at DEAR [150]. In principle, one could take into account additional constraints, *e.g.* from the simultaneous consideration of πN and K^+p scattering as done in the extensive study [190]. If all scattering data can be described consistently within our approach, the inclusion of data in other channels will further confine our results leading to even smaller error estimates. If, on the other hand, the additional data are not consistent with the K^-p sector, their inclusion may conceal the impact of the $S=-1$ data we are interested in. In this investigation we will thus restrict ourselves to experimental data from the K^-p sector.

Since we work with isospin symmetric subtraction constants, our approaches, which involve ten coupled meson-baryon channels, have six subtraction constants, $a_{\pi\Lambda}$, $a_{\pi\Sigma}$, $a_{\bar{K}N}$, $a_{\eta\Lambda}$, $a_{\eta\Sigma}$, $a_{K\Xi}$. In addition, there are the pseudoscalar decay constant f and—in the full approach only—the higher order couplings b_0, b_D, b_F, d_1, d_2, d_3, d_4. All these parameters are varied in the fits within generous limit whereas the axial-vector couplings D, F which enter the Born diagrams (Fig. 5.1b and c) are kept fixed at the values $D=0.80$, $F=0.46$ extracted from semileptonic hyperon decays [191]. We have purposely chosen ample ranges for the parameters of our approach in order to be able to take into account a large variety of qualitatively different fits to K^-p scattering data. Since our concern here is to predict the strong K^-p scattering length only from K^-p scattering data, we do not impose additional phenomenological constraints as done, *e.g.*, in the analysis [192] which includes η photoproduction as a high quality data set. In addition, the framework chosen in [192] does not exactly coincide with any of the approaches considered in the present work. We can therefore not expect the same values for the coupling constants.

We perform an overall least-squares fit to available low-energy K^-p scattering data for the three different approaches WT, WTB and full. To this end, we first calculate the individual χ_i^2 for the i^{th} observable and divide by the number of pertinent data points n_i. The total χ^2 per degree of freedom (d.o.f.) is then defined as [104]

$$\frac{\chi^2}{\text{d.o.f.}} = \frac{\sum_i n_i}{N(\sum_i n_i - p)} \sum_i \frac{\chi_i^2}{n_i} \ , \tag{5.26}$$

where N is the number of observables and p the number of free parameters in the approach. This definition of the $\chi^2/\text{d.o.f.}$ function generalizes the standard $\chi^2/\text{d.o.f.}$ for a single observable and has the advantage that all observables are weighted equally regardless of the number of data points. If one were to use instead the definition $\chi^2/\text{d.o.f.} = \sum_i \chi_i^2/(\sum_i n_i - p)$ in which all data points from different observables have the same weight, then single-valued observables (such as branching ratios) would be dominated by observables with many data points (such as scattering data). Note that the definition in Eq. (5.26) reduces to the latter one if all observables have the same number of data points.

The fitting procedure used to explore the minimum of the χ^2 function involves the combination of a Monte Carlo routine with a conjugate gradient method [193]. Using a large number a randomized starting points we perform random walks in parameter space where only those steps are allowed which lead to smaller χ^2 values. The conjugate gradient method, which is considerably slower than the random walk routine, is employed to find the global minimum of the χ^2 function. Here we use a smaller number of initial points which have already been optimized by the random walk procedure. Our method allows us to perform a large number of different fits to data distributed in parameter space so that the model-dependence of the results is reduced and a realistic error range for the K^-p scattering length derived from scattering experiments can be provided.

We obtain a large number of fits which describe the low-energy K^-p scattering data very well with the minimum $\chi^2/\text{d.o.f.}$ values given by 1.28, 0.88 and 0.71 for the different approaches WT, WTB and full, respectively. In general, if χ^2 is a function of n parameters $\boldsymbol{\theta} = (\theta_1, \ldots, \theta_n)$ the standard error range of these parameters is given by the condition [17]

$$\chi^2(\boldsymbol{\theta}) = \chi^2_{\text{min}} + \Delta\chi^2 \tag{5.27}$$

and $\Delta\chi^2$ is derived from the p-value of the χ^2 probability distribution function with the pertinent number of degrees of freedom. Strictly speaking, this relation only holds if the method of least squares is applied to one single experiment and the associated fit function depends linearly on the parameters $\boldsymbol{\theta}$. In the present investigation the situation is more involved: the free parameters of the approach enter in a highly nonlinear way into the calculation of observables and the χ^2-function which is minimized combines a variety of measurements of different quantities. Nevertheless, we will adopt the standard definition of a confidence region, Eq. (5.27), since one can expect it to be a reasonable approximation—at least in the vicinity of the minimum of the χ^2-function, where its shape should nearly be parabolic. Our fit includes a total number of 171 experimental data points and either 7 (WT, WTB) or 14 parameters (full approach). The region of one standard deviation (*i.e.* 68.27% confidence level) is then found by adding $\Delta\chi^2/\text{d.o.f.} = 1.05$ to the minimal $\chi^2/\text{d.o.f.}$ as defined in Eq. (5.26). Since the difference in the number of parameters causes only tiny modifications of $\Delta\chi^2/\text{d.o.f.}$, the same value, $\Delta\chi^2/\text{d.o.f.} = 1.05$, holds for all three approaches.

As it turns out, we also obtain fits that although having a relatively low overall $\chi^2/\text{d.o.f.}$ fail miserably in one or two observables and can thus not be classified as "good fits". In addition to the bound on the overall $\chi^2/\text{d.o.f.}$ we thus demand that each individual observable be reproduced with a χ_i^2/n_i value which does not exceed the overall $\chi^2/\text{d.o.f.}$ by more than a factor of four. Fits which do not meet this additional criterion are grouped instead with fits with the lowest $\chi^2/\text{d.o.f.}$ value which satisfies this constraint. This specific choice has proved useful in practice. These two goodness-of-fit criteria, a bound on the overall χ^2 and on the individual χ_i^2, determine the error regions specified in the following for all parameters and observables while the presented central values correspond to the fits with minimal χ^2. We also investigate analytic properties of the fits, in order to sort out solutions with unphysical pole structures. This issue will be discussed in detail in Sect. 5.4.

Finally, for the best fit of each approach we present in Table 5.1 the numerical values of the fitted parameters f, b_i, d_i and the subtraction constants in the loop integrals G. The regularization scale of G is set to $\mu = 1\,\text{GeV}$. Note that in the fits we have allowed for broad ranges for the subtraction constants $a_{\phi B}$. In fact, in the WT and WTB approaches the resulting $a_{K\Xi}$ are roughly one order of magnitude larger than the remaining subtraction constants. However, the fits are not very sensitive to variations in this parameter such that the χ^2 value is only slightly increased if $a_{K\Xi}$ is reduced to the same size as the other $a_{\phi B}$.

5.3.2 Meson-baryon scattering

The scattering of negatively charged kaons on protons, either elastically or into other meson-baryon pairs, was studied long ago in bubble chamber experiments [174–179]. Being interested in the near-threshold region, we include in our fit all available data of total cross sections for the processes $K^-p \to K^-p$, $\bar{K}^0n$, $\pi^+\Sigma^-$, $\pi^-\Sigma^+$, $\pi^0\Sigma^0$, $\pi^0\Lambda$ up to incident kaon laboratory momenta of $250\,\text{MeV}/c$. The results of the three approaches WT, WTB, full are compared to the data in Figs. 5.4, 5.5, 5.6, respectively. The shaded band indicates the 1σ confidence region of the fits whose overall agreement with the experimental data is very good for all approaches. The steep rise of the elastic cross section at small kaon momenta is due to the inclusion of the Coulomb interaction in our calculation. Note that in most channels the curves exhibit a prominent cusp effect at the $\bar{K}^0n$ threshold.

For the accurately determined threshold branching ratios γ, R_c, R_n defined in Eq. (5.25) we obtain the values presented in Table 5.2. They are in excellent agreement with the experimental numbers.

Finally, we also include the $\pi^-\Sigma^+$ event distribution from [182] in the fit. It is extracted from the decay of the $\Lambda(1405)$ which is produced in the reaction chain $K^-p \to \pi^-\Sigma^+(1660)$, $\Sigma^+(1660) \to \pi^+\Lambda(1405)$, $\Lambda(1405) \to \pi^-\Sigma^+$. To make use of these data,

	WT	WTB	full
f [MeV]	120.9	86.0	77.3
b_0 [GeV^{-1}]	—	—	-0.01
b_D [GeV^{-1}]	—	—	-0.27
b_F [GeV^{-1}]	—	—	-0.11
d_1 [GeV^{-1}]	—	—	-0.14
d_2 [GeV^{-1}]	—	—	-0.05
d_3 [GeV^{-1}]	—	—	-0.25
d_4 [GeV^{-1}]	—	—	-0.45
$a_{\bar{K}N}$ $\times 10^3$	-1.8	1.9	1.0
$a_{\pi\Lambda}$ $\times 10^3$	-12.4	2.0	-6.2
$a_{\pi\Sigma}$ $\times 10^3$	-2.9	2.4	1.9
$a_{\eta\Lambda}$ $\times 10^3$	-1.7	-0.9	-2.3
$a_{\eta\Sigma}$ $\times 10^3$	-1.4	-3.7	-1.5
$a_{K\Xi}$ $\times 10^3$	72.9	20.0	-5.2
χ^2/d.o.f.	1.28	0.88	0.71

Table 5.1: Numerical values of the fitted couplings and subtraction constants corresponding to the best fits in the three approaches. The empirical value of the average meson decay constant is $f \simeq 100\,\text{MeV}$.

	WT	WTB	full	exp. [180, 181]
γ	$2.35\,^{+0.07}_{-0.06}$	$2.36\,^{+0.03}_{-0.03}$	$2.36\,^{+0.10}_{-0.09}$	2.36 ± 0.04
R_c	$0.655\,^{+0.001}_{-0.018}$	$0.664\,^{+0.022}_{-0.024}$	$0.663\,^{+0.016}_{-0.018}$	0.664 ± 0.011
R_n	$0.191\,^{+0.027}_{-0.031}$	$0.193\,^{+0.009}_{-0.017}$	$0.190\,^{+0.026}_{-0.036}$	0.189 ± 0.015

Table 5.2: Threshold branching ratios resulting from the different approaches under consideration. The central values correspond to the best fit in each approach while the errors indicate the 1σ confidence region. See Eq. (5.25) for the definitions of γ, R_c and R_n.

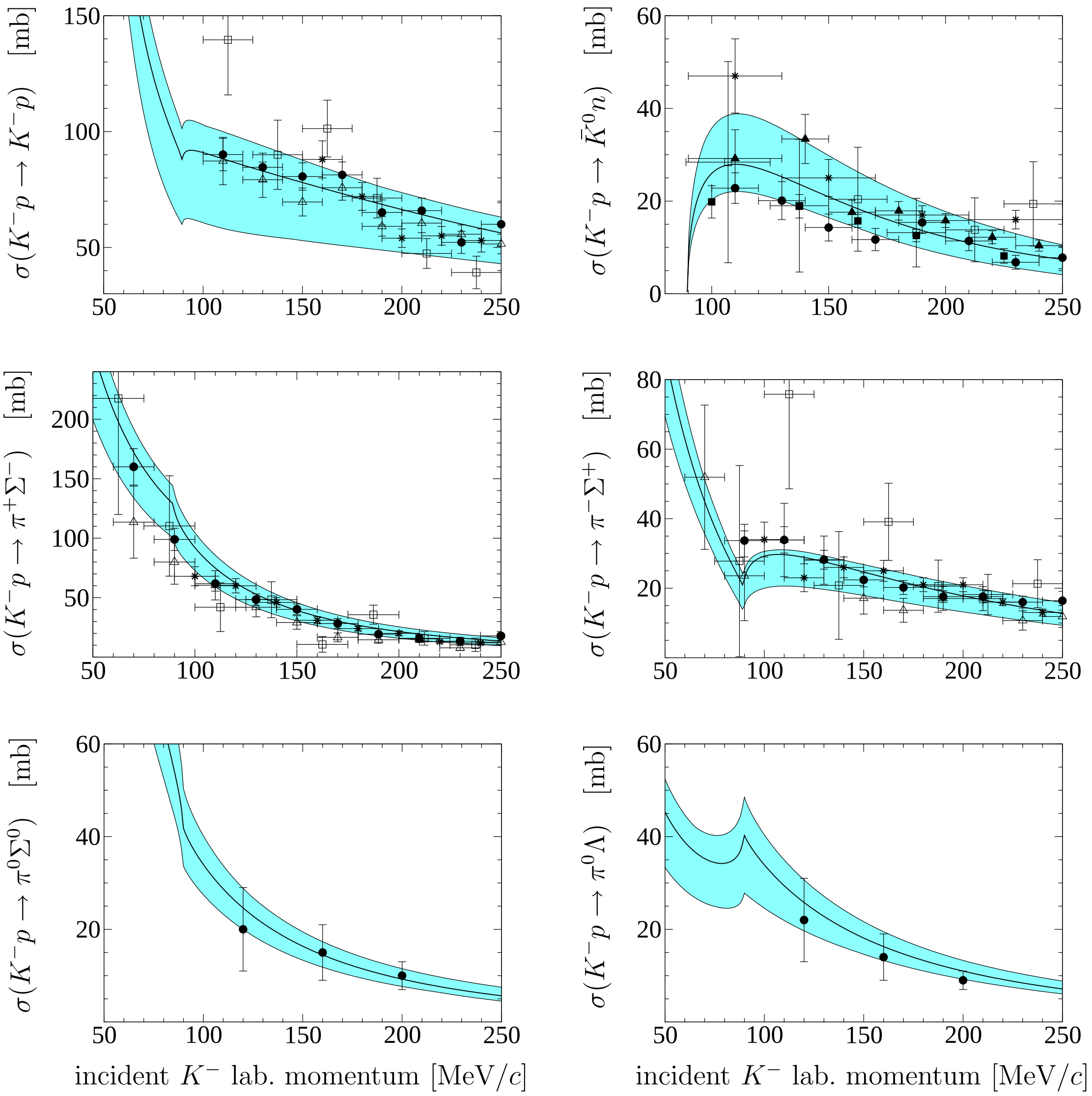

Figure 5.4: Total cross sections for K^-p scattering into various channels calculated in the WT approach. The best fit is represented by the solid line while the shaded area indicates the 1σ confidence region. The data are taken from [174] (empty squares), [175] (empty triangles), [176] (filled circles), [177] (filled squares), [179] (filled triangles), [178] (stars).

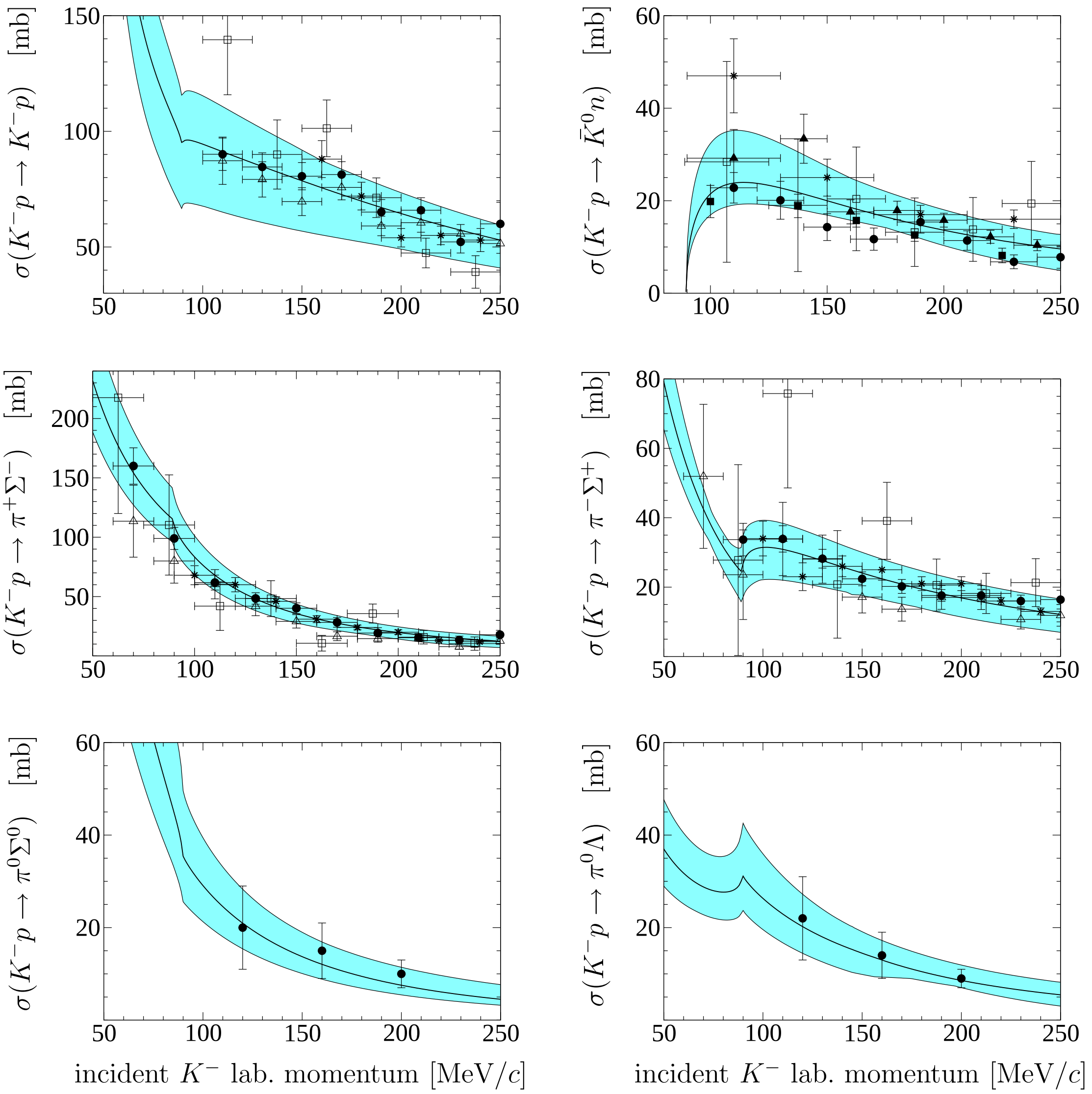

Figure 5.5: Total cross sections for K^-p scattering into various channels calculated in the WTB approach. The best fit is represented by the solid line while the shaded area indicates the 1σ confidence region. The data are taken from [174] (empty squares), [175] (empty triangles), [176] (filled circles), [177] (filled squares), [179] (filled triangles), [178] (stars).

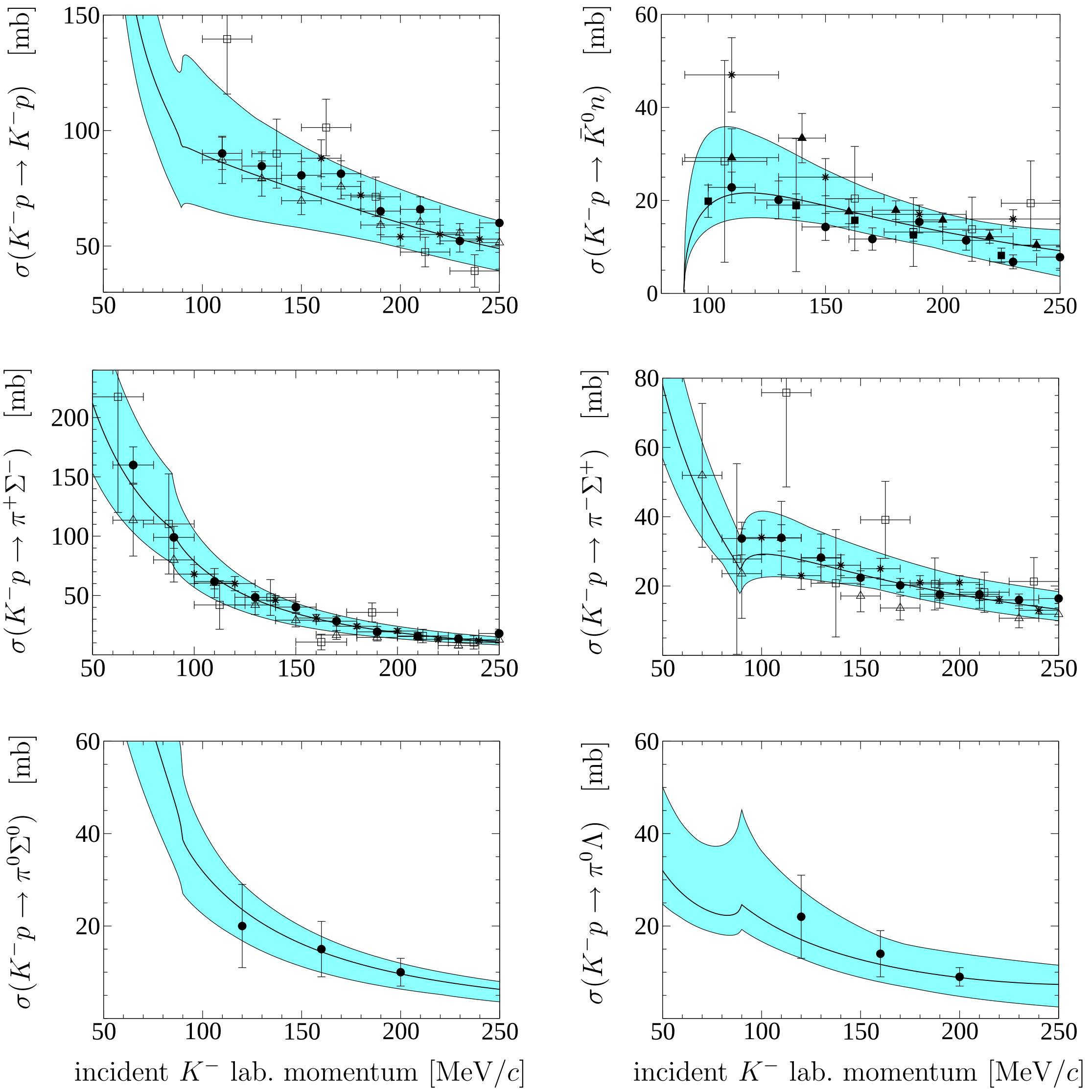

Figure 5.6: Total cross sections for K^-p scattering into various channels calculated in the full approach. The best fit is represented by the solid line while the shaded area indicates the 1σ confidence region. The data are taken from [174] (empty squares), [175] (empty triangles), [176] (filled circles), [177] (filled squares), [179] (filled triangles), [178] (stars).

which are an important constraint for the amplitudes at energies below the $\bar{K}N$ thresholds, we follow Ref. [70] and assume that the $\Lambda(1405)$ may be modeled by a generic s-wave source with $I = 0$ whose coupling to the relevant channels, $\pi\Sigma$ and $\bar{K}N$, is described by the real, energy-independent constants r_1 and r_2, respectively. The coupling to the remaining channels is neglected. One then constructs the quantity

$$F = (\mathbb{1} + V_0 G_0)^{-1} R \ , \tag{5.28}$$

where R is a vector in channel space which collects the couplings r_i, *i.e.* the non-perturbative final-state interactions generated by the chiral unitary approach are attached to the isoscalar source. The $\pi^-\Sigma^+$ event distribution is computed from F according

$$\frac{dN_{\pi^-\Sigma^+}}{dE} = |\mathbf{p}'| \ |F_{\pi^-\Sigma^+}|^2 \ , \tag{5.29}$$

where $\mathbf{p}'$ is the c.m. three-momentum of the $\pi^-\Sigma^+$ system. The coupling constants $r_{1,2}$ are treated as free constants which are fitted to the experimental distribution.

As shown in Fig. 5.7 the chiral unitary approach reproduces the experimental $\pi^-\Sigma^+$ spectrum from [182] very nicely for all choices of the interaction kernel. In addition we compare our results with the very recent measurement of the $\pi^0\Sigma^0$ event distribution with ANKE at COSY-Jülich [183] which is based on the process $pp \to pK^+\Lambda(1405)$, $\Lambda(1405) \to \pi^0\Sigma^0$. Theoretically, the event distribution is calculated using the respective analog of Eq. (5.29). Since both experimental $\pi\Sigma$ spectra originate from the decay of the $\Lambda(1405)$, we do not refit the values of the couplings $r_{1,2}$ when plotting the $\pi^0\Sigma^0$ spectrum, but only adjust the overall normalization according to the experimental numbers. Our analysis, which focuses on the K^-p threshold region, merely involves experimental data up to invariant energies of $\sqrt{s} \approx 1.47\,\text{GeV}$ (corresponding to kaon laboratory momenta of $250\,\text{MeV}/c$ in K^-p scattering). Therefore the comparison to the ANKE data in Fig. 5.7 is also performed up to this energy. One observes that the agreement with the new ANKE data is very good even though they are not included in the fit.

5.3.3 Kaon-nucleon scattering lengths

From the unitarized scattering amplitudes we may extract the kaon-nucleon scattering lengths which are given by the scattering amplitudes at the respective thresholds. In particular, the expression for the strong K^-p scattering length a_{K^-p} reads

$$a_{K^-p} = \frac{1}{8\pi\sqrt{s}} \, T_{K^-p \to K^-p}(s)\Big|_{s=(m_{K^-}+M_p)^2} \ , \tag{5.30}$$

where only the strong interaction part of the T-matrix is taken into account. The values corresponding to the best fits in the three approaches are

$$\begin{aligned} &\text{WT:} && a_{K^-p} = (-0.73 + i\,0.91)\,\text{fm} \ , \\ &\text{WTB:} && a_{K^-p} = (-1.09 + i\,0.84)\,\text{fm} \ , \\ &\text{full:} && a_{K^-p} = (-1.05 + i\,0.75)\,\text{fm} \ . \end{aligned} \tag{5.31}$$

The errors of the real and imaginary parts are, of course, correlated so instead of error bars we extract the 1σ regions in the complex a_{K^-p} plane which are plotted in Fig. 5.8.

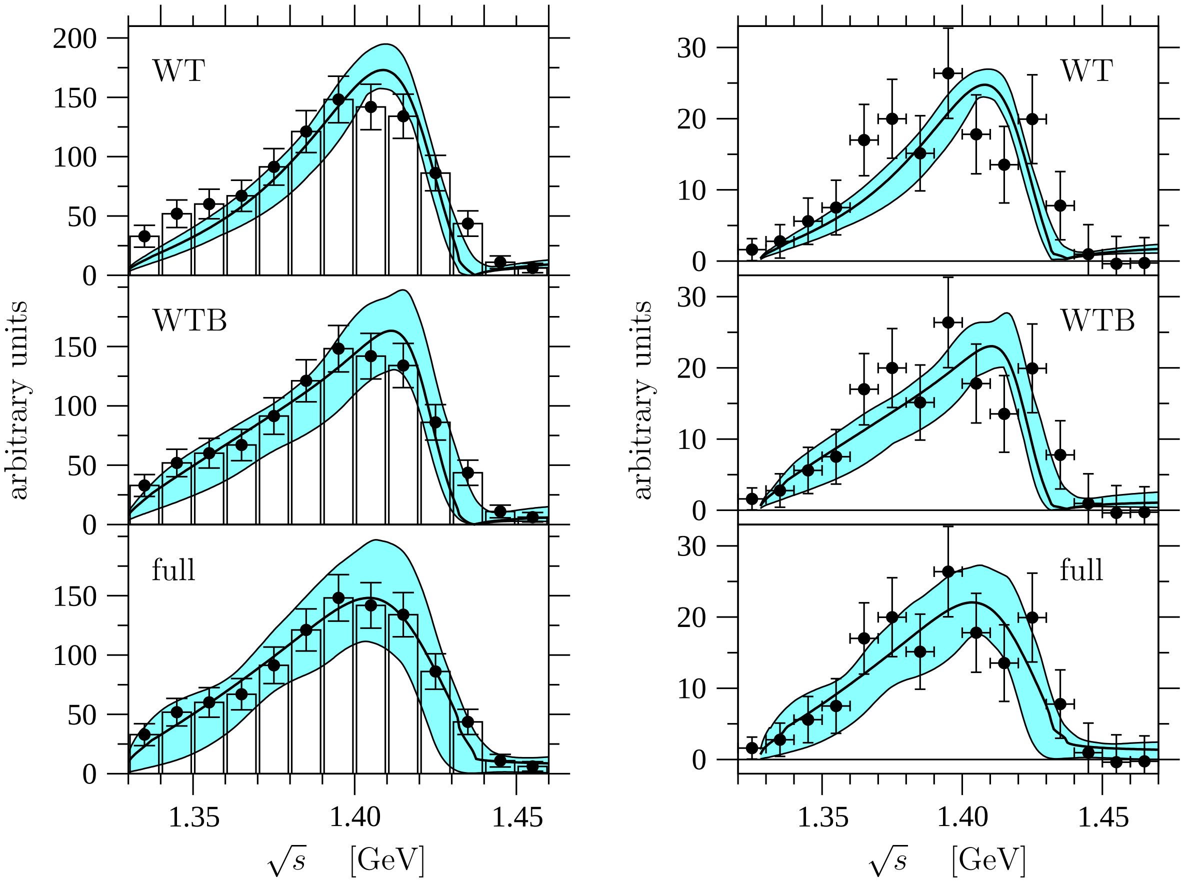

Figure 5.7: Left: $\pi^-\Sigma^+$ event distribution for the three different approaches compared to data from [182] (which have been supplemented by statistical errors following [194]). The best fits are represented by the solid lines while the shaded areas indicate the 1σ confidence regions. Right: $\pi^0\Sigma^0$ event distribution as predicted by the chiral unitary approaches compared to the recent data from [183] which were not included in the fit; only an overall normalization constant was adjusted to the data.

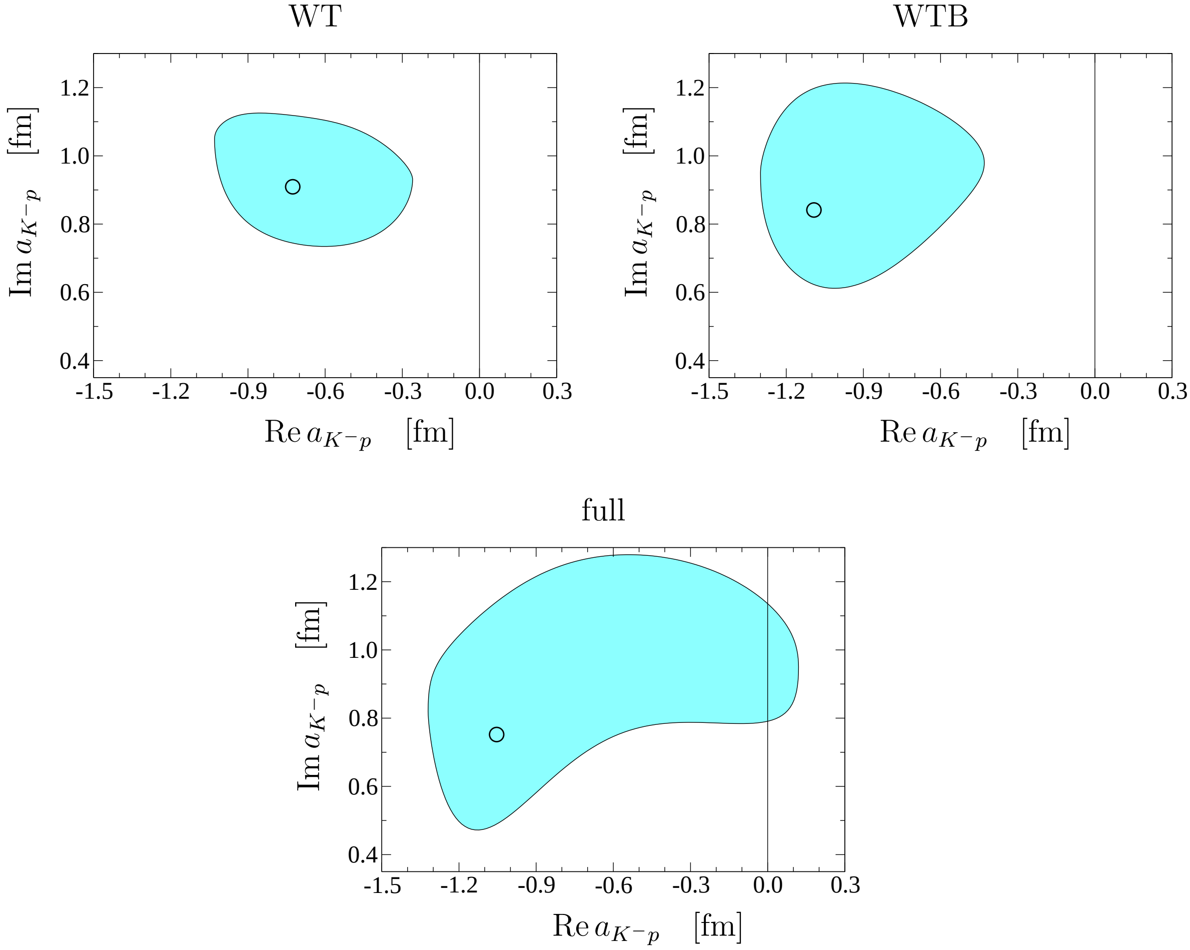

Figure 5.8: Real and imaginary parts of the scattering length a_{K^-p} for the three approaches. The circles indicate the results of the best fits, the shaded areas represent the 1σ confidence region.

While the absolute minimum of χ^2/d.o.f. is the lowest in the full approach, the χ^2 function rises steeper in the WT and WTB approaches, which have fewer parameters, leading to smaller 1σ confidence regions in the a_{K^-p} plane.

We also extract the $\bar{K}N$ s-wave scattering lengths a_0, a_1 in the isospin limit of equal up- and down-quark masses. Since we neglect isospin-breaking corrections in the Lagrangian from which the interaction kernel of the coupled-channels calculation is derived, taking the isospin limit amounts to replacing the physical masses of the particles that enter all kinematic quantities and the scalar loop integrals G by a common mass for each isospin multiplet and we disregard any electromagnetic effect. The exact choice of the masses in the isospin limit is somewhat arbitrary. To be explicit, for the pions, kaons, nucleons and Ξs we use the physical masses of the charged particles while for the Σs we employ the mass of the Σ^0. For the different approaches we obtain the

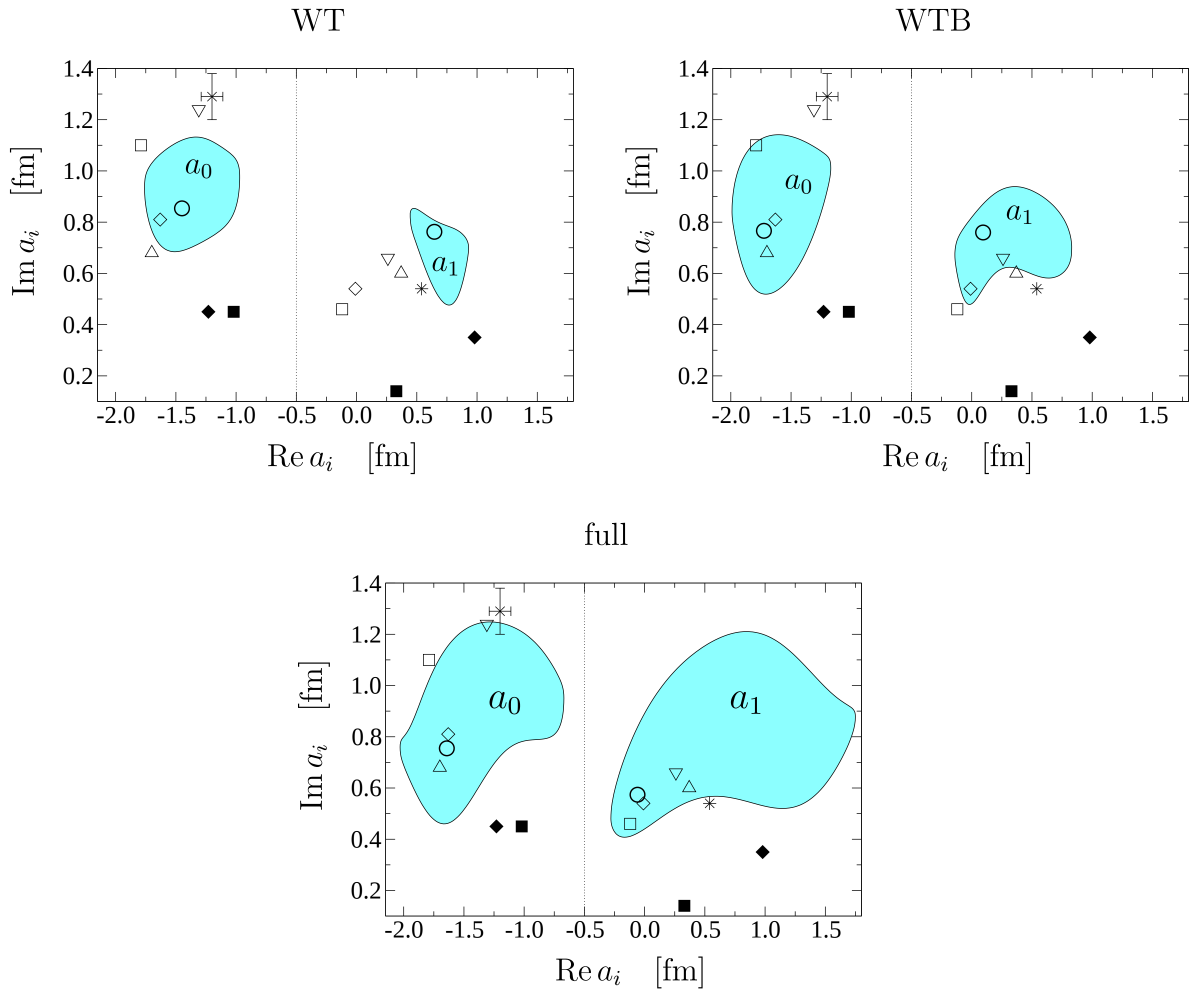

Figure 5.9: Real and imaginary parts of the isospin $\bar{K}N$ scattering lengths a_0 and a_1 for the three approaches. The circles indicate the results of the best fits, the shaded areas represent the 1σ confidence regions. Our results are compared to the values found in [195] (triangle up), [166] (star, the value $a_0 = (-2.24 + 1.94i)$ fm is not shown), [70] (triangle down), [167] (cross with error bars, a_0 only), [153] (filled diamond for fit A_4^+, empty diamond for fit B_4^+), [154] (filled square for fit I, empty square for fit II).

central values

$$\begin{aligned}
&\text{WT:} && a_0 = (-1.45 + i\,0.85)\,\text{fm}\ , && a_1 = (0.65 + i\,0.76)\,\text{fm}\ ,\\
&\text{WTB:} && a_0 = (-1.72 + i\,0.77)\,\text{fm}\ , && a_1 = (0.09 + i\,0.76)\,\text{fm}\ ,\\
&\text{full:} && a_0 = (-1.64 + i\,0.75)\,\text{fm}\ , && a_1 = (-0.06 + i\,0.57)\,\text{fm}\ .
\end{aligned} \tag{5.32}$$

In Fig. 5.9 we show the error ranges and compare the results with values found in similar chiral unitary approaches [70, 153, 154, 166, 167] and a multichannel dispersion relation analysis of $\bar{K}N$ scattering data [195]. One observes consistency of all three approaches (WT, WTB, full) within error bars and agreement with most of the values from previous investigations. However, our results do not agree with the fit A_4^+ in [153] and the similar fit I in [154]. These fits have additional poles in the complex $\sqrt{s}$ plane which cannot be associated with any known resonance and which we consider as unphysical. We will come back to this issue in Sect. 5.4, see also the discussion in [155]. Our error ranges also do not cover the a_1 value of [166], where a variant of the WT approach was employed. The approach utilized in [70] nearly coincides with WTB in the present work, however only one common subtraction constant for all channels was employed in [70] while in the present work we have the freedom to vary six (isospin symmetric) subtraction constants. This explains why the imaginary part of a_0 in [70] is larger and outside the 1σ range of the present calculation.

Due to the very high statistics of the present investigation our results provide a realistic error range for the isospin scattering lengths a_0 and a_1 within chiral unitary approaches. As shown in [196] these quantities are an important input in the theoretical analysis of the upcoming spectroscopy study of kaonic deuterium [197] and further anticipated experiments with even more complex light kaonic nuclei with AMADEUS at DAΦNE [198].

5.3.4 Kaonic hydrogen

In the absence of electromagnetic corrections the ground state strong energy shift ΔE and width Γ of kaonic hydrogen are related to the K^-p scattering length a_{K^-p} via the well-known Deser-Trueman formula [199]

$$\Delta E - \frac{i}{2}\Gamma = -2\alpha^3\mu_c^2\, a_{K^-p}\ , \tag{5.33}$$

where μ_c is the reduced mass of the K^-p system and $\alpha \approx 1/137$ is the fine-structure constant. Recently the electromagnetic corrections to the Deser-Trueman formula were calculated in a non-relativistic Lagrangian framework and were shown to be substantial [152]. In order to predict the strong energy shift and width of kaonic hydrogen from our results for the scattering length a_{K^-p} we thus utilize the updated relation derived in [152]

$$\Delta E - \frac{i}{2}\Gamma = -2\alpha^3\mu_c^2\, a_{K^-p}\, \left[1 - 2\alpha\mu_c(\ln\alpha - 1)a_{K^-p}\right]\ . \tag{5.34}$$

The obtained predictions for ΔE and Γ, which are solely based on K^-p scattering data and the $\pi\Sigma$ invariant mass spectrum, are presented in Fig. 5.10 for the three different

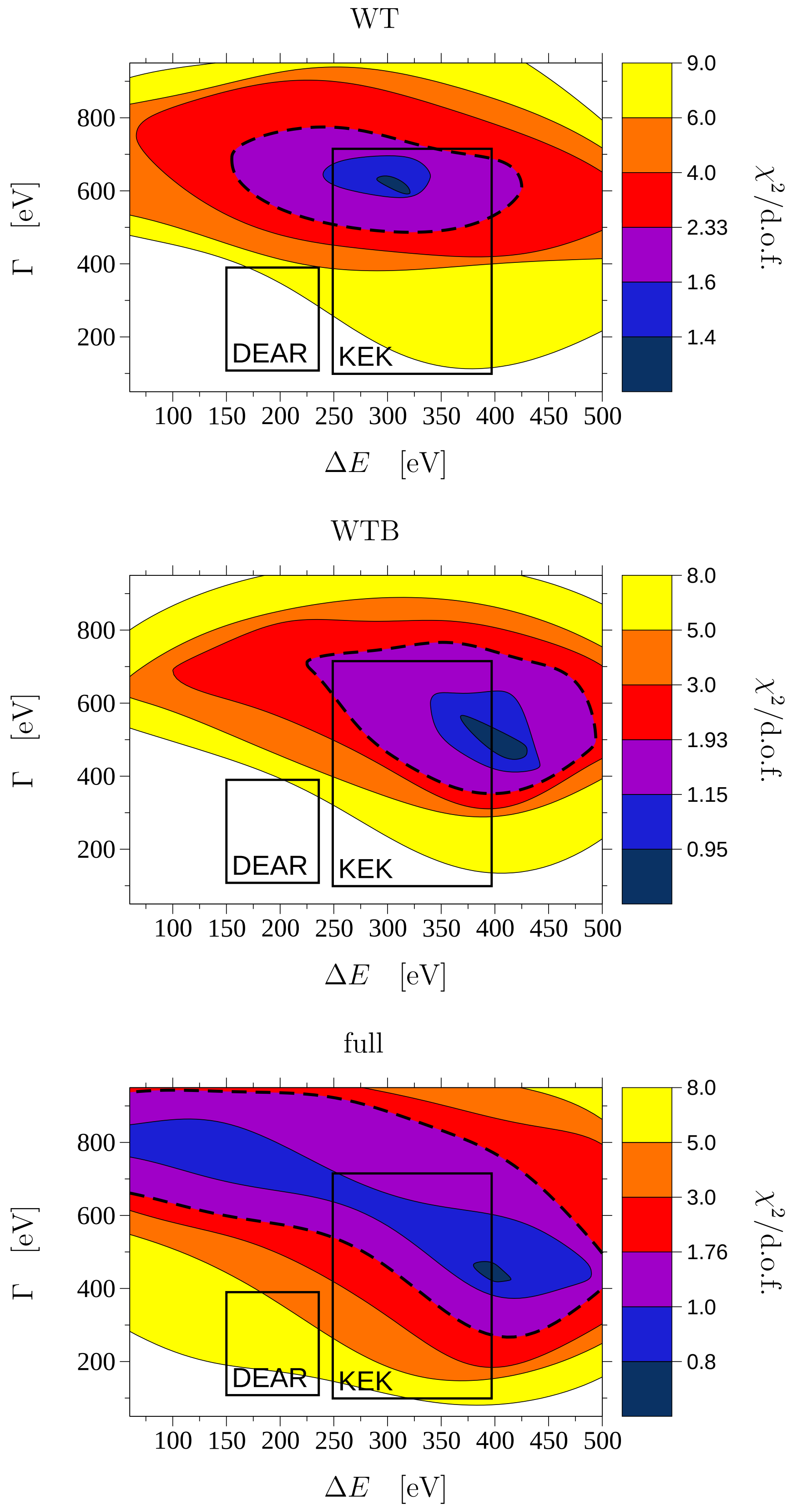

Figure 5.10: Strong energy shift ΔE and width Γ of kaonic hydrogen for the three approaches. The shaded areas represent different upper limits of the overall χ^2/d.o.f. The 1σ confidence region is bordered by the dashed line. See text for further details.

approaches. They are compared to the recent experimental determination of kaonic hydrogen observables by both the KEK [151] and the DEAR [150] collaborations. The shaded areas in the plots of Fig. 5.10 represent smoothened areas which correspond to different upper limits of the overall χ^2/d.o.f. (with the additional constraint that each individual observable is reproduced by the fit with χ_i^2/n_i of at most four times the upper limit of χ^2/d.o.f., *cf.* the discussion in Sect. 5.3.1) and are drawn on the basis of several thousands of fits (*e.g.* more than 7000 for the full approach). We point out that a comparable statistical exploration of parameter space in chiral unitary approaches for $\bar{K}N$ interactions has not been attempted before; it provides for the first time a realistic estimate of theoretical uncertainties within this framework.

Regardless of the chosen approach the fits with minimal overall χ^2 agree nicely with the result of the KEK experiment while the 1σ confidence region, which is bordered by the dashed line in the plots of Fig. 5.10, has no overlap with the error ranges given by the DEAR experiment. As explained in Sect. 5.3.1 the standard definition of the 1σ confidence region by means of Eq. (5.27) is not strictly applicable in the present investigation, where the fit function is non-linear in the parameters and the fit incorporates a variety of different observables. Therefore we refrain from showing 2σ and 3σ confidence regions since application of the standard error estimation seems more questionable in these cases. Instead we plot regions that correspond to quadratically increasing upper limits of the overall χ^2. Note that fits which are compatible with the error ranges given by DEAR have an overall χ^2/d.o.f. of at least 6.1, 5.5, 3.3 in the WT, WTB, full approach, respectively, with elastic K^-p scattering being the largest source of disagreement.

We point out that a re-measurement of kaonic hydrogen observables is foreseen at the upcoming SIDDHARTA experiment at DAΦNE [197] which aims at a high-precision determination of ΔE and Γ at the level of few eV.

5.3.5 Scattering amplitudes

The dynamics of $S = -1$ meson-baryon interactions below the $\bar{K}N$ threshold, which is governed by the $\Lambda(1405)$ resonance in the $I = 0$ channels, is a topic that is still under lively discussion, see *e.g.* [148, 149, 153–156, 200]. In particular, it is of importance for the theoretical description of deeply bound kaon nuclear states which may be formed if the attractive antikaon-nucleon interaction is strong enough below the $\pi\Sigma$ threshold, the dominant decay channel of the $\Lambda(1405)$ [157, 158, 160, 161, 163–165]. Realistic estimates of the pertinent amplitudes in this energy region are also a valuable guideline in the analysis of experimental data, *e.g.* of the reaction $pp \to ppK^+K^-$ which has recently been investigated with the ANKE detector at COSY-Jülich [162].

In this section we present our results for the s-wave meson-baryon amplitudes $f = T/(8\pi\sqrt{s})$ at energies between the $\pi\Sigma$ and $\bar{K}N$ thresholds. It appears to be most instructive to work in the isospin basis and we perform the isospin limit as explained in the previous section. Furthermore, we restrict ourselves to the lowest-lying channels and do not plot the amplitudes involving the $\eta\Lambda$, $\eta\Sigma$, $K\Xi$ channels whose physical region is far away. In Figs. 5.11, 5.12 and 5.13 we display the $I = 0$ amplitudes as they come out in the WT, WTB and full approach, respectively. The curves corresponding to the best fits (which are represented by the solid lines in Figs. 5.11, 5.12, 5.13) are qualitatively similar

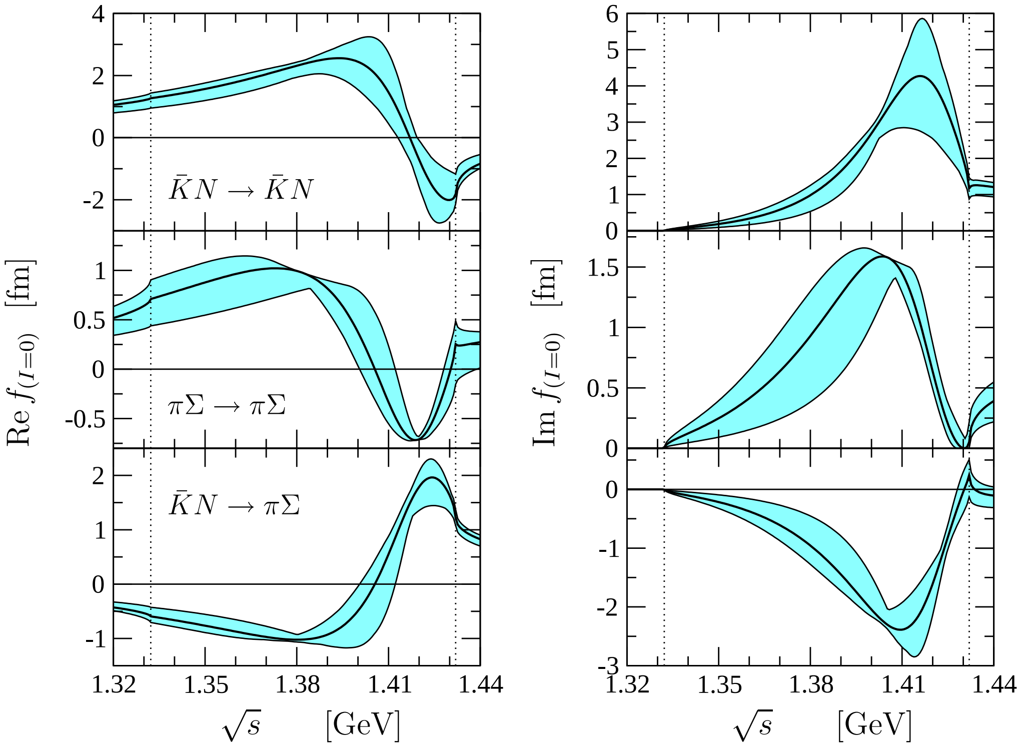

Figure 5.11: Real (left panel) and imaginary part (right panel) of the $I = 0$ $\bar{K}N$ and $\pi\Sigma$ amplitudes in the WT approach. The best fit is represented by the solid lines while the bands comprise all fits in the 1σ region. The $\pi\Sigma$ and $\bar{K}N$ thresholds are indicated by the dotted vertical lines.

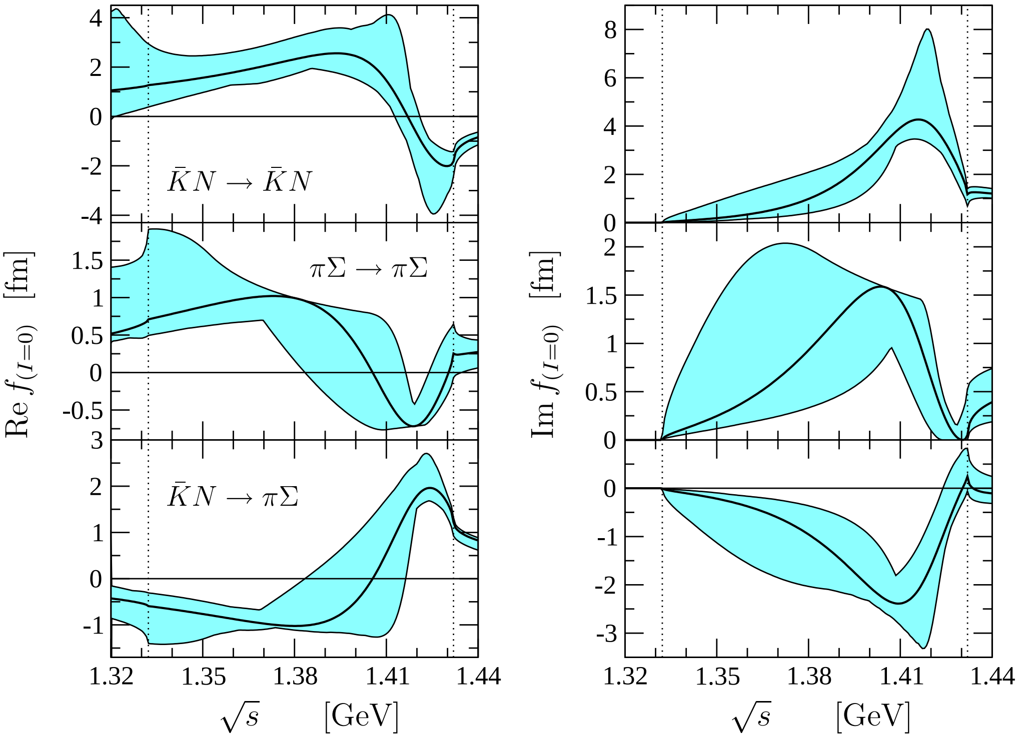

Figure 5.12: Real (left panel) and imaginary part (right panel) of the $I = 0$ $\bar{K}N$ and $\pi\Sigma$ amplitudes in the WTB approach. The best fit is represented by the solid lines while the bands comprise all fits in the 1σ region. The $\pi\Sigma$ and $\bar{K}N$ thresholds are indicated by the dotted vertical lines.

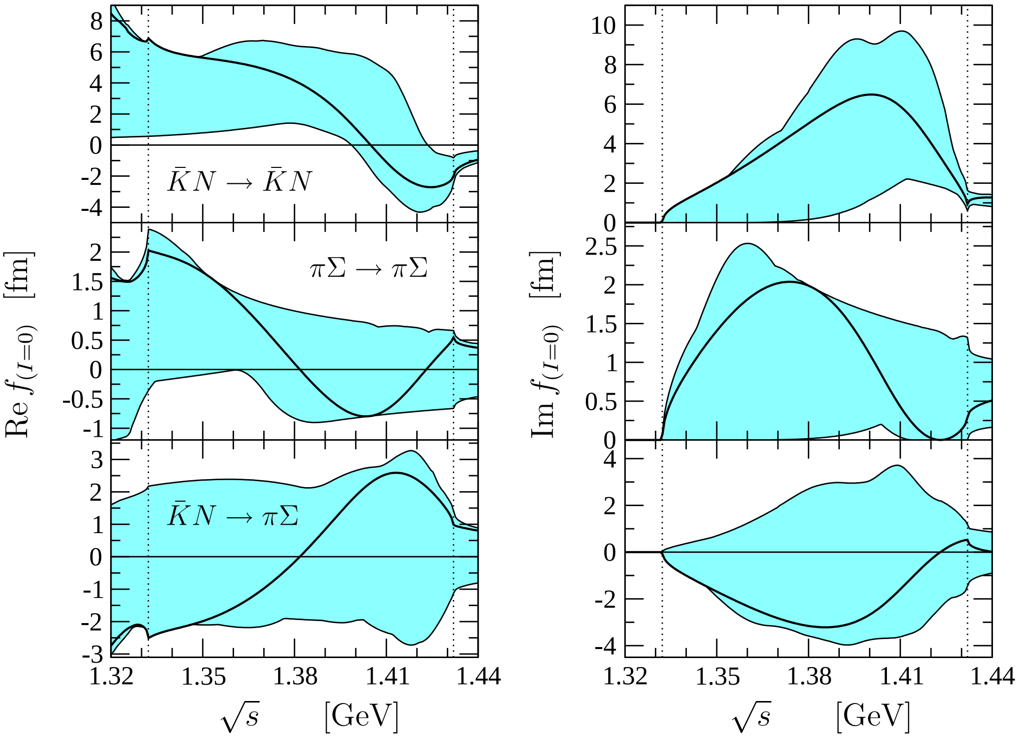

Figure 5.13: Real (left panel) and imaginary part (right panel) of the $I = 0$ $\bar{K}N$ and $\pi\Sigma$ amplitudes in the full approach. The best fit is represented by the solid lines while the bands comprise all fits in the 1σ region. The $\pi\Sigma$ and $\bar{K}N$ thresholds are indicated by the dotted vertical lines.

in all approaches. As observed for all other quantities, the error bands increase drastically by including the Born diagrams (WTB approach) and—in addition—the next-to-leading order contact terms (full approach) in the interaction kernel of the BSE.

The amplitudes with $I = 1$ and $I = 2$, which do not exhibit a distinct resonance behavior, are shown in App. B.2.

5.3.6 Coulomb effects

For small incident kaon momenta close to the K^-p threshold, the elastic K^-p scattering cross section receives sizable contributions from both the strong and the electromagnetic interaction. In this work, Coulomb interactions are taken into account by utilizing the quantum mechanical Coulomb scattering amplitude Eq. (5.23) whereas we neglect the modification of the strong amplitude via electromagnetic effects. Due to the infinite-range nature of the Coulomb potential, the scattering amplitude is infrared divergent in the limit of small incident momenta as well as small scattering angles.

As explained in Sect. 5.2.2, the divergence at vanishing relative momenta can be ignored in the energy regime accessible by the scattering experiments. However, when performing the integration over the center-of-mass scattering angle in order to calculate the total elastic cross section, a cutoff in the angle must be introduced. Two of the experiments that have produced data at the lowest kaon momenta, exclude forward scattering angles and consider only the range $-1 \leq \cos\theta_{\text{cm}} \leq 0.966$ [174, 175]. We choose to work with the same angle cutoff in order to perform consistent comparisons. The contributions of the Coulomb and the strong interaction as well as their coherent sum are displayed for the best fit of the full approach in Fig. 5.14 a. Similar results are found for the other approaches. While the corrections due to the Coulomb interaction are negligible for kaon laboratory momenta greater than 150 MeV/c, they start becoming important around 100 MeV/c. However, in the energy range covered by experiments they never exceed the size of the experimental error bars.

In Fig. 5.14 b we show the dependence of our results on the small-angle cutoff. The shaded band indicates the variation between $\cos\theta_{\text{min}} = 0.7$, for which the Coulomb amplitude is highly suppressed, and $\cos\theta_{\text{min}} = 0.99$ where it is sizable. The curves have been normalized to the solid angle covered by the experiments [174, 175], *i.e.* to the angular range $-1 \leq \cos\theta_{\text{cm}} \leq 0.966$. For incident kaon momenta larger than 150 MeV/c where the strong s-wave amplitude dominates, the results depend only weakly on the small-angle cutoff. Given the large error spread of the experiments [174–176, 178] which have provided data on elastic K^-p scattering at low energies, it is therefore justified to compare our results directly with all experimental data at the same time although the experiments differ in their angular acceptance. For instance in [178] depending on the kaon momenta only angles in the ranges $(-0.9\ldots-0.6) \leq \cos\theta_{\text{cm}} \leq (0.5\ldots0.8)$ were covered and the results were then scaled up to the full solid angle assuming a flat angular distribution. The difference between 4π and the solid angle covered with our cutoff amounts to less than 2 %.

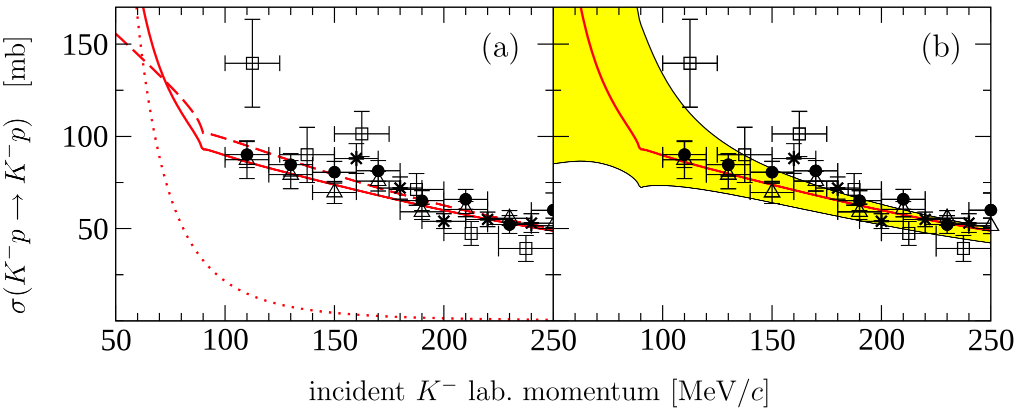

Figure 5.14: Left: Contributions to the total elastic cross section of K^-p scattering due to the Coulomb interaction (dotted), the strong interaction (dashed) and their coherent sum (solid). Right: Dependence on the small-angle cutoff excluding small center-of-mass angles. The lower boundary of the band corresponds to $\cos\theta_{\mathrm{min}} = 0.7$, the upper one to $\cos\theta_{\mathrm{min}} = 0.99$; the solid line represents the value established by the experiments [174, 175], which we also use in our calculations: $\cos\theta_{\mathrm{min}} = 0.966$.

5.4 Resonance poles

To cover a substantial region in parameter space we put only very loose constraints on the numerical values of the low-energy parameters of the chiral effective Lagrangian, *i.e.* we solely fix the order of magnitude as motivated by the naturalness assumption of couplings in the effective field theory. The subtraction constants in the loop integrals G are permitted to vary in even larger ranges. Starting from randomized initial values of the parameters the Monte Carlo routine utilized in the present investigation generates a vast number of fits and for all of them the poles of the T-matrix in the complex $W = \sqrt{s}$ plane are determined. Although we work in the physical basis, where isospin is broken by the physical masses of the particles in the loop integrals, we can classify the poles as being mainly of isospin $I = 0, 1, 2$ by their impact on channels (or channel combinations) which contain only one isospin component (*e.g.* $\eta\Lambda$, $\eta\Sigma^0$). The pole positions of the fits will serve as an additional constraint to rule out certain fits which must be considered as unphysical as we will explain in the following.

While resonances are generally associated with poles on unphysical Riemann sheets of the complex W plane, the solutions should be free of poles on the physical Riemann sheet as required by the postulate of maximal analyticity. However, within chiral unitary approaches one usually cannot exclude the existence of such pathological poles as illustrated for a simplified model in Sect. 2.3. Since it is not possible to numerically explore the entire upper half-plane, we must choose a finite region to search for poles on the physical sheet. To this end, we dismiss all fits which exhibit a pole at a distance of less than 250 MeV from the real axis in the relevant energy region (1.25 . . . 1.50 GeV). This selection criterion ensures that even if poles on the physical sheet exist, their influence on the real axis would be negligible. In particular, it guarantees that the Wigner bound [74], which is based on causality and sets a lower limit for the derivative of the phase shift with respect to energy, is not violated, see the discussion in Sect. 2.3. The order of magnitude estimate of a bound on the pole position W_0 derived from the Wigner inequality leads to $\operatorname{Im} W_0 \gtrsim 200\,\mathrm{MeV}$. Here we add a small safety margin and use $\operatorname{Im} W_0 > 250\,\mathrm{MeV}$. Note that in the same manner the influence of unphysical poles on the first Riemann sheet has been used as an exclusion criterion for certain fits in [167]. Moreover, the Wigner condition has been employed in [201] to constrain the numerical values of parameters in the context of unitarized chiral effective field theory.

Second, we reject fits which have a resonance pole on the relevant unphysical Riemann sheet that is located less than 2.5 MeV below the real axis and thus corresponds to a resonance with a width of less than 5 MeV. Such resonances would be one or two orders of magnitude narrower than what one would expect from the characteristic time-scale of the strong interactions of about $10^{-23}\,\mathrm{s}$. Lifetimes of this order translate to widths of several tens to hundreds of MeV, in agreement with typically observed hadronic resonances in this energy region. At present, there is no experimental indication for an exotically long-lived state in the energy interval under consideration and we can safely ignore such fits. The same argument has also been asserted in [167] to exclude certain fits.

The third item concerns the $\pi\Sigma$ event distribution [182] which clearly shows a peak corresponding to the $\Lambda(1405)$ resonance. We adopt the approach advocated in [70] which describes the experimental $\pi^-\Sigma^+$ event distribution as originating from a generic $I = 0$ source made up of unknown shares of $\pi\Sigma$ and $\bar{K}N$ states. As it happens we observe fits which do not exhibit a true resonance structure around 1.4 GeV, but merely show a broad bump that is generated by the intricate superposition of the two source states, $\pi\Sigma$ and $\bar{K}N$. As the $\pi\Sigma$ event distribution is not normalized, the normalization constant in the fit can be tuned in such a way that the χ^2 of the pertinent fit is relatively low. However, these fits do not have an isospin zero pole on the unphysical sheet at a position which could be associated with the $\Lambda(1405)$. In fact, if the $\pi\Sigma$ event distribution were simply approximated by the invariant mass distribution of $I = 0$ $\pi\Sigma$ states, see *e.g.* [62, 166, 167], one would observe no peak structure at all for these fits. Taking the well-established four star resonance $\Lambda(1405)$ for granted, one should identify at least one pole of the T-matrix in the near vicinity, and fits without a nearby pole must be dropped.

Finally, there is no experimental indication for an $S = -1$, $I = 1$ s-wave baryon resonance below the $\bar{K}N$ threshold, the lowest possible candidates being the $\Sigma(1480)$ (one star resonance) and $\Sigma(1560)$ (two star resonance) which are listed as "bumps" in [17]. While spin and parity of both states have not been determined yet, recent experiments [202, 203] yield controversial results even on the existence of the $\Sigma(1480)$.[†] If, however, these low lying $I = 1$ resonances should be confirmed in the future and have the required quantum numbers, their position is still above the relevant energy region considered here. Therefore we drop fits which entail a pronounced $I = 1$ resonance structure below $W = 1.44\,\mathrm{GeV}$ caused by an isospin one pole close and immediately connected to the real axis. More precisely, fits with $I = 1$ poles located at $\mathrm{Im}(W) > -50\,\mathrm{MeV}$, *i.e.* less than twice as far from the real axis as typical $\Lambda(1405)$ poles, are not taken into account.

We observe fits which agree with the DEAR results at a lower overall χ^2/d.o.f. than indicated in Fig. 5.10 (but still outside the 1σ confidence region) if the above mentioned

---

[†] One should point out, however, that the ANKE experiment [203], which found evidence for an excited hyperon at 1480 MeV, was not able to determine the isospin of this state, so it might just as well be an $I = 0$ state instead of the $\Sigma(1480)$.

criteria are omitted, *e.g.* $\chi^2/\text{d.o.f.} = 2.0$ can be obtained in the full approach. All of these fits have an isospin one pole in common which is very close to the $\bar{K}N$ thresholds and either a few MeV above (*i.e.* on the physical sheet) or below (*i.e.* on an unphysical sheet) the real axis. Solutions of this type have been reported on in [153, 154]. However, such fits clearly violate one of the criteria discussed above and are not considered here, see also [155, 156].

In the remainder of this section we will focus on the resonance pole structure of the $\Lambda(1405)$, *i.e.* the $I = 0$ poles that are located on the unphysical sheet which is directly connected to the physical real axis between the $\pi\Sigma$ and $\bar{K}N$ thresholds. The nature of the $\Lambda(1405)$ has recently attracted considerable interest. It has been claimed that instead of the usual appearance of one resonance pole the $\Lambda(1405)$ results from a pronounced two-pole structure with both poles being very close to the physical region [200]. While only the Weinberg-Tomozawa contact interaction was taken into account in [200], the inclusion of additional terms in the interaction kernel may significantly change the pole positions. In [153], *e.g.*, which also includes the next-to-leading order contact interactions the pole is located at $1321 - i\,43.5\,\text{MeV}$, *i.e.* even *below* the $\pi\Sigma$ threshold(s) and hence not immediately connected to the physical region, whereas in the WT approach a pole around a mass of 1390 MeV was found in [200].

For most fits in the 1σ confidence interval we observe two isospin zero poles in the region $\text{Re}\,W = (1250\ldots1600)\,\text{MeV}$, $\text{Im}\,W = (-2.5\ldots-250)\,\text{MeV}$. In some cases, however, it happens that there is only one $I = 0$ pole in this region. We then extend the pole search beyond the chosen limits until a second $I = 0$ pole is found. The observed pole positions are depicted in Fig. 5.15, where “first pole” refers to the pole which is closer to the real axis at 1.405 GeV, *i.e.* the position of the $\Lambda(1405)$ peak. While the variation of the position of this first pole is remarkably small in all three approaches, WT, WTB and full, the position of the second $I = 0$ pole scatters over a wide range in the complex W plane (in particular in case of the full approach) and consequently does not have in all fits a significant impact on physical observables. The positions $W_0^{(1)}$, $W_0^{(2)}$ of the first and second pole extracted from the best fit of each approach read

$$\begin{aligned}
&\text{WT:} && W_0^{(1)} = (1420 - i\,20)\,\text{MeV}\ , && W_0^{(2)} = (1440 - i\,76)\,\text{MeV}\ ,\\
&\text{WTB:} && W_0^{(1)} = (1423 - i\,15)\,\text{MeV}\ , && W_0^{(2)} = (1366 - i\,84)\,\text{MeV}\ ,\\
&\text{full:} && W_0^{(1)} = (1418 - i\,31)\,\text{MeV}\ , && W_0^{(2)} = (1348 - i\,62)\,\text{MeV}\ .
\end{aligned} \tag{5.35}$$

In Fig. 5.15 they are indicated by small circles.

We also observe very few fits with a third $I = 0$ pole which appears either at $\text{Re}\,W > 1.5\,\text{GeV}$ and thus well above the $\bar{K}N$ threshold(s) (recall that the pertinent Riemann sheet is connected to the real axis below these thresholds) or deep in the complex W plane ($\text{Im}\,W < -150\,\text{MeV}$). In these fits, the third pole is thus not expected to have much influence on physical observables.

From the discussions above it becomes clear that the analytic continuation to the complex energy plane and the resulting pole positions depend sensitively on the dynamical input of the chiral SU(3) effective Lagrangian. A rigorous extraction of the pole positions, in particular the second one, appears therefore very unlikely from the experimental data considered in the present investigation. Additional experimental input,

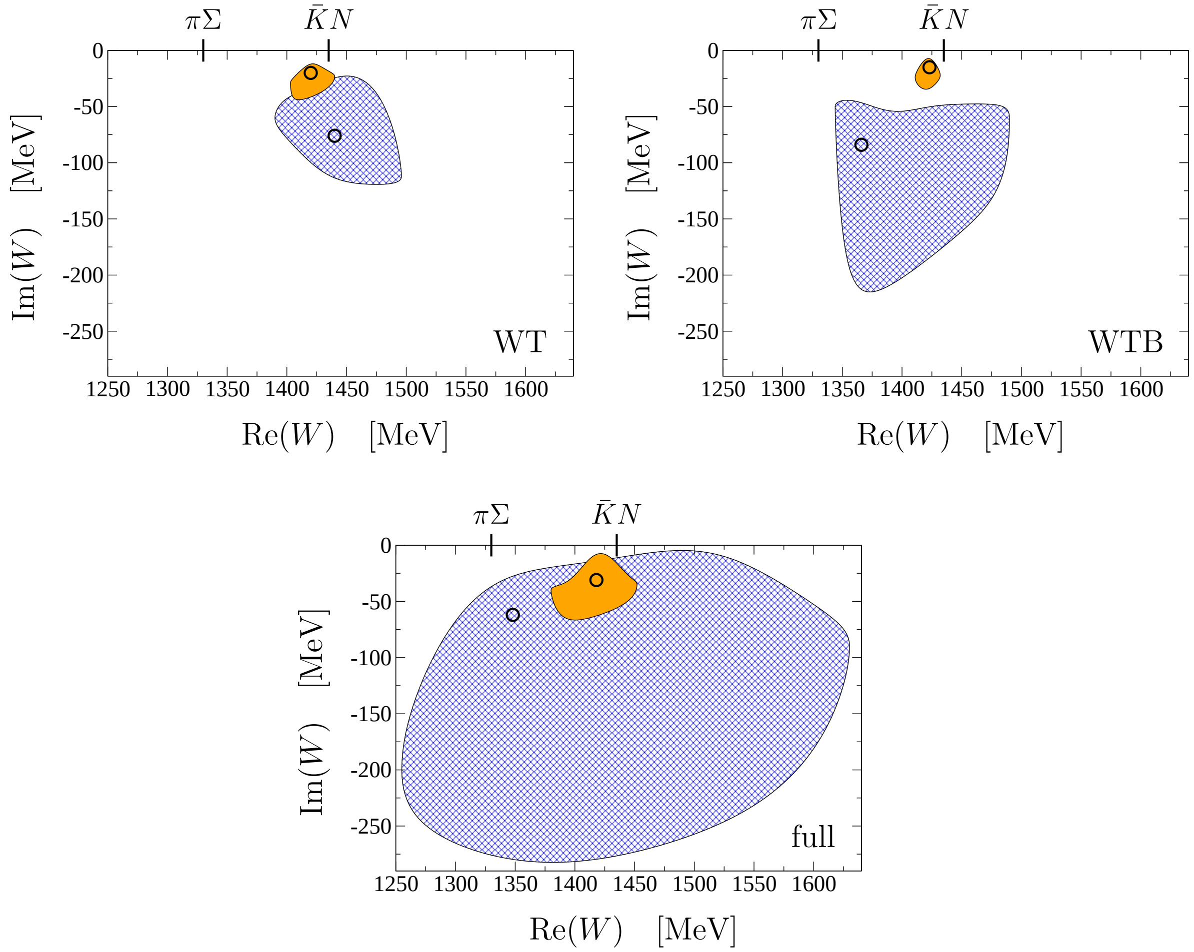

Figure 5.15: Positions of the first (shaded region) and second $I = 0$ pole (crosshatched region) in the complex W plane for the three approaches. The circles indicate the pole positions of the best fits. All poles are located on the unphysical Riemann sheet which is connected to the real axis between the $\pi\Sigma$ and the $\bar{K}N$ thresholds.

however, may help to further constrain the position of the second pole, see *e.g.* Ref. [187]. But in any case, as illustrated above and also pointed out in [167], the pole positions can very well serve as an additional constraint to rule out certain fits.

5.5 Conclusions

In this chapter we have investigated $S = -1$ meson-baryon scattering at low energies using three variants of chiral unitary approaches which differ in the choice of the interaction kernel that is iterated using the Bethe-Salpeter equation. In the first approach, the interaction kernel is derived from the Weinberg-Tomozawa contact interaction at leading chiral order which is successively supplemented by the Born terms and the contact interactions of next-to-leading chiral order in the second and third framework, respectively. The usage of three different interaction kernels helps to estimate the inherent model-dependence of such approaches.

The BSE is treated in the so-called on-shell approximation where the external momenta in the interaction kernel are put on their mass shells. In this framework the inclusion of the u-channel Born diagram introduces unphysical subthreshold cuts as explained in some detail in Sect. 5.2.1. In order to produce sensible results these artificial singularities have to be removed.

For all three approaches a least-squares fit to low-energy data in $S = -1$ meson-baryon channels is performed. These are in detail elastic and inelastic K^-p scattering cross sections, the $\pi\Sigma$ mass spectrum in the $\Lambda(1405)$ region and the precisely measured K^-p threshold decay ratios. Fits with the lowest χ^2/d.o.f. value are found in the full approach including the higher order couplings while the minimum χ^2/d.o.f. value is largest in the Weinberg-Tomozawa approach.

Due to an exhaustive sampling of parameter space based on Monte Carlo methods we can provide for the first time in a chiral unitary study a realistic error range for the K^-p scattering length. This quantity is directly related to the strong interaction shift ΔE and width Γ of the ground state in kaonic hydrogen. In all three approaches we obtain values for ΔE, Γ which are in agreement with the KEK experiment, but disagree with DEAR. The present analysis confirms the findings of [152] by pointing at questions of consistency of the recent DEAR measurement with previous K^-p scattering data. The conservative error ranges for ΔE, Γ deduced from chiral unitary approaches are in clear disagreement with the DEAR experiment. In this respect, we are looking forward to the upcoming re-measurement of kaonic hydrogen observables with SIDDHARTA at DAΦNE [197] which aims at a precision of few eV and will certainly clarify the situation.

We have also presented our results for the meson-baryon scattering amplitudes at energies below the $\bar{K}N$ threshold which are of relevance for the analysis of hadronic reactions in the domain of the $\Lambda(1405)$ and may help to improve our understanding of deeply bound kaon nuclear states. Moreover, we have estimated the importance of the Coulomb interaction in elastic K^-p scattering which turns out to be substantial only rather close to threshold.

Finally, we have critically investigated the pole structure of the fits. The first isospin zero pole corresponding to the $\Lambda(1405)$ remains relatively fixed in all fits and close to the physical axis, whereas the second $I = 0$ pole is quite sensitive to the chosen parameters of the approach. In particular, the influence of the second pole on physical observables is substantially reduced if it is further away from the real axis and can even dissolve in the non-resonant background. Although the pole positions depend sensitively on the dynamical input of the chiral SU(3) effective Lagrangian, we have illustrated that the general pole structure of a fit can serve as an additional criterion to consider the fit as unphysical.

Outlook

At the end of each chapter we have summarized our respective findings, hence we are not going to list all the results here once again. Instead we would like to briefly address a few possible continuations of the present work.

Our treatment of final-state interactions in η and η' decays relies on the dominance of two-body interactions which is usually a good approximation in low-energy hadron physics. In fact, we have estimated some three-body effects in the decay modes $\eta \to 3\pi$, $\eta' \to \eta\pi\pi$ and found only moderate contributions. For the decays of the η' into three pions, however, three-body contributions to final-state interactions could be more important due to larger phase space. A rigorous inclusion of three-body interactions would thus improve our predictions for $\eta' \to 3\pi$, where experimental information is sparse so far, and at the same time it would make our error estimates for the remaining hadronic decay modes of η and η' more reliable. However, we are aware of the fact that such an improved approach would require a great deal of extra work—if it is feasible at all. As a guideline one could use the time-honored work of Mandelstam [95].

There are of course a few more decay modes of the η and the η' which we have not studied so far in the chiral unitary framework. Interesting examples are given by the anomalous decay $\eta' \to \pi^+\pi^-\pi^+\pi^-$, whose leading contribution is of sixth chiral order, and by the rare decays of η and η' into a lepton-antilepton pair which involve a two-photon intermediate state. Rare decay modes of η and η', *e.g.* the CP violating decays into two pions or into $4\pi^0$, could be employed to search for non-conventional effects beyond the Standard Model once sufficient experimental precision is reached. A decay mode which appears to be accessible more easily in experiments due to its not so tiny branching fraction is $\eta, \eta' \to \pi^0\gamma\gamma$. The occurrence of two photons in these non-anomalous decays, however, makes the preservation of electromagnetic gauge invariance a difficult task and hampers a straightforward application of the chiral unitary approach.

In general, our approach suffers from the lack of crossing symmetry which is spoilt by the resummation of s-channel bubbles via the Bethe-Salpeter equation. As explained in Sect. 2.3 chiral unitary approaches also do not guarantee maximal analyticity of the amplitudes as postulated in S-matrix theory. One possibility to overcome these handicaps—at least in the domain of two-particle scattering such as K^-p scattering—could be the use of Roy equations [204] or extensions thereof. Up to now, however, Roy equations have only been used to describe $\pi\pi$ and πK scattering although there has been work towards an application also to pion-nucleon scattering, see [205] and references therein.

In view of the upcoming experimental investigations of kaonic deuterium at SIDDHARTA and deeply bound kaon nuclear states by the AMADEUS Collaboration it would be evident to extend our studies of $\bar{K}N$ interactions to the $\bar{K}NN$ system. For the investigation of possible bound states, establishing a non-relativistic effective field theory could be most beneficial [206].

Appendix A

Mesonic interactions

A.1 The groups U(3) and SU(3)

The unitary group U(3) consists of all unitary 3×3 matrices U, *i.e.*

$$U^\dagger U = U U^\dagger = \mathbb{1} \,. \tag{A.1}$$

The special unitary group SU(3) is the subgroup of U(3) whose members have unit determinant. Any unitary matrix U may be expressed in terms of a Hermitian matrix H as $U = e^{iH}$. Since for any matrix A we have $\det e^A = e^{\operatorname{tr} A}$, H must be traceless if $U \in \mathrm{SU}(3)$. Consequently, the nine (eight) generators t^a of U(3) (SU(3)) are given by a set of linearly independent Hermitian (Hermitian and traceless) 3×3 matrices such that

$$U = \exp\{i\alpha^a t^a\} \tag{A.2}$$

where the index a runs from 0 (1) to 8 and the α^a are the real group parameters. Conventionally, the generators of U(3) and SU(3) are normalized according to

$$\operatorname{tr}\bigl(t^a t^b\bigr) = \frac{1}{2}\delta^{ab} \,, \tag{A.3}$$

and they satisfy the Lie algebra relation

$$[t^a, t^b] = i f^{abc} t^c \tag{A.4}$$

with real structure constants f^{abc}. The structure constants are totally antisymmetric and the non-vanishing ones read

$$\begin{aligned} f^{123} &= 1 \,, & f^{147} &= f^{246} = f^{257} = f^{345} = \frac{1}{2} \\ f^{156} &= f^{367} = -\frac{1}{2} \,, & f^{458} &= f^{678} = \frac{\sqrt{3}}{2} \,. \end{aligned} \tag{A.5}$$

Furthermore, one defines the anti-commutator

$$\{t^a, t^b\} = d^{abc} t^c \tag{A.6}$$

with totally symmetric real coefficients d^{abc} which are given by

$$\begin{aligned}
&d^{0ab} = \sqrt{\frac{2}{3}}\,\delta^{ab}\,, && d^{118} = d^{228} = d^{338} = -d^{888} = \sqrt{\frac{1}{3}}\,,\\
&d^{146} = d^{157} = d^{256} = d^{344} = d^{355} = \frac{1}{2}\,, && d^{247} = d^{366} = d^{377} = -\frac{1}{2}\,,\\
&d^{448} = f^{558} = f^{668} = f^{778} = -\frac{1}{2\sqrt{3}}\,,
\end{aligned} \tag{A.7}$$

and zero otherwise. The product of two generators may thus be written as

$$t^a t^b = \frac{1}{2}(d^{abc} + i f^{abc})\, t^c\ . \tag{A.8}$$

By means of the relation

$$t^a = \frac{1}{2}\,\lambda^a\ , \tag{A.9}$$

the generators of U(3) and SU(3) are conventionally expressed in terms of the matrices

$$\begin{aligned}
&\lambda^0 = \sqrt{\frac{2}{3}}\begin{pmatrix} 1 & 0 & 0\\ 0 & 1 & 0\\ 0 & 0 & 1\end{pmatrix}, \quad \lambda^1 = \begin{pmatrix} 0 & 1 & 0\\ 1 & 0 & 0\\ 0 & 0 & 0\end{pmatrix}, \quad \lambda^2 = \begin{pmatrix} 0 & -i & 0\\ i & 0 & 0\\ 0 & 0 & 0\end{pmatrix},\\
&\lambda^3 = \begin{pmatrix} 1 & 0 & 0\\ 0 & -1 & 0\\ 0 & 0 & 0\end{pmatrix}, \quad \lambda^4 = \begin{pmatrix} 0 & 0 & 1\\ 0 & 0 & 0\\ 1 & 0 & 0\end{pmatrix}, \quad \lambda^5 = \begin{pmatrix} 0 & 0 & -i\\ 0 & 0 & 0\\ i & 0 & 0\end{pmatrix},\\
&\lambda^6 = \begin{pmatrix} 0 & 0 & 0\\ 0 & 0 & 1\\ 0 & 1 & 0\end{pmatrix}, \quad \lambda^7 = \begin{pmatrix} 0 & 0 & 0\\ 0 & 0 & -i\\ 0 & i & 0\end{pmatrix}, \quad \lambda^8 = \frac{1}{\sqrt{3}}\begin{pmatrix} 1 & 0 & 0\\ 0 & 1 & 0\\ 0 & 0 & -2\end{pmatrix}.
\end{aligned} \tag{A.10}$$

The $\lambda^1, \ldots, \lambda^8$ are known as the Gell-Mann matrices. In analogy to Eq. (A.3) the matrices λ^a obey the following normalization

$$\mathrm{tr}\big(\lambda^a \lambda^b\big) = 2\,\delta^{ab}\ . \tag{A.11}$$

A.2 Fourth-order Lagrangian

The fourth-order chiral Lagrangian in the U(3) framework is of the form

$$\mathcal{L}^{(4)} = \sum_{i=0}^{57} \beta_i\, \mathcal{O}_i\,, \tag{A.12}$$

where the coefficients β_i are functions of the chirally invariant combination $\sqrt{\lambda}\bar{\varphi}_0 = \eta_0 + \sqrt{\lambda}\theta$ which involves the singlet field η_0 and does not depend on the QCD renormalization scale, see Sect. 1.5.1 for details. The β_i can be expanded in terms of $\sqrt{\lambda}\bar{\varphi}_0$ and due to parity conservation they are either even or odd functions of this variable. The full list of operators $\mathcal{O}_i$ was given in [41, 46]; they read

$$
\begin{aligned}
\mathcal{O}_0 &= \langle C^\mu C^\nu C_\mu C_\nu \rangle\,, & \mathcal{O}_1 &= \langle C^\mu C_\mu \rangle \langle C^\nu C_\nu \rangle\,,\\
\mathcal{O}_2 &= \langle C^\mu C^\nu \rangle \langle C_\mu C_\nu \rangle\,, & \mathcal{O}_3 &= \langle C^\mu C_\mu C^\nu C_\nu \rangle\,,\\
\mathcal{O}_4 &= -\langle C^\mu C_\mu \rangle \langle M \rangle\,, & \mathcal{O}_5 &= -\langle C^\mu C_\mu M \rangle\,,\\
\mathcal{O}_6 &= \langle M \rangle \langle M \rangle\,, & \mathcal{O}_7 &= \langle N \rangle \langle N \rangle\,,\\
\mathcal{O}_8 &= \tfrac{1}{2}\langle MM + NN \rangle\,, & \mathcal{O}_9 &= i\langle C^\mu C^\nu F^+_{\mu\nu} \rangle\,,\\
\mathcal{O}_{10} &= \tfrac{1}{4}\langle F_+^{\mu\nu} F^+_{\mu\nu} - F_-^{\mu\nu} F^-_{\mu\nu} \rangle\,, & \mathcal{O}_{11} &= \tfrac{1}{2}\langle F_+^{\mu\nu} F^+_{\mu\nu} + F_-^{\mu\nu} F^-_{\mu\nu} \rangle\,,\\
\mathcal{O}_{12} &= \tfrac{1}{4}\langle MM - NN \rangle\,, & \mathcal{O}_{13} &= -\langle C^\mu \rangle \langle C_\mu C^\nu C_\nu \rangle\,,\\
\mathcal{O}_{14} &= -\langle C^\mu \rangle \langle C_\mu \rangle \langle C^\nu C_\nu \rangle\,, & \mathcal{O}_{15} &= -\langle C^\mu \rangle \langle C^\nu \rangle \langle C_\mu C_\nu \rangle\,,\\
\mathcal{O}_{16} &= \langle C^\mu \rangle \langle C_\mu \rangle \langle C^\nu \rangle \langle C_\nu \rangle\,, & \mathcal{O}_{17} &= \langle C^\mu \rangle \langle C_\mu \rangle \langle M \rangle\,,\\
\mathcal{O}_{18} &= -\langle C^\mu \rangle \langle C_\mu M \rangle\,, & \mathcal{O}_{19} &= \tfrac{1}{2}\langle F_+^{\mu\nu} \rangle \langle F^+_{\mu\nu} \rangle + \tfrac{1}{2}\langle F_-^{\mu\nu} \rangle \langle F^-_{\mu\nu} \rangle\,,\\
\mathcal{O}_{20} &= \tfrac{1}{4}\langle F_+^{\mu\nu} \rangle \langle F^+_{\mu\nu} \rangle - \tfrac{1}{4}\langle F_-^{\mu\nu} \rangle \langle F^-_{\mu\nu} \rangle\,, & \mathcal{O}_{21} &= i\langle C^\mu C_\mu N \rangle\,,\\
\mathcal{O}_{22} &= i\langle C^\mu C_\mu \rangle \langle N \rangle\,, & \mathcal{O}_{23} &= i\langle C^\mu \rangle \langle C_\mu N \rangle\,,\\
\mathcal{O}_{24} &= i\langle C^\mu \rangle \langle C_\mu \rangle \langle N \rangle\,, & \mathcal{O}_{25} &= i\langle MN \rangle\,,\\
\mathcal{O}_{26} &= i\langle M \rangle \langle N \rangle\,, & \mathcal{O}_{27} &= \langle C^\mu \rangle \langle C^\nu F^-_{\mu\nu} \rangle\,,\\
\mathcal{O}_{28} &= \tfrac{1}{4}\epsilon^{\mu\nu\alpha\beta}\langle F^+_{\mu\nu} F^+_{\alpha\beta} - F^-_{\mu\nu} F^-_{\alpha\beta} \rangle\,, & \mathcal{O}_{29} &= i\epsilon^{\mu\nu\alpha\beta}\langle C_\mu C_\nu F^+_{\alpha\beta} \rangle\,,\\
\mathcal{O}_{30} &= i\epsilon^{\mu\nu\alpha\beta}\langle C_\mu \rangle \langle C_\nu F^-_{\alpha\beta} \rangle\,, & \mathcal{O}_{31} &= T^\mu \langle C_\mu C^\nu C_\nu \rangle\,,\\
\mathcal{O}_{32} &= T^\mu \langle C_\mu \rangle \langle C^\nu C_\nu \rangle\,, & \mathcal{O}_{33} &= T^\mu \langle C_\mu C^\nu \rangle \langle C_\nu \rangle\,,\\
\mathcal{O}_{34} &= T^\mu \langle C_\mu \rangle \langle C^\nu \rangle \langle C_\nu \rangle\,, & \mathcal{O}_{35} &= T^\mu T_\mu \langle C^\nu C_\nu \rangle\,,\\
\mathcal{O}_{36} &= T^\mu T^\nu \langle C_\mu C_\nu \rangle\,, & \mathcal{O}_{37} &= T^\mu T_\mu \langle C^\nu \rangle \langle C_\nu \rangle\,,\\
\mathcal{O}_{38} &= T^\mu T^\nu \langle C_\mu \rangle \langle C_\nu \rangle\,, & \mathcal{O}_{39} &= T^\mu T_\mu T^\nu \langle C_\nu \rangle\,,\\
\mathcal{O}_{40} &= T^\mu T_\mu T^\nu T_\nu\,, & \mathcal{O}_{41} &= i\nabla^\mu T_\mu \langle C^\nu C_\nu \rangle\,,\\
\mathcal{O}_{42} &= i\nabla^\mu T_\mu \langle C^\nu \rangle \langle C_\nu \rangle\,, & \mathcal{O}_{43} &= i\nabla^\mu T_\mu T^\nu \langle C_\nu \rangle\,,\\
\mathcal{O}_{44} &= i\nabla^\mu T_\mu T^\nu T_\nu\,, & \mathcal{O}_{45} &= \nabla^\mu T_\mu \nabla^\nu T_\nu\,,\\
\mathcal{O}_{46} &= T^\mu \langle C_\mu M \rangle\,, & \mathcal{O}_{47} &= T^\mu \langle C_\mu \rangle \langle M \rangle\,,\\
\mathcal{O}_{48} &= iT^\mu \langle C_\mu N \rangle\,, & \mathcal{O}_{49} &= iT^\mu \langle C_\mu \rangle \langle N \rangle\,,\\
\mathcal{O}_{50} &= T^\mu T_\mu \langle M \rangle\,, & \mathcal{O}_{51} &= iT^\mu T_\mu \langle N \rangle\,,\\
\mathcal{O}_{52} &= i\nabla^\mu T_\mu \langle M \rangle\,, & \mathcal{O}_{53} &= \nabla^\mu T_\mu \langle N \rangle\,,\\
\mathcal{O}_{54} &= T^\mu \langle C^\nu F^-_{\mu\nu} \rangle\,, & \mathcal{O}_{55} &= T^\mu \langle C^\nu \rangle \langle F^-_{\mu\nu} \rangle\,,\\
\mathcal{O}_{56} &= -\epsilon^{\mu\nu\alpha\beta} T_\mu \langle C_\nu F^-_{\alpha\beta} \rangle\,, & \mathcal{O}_{57} &= -\epsilon^{\mu\nu\alpha\beta} T_\mu \langle C_\nu \rangle \langle F^-_{\alpha\beta} \rangle\,,
\end{aligned}
\tag{A.13}
$$

where we have made use of the abbreviations

$$
\begin{aligned}
C_\mu &= U^\dagger \nabla_\mu U\,, & M &= U^\dagger \chi + \chi^\dagger U\,, & N &= U^\dagger \chi - \chi^\dagger U\,,\\
T_\mu &= i\nabla_\mu \theta\,, & F^\pm_{\mu\nu} &= L_{\mu\nu} \pm U^\dagger R_{\mu\nu} U\,.
\end{aligned}
\tag{A.14}
$$

The covariant derivatives and field strength tensors have been defined in Eqs. (1.99) and (1.116), respectively, see Sects. 1.5.1 and 1.5.3. Note that there is a Cayley-Hamilton identity which relates the operators $\mathcal{O}_i$ with $i = 0, 1, 2, 3, 13, 14, 15, 16$ and allows one to eliminate one of these operators. Conventionally, $\mathcal{O}_0$ is removed, but in this work we do not make use the Cayley-Hamilton identity since it mixes terms of different orders in the large N_c counting scheme which we utilize to estimate the size of the different couplings.

A.3 $\mathcal{O}(p^6)$ contact terms in $\eta^{(\prime)} \to \pi^+\pi^-\gamma^*$

There are several terms in the unnatural parity part of the effective Lagrangian of sixth chiral order which contribute to $\eta^{(\prime)} \to \pi^+\pi^-\gamma^*$ at tree level. The full set of Lagrangian terms in the SU(3) framework can be found in [55] whereas in the extended U(3) framework—necessary to describe η' decays—the terms relevant for $\eta^{(\prime)} \to \pi^+\pi^-\gamma$ have been given in [136]. In this appendix we repeat the construction of the pertinent Lagrangian terms extending the findings of [136] to the description of off-shell photons.

The building blocks for the construction of the chiral Lagrangian read

$$\begin{aligned} &C_\mu = U^\dagger \nabla_\mu U\,, && M = U^\dagger\chi + \chi^\dagger U\,, && N = U^\dagger\chi - \chi^\dagger U\,, \\ &F^\pm_{\mu\nu} = L_{\mu\nu} \pm U^\dagger R_{\mu\nu} U\,, && E_{\mu\nu} = U^\dagger \nabla_\mu\nabla_\nu U - (\nabla_\mu\nabla_\nu U)^\dagger U\,, && \end{aligned} \tag{A.15}$$

where the covariant derivatives and field strength tensors have been defined in Eqs. (1.99) and (1.116), respectively, see Sects. 1.5.1 and 1.5.3. Note that we do not consider terms which involve the derivative of the external field θ, $\nabla_\mu\theta$, since they are not relevant for our discussion of the decays $\eta^{(\prime)} \to \pi^+\pi^-\gamma^*$.

The terms of $\mathcal{O}(p^6)$ which contribute to $\eta^{(\prime)} \to \pi^+\pi^-\gamma^*$ read

$$\begin{aligned} \mathcal{L}^{(6)} = \epsilon^{\mu\nu\alpha\beta}\Big\{ & \bar{W}_7 \langle N(F^+_{\mu\nu}C_\alpha C_\beta + C_\alpha C_\beta F^+_{\mu\nu} + 2C_\alpha F^+_{\mu\nu} C_\beta)\rangle \\ & + \bar{W}_8 \big(\langle N\rangle\langle F^+_{\mu\nu}C_\alpha C_\beta\rangle - \langle MC_\mu\rangle\langle C_\nu F^-_{\alpha\beta}\rangle\big) \\ & + \bar{W}_9 \big(\langle N(F^+_{\mu\nu}C_\alpha - C_\alpha F^+_{\mu\nu})\rangle - \langle M(F^-_{\mu\nu}C_\alpha + C_\alpha F^-_{\mu\nu})\rangle\big)\langle C_\beta\rangle \\ & - \bar{W}_{10}\langle M\rangle\langle F^-_{\mu\nu}C_\alpha\rangle\langle C_\beta\rangle \\ & + \bar{W}_{11}\langle F^+_{\mu\nu}(E^\lambda{}_\alpha C_\beta C_\lambda - C_\lambda C_\beta E^\lambda{}_\alpha)\rangle \\ & + \bar{W}_{12}\langle F^+_{\mu\nu}(E^\lambda{}_\alpha C_\lambda C_\beta - C_\beta C_\lambda E^\lambda{}_\alpha)\rangle \\ & + \bar{W}_{13}\langle F^+_{\mu\nu}(E^\lambda{}_\alpha C_\lambda - C_\lambda E^\lambda{}_\alpha)\rangle\langle C_\beta\rangle \\ & + \bar{W}_{14}\langle F^+_{\mu\nu}(E^\lambda{}_\alpha C_\beta - C_\beta E^\lambda{}_\alpha)\rangle\langle C_\lambda\rangle\Big\}\,. \end{aligned} \tag{A.16}$$

The coefficients $\bar{W}_i$ $(i = 7, \ldots, 14)$ are even functions of the variable $\sqrt{\lambda}\bar{\varphi}_0 = \eta_0 + \sqrt{\lambda}\theta$ which involves the singlet field η_0. For $\theta \equiv 0$ they can be expanded in terms of η_0 according to

$$\bar{W}_i\Big(\frac{\eta_0}{f}\Big) = \bar{w}_i^{(0)} + \bar{w}_i^{(2)}\frac{\eta_0^2}{f^2} + \bar{w}_i^{(4)}\frac{\eta_0^4}{f^4} + \cdots \tag{A.17}$$

with expansion coefficients $\bar{w}_i^{(j)}$ not fixed by chiral symmetry. At tree level we find the following contribution to the amplitude of $\eta^{(\prime)} \to \pi^+\pi^-\gamma^*$

$$\mathcal{A}^{(\mathrm{ct})}(\eta^{(\prime)} \to \pi^+\pi^-\gamma^*) = -ek_\mu\epsilon_\nu p_\alpha^+ p_\beta^- \epsilon^{\mu\nu\alpha\beta}\frac{1}{4\pi^2 f^3}\,\beta_{\eta^{(\prime)}}^{(\mathrm{ct})} \tag{A.18}$$

with

$$\begin{aligned}
\beta_\eta^{(\mathrm{ct})} &= \frac{64\pi^2}{\sqrt{3}}\Big\{-4\bar{w}_7^{(0)}m_\pi^2 + 8\bar{w}_8^{(0)}(m_K^2 - m_\pi^2) \\
&\qquad + \bar{w}_{11}^{(0)}(m_\eta^2 - 2m_\pi^2 + 2s_{+-} - k^2) - \bar{w}_{12}^{(0)}(2m_\pi^2 - s_{+-})\Big\}\ , \\
\beta_{\eta'}^{(\mathrm{ct})} &= 32\pi^2\sqrt{\frac{2}{3}}\Big\{8(-\bar{w}_7^{(0)} + 3\bar{w}_9^{(0)})m_\pi^2 + (4\bar{w}_8^{(0)} + 6\bar{w}_{10}^{(0)})(2m_K^2 + m_\pi^2) \\
&\qquad + 2\bar{w}_{11}^{(0)}(m_{\eta'}^2 - 2m_\pi^2 + 2s_{+-} - k^2) + 3\bar{w}_{14}^{(0)}(m_{\eta'}^2 + s_{+-} - k^2) \\
&\qquad - 2(\bar{w}_{12}^{(0)} + 3\bar{w}_{13}^{(0)})(2m_\pi^2 - s_{+-})\Big\}\ .
\end{aligned} \tag{A.19}$$

By defining the combinations

$$\begin{aligned}
\bar{w}_\eta^{(m)} &= -2(2\bar{w}_7^{(0)} + \bar{w}_{11}^{(0)} + \bar{w}_{12}^{(0)})m_\pi^2 + 8\bar{w}_8^{(0)}(m_K^2 - m_\pi^2) + \bar{w}_{11}^{(0)}m_\eta^2\,, \\
\bar{w}_\eta^{(s)} &= 2\bar{w}_{11}^{(0)} + \bar{w}_{12}^{(0)}\,, \\
\bar{w}_\eta^{(k)} &= -\bar{w}_{11}^{(0)}\,, \\
\bar{w}_{\eta'}^{(0)} &= 2\bar{w}_{11}^{(0)} + 3\bar{w}_{14}^{(0)}\,, \\
\bar{w}_{\eta'}^{(m)} &= -4(2\bar{w}_7^{(0)} - 6\bar{w}_9^{(0)} + \bar{w}_{11}^{(0)} + \bar{w}_{12}^{(0)} + 3\bar{w}_{13}^{(0)})m_\pi^2 + (4\bar{w}_8^{(0)} + 6\bar{w}_{10}^{(0)})(2m_K^2 + m_\pi^2)\,, \\
\bar{w}_{\eta'}^{(s)} &= 4\bar{w}_{11}^{(0)} + 2\bar{w}_{12}^{(0)} + 6\bar{w}_{13}^{(0)} + 3\bar{w}_{14}^{(0)}\,, \\
\bar{w}_{\eta'}^{(k)} &= -2\bar{w}_{11}^{(0)} - 3\bar{w}_{14}^{(0)}\,,
\end{aligned} \tag{A.20}$$

which are obviously linearly independent, we arrive at a simple form for the $\beta_{\eta^{(\prime)}}^{(\mathrm{ct})}$:

$$\begin{aligned}
\beta_\eta^{(\mathrm{ct})} &= \frac{64\pi^2}{\sqrt{3}}\Big(\bar{w}_\eta^{(m)} + \bar{w}_\eta^{(s)}s_{+-} + \bar{w}_\eta^{(k)}k^2\Big)\ , \\
\beta_{\eta'}^{(\mathrm{ct})} &= 32\pi^2\sqrt{\frac{2}{3}}\Big(\bar{w}_{\eta'}^{(0)}m_{\eta'}^2 + \bar{w}_{\eta'}^{(m)} + \bar{w}_{\eta'}^{(s)}s_{+-} + \bar{w}_{\eta'}^{(k)}k^2\Big)\ .
\end{aligned} \tag{A.21}$$

Since the mass of the η' is counted as of zeroth chiral order, the $\bar{w}_{\eta'}^{(0)}$ piece in $\beta_{\eta'}^{(\mathrm{ct})}$ violates the chiral counting scheme. However, as shown in [136], it can be absorbed into the $\mathcal{O}(p^4)$ coupling $w_3^{(1)}$ and in Sect. 4.3 we have employed the renormalized value, $\beta_{\eta'}^{(\mathrm{ct})} = 32\pi^2\sqrt{2/3}(\bar{w}_{\eta'}^{(m)} + \bar{w}_{\eta'}^{(s)}s_{+-} + \bar{w}_{\eta'}^{(k)}k^2)$, without changing the notation.

Appendix B

Meson-baryon interactions

B.1 Coupling constants

The leading order contact interaction derived from the chiral effective meson-baryon Lagrangian $\mathcal{L}^{(1)}_{\hat{\phi}B}$ is known as the Weinberg-Tomozawa term. For the ten $S = -1$ meson baryon channels the pertinent coefficients, which we denote by $C^{(\mathrm{a})}_{jb,ia}$ (*cf.* Eqs. (5.2), (5.7)), are given in Table B.1. The next-to-leading order contact terms involve the coefficients $C^{(\mathrm{d}_1)}_{jb,ia}$, $C^{(\mathrm{d}_2)}_{jb,ia}$ (see Eq. (5.10)) whose values can be found in Tables B.2, B.3, respectively.

The axial-vector couplings $C^{(\mathrm{b})}_{ia,b}$ enter the direct and crossed Born diagrams, *cf.* Eqs. (5.8), (5.9). They are symmetric under the combined transformation $a \leftrightarrow b$ and charge conjugation of the meson i. The non-zero values relevant for the present work read

$$
\begin{aligned}
C^{(\mathrm{b})}_{K^-p,\Lambda} &= C^{(\mathrm{b})}_{\bar{K}^0n,\Lambda} = C^{(\mathrm{b})}_{\eta\Xi^-,\Xi^-} = C^{(\mathrm{b})}_{\eta\Xi^0,\Xi^0} = -D - 3F\,, \\
C^{(\mathrm{b})}_{\eta p,p} &= C^{(\mathrm{b})}_{\eta n,n} = C^{(\mathrm{b})}_{K^+\Xi^-,\Lambda} = C^{(\mathrm{b})}_{K^0\Xi^0,\Lambda} = -D + 3F\,, \\
C^{(\mathrm{b})}_{\pi^0\Sigma^0,\Lambda} &= C^{(\mathrm{b})}_{\pi^+\Sigma^-,\Lambda} = C^{(\mathrm{b})}_{\pi^-\Sigma^+,\Lambda} = C^{(\mathrm{b})}_{\eta\Sigma^+,\Sigma^+} = C^{(\mathrm{b})}_{\eta\Sigma^-,\Sigma^-} = C^{(\mathrm{b})}_{\eta\Sigma^0,\Sigma^0} = -C^{(\mathrm{b})}_{\eta\Lambda,\Lambda} = 2D\,, \\
C^{(\mathrm{b})}_{\pi^+\Sigma^-,\Sigma^0} &= -C^{(\mathrm{b})}_{\pi^-\Sigma^+,\Sigma^0} = -C^{(\mathrm{b})}_{\pi^0\Sigma^-,\Sigma^-} = C^{(\mathrm{b})}_{\pi^0\Sigma^+,\Sigma^+} = 2\sqrt{3}F\,, \\
C^{(\mathrm{b})}_{\bar{K}^0p,\Sigma^+} &= C^{(\mathrm{b})}_{K^-n,\Sigma^-} = \sqrt{2}\,C^{(\mathrm{b})}_{K^-p,\Sigma^0} = -\sqrt{2}\,C^{(\mathrm{b})}_{\bar{K}^0n,\Sigma^0} = C^{(\mathrm{b})}_{\pi^+\Xi^-,\Xi^0} = \sqrt{2}\,C_{\pi^0\Xi^-,\Xi^-} \\
&= -\sqrt{2}\,C_{\pi^0\Xi^0,\Xi^0} = \sqrt{6}\,(D - F)\,, \\
C^{(\mathrm{b})}_{\pi^-p,n} &= \sqrt{2}\,C^{(\mathrm{b})}_{\pi^0p,p} = -\sqrt{2}\,C^{(\mathrm{b})}_{\pi^0n,n} = \sqrt{2}\,C^{(\mathrm{b})}_{K^+\Xi^-,\Sigma^0} = -\sqrt{2}\,C^{(\mathrm{b})}_{K^0\Xi^0,\Sigma^0} = C^{(\mathrm{b})}_{\bar{K}^0\Sigma^-,\Xi^-} \\
&= C^{(\mathrm{b})}_{K^-\Sigma^+,\Xi^0} = \sqrt{6}\,(D + F)\,. \qquad \text{(B.1)}
\end{aligned}
$$

	K^-p	$\bar{K}^0n$	$\pi^0\Lambda$	$\pi^0\Sigma^0$	$\pi^+\Sigma^-$	$\pi^-\Sigma^+$	$\eta\Lambda$	$\eta\Sigma^0$	$K^+\Xi^-$	$K^0\Xi^0$
K^-p	4	2	$\sqrt{3}$	1	0	2	3	$\sqrt{3}$	0	0
$\bar{K}^0n$		4	$-\sqrt{3}$	1	2	0	3	$-\sqrt{3}$	0	0
$\pi^0\Lambda$			0	0	0	0	0	0	$\sqrt{3}$	$-\sqrt{3}$
$\pi^0\Sigma^0$				0	4	4	0	0	1	1
$\pi^+\Sigma^-$					4	0	0	0	2	0
$\pi^-\Sigma^+$						4	0	0	0	2
$\eta\Lambda$							0	0	3	3
$\eta\Sigma^0$								0	$\sqrt{3}$	$-\sqrt{3}$
$K^+\Xi^-$									4	2
$K^0\Xi^0$										4

Table B.1: Coefficients $C^{(a)}_{jb,ia} = C^{(a)}_{ia,jb}$ of the leading-order contact interaction.

B.2 Isospin amplitudes

In this appendix we plot the amplitudes of meson-baryon scattering in the isospin limit at energies between the $\pi\Sigma$ and $\bar{K}N$ thresholds. The relevant channels with isospin one are $\bar{K}N$, $\pi\Sigma$, $\pi\Lambda$. The plots are shown in Figs. B.1, B.2 and B.3 for the approaches WT, WTB and full, respectively. The meson-baryon pair $\pi\Sigma$ is the only one which involves an $I = 2$ component. The pertinent amplitudes corresponding to the WT, WTB and full approach are displayed in Figs. B.4, B.5 and B.6, respectively. The $I = 0$ amplitudes have already been shown in Sect. 5.3.5.

	K^-p	$\bar{K}^0n$	$\pi^0\Lambda$	$\pi^0\Sigma^0$	$\pi^+\Sigma^-$	$\pi^-\Sigma^+$	$\eta\Lambda$	$\eta\Sigma^0$	$K^+\Xi^-$	$K^0\Xi^0$
K^-p	$4(b_0{+}b_D)m_K^2$	$2(b_D{+}b_F)m_K^2$	$\frac{-(b_D+3b_F)\mu_1^2}{2\sqrt{3}}$	$\frac{(b_D-b_F)\mu_1^2}{2}$	0	$(b_D{-}b_F)\mu_1^2$	$\frac{(b_D+3b_F)\mu_2^2}{6}$	$\frac{-(b_D-b_F)\mu_2^2}{2\sqrt{3}}$	0	0
$\bar{K}^0n$		$4(b_0{+}b_D)m_K^2$	$\frac{(b_D+3b_F)\mu_1^2}{2\sqrt{3}}$	$\frac{(b_D-b_F)\mu_1^2}{2}$	$(b_D{-}b_F)\mu_1^2$	0	$\frac{(b_D+3b_F)\mu_2^2}{6}$	$\frac{(b_D-b_F)\mu_2^2}{2\sqrt{3}}$	0	0
$\pi^0\Lambda$			$\frac{4(3b_0+b_D)m_\pi^2}{3}$	0	0	0	0	$\frac{4b_Dm_\pi^2}{3}$	$\frac{-(b_D-3b_F)\mu_1^2}{2\sqrt{3}}$	$\frac{(b_D-3b_F)\mu_1^2}{2\sqrt{3}}$
$\pi^0\Sigma^0$				$4(b_0{+}b_D)m_\pi^2$	0	0	$\frac{4b_Dm_\pi^2}{3}$	0	$\frac{(b_D+b_F)\mu_1^2}{2}$	$\frac{(b_D+b_F)\mu_1^2}{2}$
$\pi^+\Sigma^-$					$4(b_0{+}b_D)m_\pi^2$	0	$\frac{4b_Dm_\pi^2}{3}$	$\frac{4b_Fm_\pi^2}{\sqrt{3}}$	$(b_D{+}b_F)\mu_1^2$	0
$\pi^-\Sigma^+$						$4(b_0{+}b_D)m_\pi^2$	$\frac{4b_Dm_\pi^2}{3}$	$\frac{-4b_Fm_\pi^2}{\sqrt{3}}$	0	$(b_D{+}b_F)\mu_1^2$
$\eta\Lambda$							$\frac{4(3b_0\mu_3^2+b_D\mu_4^2)}{9}$	0	$\frac{(b_D-3b_F)\mu_2^2}{6}$	$\frac{(b_D-3b_F)\mu_2^2}{6}$
$\eta\Sigma^0$								$\frac{4(b_0\mu_3^2+b_Dm_\pi^2)}{3}$	$\frac{-(b_D+b_F)\mu_2^2}{2\sqrt{3}}$	$\frac{(b_D+b_F)\mu_2^2}{2\sqrt{3}}$
$K^+\Xi^-$									$4(b_0{+}b_D)m_K^2$	$2(b_D{-}b_F)m_K^2$
$K^0\Xi^0$										$4(b_0{+}b_D)m_K^2$

Table B.2: Coefficients $C^{(d_1)}_{jb,ia} = C^{(d_1)}_{ia,jb}$ of the next-to-leading order contact interaction where we have made use of the abbreviations $\mu_1^2 = m_K^2 + m_\pi^2$, $\mu_2^2 = 5m_K^2 - 3m_\pi^2$, $\mu_3^2 = 4m_K^2 - m_\pi^2$ and $\mu_4^2 = 16m_K^2 - 7m_\pi^2$.

	K^-p	$\bar{K}^0n$	$\pi^0\Lambda$	$\pi^0\Sigma^0$	$\pi^+\Sigma^-$	$\pi^-\Sigma^+$	$\eta\Lambda$	$\eta\Sigma^0$	$K^+\Xi^-$	$K^0\Xi^0$
K^-p	$2d_2+d_3+2d_4$	$d_1+d_2+d_3$	$\frac{-\sqrt{3}(d_1+d_2)}{2}$	$\frac{-d_1-d_2+2d_3}{2}$	$-2d_2+d_3$	$-d_1+d_2+d_3$	$\frac{d_1-3d_2+2d_3}{2}$	$\frac{d_1-3d_2}{2\sqrt{3}}$	$-4d_2+2d_3$	$-2d_2+d_3$
$\bar{K}^0n$		$2d_2+d_3+2d_4$	$\frac{\sqrt{3}(d_1+d_2)}{2}$	$\frac{-d_1-d_2+2d_3}{2}$	$-d_1+d_2+d_3$	$-2d_2+d_3$	$\frac{d_1-3d_2+2d_3}{2}$	$\frac{-(d_1-3d_2)}{2\sqrt{3}}$	$-2d_2+d_3$	$-4d_2+2d_3$
$\pi^0\Lambda$			$2d_4$	0	0	0	0	d_3	$\frac{\sqrt{3}(d_1-d_2)}{2}$	$\frac{-\sqrt{3}(d_1-d_2)}{2}$
$\pi^0\Sigma^0$				$2(d_3+d_4)$	$-2d_2+d_3$	$-2d_2+d_3$	d_3	0	$\frac{d_1-d_2+2d_3}{2}$	$\frac{d_1-d_2+2d_3}{2}$
$\pi^+\Sigma^-$					$2d_2+d_3+2d_4$	$-4d_2+2d_3$	d_3	$\frac{2d_1}{\sqrt{3}}$	$d_1+d_2+d_3$	$-2d_2+d_3$
$\pi^-\Sigma^+$						$2d_2+d_3+2d_4$	d_3	$\frac{-2d_1}{\sqrt{3}}$	$-2d_2+d_3$	$d_1+d_2+d_3$
$\eta\Lambda$							$2(d_3+d_4)$	0	$\frac{-d_1-3d_2+2d_3}{2}$	$\frac{-d_1-3d_2+2d_3}{2}$
$\eta\Sigma^0$								$2d_4$	$\frac{-(d_1+3d_2)}{2\sqrt{3}}$	$\frac{d_1+3d_2}{2\sqrt{3}}$
$K^+\Xi^-$									$2d_2+d_3+2d_4$	$-d_1+d_2+d_3$
$K^0\Xi^0$										$2d_2+d_3+2d_4$

Table B.3: Coefficients $C^{(d_2)}_{jb,ia} = C^{(d_2)}_{ia,jb}$ of the next-to-leading order contact interaction.

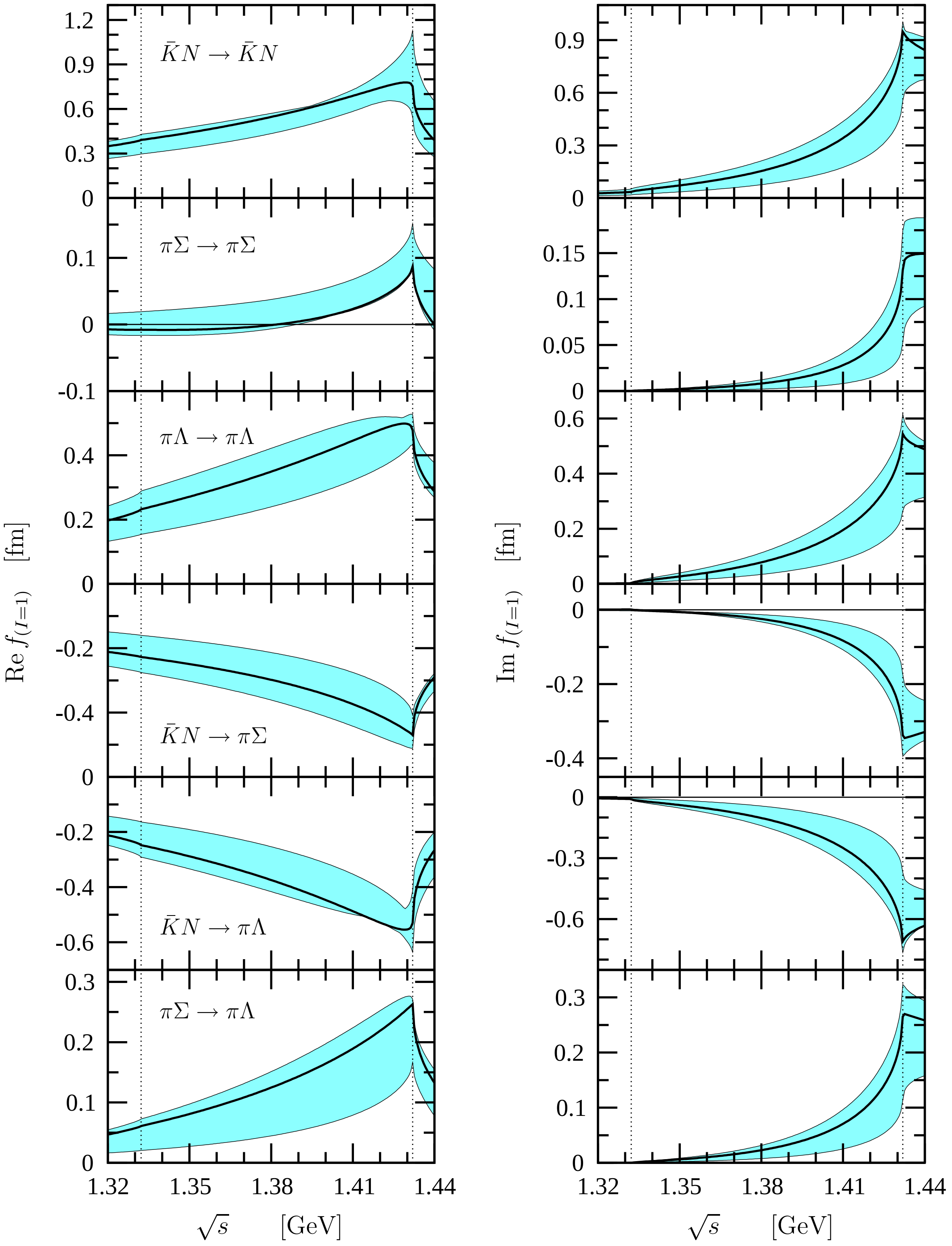

Figure B.1: Real (left panel) and imaginary part (right panel) of the $\bar{K}N$, $\pi\Sigma$, $\pi\Lambda$ $I = 1$ scattering amplitudes in the WT approach. The best fit is represented by the solid lines while the bands comprise all fits in the 1σ region. The $\pi\Sigma$ and $\bar{K}N$ thresholds are indicated by the dotted vertical lines.

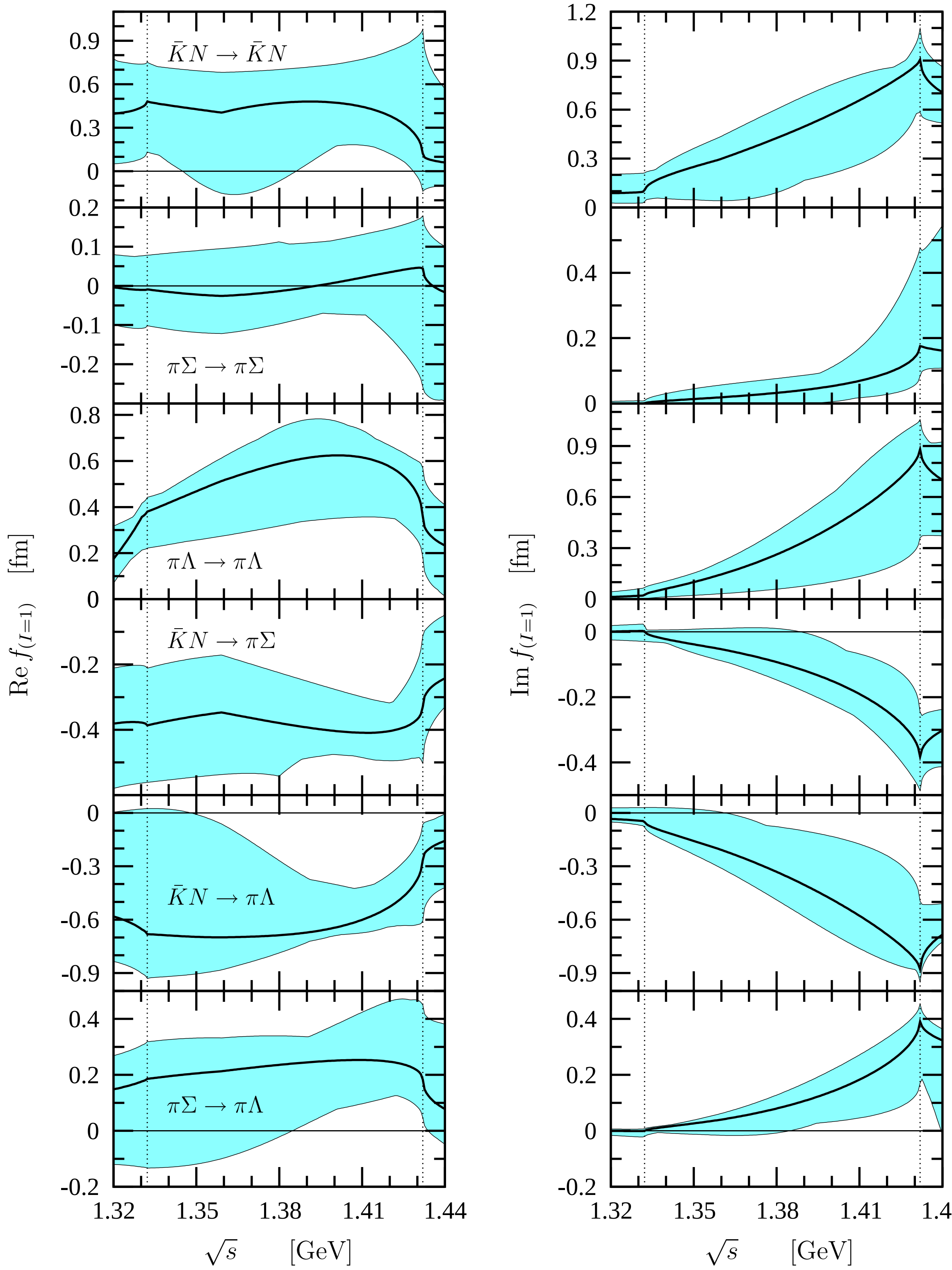

Figure B.2: Real (left panel) and imaginary part (right panel) of the $\bar{K}N$, $\pi\Sigma$, $\pi\Lambda$ $I = 1$ scattering amplitudes in the WTB approach. The best fit is represented by the solid lines while the bands comprise all fits in the 1σ region. The $\pi\Sigma$ and $\bar{K}N$ thresholds are indicated by the dotted vertical lines.

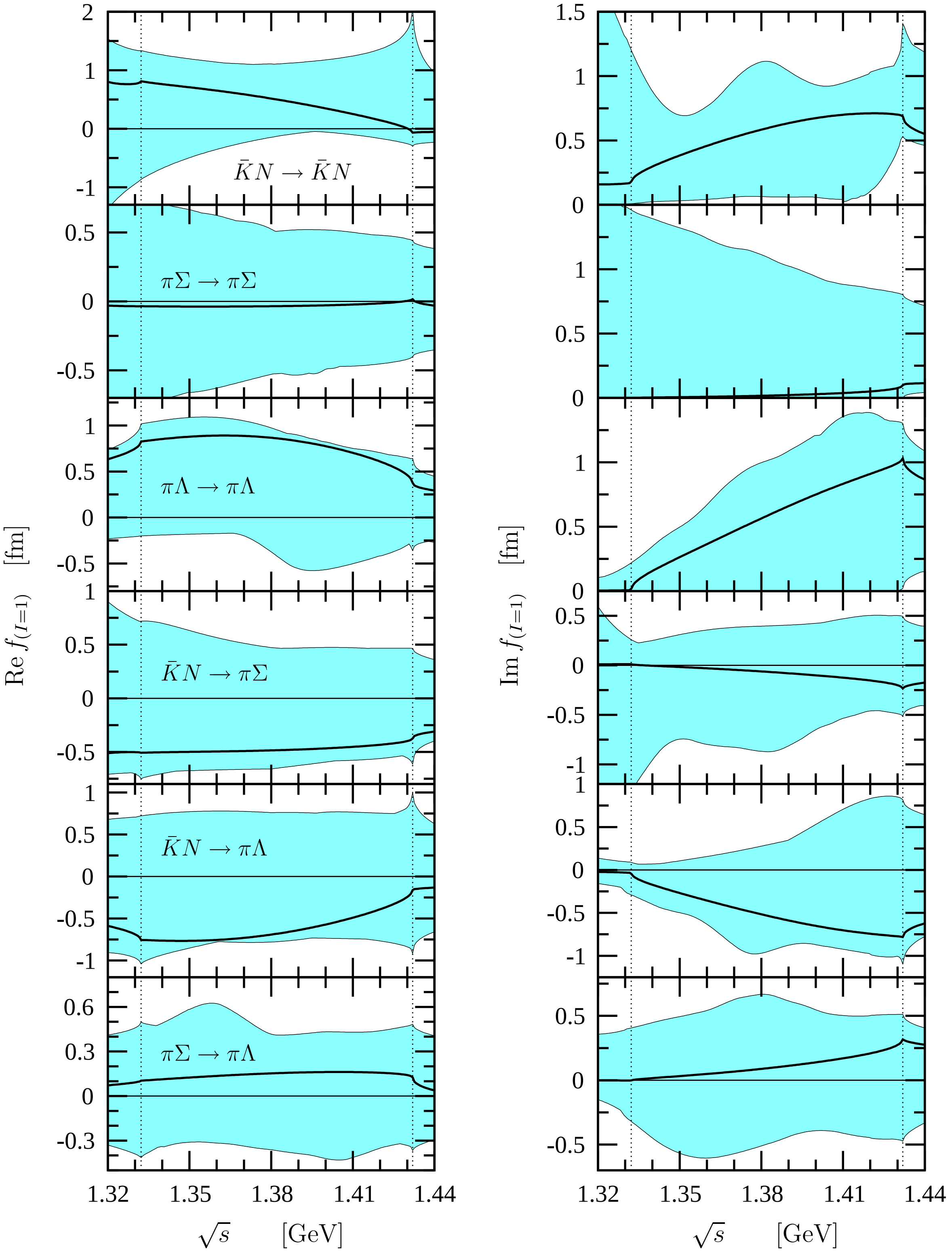

Figure B.3: Real (left panel) and imaginary part (right panel) of the $\bar{K}N$, $\pi\Sigma$, $\pi\Lambda$ $I = 1$ scattering amplitudes in the full approach. The best fit is represented by the solid lines while the bands comprise all fits in the 1σ region. The $\pi\Sigma$ and $\bar{K}N$ thresholds are indicated by the dotted vertical lines.

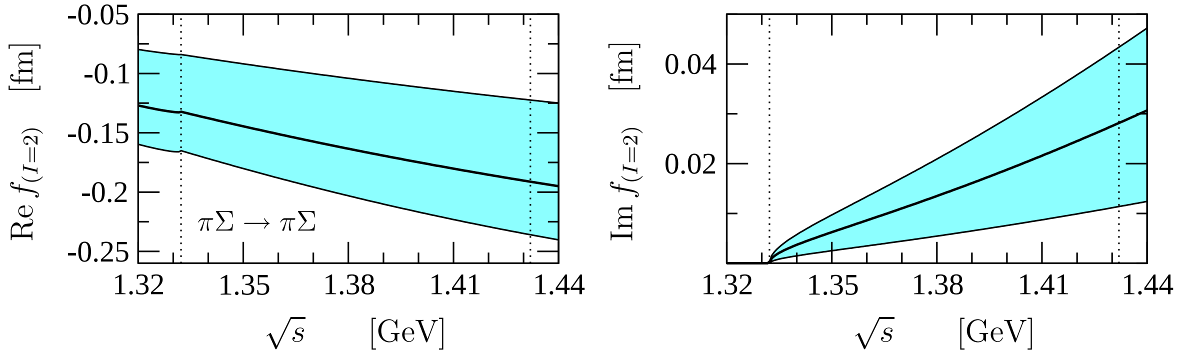

Figure B.4: Real (left panel) and imaginary part (right panel) of the $I = 2$ $\pi\Sigma$ scattering amplitude in the WT approach. The best fit is represented by the solid lines while the bands comprise all fits in the 1σ region. The $\pi\Sigma$ and $\bar{K}N$ thresholds are indicated by the dotted vertical lines.

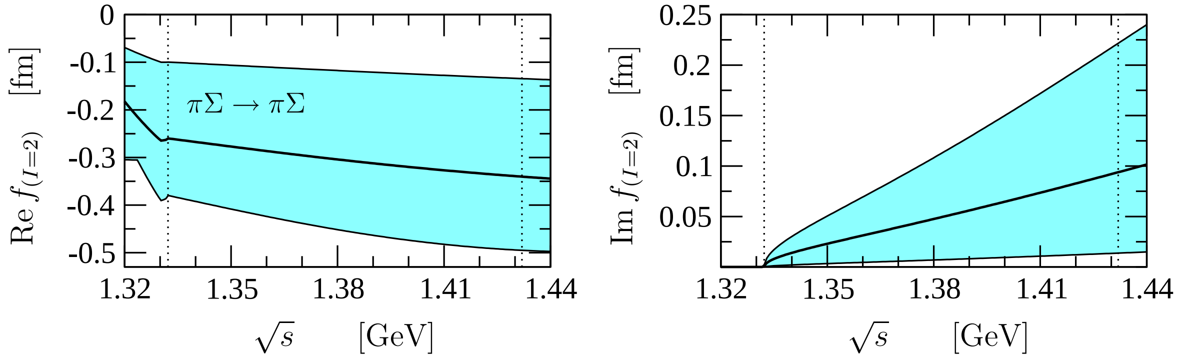

Figure B.5: Real (left panel) and imaginary part (right panel) of the $I = 2$ $\pi\Sigma$ scattering amplitude in the WTB approach. The best fit is represented by the solid lines while the bands comprise all fits in the 1σ region. The $\pi\Sigma$ and $\bar{K}N$ thresholds are indicated by the dotted vertical lines.

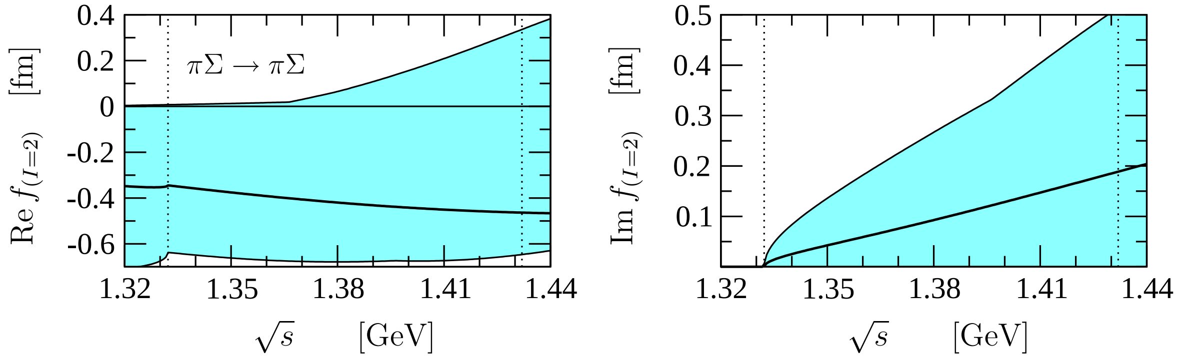

Figure B.6: Real (left panel) and imaginary part (right panel) of the $I = 2$ $\pi\Sigma$ scattering amplitude in the full approach. The best fit is represented by the solid lines while the bands comprise all fits in the 1σ region. The $\pi\Sigma$ and $\bar{K}N$ thresholds are indicated by the dotted vertical lines.

Acknowledgements

I would like to round off this thesis by expressing my gratitude to all those who have contributed in various ways to my research work over the past four years and helped me to finally finish this thesis.

I am deeply grateful to my mentor and friend Dr. Buḡra Borasoy who constantly accompanied me on my path in science. He supported me at all times with his advice and was always patient with me. He shared his insights into physics with me and his new ideas about research projects. Collaborating with him was always a great pleasure, not least due to his invincible sense of humor.

I am very much thankful to my Ph.D. supervisor Prof. Ulf-G. Meißner for his interest in my research work, constructive criticism, his kind support and his collaboration over the past years here in Bonn. I have always appreciated his keen perception and and his quick way of thinking.

Furthermore, sincere thanks go to Prof. Wolfram Weise for supporting me during the early stages of this work in Munich, for his interest and cooperation.

I am grateful to PD Dr. Akaki Rusetsky for many enlightening discussions and for agreeing to carefully read and assess this thesis.

I thank all members of the theory division of the HISKP for creating a pleasant and stimulating atmosphere at work. In particular, I am grateful to my office mate Peter Bruns for countless conversations about physics, philosophy, politics and all that, for fruitful cooperation and for proof-reading this thesis with great care. I thank Prof. Hans-Werner Hammer, Prof. Herbert R. Petry, PD Dr. Bernard Metsch, Matthias Frink, Dr. Hermann Krebs, Dr. Bastian Kubis and Dr. Udit Raha for many interesting discussions. Special thanks go to Dr. Maxim Belushkin and Dr. Hermann Krebs for their help with programming issues and to Dr. Bastian Kubis for providing me with LaTeX templates which eased typesetting this thesis a lot. I thank our “native speaker” David Canham for helping me out with some English problems. Many thanks also go to our system administrators PD Dr. Bernard Metsch, Dr. Paul Büttiker, Dr. Christian Haupt and Simon Kreuzer. Finally, I would like to thank Barbara Mosblech for managing all bureaucratic necessities smoothly and for cheering up the whole corridor with her sunny nature.

I am thankful to Prof. Jürg Gasser and Prof. Dean Lee, who have both been frequent guests at our institute, for inspiring discussions.

I am grateful to many experimental colleagues for valuable discussions and their interest in my work: Prof. Reinhard Beck and Prof. Ulrike Thoma from the HISKP, Prof. Michael Ostrick from Mainz, Prof. Bo Höistad, Dr. Magnus Wolke, Dr. Andrezj Kupsc, Dr. Paweł Moskal, Benedykt Jany, Michal Janusz, Leonid Yurev and Christoph Redmer from the WASA-at-COSY Collaboration.

I would like to thank Andreas Ehmer for broadening my philosophical background by providing me with this little booklet by Heidegger from which I quote at the beginning of this thesis.

I thank my family for their support which I could always rely upon. In particular, I am grateful to my sister Dominique Nißler and my stepfather Heinz Hofstetter for many motivating phone-calls. They always helped me to stay grounded.

Nikola, thank you for your patience, for your understanding and your love.

Bibliography

[1] D. J. Gross and F. Wilczek, Phys. Rev. Lett. **30** (1973) 1343;
H. D. Politzer, Phys. Rev. Lett. **30** (1973) 1346.

[2] S. Weinberg, Physica A **96** (1979) 327.

[3] J. Gasser and H. Leutwyler, Annals Phys. **158** (1984) 142.

[4] J. Gasser and H. Leutwyler, Nucl. Phys. B **250** (1985) 465.

[5] J. Wess and B. Zumino, Phys. Lett. B **37** (1971) 95.

[6] E. Witten, Nucl. Phys. B **223** (1983) 422.

[7] Y. Nambu, Phys. Rev. Lett. **4** (1960) 380;
J. Goldstone, Nuovo Cim. **19** (1961) 154;
J. Goldstone, A. Salam and S. Weinberg, Phys. Rev. **127** (1962) 965 Phys. Rev. **127** (1962) 965.

[8] S. Weinberg, Phys. Rev. **166** (1968) 1568.

[9] S. Coleman, J. Wess and B. Zumino, Phys. Rev. **177** (1969) 2239;
C. G. Callan, S. Coleman, J. Wess and B. Zumino, Phys. Rev. **177** (1969) 2247.

[10] H. Leutwyler, Lectures given at Theoretical Advanced Study Institute, Boulder (1991), published in *Perspectives of the Standard Model*, edited by R. K. Ellis, C. T. Hill and J. D. Lykken (World Scientific, Singapore, 1992), BUTP-91-26.

[11] S. Scherer, Adv. Nucl. Phys. **27** (2003) 277 [arXiv:hep-ph/0210398].

[12] B. Kubis, arXiv:hep-ph/0703274.

[13] B. Borasoy, arXiv:hep-ph/0703297.

[14] V. Bernard and U.-G. Meißner, Annu. Rev. Nucl. Part. Sci. **57** (2007) 33.

[15] V. Bernard, Prog. Part. Nucl. Phys. **60** (2008) 82 [arXiv:0706.0312 [hep-ph]].

[16] J. F. Donoghue, E. Golowich and B. R. Holstein, *Dynamics Of The Standard Model* (Cambridge University Press, Cambridge, 1992).

[17] W. M. Yao *et al.* [Particle Data Group], J. Phys. G **33** (2006) 1.

[18] G. Colangelo and S. Dürr, Eur. Phys. J. C **33** (2004) 543 [arXiv:hep-lat/0311023].

[19] R. P. Feynman and A. R. Hibbs, *Quantum Mechanics and Path Integrals* (McGraw-Hill, New York, 1965).

[20] M. E. Peskin and D. V. Schroeder, *An Introduction To Quantum Field Theory* (Addison-Wesley, Reading, Massachusetts, 1995).

[21] N. H. Fuchs, H. Sazdjian and J. Stern, Phys. Lett. B **269** (1991) 183.

[22] M. Gell-Mann, R. J. Oakes and B. Renner, Phys. Rev. **175** (1968) 2195.

[23] M. Gell-Mann, California Institute of Technology Synchrotron Laboratory Report No. CTSL-20;
M. Gell-Mann and Y. Ne'eman, *The eightfold way* (Benjamin, New York, 1964).

[24] S. Okubo, Prog. Theor. Phys. **27** (1962) 949.

[25] M. Veltman, Proc. Roy. Soc. A **301** (1967) 107;
D. G. Sutherland, Nucl. Phys. B **2** (1967) 433.

[26] S. Adler, Phys. Rev. **177** (1969) 2426.

[27] J. S. Bell and R. Jackiw, Nuovo Cim. A **60** (1969) 47.

[28] K. Fujikawa, Phys. Rev. Lett. **42** (1979) 1195.

[29] S. Weinberg, *The Quantum Theory of Fields*, Vol. II, (Cambridge University Press, Cambridge, 1996).

[30] G. 't Hooft, Phys. Rev. D **14** (1976) 3432 [Erratum-ibid. D **18** (1978) 2199].

[31] G. 't Hooft, Nucl. Phys. B **72** (1974) 461.

[32] E. Witten, Nucl. Phys. B **156** (1979) 269.

[33] O. Bär and U. J. Wiese, Nucl. Phys. B **609** (2001) 225 [arXiv:hep-ph/0105258].

[34] B. Borasoy, Eur. Phys. J. C **34** (2004) 317 [arXiv:hep-ph/0402294].

[35] B. Borasoy and E. Lipartia, Phys. Rev. D **71** (2005) 014027 [arXiv:hep-ph/0410141].

[36] W. A. Bardeen, Phys. Rev. **184** (1969) 1848.

[37] R. Kaiser and H. Leutwyler, Eur. Phys. J. C **17** (2000) 623 [arXiv:hep-ph/0007101].

[38] C. Rosenzweig, J. Schechter and C. G. Trahern, Phys. Rev. D **21** (1980) 3388.

[39] E. Witten, Annals Phys. **128** (1980) 363.

[40] P. Di Vecchia and G. Veneziano, Nucl. Phys. B **171** (1980) 253.

[41] P. Herrera-Siklody, J. I. Latorre, P. Pascual and J. Taron, Nucl. Phys. B **497** (1997) 345 [arXiv:hep-ph/9610549].

[42] R. Kaiser and H. Leutwyler, in *Proceedings of the Workshop Nonperturbative Methods in Quantum Field Theory, Adelaide, Australia, 1998*, edited by A. W. Schreiber, A. G. Williams and A. W. Thomas (World Scientific, Singapore, 1998) [arXiv:hep-ph/9806336].

[43] B. Borasoy and S. Wetzel, Phys. Rev. D **63** (2001) 074019 [arXiv:hep-ph/0105132].

[44] J. Kodaira, Nucl. Phys. B **165** (1980) 129.

[45] T. Becher and H. Leutwyler, Eur. Phys. J. C **9** (1999) 643 [arXiv:hep-ph/9901384].

[46] N. Beisert and B. Borasoy, Eur. Phys. J. A **11** (2001) 329 [arXiv:hep-ph/0107175].

[47] N. Beisert and B. Borasoy, Nucl. Phys. A **705** (2002) 433 [arXiv:hep-ph/0201289].

[48] E. E. Salpeter and H. A. Bethe, Phys. Rev. **84** (1951) 1232.

[49] N. Beisert and B. Borasoy, Nucl. Phys. A **716** (2003) 186 [arXiv:hep-ph/0301058].

[50] F. J. Gilman and R. Kauffman, Phys. Rev. D **36** (1987) 2761 [Erratum-ibid. D **37** (1988) 3348].

[51] A. Bramon, R. Escribano and M. D. Scadron, Eur. Phys. J. C **7** (1999) 271 [arXiv:hep-ph/9711229].

[52] B. R. Holstein, Phys. Scripta **T99** (2002) 55 [arXiv:hep-ph/0112150].

[53] N. F. Nasrallah, Phys. Rev. D **70** (2004) 116001 [Erratum-ibid. D **72** (2005) 019903] [arXiv:hep-ph/0410240].

[54] V. Bernard, R. L. Jaffe and U.-G. Meißner, Nucl. Phys. B **308** (1988) 753.

[55] D. Issler, Report SLAC-PUB-4943, 1990 (unpublished);
R. Akhoury and A. Alfakih, Annals Phys. **210** (1991) 81;
H. W. Fearing and S. Scherer, Phys. Rev. D **53** (1996) 315 [arXiv:hep-ph/9408346];
J. Bijnens, L. Girlanda and P. Talavera, Eur. Phys. J. C **23** (2002) 539 [arXiv:hep-ph/0110400];
T. Ebertshäuser, H. W. Fearing, S. Scherer, Phys. Rev. D **65** (2002) 054033 [arXiv:hep-ph/0110261].

[56] V. Bernard, N. Kaiser and U.-G. Meißner, Int. J. Mod. Phys. E **4** (1995) 193 [arXiv:hep-ph/9501384].

[57] A. Krause, Helv. Phys. Acta **63** (1990) 3.

[58] J. A. Oller, M. Verbeni and J. Prades, JHEP **0609** (2006) 079 [arXiv:hep-ph/0608204].

[59] M. Frink and U.-G. Meißner, Eur. Phys. J. A **29** (2006) 255 [arXiv:hep-ph/0609256].

[60] B. Ananthanarayan, G. Colangelo, J. Gasser and H. Leutwyler, Phys. Rept. **353** (2001) 207 [arXiv:hep-ph/0005297].

[61] T. N. Truong, Phys. Rev. Lett. **61** (1988) 2526.

[62] N. Kaiser, P. B. Siegel and W. Weise, Nucl. Phys. A **594** (1995) 325 [arXiv:nucl-th/9505043].

[63] J. A. Oller and E. Oset, Nucl. Phys. A **620** (1997) 438 [Erratum-ibid. A **652** (1999) 407] [arXiv:hep-ph/9702314].

[64] N. Beisert, Diploma thesis, TU München (2001), unpublished.

[65] B. Borasoy, P. C. Bruns, U.-G. Meißner and R. Nißler, Eur. Phys. J. A **34** (2007) 161 [arXiv:0709.3181 [nucl-th]].

[66] J. Gasser and U.-G. Meißner, Nucl. Phys. B **357** (1991) 90.

[67] J. Nieves and E. Ruiz Arriola, Nucl. Phys. A **679** (2000) 57 [arXiv:hep-ph/9907469].

[68] D. Djukanovic, J. Gegelia and S. Scherer, Eur. Phys. J. A **29** (2006) 337 [arXiv:hep-ph/0604164].

[69] U.-G. Meißner and J. A. Oller, Nucl. Phys. A **673** (2000) 311 [arXiv:nucl-th/9912026].

[70] J. A. Oller and U.-G. Meißner, Phys. Lett. B **500** (2001) 263 [arXiv:hep-ph/0011146].

[71] G. Höhler and A. Schulte, πN Newsletter **7** (1992) 94.

[72] N. M. Queen and G. Violini, *Dispersion Theory in High-Energy Physics* (Macmillan, London, 1974).

[73] J. R. Taylor, *Scattering Theory* (Wiley, New York, 1972).

[74] L. Eisenbud, Thesis, Princeton University (1948), unpublished;
E. P. Wigner, Phys. Rev. **98** (1955) 145.

[75] B. Borasoy and R. Nißler, Eur. Phys. J. A **26** (2005) 383 [arXiv:hep-ph/0510384].

[76] B. Borasoy, U.-G. Meißner and R. Nißler, Phys. Lett. B **643** (2006) 41 [arXiv:hep-ph/0609010].

[77] D. G. Sutherland, Phys. Lett. **23** (1966) 384.

[78] R. Baur, J. Kambor and D. Wyler, Nucl. Phys. B **460** (1996) 127 [arXiv:hep-ph/9510396].

[79] C. Ditsche, Diploma thesis, Universität Bonn (2007), HISKP-TH-07-23.

[80] J. Gasser and H. Leutwyler, Nucl. Phys. B **250** (1985) 539.

[81] J. Kambor, C. Wiesendanger and D. Wyler, Nucl. Phys. B **465** (1996) 215 [arXiv:hep-ph/9509374].

[82] A. V. Anisovich and H. Leutwyler, Phys. Lett. B **375** (1996) 335 [arXiv:hep-ph/9601237].

[83] J. Bijnens and K. Ghorbani, JHEP **0711** (2007) 030 [arXiv:0709.0230 [hep-ph]].

[84] D. J. Gross, S. B. Treiman and F. Wilczek, Phys. Rev. D **19** (1979) 2188.

[85] C. Roiesnel and T. N. Truong, Nucl. Phys. B **187** (1981) 293.

[86] A. H. Fariborz and J. Schechter, Phys. Rev. D **60** (1999) 034002 [arXiv:hep-ph/9902238].

[87] S. Giovannella *et al.* [KLOE Collaboration], arXiv:hep-ex/0505074;
T. Capussela *et al.* [KLOE Collaboration], Acta Phys. Slov. **56** (2005) 341.

[88] V. Nikolaenko *et al.* [VES Collaboration], AIP Conf. Proc. **796** (2005) 154;
V. Dorofeev *et al.* [VES Collaboration], [arXiv:hep-ph/0607044].

[89] W. B. Tippens *et al.* [Crystal Ball Collaboration], Phys. Rev. Lett. **87** (2001) 192001.

[90] F. Ambrosino *et al.* [KLOE collaboration], arXiv:0707.4137 [hep-ex].

[91] H. Osborn and D. J. Wallace, Nucl. Phys. B **20** (1970) 23.

[92] R. F. Dashen, Phys. Rev. **183** (1969) 1245.

[93] M. Walker, Diploma thesis, Universität Bern (1998),
http://www.itp.unibe.ch/diploma_thesis/walker/eta3pi.pdf

[94] R. E. Cutkosky, Phys. Rev. **96** (1954) 1135.

[95] S. Mandelstam, Phys. Rev. **140** (1965) B375.

[96] S. Eidelman *et al.* [Particle Data Group], Phys. Lett. B **592** (2004) 1.

[97] A. Abele *et al.* [Crystal Barrel Collaboration], Phys. Lett. B **417** (1998) 197.

[98] M. Bashkanov *et al.*, arXiv:0708.2014 [nucl-ex].

[99] Talks by M. Unverzagt and S. Prakhov at the *EtaMesonNet Meeting, Mainz, Germany, 2006.*

[100] H. H. Adam *et al.* [WASA-at-COSY Collaboration], arXiv:nucl-ex/0411038.

[101] F. Ambrosino *et al.* [KLOE Collaboration], arXiv:0707.2355 [hep-ex].

[102] A. Starostin, in *Proceedings of the Second International Workshop on Eta Meson Physics, Peñiscola, Spain, 2007*, edited by M. Jacewicz and B. Höistad, arXiv:0710.1809 [nucl-ex].

[103] KLOE-2, Letter of Intent,
http://www.lnf.infn.it/lnfadmin/direzione/roadmap/LoIKLOE.pdf

[104] G. Höhler, E. Pietarinen, I. Sabba Stefanescu, F. Borkowski, G. G. Simon, V. H. Walther and R. D. Wendling, Nucl. Phys. B **114** (1976) 505.

[105] B. Hyams *et al.*, Nucl. Phys. B **64**, 134 (1973) [AIP Conf. Proc. **13**, 206 (1973)];
C. D. Froggatt and J. L. Petersen, Nucl. Phys. B **129**, 89 (1977).

[106] A. D. Martin and E. N. Ozmutlu, Nucl. Phys. B **158**, 520 (1979);
D. H. Cohen, D. S. Ayres, R. Diebold, S. L. Kramer, A. J. Pawlicki and A. B. Wicklund, Phys. Rev. D **22**, 2595 (1980).

[107] M. J. Losty *et al.*, Nucl. Phys. B **69** (1974) 185;
W. Hoogland *et al.*, Nucl. Phys. B **126** (1977) 109.

[108] S. D. Protopopescu *et al.*, Phys. Rev. D **7**, 1279 (1973);
P. Estabrooks and A. D. Martin, Nucl. Phys. B **79**, 301 (1974).

[109] J. A. Oller, E. Oset and J. R. Pelaez, Phys. Rev. D **59** (1999) 074001 [Erratum-ibid. D **60** (1999 ERRAT,D75,099903.2007) 099906] [arXiv:hep-ph/9804209].

[110] I. Caprini, G. Colangelo and H. Leutwyler, Phys. Rev. Lett. **96** (2006) 132001 [arXiv:hep-ph/0512364].

[111] A. Lopez *et al.* [CLEO Collaboration], arXiv:0707.1601 [hep-ex].

[112] J. F. Donoghue, B. R. Holstein and D. Wyler, Phys. Rev. D **47** (1993) 2089;
J. Bijnens, Phys. Lett. B **306** (1993) 343 [arXiv:hep-ph/9302217];
R. Urech, Nucl. Phys. B **433** (1995) 234 [arXiv:hep-ph/9405341];
R. Baur and R. Urech, Phys. Rev. D **53** (1996) 6552 [arXiv:hep-ph/9508393]; Nucl. Phys. B **499** (1997) 319 [arXiv:hep-ph/9612328];
J. Bijnens and J. Prades, Nucl. Phys. B **490** (1997) 239 [arXiv:hep-ph/9610360];
J. F. Donoghue and A. F. Pérez, Phys. Rev. D **55** (1997) 7075 [arXiv:hep-ph/9611331];
B. Moussallam, Nucl. Phys. B **504** (1997) 381 [arXiv:hep-ph/9701400].

[113] G. R. Kalbfleisch, Phys. Rev. D **10** (1974) 916.

[114] D. Alde *et al.* [Serpukhov-Brussels-Los Alamos-Annecy(LAPP) Collaboration], Phys. Lett. B **177** (1986) 115.

[115] B. R. Jany, arXiv:0709.2834 [nucl-ex].

[116] R. R. Akhmetshin *et al.* [CMD-2 Collaboration], Phys. Lett. B **509** (2001) 217 [arXiv:hep-ex/0103043].

[117] C. Zemach, Phys. Rev. **133** (1964) B1201.

[118] N. Cabibbo, Phys. Rev. Lett. **93** (2004) 121801 [arXiv:hep-ph/0405001].

[119] N. Cabibbo and G. Isidori, JHEP **0503** (2005) 021 [arXiv:hep-ph/0502130].

[120] E. Gamiz, J. Prades and I. Scimemi, Eur. Phys. J. C **50** (2007) 405 [arXiv:hep-ph/0602023].

[121] G. Colangelo, J. Gasser, B. Kubis and A. Rusetsky, Phys. Lett. B **638** (2006) 187 [arXiv:hep-ph/0604084].

[122] U.-G. Meißner, G. Müller and S. Steininger, Phys. Lett. B **406** (1997) 154 [Erratum-ibid. B **407** (1997) 454] [arXiv:hep-ph/9704377].

[123] J. R. Batley *et al.* [NA48/2 Collaboration], Phys. Lett. B **633** (2006) 173 [arXiv:hep-ex/0511056].

[124] J. Belina, Diploma thesis, Universität Bern (2006), http://www.itp.unibe.ch/diploma_thesis/belina/totalcor.pdf

[125] J. Gasser and H. Leutwyler, Phys. Rept. **87** (1982) 77.

[126] H. Leutwyler, Nucl. Phys. B **337** (1990) 108.

[127] J. F. Donoghue and D. Wyler, Phys. Rev. D **45** (1992) 892.

[128] H. Leutwyler, Phys. Lett. B **378** (1996) 313 [arXiv:hep-ph/9602366].

[129] G. Amoros, J. Bijnens and P. Talavera, Nucl. Phys. B **602** (2001) 87 [arXiv:hep-ph/0101127].

[130] D. B. Kaplan and A. V. Manohar, Phys. Rev. Lett. **56** (1986) 2004.

[131] B. V. Martemyanov and V. S. Sopov, Phys. Rev. D **71** (2005) 017501 [arXiv:hep-ph/0502023].

[132] B. Borasoy and R. Nißler, Eur. Phys. J. A **19** (2004) 367 [arXiv:hep-ph/0309011].

[133] B. Borasoy and R. Nißler, Eur. Phys. J. A **33** (2007) 95 [arXiv:0705.0954 [hep-ph]].

[134] J. Bijnens, in *Proceedings of the Workshop on Chiral Dynamics: Theory and Experiment, Mainz, Germany, 1997*, edited by A. M. Bernstein, D. Drechsel and T. Walcher, (Springer, Berlin, 1998) [arXiv:hep-ph/9710555].

[135] H. J. Arends [A2 Collaboration], AIP Conf. Proc. **870** (2006) 481.

[136] B. Borasoy and R. Nißler, Nucl. Phys. A **740** (2004) 362 [arXiv:hep-ph/0405039]; see also R. Nißler, Diploma thesis, TU München (2003), unpublished.

[137] A. Faessler, C. Fuchs and M. I. Krivoruchenko, Phys. Rev. C **61** (2000) 035206 [arXiv:nucl-th/9904024].

[138] Ö. Kaymakcalan, S. Rajeev and J. Schechter, Phys. Rev. D **30** (1984) 594.

[139] J. Bijnens, Int. J. Mod. Phys. A **8** (1993) 3045.

[140] A. Abele *et al.* [Crystal Barrel Collaboration], Phys. Lett. B **402** (1997) 195.

[141] S. I. Bityukov *et al.* [GAMS-200 Collaboration], Z. Phys. C **50** (1991) 451.

[142] C. Picciotto, Phys. Rev. D **45** (1992) 1569.

[143] C. Picciotto and S. Richardson, Phys. Rev. D **48** (1993) 3395.

[144] M. Gormley *et al.*, Phys. Rev. D **2** (1970) 501.

[145] J. G. Layter *et al.*, Phys. Rev. D **7** (1973) 2565.

[146] Talk by C. Bloise at the *Symposium on Meson Physics at COSY-11 and WASA-at-COSY, Kraków, Poland, 2007.*

[147] C. Bargholtz *et al.* [CELSIUS-WASA Collaboration], Phys. Lett. B **644** (2007) 299 [arXiv:hep-ex/0609007].

[148] B. Borasoy, R. Nißler and W. Weise, Phys. Rev. Lett. **94** (2005) 213401 [arXiv:hep-ph/0410305]; Eur. Phys. J. A **25** (2005) 79 [arXiv:hep-ph/0505239].

[149] B. Borasoy, U.-G. Meißner and R. Nißler, Phys. Rev. C **74** (2006) 055201 [arXiv:hep-ph/0606108].

[150] G. Beer *et al.* [DEAR Collaboration], Phys. Rev. Lett. **94** (2005) 212302;
M. Cargnelli *et al.* [DEAR Collaboration], Int. J. Mod. Phys. A **20** (2005) 341.

[151] M. Iwasaki *et al.*, Phys. Rev. Lett. **78** (1997) 3067;
T. M. Ito *et al.*, Phys. Rev. C **58** (1998) 2366.

[152] U.-G. Meißner, U. Raha and A. Rusetsky, Eur. Phys. J. C **35** (2004) 349 [arXiv:hep-ph/0402261].

[153] J. A. Oller, J. Prades and M. Verbeni, Phys. Rev. Lett. **95** (2005) 172502 [arXiv:hep-ph/0508081].

[154] J. A. Oller, Eur. Phys. J. A **28** (2006) 63 [arXiv:hep-ph/0603134].

[155] B. Borasoy, R. Nißler and W. Weise, Phys. Rev. Lett. **96** (2006) 199201 [arXiv:hep-ph/0512279].

[156] J. A. Oller, J. Prades and M. Verbeni, Phys. Rev. Lett. **96** (2006) 199202 [arXiv:hep-ph/0601109].

[157] Y. Akaishi and T. Yamazaki, Phys. Rev. C **65** (2002) 044005.

[158] T. Yamazaki and Y. Akaishi, Phys. Lett. B **535** (2002) 70.

[159] M. Agnello *et al.* [FINUDA Collaboration], Phys. Rev. Lett. **94** (2005) 212303.

[160] E. Oset and H. Toki, Phys. Rev. C **74** (2006) 015207 [arXiv:nucl-th/0509048].

[161] V. K. Magas, E. Oset, A. Ramos and H. Toki, Phys. Rev. C **74** (2006) 025206 [arXiv:nucl-th/0601013].

[162] Y. Maeda *et al.*, arXiv:0710.1755 [nucl-ex].

[163] Y. Ikeda and T. Sato, Phys. Rev. C **76** (2007) 035203 [arXiv:0704.1978 [nucl-th]].

[164] N. V. Shevchenko, A. Gal, J. Mares and J. Revai, Phys. Rev. C **76** (2007) 044004 [arXiv:0706.4393 [nucl-th]].

[165] T. Yamazaki and Y. Akaishi, Phys. Rev. C **76** (2007) 045201 [arXiv:0709.0630 [nucl-th]].

[166] E. Oset and A. Ramos, Nucl. Phys. A **635** (1998) 99 [arXiv:nucl-th/9711022].

[167] C. García-Recio, J. Nieves, E. Ruiz Arriola and M. J. Vicente Vacas, Phys. Rev. D **67** (2003) 076009 [arXiv:hep-ph/0210311].

[168] N. Kaiser, P. B. Siegel and W. Weise, Phys. Lett. B **362** (1995) 23 [arXiv:nucl-th/9507036];
N. Kaiser, T. Waas and W. Weise, Nucl. Phys. A **612** (1997) 297 [arXiv:hep-ph/9607459];
J. Caro Ramon, N. Kaiser, S. Wetzel and W. Weise, Nucl. Phys. A **672** (2000) 249 [arXiv:nucl-th/9912053].

[169] J. Gasser, M. E. Sainio and A. Švarc, Nucl. Phys. B **307** (1988) 779.

[170] G. Höhler, in *Landolt-Börnstein*, Vol. 9b2, edited by H. Schopper (Springer, Berlin, 1983) Appendix A7.

[171] J. C. Jackson and H. W. Wyld, Phys. Rev. Lett. **8** (1959) 355.

[172] R. H. Dalitz and S. F. Tuan, Annals Phys. **10** (1960) 307.

[173] L. D. Landau and E. M. Lifshitz, *Quantum Mechanics* (Pergamon Press, Oxford, 1977).

[174] W. E. Humphrey and R. R. Ross, Phys. Rev. **127** (1962) 1305.

[175] M. Sakitt *et al.* Phys. Rev. **139** (1965) B719.

[176] J. K. Kim, Phys. Rev. Lett. **14** (1965) 29;
Columbia University Report, Nevis **149** (1966);
Phys. Rev. Lett. **19** (1967) 1074.

[177] W. Kittel, G. Otter and I. Wacek, Phys. Lett. **21** (1966) 349.

[178] J. Ciborowski *et al.*, J. Phys. G **8** (1982) 13.

[179] D. Evans *et al.*, J. Phys. G **9** (1983) 885.

[180] D. N. Tovee *et al.*, Nucl. Phys. B **33** (1971) 493.

[181] R. J. Nowak *et al.*, Nucl. Phys. B **139** (1978) 61.

[182] R. J. Hemingway, Nucl. Phys. B **253** (1985) 742.

[183] I. Zychor *et al.*, arXiv:0705.1039 [nucl-ex].

[184] J. C. Nacher, E. Oset, H. Toki and A. Ramos, Phys. Lett. B **461** (1999) 299 [arXiv:nucl-th/9902071].

[185] T. Hyodo, A. Hosaka, M. J. Vicente Vacas and E. Oset, Phys. Lett. B **593** (2004) 75 [arXiv:nucl-th/0401051].

[186] J. K. Ahn [LEPS Collaboration], Nucl. Phys. A **721** (2003) C715.

[187] V. K. Magas, E. Oset and A. Ramos, Phys. Rev. Lett. **95** (2005) 052301 [arXiv:hep-ph/0503043].

[188] S. Prakhov *et al.* [Crystall Ball Collaboration], Phys. Rev. C **70** (2004) 034605.

[189] B. Borasoy, P. C. Bruns, U.-G. Meißner and R. Nißler, Phys. Rev. C **72** (2005) 065201 [arXiv:hep-ph/0508307].

[190] M. F. M. Lutz and E. E. Kolomeitsev, Nucl. Phys. A **700** (2002) 193 [arXiv:nucl-th/0105042].

[191] F. E. Close and R. G. Roberts, Phys. Lett. B **316** (1993) 165 [arXiv:hep-ph/9306289];
B. Borasoy, Phys. Rev. D **59** (1999) 054021 [arXiv:hep-ph/9811411].

[192] B. Borasoy, E. Marco and S. Wetzel, Phys. Rev. C **66** (2002) 055208 [arXiv:hep-ph/0212256].

[193] M. Galassi *et al.*, *GNU Scientific Library Reference Manual (2nd Ed.)*, ISBN 0954161734.
http://www.gnu.org/software/gsl/

[194] R. H. Dalitz and A. Deloff, J. Phys. G **17** (1991) 289.

[195] A. D. Martin, Nucl. Phys. B **179** (1981) 33.

[196] U.-G. Meißner, U. Raha and A. Rusetsky, Eur. Phys. J. C **47** (2006) 473 [arXiv:nucl-th/0603029].

[197] M. Cargnelli *et al.* [SIDDHARTA Collaboration], in *Proceedings of the International Conference on Exotic Atoms and Related Topics (EXA '05), Vienna, Austria, 2005*, edited by A. Hirtl, J. Marton, E. Widmann and J. Zmeskal (Austrian Academy of Sciences Press, Vienna, Austria, 2006) 313;
C. Curceanu-Petrascu *et al.*, Eur. Phys. J. A **31** (2007) 537.

[198] M. Cargnelli *et al.* [AMADEUS Collaboration], Letter of Intent, http://www.lnf.infn.it/esperimenti/siddharta/ LOI_AMADEUS_March2006.pdf

[199] S. Deser, M. L. Goldberger, K. Baumann and W. E. Thirring, Phys. Rev. **96** (1954) 774;
T. L. Trueman, Nucl. Phys. **26** (1961) 57.

[200] D. Jido, J. A. Oller, E. Oset, A. Ramos and U.-G. Meißner, Nucl. Phys. A **725** (2003) 181 [arXiv:nucl-th/0303062].

[201] J. R. Pelaez, Phys. Rev. D **55** (1997) 4193 [arXiv:hep-ph/9609427].

[202] S. Prakhov *et al.*, Phys. Rev. C **69** (2004) 042202.

[203] I. Zychor *et al.*, Phys. Rev. Lett. **96** (2006) 012002 [arXiv:nucl-ex/0506014].

[204] S. M. Roy, Phys. Lett. B **36** (1971) 353.

[205] T. Becher and H. Leutwyler, JHEP **0106** (2001) 017 [arXiv:hep-ph/0103263].

[206] A. Rusetsky (private communication).